UNCLASSIFIED

AD 295 829

Reproduced
by the

ARMED SERVICES TECHNICAL INFORMATION AGENCY
ARLINGTON HALL STATION
ARLINGTON 12, VIRGINIA

UNCLASSIFIED

NOTICE: When government or other drawings, specifications or other data are used for any purpose other than in connection with a definitely related government procurement operation, the U. S. Government thereby incurs no responsibility, nor any obligation whatsoever; and the fact that the Government may have formulated, furnished, or in any way supplied the said drawings, specifications, or other data is not to be regarded by implication or otherwise as in any manner licensing the holder or any other person or corporation, or conveying any rights or permission to manufacture, use or sell any patented invention that may in any way be related thereto.

62-1142

295 829

FUNDAMENTALS OF DESIGN FOR SOLID-PROPELLANT ROCKET MISSILES

By

V. D. Kurov and Yu. M. Dolzhanskiy

295829

ASTIA

FEB 11 1963

TISIA

UNEDITED ROUGH DRAFT TRANSLATION

FUNDAMENTALS OF DESIGN FOR SOLID-PROPELLANT ROCKET MISSILES

BY: V. D. Kurov and Yu. M. Dolzhanskiy

English Pages: 394

THIS TRANSLATION IS A RENDITION OF THE ORIGINAL FOREIGN TEXT WITHOUT ANY ANALYTICAL OR EDITORIAL COMMENT. STATEMENTS OR THEORIES ADVOCATED OR IMPLIED ARE THOSE OF THE SOURCE AND DO NOT NECESSARILY REFLECT THE POSITION OR OPINION OF THE FOREIGN TECHNOLOGY DIVISION.

PREPARED BY:

TRANSLATION SERVICES BRANCH
FOREIGN TECHNOLOGY DIVISION
WP-AFB, OHIO.

V. D. Kurov and Yu. M. Dolzhanskiy

OSNOVY PROYEKTIROVANIYA POROKHOVYKH RAKETNYKH SNARYADOV

Gosudarstvennoye Nauchno-Tekhnicheskoye Izdatel'stvo
Oborongiz

Moskva - 1961

Pages: 1-294

FTD-TT-62-1142/1+2

TABLE OF CONTENTS

This book contains basic data on the construction of contemporary solid-propellant rocket-powered missiles, as well as information on their most important component parts and units. The book also outlines the methods employed to select optimum missile parameters as well as the parameters required for the design and planning stages of missile warhead and rocket sections; in addition, methods are presented for the determination of the laws governing the combustion of solid propellants and the discharge of the gases produced on the combustion of the solid propellants; further, methods are presented on the calculation of maximum pressure of solid-propellant combustion gases, and methods for the calculation of specific impulse and reaction thrust. A complete system of equations of missile motion is presented, as well as a method for the calculation of missile trajectory; the various possibilities of stabilizing a missile in flight are also examined. The test-stand investigations of a solid-propellant engine and missile firing tests are described.

The book is intended as a text for secondary educational institutions; at the same time, it may be useful for students of higher educational institutions as well as for engineers who are specializing in the field of rocket-system design.

FOREWORD

Reaction-thrust systems employing power plants operating on solid propellants are in wide use in various areas of rocket engineering.

Solid-propellant engines are comparatively simple in design, they are mobile, convenient in operation, and yet sufficiently reliable and effective. In the opinion of foreign specialists, achievements in the chemistry of solid propellants and the solution of problems in the design of large-scale engines make it possible to regard this class of power plants as extremely promising. It is for this reason that in recent years particular attention has been devoted abroad to problems of designing rockets using solid-propellant engines.

The present book contains basic information required for the design of the simplest reaction-thrust systems involving the use of solid-propellant engines – field-artillery rocket shells employing a powder charge. Individual design problems are discussed within the scope of the program of the course taught in secondary educational institutions.

The book consists of seven chapters. Chapter 1 presents a brief examination of the basic stages in the historical development of rocket artillery and the characteristics of certain contemporary rocket missile specimens using solid-propellant engines are presented. Chapter 2 is a direct introduction to problems encountered

in the design of solid-propellant rocket missiles. This chapter undertakes a consideration and analysis of the tactical-engineering problem of designing new missiles, and diagrams are examined in detail with respect to the design of the most important structural elements of a missile; in addition, a method is presented for the tentative selection of the basic parameters of the missile being designed. Chapters 3 and 5 are devoted to problems of working out the design of the missile warhead and its power plant. The fundamentals of the theory of interior ballistics for solid-propellant rocket engines and the elements of exterior rocket-missile ballistics are covered in Chapters 4 and 6. Finally, Chapter 7 contains the basic data on the testing of experimental missiles and their engines.

Chapters 4 and 6 cover a somewhat greater scope than the school course in order to make the material contained in these chapters more interesting and useful for a wider circle of readers. All of the data and specific figures in the book have been taken primarily from foreign literature.

Chapters 1 and 7 of the book were written by V.D. Kurov, Chapter 4 was written by Yu.M. Dolzhanskiy, and Chapters 2, 3, 5, and 6 were written jointly by Dolzhanskiy and Kurov.

The authors wish to express their gratitude to Professor V.I. Feodos'yev, who undertook the task of examining the initial manuscript, and the authors also wish to express their sincere gratitude to all of the individuals who assisted them in selecting the contents and format of this book; the authors wish especially to acknowledge the assistance and valuable advice given by Candidate of Technical Sciences M.F. Dyunze who reviewed the manuscript.

The authors will be glad to consider any complaints and criti-

cal comments with regard to the book and request that all inquiries be addressed to the publishers: Moscow, I-51, Petrovka 24, Oborongiz.

Chapter 1

BRIEF HISTORY OF THE DEVELOPMENT OF ROCKET WEAPONS USING SOLID-PROPELLANT ENGINES

There are references in the chronicles of ancient India, China, and other eastern countries to "firebolts" (incendiary arrows) — the forerunners of powder-propelled rockets. Structurally, these were made in the form of a conventional arrow that terminated in a bamboo tube which was filled with black powder (Fig. 1.1). As the black powder was ignited, the arrow flew forward under the action of a reactive force which was produced by the gases flowing out of the tube.

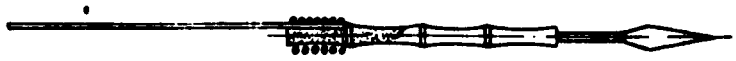

Fig. 1.1. "Firebolt."

These "incendiary arrows" were developed on a large scale in India. The Indians used these arrows both for hunting as well as for such military purposes as the repulsion of their enemies. During the colonization of India, the British ran up against the "rocket arrows" for the first time. The British military engineer, William Congreve, undertook the study of these rockets. By that time, the Indian rocket was being made of iron, and it was fitted with a pointed tip, thus giving it the appearance of sharp spears. A reed tube was fastened to the body of the arrow in order to provide for stability in flight. The British were able to increase the

dimensions of the rocket casing and attached a wooden stick in the place of the reed at the end, and in front they installed a cap with an incendiary charge. These rocket-arrows were now so heavy that it became necessary to build special launching racks to fire them.

The appearance of rockets in England compelled other European nations to undertake their use. In 1867, on the day that war was declared between Denmark and England, British naval vessels attacked the city of Copenhagen and fired some 40,000 rockets at the city. As a result, the entire city was engulfed in flames, and Denmark was forced to capitulate. After this one-day war, the Dane, Shumakher [sic], designed his own rocket on the basis of the one used by the British, and this Danish rocket was essentially the same as the one used by the British, with the exception that it had a removable warhead that was fastened to the combustion chamber by means of tape which burned up during the flight, and in addition, the powder cavity of this rocket was somewhat larger.

The Austrian, Avgustin [sic], having studied the British and Danish rockets, constructed a rocket missile on the basis of these forerunners, which was structurally a riveted iron casing filled with a powder charge throughout its entire length. The forward part of the casing was filled either with an incendiary charge or a shot grenade. The flight of this missile was stabilized by means of a stick attached to the side of the casing.

A description of the first Russian rocket appears in the "Regulations" of Onisim Mikhalyov, written by him in 1607-1621. Structurally, these rockets were made in the form of a shell (along the lines of an artillery shell), and they were filled with a special powder charge shaped so as to have a channel ("a rocket void") on

the inside. At that time, there was no theoretical justification for the need of this channel. The channel was made, because it had been established in practice that it served to increase reaction thrust.

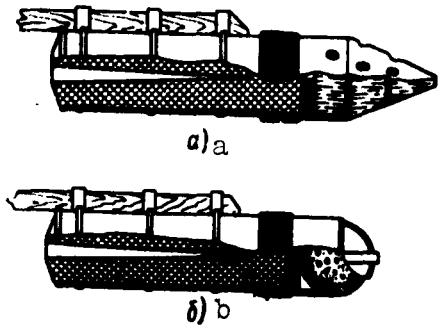

Fig. 1.2. Rocket missile designed by A.D. Zasyad'ko. a) Incendiary rocket; b) demolition rocket.

During the reign of Peter I rockets came into ever-increasing use. During this period, the numerous holidays on the occasion of Russian military victories were generally celebrated by tremendous exhibitions of fireworks which employed the principle of rockets. At the same time, rockets came into widespread use in the army. An extremely successful rocket was designed in 1707, and this signal rocket remained in the arsenal of weapons for almost 150 years.

The first Russian military rockets were designed by Aleksandr Dmitriyevich Zasyad'ko (1779-1838). He designed demolition and incendiary rockets of three calibers: 2, 2.5, and 4 inches. Structurally, Zasyad'ko's rockets were made with cylindrical iron casings filled with powder, and a conical channel was drilled into the charge, said channel extending 3/4 of the length into the charge. A perforated cap filled with an incendiary mass [paste] was mounted at the front end of the rocket casing. Flames shot out of the openings of the perforated cap (in the zone of rocket impact), igniting all objects in the vicinity. A wooden stick was mounted at the rear end of the rocket in order to achieve flight stability.

Thus was built the first Russian incendiary rocket. The construction of a demolition rocket is in no way different from that

of an incendiary rocket; the only exception here is the fact that instead of a cap with an incendiary paste, a round shell containing explosives (Fig. 1.2) is attached to the casing.

A.D. Zasyad'ko designed a launching installation for the firing of his rockets; this installation consisted of tubes mounted on a tripod so that it could rotate freely in both the horizontal and vertical planes. Such a launching device was easily portable and could be set up in any small area, thus attaining greater maneuverability.

Because of its small weight and simplicity of design, a great number of these launching installations could quickly be concentrated in a given sector, thus making it possible to mount massive fire power against an enemy. Later on, Zasyad'ko designed launching installations which made it possible to fire simultaneous salvos of six rockets. These installations were also unique in the simplicity of their design and limited weight.

During the period being described, the successful waging of military campaigns depended in great measure on the ability to defend and take fortresses. Special means were developed for the capture and defense of fortresses. The Russian general A.A. Shil'der developed a new system of fortress defense involving the use of rocket missiles. He also developed an underwater craft to operate in minor bodies of water; this craft was armed primarily with rocket missiles which could be launched electrically both beneath the surface as well as from the surface. This application of rocket missiles was yet another important achievement in the area of Russian rocket engineering.

The eminent Russian designer-rocketeer Konstantin Ivanovich Konstantinov (1819-1871) began his activities in this same period

of widespread development of Russian rocket engineering. One of Konstantinov's first inventions was the electroballistic installation for the measurement of missile velocity during flight (on its trajectory).

In 1847-1850, K.I. Konstantinov, using his electroballistic installation as the basis, designed a remarkable device – a rocket electroballistic pendulum. This device makes it possible to construct the curve of change in missile reaction force during missile flight. The existence of this device made it possible to undertake a solution of the problems associated with range and accuracy of missile flight over a given trajectory on a scientific basis.

Both of the devices produced by K.I. Konstantinov made it possible to lay the foundations of the theory of interior and exterior ballistics for rocket missiles. On the basis of his research, Konstantinov sought to design new rockets which could achieve the firing accuracy of artillery weapons.

Prior to this, rockets of identical caliber and designation, and even rockets produced in a single production batch, exhibited substantial production deviations, thus sharply reducing the accuracy of their firing. After a number of investigations, K.I. Konstantinov established that it was impossible to obtain stable rocket characteristics under the existing methods of production. It is for this reason that he implemented a series of measures intended to obtain technological uniformity for the production of rockets. New machines and mechanisms were installed in the rocket institution for the production of casings, the drilling of channels into the powder, the preparation of uniform rocket mixtures, etc.

In addition to improving production, Konstantinov did much in

the field of improving the design of the rocket systems themselves. For example, he proposed a dry method of filling the rocket casings with powder in order to increase the accuracy of firing with rocket missiles and to increase the length of time for which these missiles could be stored; in addition, he selected the optimum shape, weight, and dimensions of rocket missiles in order to attain the greatest flight range. He also improved the design of the launching installations – they became more stable, and the rockets could be housed in these installations with smaller clearances, thus making it possible to obtain more stable missile characteristics on departure from the guide rails, and consequently, it was possible to obtain greater firing accuracy in flight.

Fig. 1.3. Rocket missile from the 1860's.

All of the above-enumerated measures made it possible to produce domestic rocket missiles exhibiting the best characteristics both with respect to firing accuracy, as well as with respect to range in comparison with rocket missiles produced by other governments (Great Britain, France, Austria, etc.).

Three basic rocket-missile calibers were selected in Russia: 2, 2.5, and 4 inches (102, 64, and 51 mm [sic]).

In terms of designation, the rockets were subdivided into field rockets armed with explosive shells and shot, and fortress rockets which, in addition to the demolition charges, were also armed with incendiary and illumination charges.

Rockets attained a range of 4000-4500 m, with a lateral deviation of 30 m. An example of this type of missile design is presented

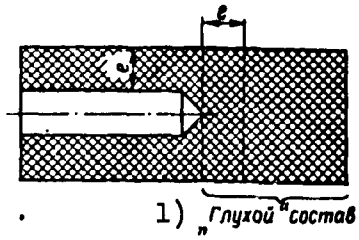

Fig. 1.4. For the selection of the optimum thickness e of the "blind" propellant grain (e is the optimum thickness).
1) "Blind" grain.

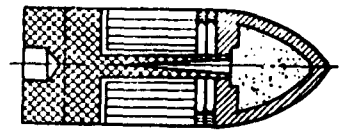

Fig. 1.5. Rocket missile designed in accordance with Konstantinov's system, 1862.

in Fig. 1.3.

By the middle of the 19th century, the European armies were already using rifled bores, whereas in Russia smooth-bore weapons were still in use. This backwardness in the armament of the Russian army had to be overcome. In this connection, military specialists in the Russian press started expounding the idea that rocket systems were obsolete and that it would be necessary to replace these with systems involving rifled artillery; the positive aspects of rocket weaponry were deliberately covered up, and only the shortcomings of rockets were stressed. However, Konstantinov and his followers wrote articles against this underestimation of rocket weapons and continued to work on the theory and design of rocket missiles.

In particular, Konstantinov established that the entire powder (propellant) charge does not participate in the development of reaction force, but only that portion in which there is an internal channel, and a portion of the blind (without channel) charge, the length of which must be equal to the thickness of the propellant spacer (Fig. 1.4). Later on, he established that if the length of the blind charge is greater than the thickness of the propellant spacer, the center of missile gravity shifts more significantly during the combustion of the powder, causing the trajectory of mis-

sile flight to change during the active phase, and as a result we have great scattering of the rockets.

A reduction in the length of the blind charge to the thickness of the propellant spacer immediately eliminated this shortcoming from the rockets, and this, of course, had an immediate positive effect on the accuracy of firing. In addition, this step served to eliminate yet another shortcoming that was inherent not only in rockets, but in the artillery missiles of the time; this shortcoming is related to the spherical shape of the missile head. Konstantinov not only proposed to replace the spherical heads with heads that were somewhat elongated, but he lengthened the guide rails of the launching installation as well. The guide rails were somewhat too short and as a result the missiles left the guide rails at a time when the charge had not yet entered the stage of complete combustion, i.e., under the action of incomplete reaction force. As a result, the initial segment of the trajectory was observed to sag, the missile would deviate from its assigned heading, etc., and this sharply reduced the firing characteristics of the rockets. Konstantinov also proposed a new design for the empennage of the rocket, reducing its length by one half.

All of these innovations sharply increased range and the firing characteristics of the rocket missiles. An example of a rocket-missile designed by Konstantinov in 1862 is presented in Fig. 1.5.

Despite the number of achievements, in 1887 rocket weapons in Russia were officially removed from the arsenal of armaments, but the production of rockets continued until 1908, since they still found application during the military expeditions carried out by the Russian army as, for example, in Central Asia. Certain types of rockets – signal rockets, rescue rockets, and illumination rockets –

remained in the armament of the army even after the closing, in 1910, of the Nikolayevskiy Rocket Institution, the chief supplier of rockets. However, despite the official rejection of rockets, work on their improvement continued. Along these lines, we should mention the work of Pomortsev in the area of improving rocket-missile design. Pomortsev proposed, in particular, that rockets be stabilized not by means of long tail sections, as was the case before, but by means of annular stabilizers whose dimensions virtually did not exceed those of the rocket. He also proposed rockets that would function on compressed air.

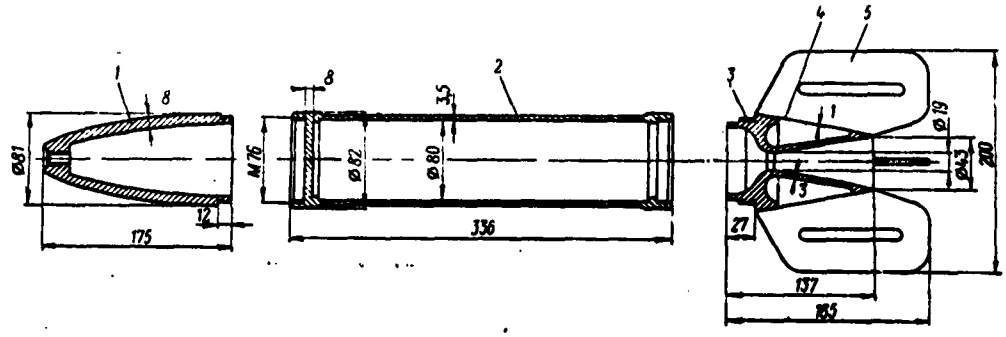

Fig. 1.6. The M8 rocket missile (USSR), caliber 82 mm, launching weight 8 kg, maximum velocity 315 m/sec. 1) Warhead; 2) combustion chamber (with fixed forward plate); 3) nozzle; 4) cowling; 5) stabilizer.

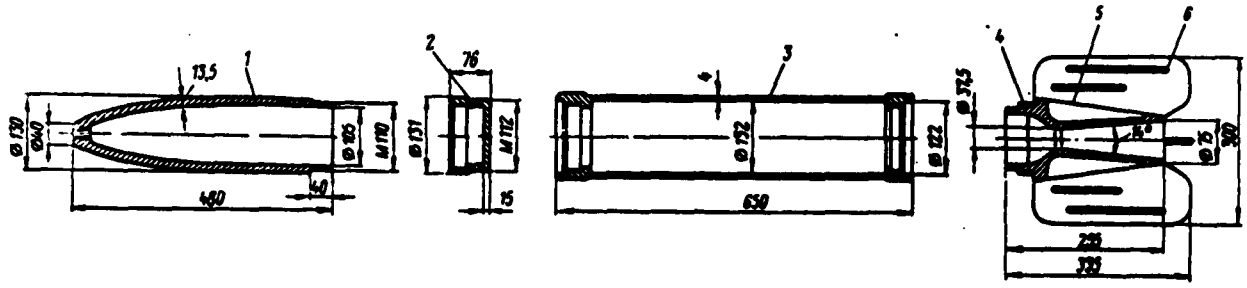

Fig. 1.7. The M13 rocket missile (USSR), caliber 132 mm, launching weight 42.5 kg, maximum velocity 355 m/sec. 1) Warhead; 2) spacer; 3) combustion chamber; 4) nozzle; 5) cowling; 6) stabilizer.

In addition to the development of new designs, Russian scientists worked on a series of significant theoretical problems in rocket

engineering.

It is well known that the mass of the rocket in the active segment of the trajectory continuously undergoes change as a result of the combustion of the propellant and the exhaust of the propellant gases. This made the calculation of the exterior rocket ballistics extremely difficult. The solution to the problem of the motion of a body with a variable mass in air was sought by many investigators abroad, but only our scientists were able to solve this problem, thus laying the foundations for subsequent work, resulting in the final analysis in the development of contemporary rockets.

The problem of the motion of rockets, as a special case of the motion of a body with a variable mass, was solved by Professor I.V. Meshcherskiy in 1895. He proposed a mathematical expression for the determination of rocket velocity and the distance covered, which was a function of air resistance, gravitational forces, propellant weight, gas pressure, and exhaust velocity.

In 1897, Meshcherskiy published yet another work, in which he presented the equations of the mechanics for the motion of bodies of variable mass, and in 1904 he provided the solution to yet another important problem on the motion of a body with the simultaneous addition and removal of mass from the body, thus laying the groundwork for the theory of air-reaction engines.

The work of another Russian scientist – K.E. Tsiolkovskiy – also became well known throughout the world. In 1903, he published the work "Investigation of Space by Means of Reaction-Thrust Devices," in which Tsiolkovskiy, for the first time anywhere, developed the theory of rocket flight into outer space. In particular, he proposed a liquid-fuel rocket engine (ZhRD) with all of its basic units – a pump for the supply of propellant to the combustion chamber,

a device for the cooling of the combustion chamber by means of one of the propellant components, an expanding jet nozzle, etc.

K.E. Tsiolkovskiy also proposed the idea of artificial satellites of the earth and planets, setting down the principal structural diagrams. The derivation of the formulas for the determination of rocket-flight velocities at any point of the active phase of the trajectory is also credited to him.

These works and a number of others, produced both in Russia as well as abroad, permitted many scientists subsequently to return to the idea of developing rocket weapons, but now they were in a position to work on a higher theoretical level.

After the October Revolution in our country, scientists and designers achieved the necessary conditions for the continuation of work in the area of improving rockets. As a result of these works, reaction-thrust missiles of the following calibers were designed: 82, 132, and 300 mm (Figs. 1.6, 1.7, and 1.8), which were used successfully at the front during the Great Fatherland War.

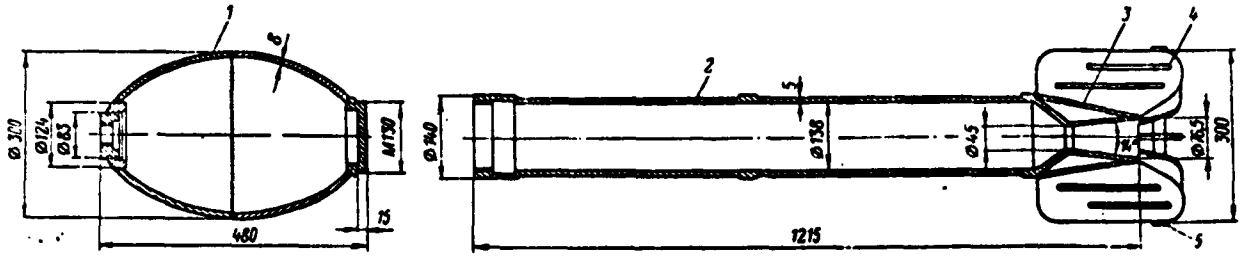

Fig. 1.8. The M31 rocket missile (USSR), caliber 300 mm, launching weight 94.6 kg, maximum velocity 255 m/sec. 1) Warhead (assembly); 2) combustion chamber (made in a single unit, together with the nozzle); 3) cowling; 4) stabilizer; 5) stabilizer guide ring.

It was during the 1930's that all countries undertook the most serious development of rockets. In Germany these projects were being worked on particularly intensively. In 1931, the Germans developed

a solid-propellant rocket missile, but this was not completed until 1935.

In 1936, Germany set up special organizations that were responsible for the design and production of rocket weapons exclusively. Later on, an ever-increasing number of scientists joined these organizations, as well as scientists and commercial firms from countries occupied by Germany.

In 1941, the Germans began using a multiperforated grain and they also began work on the design of the "D" mortar-firing system, which fired a 158-mm rocket missile. Subsequently, on the basis of this missile, they developed a 300-mm fragmentation-demolition shell, as well as a 280-mm demolition and 210- and 320-mm incendiary shells. During the course of the war, the Germans developed 80- and 150-mm rocket missiles.

It should be pointed out that the German reaction-thrust missiles were turbojet missiles for the most part and therefore exhibited rather high firing accuracy. The German launching installations made it possible to fire a salvo of only 5-10 rocket missiles, and this did not provide sufficient fire power.

The Germans were the first to develop and use long-range liquid-fuel rockets (V-2) and pilotless airplane-missiles with air-reaction engines (V-1) for military purposes. In Fig. 1.9 we present diagrams of several types of German rocket missiles.

In addition to Germany, the British, although admittedly not as intensively, were working on the design of rocket missiles. Here the work was directed primarily toward means of defense against the rapidly developing bomber-aircraft forces. It was for this purpose that the British, in 1938, developed the 76-mm antiaircraft solid-propellant rocket whose weight came to 22.4 kg, which carried

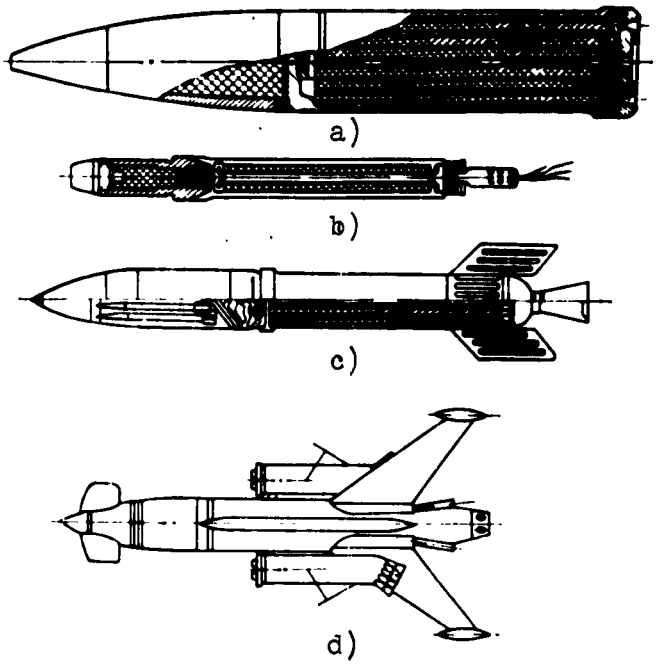

Fig. 1.9. German rocket missiles from the Second World War. a) 210-mm fragmentation-demolition missile; b) the antiaircraft missile "Luftfaust"; c) the antiaircraft missile-mothership "Rheinkind"; d) a version of the R-ShR antiaircraft guided rocket "Rheintochter".

an explosive charge weighing 1.6 kg. This rocket played an important role in the defense of England against the raids of German aircraft. Mention should also be made of the successful work done in England on the development of aviation rocket missiles, this work begun in 1941; certain of these designs were also taken over by the USAF.

The United States did almost no work in rocket engineering prior to the war; it was only in 1940 that intensive planning for military rockets was begun. First a rocket booster for aviation bombs was developed, and this booster increased the penetration capacity of the bomb. In addition, the improvement of the antitank "bazooka" weapon continued until the end of the war; work on this weapon was begun in 1941. This weapon was capable of destroying a

tank at a distance of 100-200 m. By the end of the war, a new type of antitank rocket had been developed; this was the "Super-Bazooka" which had increased penetrating power.

Much work was done in the USA during this period on equipping the Air Force and Navy with rockets. In December of 1944, a booster engine was developed for purposes of accelerating the takeoff run of an aircraft by a factor of 4. Somewhat earlier, in 1942, naval rocket bombs weighing 21-29 kg were developed for antisubmarine action. Launching racks for rocket weapons were demountable and were installed on decks of vessels.

The Americans also did much work on equipping naval and airborne landing units with rocket weapons. However, rocket engineering in the USA underwent particularly great development only in the postwar period.

We will present below data on certain military rockets of the USA and other capitalistic countries.

THE "GROUND-TO-GROUND" CLASSIFICATION OF ROCKETS FOR FIRING FROM THE GROUND AGAINST GROUND TARGETS

SHORT RANGE ANTITANK MISSILES

The "Dart" (USA)
(Fig. 1.10)

Basic Missile Characteristics

Length	1.52 m
Wingspan	1.27 m
Span of tail unit	0.914 m
Engine	Solid-propellant rocket (PRD)

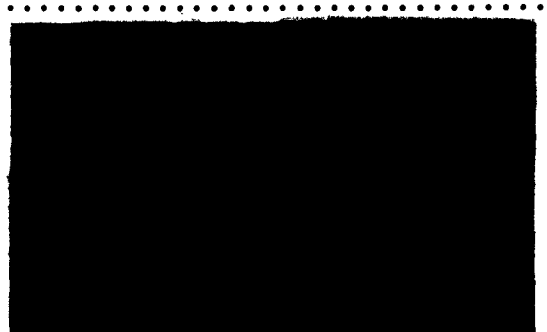

Fig. 1.10. The antitank missile "Dart" (USA) on its launching installation.

The "891 Vickers-Armstrong" (Great Britain)

Basic Missile Characteristics

Length	0.819 m
Tail unit span	0.279 m
Caliber	114 mm
Engine	PRD
Weight of missile with launching container	18 kg

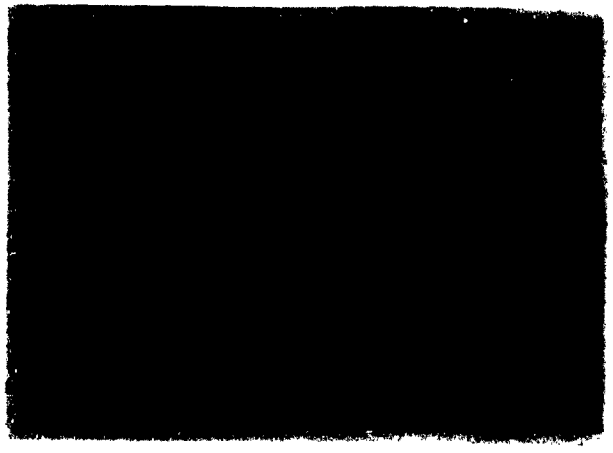

Fig. 1.11. The antitank missile 891 "Vickers-Armstrong" (Great Britain).

Figure 1.11 shows this missile at instant of firing, and it also shows the portable container which serves, at the same time, as the launching installation.

ARMY FIELD ROCKETS

The "Lacrosse" (USA)

(Fig. 1.12)

Basic Characteristics

Length	6.1 m
Wingspan	2.75 m
Tail-unit span	1.5 m
Caliber	500 mm
Engine	PRD
Range	35 km
Weight of rocket	1150 kg

MEDIUM-RANGE BALLISTIC ROCKETS

The "Polaris" (USA)

Basic Characteristics

Over-all length	8.07 m

Caliber ..... 1370 mm
Engine ..... Two-stage PRD

Weight of rocket ..... 13,600 kg
Relative weight of propellant 0.9
Weight of Warhead ..... 450 kg

Fig. 1.12. The "Lacrosse" rocket (USA) in firing position.

The proposed propellant for the two stages is a solid propellant with a mixture based on polyurethane, exhibiting a specific impulse of j_1 = 240 kg·sec/kg.

"GROUND-TO-AIR" CLASSIFICATION OF ROCKETS FOR FIRING FROM THE GROUND AGAINST AIR TARGETS

The "Nike-Hercules" (USA)

(Fig. 1.13)

Basic Characteristics

Length ..... 12.65 m
Wingspan ..... 1.88 m
Caliber ..... 635 mm
Engine (Fig. 1.14) ..... Two-state PRD

Fig. 1.13. The antiaircraft rocket "Nike-Hercules" (USA) on launching installation.

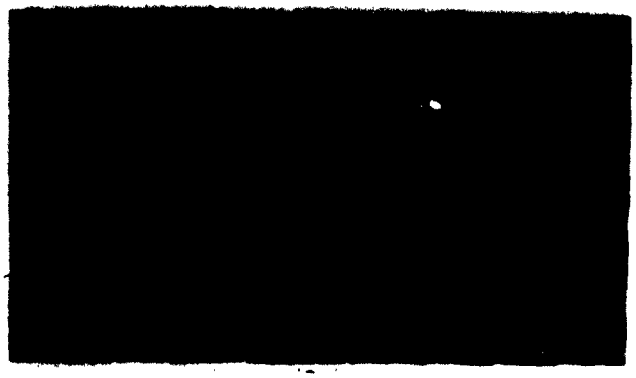

Fig. 1.14. The engine of the second stage of the antiaircraft "Nike-Hercules" rocket.

The "Hawk" (USA)

(Fig. 1.15)

Basic Characteristics

Length	4.98 m
Wingspan	1.19 m
Caliber	355 mm
Engine	PRD, with two thrust stages
Weight of rocket	450 kg

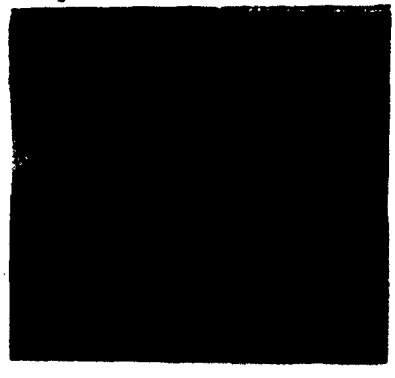

Fig. 1.15. Launching installation with three "Hawk" rockets (USA).

The "Thunderbird" (Great Britain)

(Fig. 1.16)

Basic Characteristics

Length	6 m
Wingspan	1.69 m
Tail-unit span	1.6 m
Caliber	400 mm
Engine	Two-stage PRD

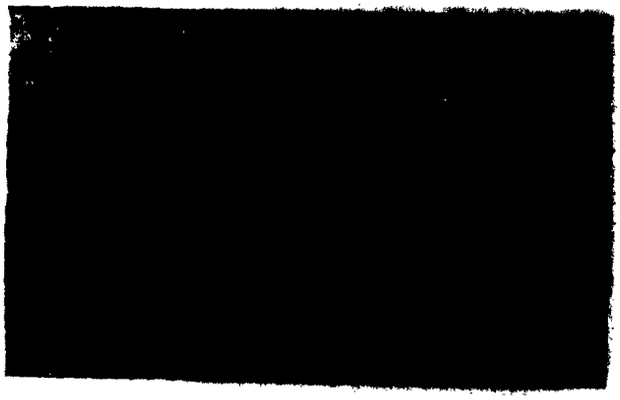

Fig. 1.16. The antiaircraft "Thunderbird" rocket (Great Britain) at the annual air-show of Farnborough.

"AIR-TO-AIR" CLASSIFICATION OF ROCKETS FOR FIRING FROM AIRCRAFT AGAINST AIR TARGETS

The "Falcon" (USA)

(Fig. 1.17)

Basic Characteristics

Length	1.95 m
Tail-unit span	0.5 m
Caliber	160 mm
Engine	PRD
Operating range	2-8 km
Velocity	2 M(ach)
Weight of missile	50 kg

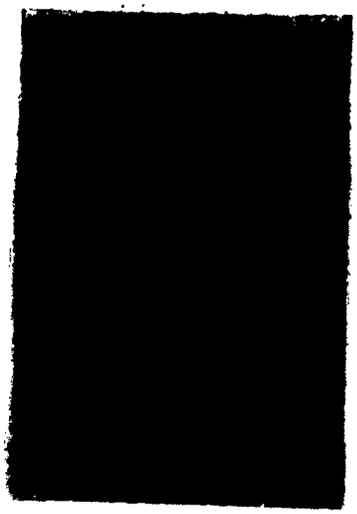

Fig. 1.17. Two of the last models of the "Falcon" missile (USA).

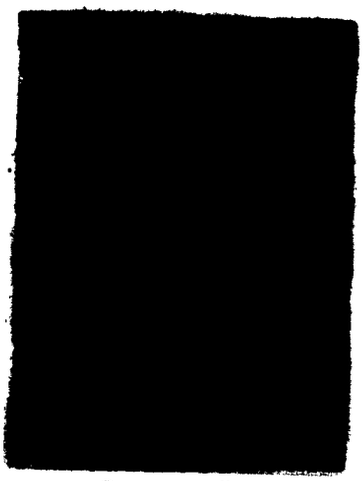

Fig. 1.18. The "Sidewinder" rocket (USA) on the ground.

The "Sidewinder" (USA)

(Figs. 1.18 and 1.19)

Basic Characteristics

Length	2.8 m
Tail-unit span	0.48 m
Caliber	110 mm
Engine	PRD, with an operating time of 2 sec
Weight of missile	70 kg

Fig. 1.19. A USAF interceptor (USA) equipped with four "Sidewinder" rockets, mounted beneath the winds of the aircraft.

The "Fireflash" (Great Britain)

(Fig. 1.20)

Basic Characteristics

Length	3.7 m
Wingspan	0.714 m
Tail-unit span	0.656 m
Altitude, with boosters	0.602 m
Length of missile airframe	2.26 m
Caliber	150 mm
Engine	Two PRD, jettisoned after burnout of propellant
Weight of missile	140 kg

We can see clearly in Fig. 1.20 the unique assembly of a missile with two engines fastened at the sides of the missile airframe and jettisoned after the complete burnout of the propellant.

Fig. 1.20. The "Fireflash" missile, mounted beneath the wind of an English interceptor.

The "Firestrike" (Great Britain)

(Fig. 1.21)

Basic Characteristics

Length	3.18 m
Wingspan	0.74 m
Tail-unit span	0.46 m
Caliber	220 mm
Engine	PRD

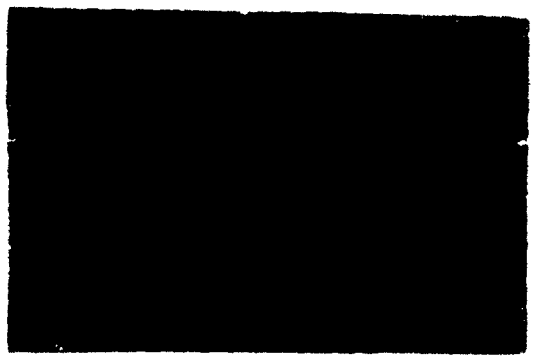

Fig. 1.21. The "Firestrike" missile mounted beneath an aircraft wing.

The "Matra 2-510" (France)

Basic Characteristics

Length	3.2 m
Wingspan	1.0 m
Caliber	200 mm
Engine	PRD, with booster

"AIR-TO-GROUND" CLASSIFICATION OF ROCKETS FOR FIRING FROM AN AIRCRAFT AGAINST GROUND TARGETS

The "Bull Pup" (USA)

(Fig. 1.22)

Basic Characteristics

Length	3.35 m
Wingspan	0.9 m
Caliber	300 mm
Engine	PRD
Total weight of missile	270 kg

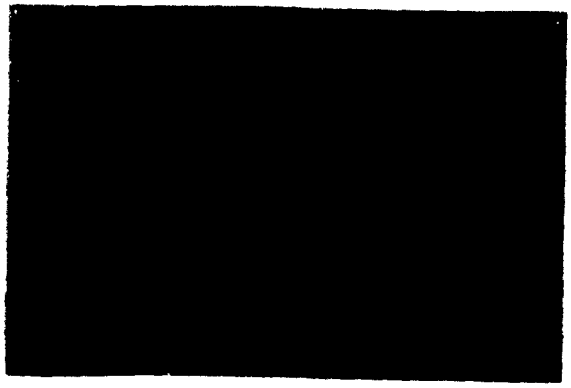

Fig. 1.22. Mounting of the "Bull Pup" missiles (USA) beneath the wing of an aircraft of the tactical branch of the USAF.

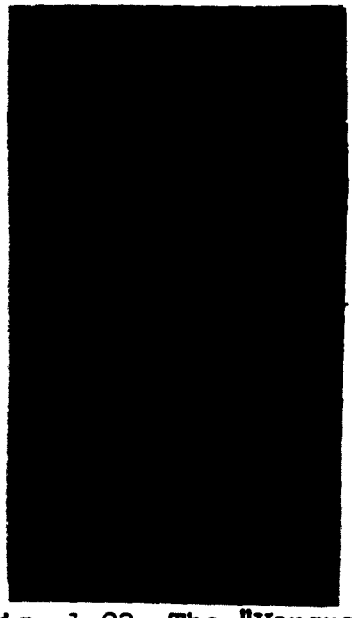

Fig. 1.23. The "Vanguard" rocket with its last-stage engine operating on solid propellant.

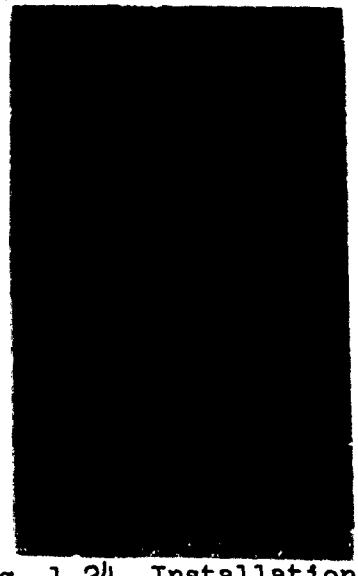

Fig. 1.24. Installation of the container with scientific equipment on the "Jupiter-C" rocket. The last stage of this rocket operates on solid propellants.

The "BB-10" (France)

Basic Characteristics

Length	3.4 m
Tail-unit span	0.8 m
Engine	PRD
Weight of rocket	400 kg

The extensive use of solid-propellant rocket engines was not restricted to military purposes. Solid-propellant rocket engines have proved themselves reliable and effective power plants for powerful rockets used for such civilian purposes as the investigation of outer layers of the terrestrial atmosphere, the launching of artificial satellites and the mastery of outer space. As an example, we can cite the well-known "Vanguard" system with a last-stage engine that operates on solid propellants.(Fig. 1.23), or the "Jupiter-C" (Fig. 1.24). By means of these rockets the Americans were able to launch several artificial satellites and to carry out a series of other investigations in conjunction with the International Geophysical Year.

Chapter 2

TENTATIVE SELECTION OF BASIC DESIGN PARAMETERS FOR A MISSILE

§ 1. REQUIREMENTS IMPOSED ON SOLID-PROPELLANT ROCKET MISSILES*

Of the basic requirements imposed on the design and parameters of a missile, we can mention the following:

1) tactical-technical requirements;

2) production-economic requirements.

Tactical-technical requirements include the requirements which pertain to the missile, its launching installation, and the method of missile utilization (the firing method).

Here, the requirements imposed on the missile are the most essential; however, an underestimation of the requirements imposed on the launching installation or the method of missile utilization may result in having the entire complex of weapons prove to be inadequately perfected or simply not fit for combat, even if the basic element of the complex — the rocket missile — has been designed properly. The requirements imposed on the missile include the parameters and the characteristics of the rocket engine and the missile warhead, as well as information on the required combat effectiveness of the weapons system being developed. Of these, the following are the most important.

The combat designation of the missile (the type of warhead). The combat designation of a missile is determined by the required effect that the missile is to have at the target. In the classifica-

tion of missiles according to combat designation, the following types of missiles have been adopted:

– missiles of basic designation: demolition, fragmentation, fragmentation-demolition, armor-piercing, incendiary, etc.;

– missiles of special designation: illumination, smoke, propaganda, etc.

Missiles of basic designation are used for the direct destruction of targets. The area in which such missiles can be used is determined by the military assignments of the field artillery.

If the combat designation (type of warhead) of the missile is given in the tactical-technical requirements, the designer is better able to select the structural procedure of missile assembly during the planning and design stage, he is in a position to decide on the shape of the warhead, etc., and he can also make a decision as to the type of fuse to be employed in the missile warhead being developed.

Requirements with respect to missile effectiveness at the target. For missiles of basic designation, the requirement for effectiveness at the target is a single-valued function of the payload weight of the system. Let us examine this in greater detail.

Demolition missiles are intended primarily for nonconcrete field-type defense installations such as trenches, shelters, fire points, observation points, etc. Demolition missiles of large caliber can be used in coordinated raids against concrete and reinforced-concrete structures.

Demolition bombs destroy the target with the destructive force produced by the shock wave that is generated on the detonation of the explosives and, in part, by the force of impact against the obstacle. In accordance with this, the force of demolition-missile

effect at the target is determined primarily by the characteristics and quantity of the explosive material used, said material enclosed within the body of the missile warhead; given a certain explosive, the force is uniquely defined by the weight of the explosive charge in the warhead.

Fragmentation missiles are intended for air or ground targets (primarily against objects), for the destruction of light field shelters, etc.

In accordance with the designation of the fragmentation missile, the basic requirement imposed on the force of such a missile can be reduced to the necessity of obtaining the maximum number of effective fragments over the greatest possible effective range.

As a rule, a fragmentation warhead must have a rather thick shell and needs a quantity of explosives adequate only to fragment the shell into pieces of shrapnel and to impart the required initial velocity to the shrapnel. The effective force of a fragmentation missile at the target, as a rule, is determined by the maximum weight of the metal used in the warhead of the missile, and this factor will make it possible to estimate the minimum weight of explosive charge required to achieve the fragmentation.

Fragmentation-demolition missiles are an example of the unification of various types of missiles and these are employed to produce an effect of shell fragmentation as well as the destructive demolition force of the explosion at the target. The requirement imposed on the effective force of the warhead of this type of missile involves the selection of the correct weight of the explosive charge and the desired quantity of fragments.

For certain types of rocket ammunition such as, for example, hollow-charge antitank mines, the force is completely determined

by the geometry of the warhead. In fact, the effective force of a hollow-charge mine at the target is characterized by the thickness of the armor plating that is penetrated by the stream of products of the explosion of the hollow-charge warhead of the mine. On the other hand, it has been established that the armor-piercing capability of a hollow charge depends on the geometry of the warhead charge and primarily on the diameter D_v of the hollow funnel; here, as a rough estimation, we may hold that

$$D_в \approx \frac{b_{max}}{n_ф},$$

where b_{max} is the maximum thickness of the armor plate being penetrated; n_f is some coefficient that is a function of the shape of the funnel.

Thus with a given magnitude of b we can immediately determine the basic dimension D_v of the hollow charge, and this dimension is then employed to select the dimensions of the remaining elements in the geometry of the hollow charge and the warhead.

In addition to the basic stipulation of effective force for the missile being designed, the tactical-technical requirements may include certain additional requirements with respect to the nature of missile effectiveness at the target; as a rule, these additional requirements are imposed on antiaircraft missiles, incendiary missiles, and certain others.

Firing range (or range of direct fire). Rocket missiles of the field artillery are a means employed to destroy various enemy targets and objects, even if they are situated at considerable distances from the firing position. In this connection, the maximum firing range is one of the most important missile characteristics and must be included in the tactical-technical requirements.

The range requirement uniquely defines the magnitude of required

missile-flight velocity at the end of the active phase of the trajectory, since, as has been demonstrated by the solution of the basic problem of exterior ballistics, the initial velocity of a body in flight, launched at a certain angle to the horizon, in turn uniquely defines the flight range of this body. The magnitude of the required velocity v_{max} is extremely important, since it is one of the input parameters in the planning stage for the calculation of the interior ballistic characteristics of the rocket engine of the missile.

For missiles of the "air-to-air" class and for antitank hollow-charge mines, we impose the requirement of passing the so-called combat control distance within a definite period of time rather than the maximum firing range.

For example, "a missile is designated for ... and must pass a distance of 1000 m in no less than 2 sec." A similar requirement is imposed by the features of aerial combat and the nature of aircraft maneuvering on approach. The control distance is that distance at which the enemy aircraft cannot escape the attacking fire nor return the fire.

Firing accuracy. The probability of an unguided rocket missile hitting a target is generally characterized by missile firing accuracy.

Missile firing accuracy is that dimensionless quantity which characterizes the possible maximum deviation of the missile from the calculated (theoretical) point of impact. If the greatest deviation of the missile from the target is equal to B^{max}[m], the firing accuracy will be characterized by the following quantity:

$$\eta = \frac{B^{max}}{X},$$

where X is the firing range (the distance from the point of missile launch to the target).

In firing, the scattering of missile impact points around a central sighting point is generally estimated by means of the quantities which characterize the mean probable deviation (B_d) of the missile with respect to range [distance] and in the lateral direction (B_b). In accordance with this, the firing accuracy with respect to range is generally regarded as

$$\eta_д = \frac{B_д}{X}$$

and in the lateral direction

$$\eta_б = \frac{B_б}{X}.$$

As an example of the formulation of tactical-technical requirements with respect to firing accuracy we can cite, for example: "...over the entire range of possible missile flight velocities and ...the stabilization elements of the missile must provide for a firing accuracy with respect to range that must not exceed

$$\eta_д = \frac{B_д}{X} < 0{,}03$$

and in the lateral direction not to exceed

$$\eta_б = \frac{B_б}{X} < 0{,}01».$$

This means that the mean probable deviation of impact points with respect to range must not exceed 3%, and in the lateral direction it must not exceed 1% of the firing distance.

The establishment of firing-accuracy requirements enables the designer to select the type of missile stabilization, the general scheme of missile assembly, and it also enables him to solve certain other problems in the planning stage.

Total missile weight. For the majority of missiles used in the field rocket artillery, the total weight is stipulated tentatively in the tactical-technical requirements, within a rather wide range. Short-range antitank missiles, as well as "ground-to-air" and "air-to-air" missiles are narrowly restricted in terms of weight.

The temperature interval for missile utilization. As a rule, the tactical-technical requirements stipulate the maximum temperature interval within which a rocket missile must assure faultless combat capability.

The necessity of taking into consideration a certain interval of operating temperatures can be explained by the fact that the basic parameters of a solid-propellant rocket engine depend strongly on the initial temperature of the charge and, at various temperatures, may undergo substantial change. This brings forth a series of specific problems which must be borne in mind at the very beginning of the missile planning stage.

The reliability of the entire weapons system (faultless missile operation).

The possibility and convenience of transporting a missile in crates or directly on combat vehicles, and here it is assumed, as a rule, that the missile should not surrender any of its combat readiness as a result of the transportation process.

Permissible prelaunch checks and similar regulation operations and their duration.

The possibility of long missile storage.

The above-mentioned requirements and periods make it possible for the designer to approach intelligently and with justification the solution of, for example, the problem of the selection of the material for certain missile units, the selection of anticorrosion coatings, etc., and to select the method of protecting the missile during storage in warehouses and arsenals.

In the production-economic requirements we present the technological and economic indicators that are required for the missile design being planned. This group of requirements is difficult to

break down unless they are referred specifically to a certain end product; however, some of the following may be classified as general requirements:

– restriction of material expenditures during the planning phase, and in the production and testing of the missile and all of its systems;

– the adaptability of individual units and missile component parts to production processes;

– the utilization of inexpensive construction materials, as well as those that are not in short supply, etc.

The contents of the tactical-technical requirements for the design of a missile, as well as an analysis of the corresponding conclusions, must always precede the direct development of a design and the calculations. Only in this case can the new design fully meet all of the requirements imposed, and it is only in this way that the missile being planned will be in a position to cope with all of the problems before it.

§ 2. SELECTION AND JUSTIFICATION OF STRUCTURAL MISSILE DIAGRAMS

The structural diagram of a rocket missile refers to that interrelated positioning of the basic missile parts – warhead and rocket – into an over-all assembly.

There are several possible ways of assembling a solid-propellant rocket missile. Examples of such structural diagrams are presented in Fig. 2.1.

The structural diagram for the missile should be selected after the careful analysis of the tactical-technical requirements for the missile.

Most frequently, in the planning stage, a normal diagram (Fig. 2.1a) is selected. However, this diagram in no way can be regarded

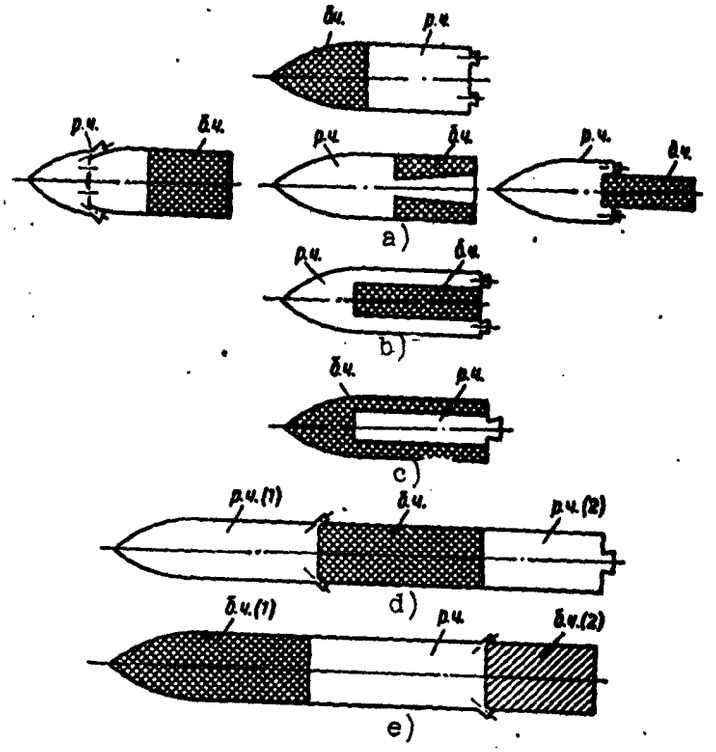

Fig. 2.1. Possible structural diagrams for the assembly of a solid-propellant rocket missile.
р.ч = r.ch. = rocket part
б.ч = b.ch. = warhead.

as optimum for missiles of various designations. Apparently, it is only for armor- and concrete-piercing missiles that this normal diagram is the only one possible. As a matter of fact, fragmentation missiles with a contact fuse will exhibit greater effectiveness if they are executed in accordance with a completely opposite diagram (Fig. 2.1b). Indeed, it is precisely in this case that the maximum number of warhead fragments will be scattered against the obstacle at the instant that the explosive charge is set off as the missile strikes the obstacle, whereas in the case of the normal diagram a substantial number of the fragments would move into the ground directly at the point of missile impact. When noncontact fuses are employed, the structural diagram which assumes an internal position of the warhead (Fig. 2.1c) is extremely effective in the case of a

fragmentation missile. In this case, the total number of fragments increases substantially because both the warhead and the combustion chamber are blown apart on detonation.

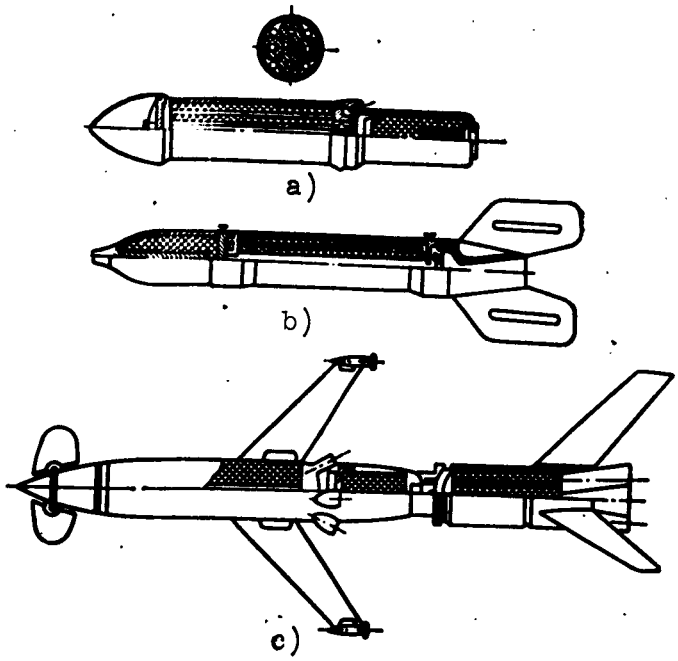

Fig. 2.2. Examples of the utilization of various structural diagrams in the design of actual missiles shapes. a) inverse diagram (158.5-mm German turbojet missile); b) normal diagram (82-mm German finned missile); c) diagram of intermediate warhead position (German guided antiaircraft rocket "Rheintochter").

The structural diagram of an internal rocket portion (Fig. 2.1d) as well as the diagram of an intermediate rocket-portion position (Fig. 2.1f), may be recommended for powerful demolition missiles. Moreover, the structural diagram of the internal positioning of the rocket missile is efficient even when it is necessary to decrease the over-all length of the missile from the standpoint, for example, of missile flight stability or for any other reasons. The structural diagram of intermediate warhead positioning (Fig. 2.1e) is particularly promising for the design of high-speed and superlong-range missiles; in this case, it is sometimes sensible to provide for separation

(jettisoning) as the afterburner (rear combustion chamber) is put into operation.

Effective demolition-fragmentation missiles can be designed on the basis of a structural diagram involving the intermediate positioning of the rocket portion, if the forward warhead of such a missile is of the demolition or fragmentation-demolition type, and the rear warhead is of the fragmentation type.

Examples of specific designs, developed with the use of various diagrams for the interrelated positioning of warhead and rocket parts are presented in Fig. 2.2.

It is important to underscore once again that the selection of the structural diagram is an extremely important and responsible stage of missile planning, a stage that frequently offers tremendous hidden possibilities of increasing the effectiveness of the weapon being developed as well as improving other parameters of the shape of missiles in question. Sometimes, the possibility of satisfying the tactical-technical requirements depends on the very selection of the structural diagram for the upcoming missile.

As justification for the selected diagram, it becomes necessary to evaluate the advantages and shortcomings of this structural diagram from the standpoint of satisfying the tactical-technical requirements.

All other conditions being equal, a good guide to follow is the selection of the simplest possible structural diagram and to select a more complicated diagram only if convincing proof is at hand to justify the need for such a selection.

§ 3. TENTATIVE SELECTION OF BASIC CALCULATION PARAMETERS FOR THE MISSILE BEING PLANNED

The initial parameters for all theoretical calculations carried

out during the design stage for a solid-propellant rocket missile are the following:

a) the weight parameters of the missile:

P_* is the weight of the explosive charge;

P_0 is the total weight of the fully armed missile;

ω is the weight of the solid-propellant charge;

q_k is the weight of the engine;

q_p is the passive weight of the missile (the missile weight when all of the solid propellant has been consumed);

b) geometric characteristics of the missile:

$\underline{d}$ is the caliber;

$\underline{l}$ is the total length;

$2L_{op}$ is the tail-unit span;

c) basic trajectory parameters of missile flight:

X_{max} is the maximum firing range;

H_{max} is maximum altitude of missile ascent during flight (on the trajectory);

v_{max} is the velocity of the missile at the end of the active phase of the trajectory;

$B_{d(b)}/X_{max}$ is the characteristic of missile firing accuracy;

d) working characteristics and basic parameters of the interior ballistics of the rocket engine:

$p = p(t)$ is the change in pressure within the combustion chamber as a function of time (the pressure curve);

$\pm t^o$ is the temperature interval of engine operation;

τ is the time of engine operation;

p_{max} is the maximum pressure within the combustion chamber.

Some of the enumerated characteristics are presented in tactical-technical requirements (X, P_0, P_*, $p = p(t)$, τ, etc.); of these,

those that are not defined in the requirements, must be tentatively selected at the beginning of the planning stage.

The calculated (theoretical) parameters for the preliminary tentative assembly of the future end product are selected on the basis of experience gained in design and theoretical projects as well as on the basis of the existing requirements.

Calculation of weight characteristics for the missile. As a rule, the tactical-technical requirements with respect to the combat effectiveness at the target on the part of the missile being planned either give or make it possible to define uniquely the weight of the missile warhead explosive charge (the weight of the missile payload). Therefore the quantity P_* can always be regarded as known.

Having P_* and knowing the combat designation of the missile (the type of warhead), we can tentatively estimate the total weight of the missile warhead. Here we use statistical data on the so-called fill factor η by which we mean the ratio between the weight of the warhead payload and the total warhead weight:

$$\eta = \frac{P_*}{P_0^{b.ch}} 100\%. \qquad (2.1)$$

where $P_0^{b.ch}$ is the weight of the armed warhead.

The characteristic values of the fill factor η for missiles of various designations are as follows:

55%, for demolition missiles (M31, USSR);

15%, for fragmentation missiles ("Luftfaust," Germany);

25%, for fragmentation-demolition missiles (M13, USSR).

The tentative value of the total weight of the missile warhead is determined by η in the following form:

$$P_0^{b.ch} = \frac{P_*}{\eta^{\%}} 100. \qquad (2.2)$$

If the caliber d of the missile being designed is indicated in

tactical-technical requirements, we can use the statistical coefficient k_s of relative missile weight and the coefficient k_* of relative payload weight for a tentative determination of the weight characteristics of the warhead in the missile being designed.

The above-mentioned coefficients are determined by the following relationships:

$$k_c = \frac{P_0^{b.ch}}{d^3} \text{ kg/dm}^3, \tag{2.3}$$

$$k_* = \frac{P_*}{d^3} \text{ kg/dm}^3. \tag{2.4}$$

The values of the coefficients k_s for missiles with various combat designations are approximately the following:

2, for demolition missiles (300-mm missile, Germany);

6, for fragmentation missiles (M8, USSR);

8, for fragmentation-demolition missiles (M13, USSR).

Accordingly, the values of k_* are equal to:

3, for demolition missiles (300-mm missile, Germany);

1, for fragmentation missiles (M8, USSR);

2, for fragmentation-demolition missiles (M13, USSR).

The total weight of the rocket missile is comprised of the weight $P_0^{b.ch}$ of the warhead, the weight q_k of the rocket engine, and the weight ω of the solid-propellant charge. If the magnitude of the total weight P_0 is given in the tactical-technical requirements, the remaining combat characteristics can be determined comparatively simply.

In fact, expanding the right-hand part of Tsiolkovskiy's formula in series, we will have for the maximum velocity of the rocket

$$v_{max} = U_e \ln\left(1 + \frac{\omega}{q_k}\right)$$

and keeping only the first-degree terms in the expansion, it is easy to obtain the following approximate relationship:

$$v_{max} \approx U_e \frac{2\omega}{2q_p + \omega}. \qquad (2.5)$$

From (2.5) the quantity ω is defined as

$$\omega = q_p \frac{2v_{max}}{2U_e - v_{max}} \qquad (2.6)$$

or, taking into consideration that $q_p = P_0 - \omega$,

$$\omega = P_0 \frac{2v_{max}}{2U_e + v_{max}}. \qquad (2.6')$$

The quantity ω, found from Relationship (2.6) or (2.6'), represents the weight of the solid-propellant charge required to impart a velocity v_{max} to a rocket having a launching weight of P_0 and a passive weight q_p (under the condition that the exhaust velocity for the products of combustion amounts to U_e).

The quantity v_{max} which must be known in order to use Relationship (2.6) or (2.6') in specific calculations, is estimated approximately on the basis of the given firing range. In this case, it is possible to use either ballistic tables or the tentative formulas derived in Chapter 6. With respect to U_e it has been demonstrated that

$$U_e = j_1 g \text{ m/sec},$$

where j_1 is the specific impulse of the engine; g is the acceleration of gravity, and since for the majority of solid-propellant rocket engines the quantity j_1 is sufficiently stable and amounts, on the average, to $j_1 \approx 200$ kg·sec/kg,* we can assume in approximate terms that

$$U_e = 1950\text{—}2000 \text{ m/sec}.$$

Thus it becomes possible to determine with sufficient accuracy one of the most important weight characteristics of a rocket missile — the weight of the solid-propellant charge of the engine. After this, the passive weight of the missile will be

$$q_p = P_0 - \omega, \qquad (2.7)$$

and since the passive weight is composed of the weight of the armed warhead and the structural weight of the engine, the quantity q_k is determined by the difference

$$q_к = q_п - P_0^{б.ч}. \qquad (2.8)$$

It is more complicated to estimate the weight characteristics of the missile, if the quantity P_0 is not indicated in the tactical-technical requirements. In this case, the following calculation method may be employed.

It has been established that for almost all types of rocket missiles used in the field artillery, the weight of the metal which goes into the combustion chamber can be determined in terms of the weight of the metal used in the warhead by means of a certain proportionality function Φ which represents the product of special coefficients:

$$\Phi = k_{т.с} k_d k_p \ldots,$$

where $k_{t.s}$ is the coefficient of the type of missile warhead; k_d is the coefficient of missile caliber; k_p is the coefficient by which we take into consideration the effect on q_k of the magnitude of pressure in the combustion chamber (at d = const); .....

.....

.....

Thus, in this case,

$$q_к \approx \Phi (P_0^{б.ч} - P_ф) = k_{т.с} k_d k_p \ldots (P_0^{б.ч} - P_ф), \qquad (2.9)$$

where for demolition missiles of medium caliber with pressure in the combustion chamber not exceeding p = 100 kg/cm^2 (of the 300-mm type demolition missile, Germany) we can assume

$$q_к \approx (2{,}0 \div 2{,}1)(P_0^{б.ч} - P_ф),$$

while for fragmentation missiles (of the M8 type, USSR)

$$q_к = (1{,}8 \div 1{,}9)(P_0^{б.ч} - P_ф).$$

After the determination of q_k, the remaining unknown weight characteristics can be found without difficulty. In fact, according to (2.8)

$$q_n = q_n + P_0^{k-1},$$

after which, in accordance with (2.6), it is easy to calculate ω and to find the total weight of the missile:

$$P_0 = q_n + \omega.$$

The tentative relationships that have been presented here make it possible to estimate the theoretical weight characteristics of the missile with sufficient accuracy; these characteristics must be known in order to design each specific end product.

The selection of the basic weight characteristics is of great significance not only for the direct planning of the rocket missile, but for the issuance of preliminary requirements with respect to the design of the launching installation and other auxiliary ground equipment.

The determination of geometric missile characteristics. Of the geometric characteristics, as a rule, the caliber of the missile is indicated in the tactical-technical requirements, at least for missiles of the "air-to-air" classification, as well as for anti-tank and certain other missiles. If the caliber is not given in the tactical-technical requirements, a tentative magnitude of caliber can be estimated on the basis of the statistical coefficients k_s or k_*. The following may be regarded as a calculation formula for the determination of the magnitude of d:

$$d = \sqrt[3]{\frac{P_0^{k-1}}{k_s}\left(\text{or } \frac{P_0}{k_*}\right)} \text{ dm}. \qquad (2.10)$$

The second basic geometric characteristic of a rocket missile is the total length of the rocket missile and this can be determined conclusively only by consideration of the conditions of mis-

sile stability during flight, i.e., in fact only after the model has passed its windtunnel tests and after the test firing of control prototypes. However, we can bear in mind, even during the preliminary calculations, that for missiles stabilized by fins, the optimum length is approximately

$$\underline{l} = (8\text{-}10)\ d\ (\text{to } 15d) \qquad (2.11)$$

(M8, M13, M13DD, USSR),

whereas for turbojet missiles

$$\underline{l} = (4\text{-}6)\ d\ (\text{to } 10\ d) \qquad (2.11')$$

(300- and 210-mm missiles, Germany).

The span $2L_{op}$ of the stabilization fins of a rocket missile are determined by the aerodynamic characteristics of the object, as well as by the in-plan view of the shape and the number of fins in the stabilizer. There is, apparently, no point in enumerating all of the special cases which might occur in the determination of the dimension $2L_{op}$, and we need only point out that for the most frequently employed four-finned tail unit (in the shape of a blade in the in-plan view) that is almost rectangular, the dimension $2L_{op}$ generally does not exceed

$$(2L_{on})_{max} = 3d.$$

The parameters of flight trajectory. The most important flight-trajectory parameters may be regarded as maximum firing range and missile firing accuracy. Both of these characteristics are given in the tactical-technical requirements for the design of the object. The remaining parameters can be estimated with comparative ease on the basis of the simplified theory of missile flight along a trajectory (see Chapter 6).

The working characteristics and the basic parameters of interior ballistics of rocket engines. The sequence of selecting the basic

rocket-engine parameters and the working characteristics of a rocket engine are examined in detail in Chapter 4.

After the selection of the basic parameters of the missile being designed, we undertake the working out of the various missile design versions and the detailed calculation of the interior ballistics of the engine as well as the flight characteristics of the missile. During the process of this work, the parameters that were initially assumed are refined and corrected.

§ 4. THE PLANNING PROCEDURE FOR A FIELD-ARTILLERY ROCKET MISSILE AND ITS INDIVIDUAL ELEMENTS

The initial design of a field-artillery rocket missile is presented in Fig. 2.3.

In accordance with the construction of a solid-propellant rocket missile, the planning stage includes:

1) the designing of the missile elements:

– the warhead;

– the combustion chamber;

– the nozzle unit;

– the stabilization systems, the spacers, and other auxiliary elements of the structure;

2) the design of the solid-propellant charge of the engine:

– the selection of the type of working charge and its insertion into the combustion chamber;

– the design of the igniter.

The design of each of the missile elements can be reduced to a series of successive calculations and the seeking of the most promising design solutions. In this case, the approximate sequence of the planning of individual missile elements can be carried out in accordance with the following procedures.

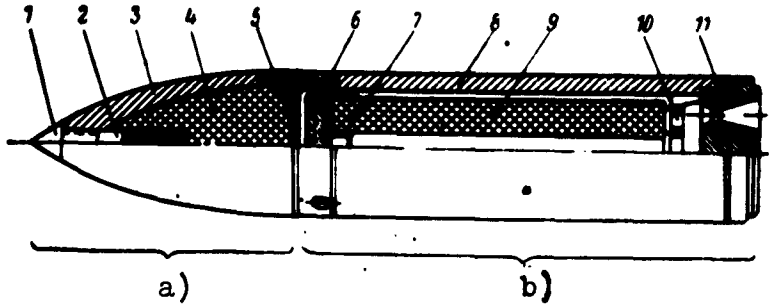

Fig. 2.3. Basic design of a contemporary solid-propellant field-artillery rocket missile. a) Warhear; b) rocket; 1) fuse; 2) auxiliary detonator; 3) warhead frame; 4) bursting charge; 5) spacer; 6) igniter, with electroigniter system; 7) forward grid (trap), for retention of igniter and grain (charge); 8) body of combustion chamber; 9) solid-propellant working charge of engine; 10) diaphragm; 11) nozzle assembly.

The procedure for the planning and design of the warhead:

1) selection of the warhead type in accordance with missile designation;

2) selection of warhead shape, and justification for this selection;

3) calculation of thickness of head wall, based on the standpoint of providing strength on impact against obstacle (demolition warheads) or on other considerations (for example, for fragmentation missiles, the obtaining of a definite number of fragments of given weight, etc.);

4) the development of a production process for the fabrication of the warhead frame, geared to mass production;

5) the selection of the type of fuse and the working out of the tactical-technical requirements for the design of this item.

The procedure for the planning and design of the combustion chamber:

1) the selection of the combustion-chamber design;

2) the calculation of the wall thickness which will guarantee

engine durability at the working pressure and gas temperature within the combustion chamber;

3) an analysis of the possibilities of reducing the thickness of the combustion-chamber wall by employing thermal insulation or other special measures;

4) the selection of the system to be employed to connect the warhead and rocket parts of the missile, and the type of connection device to be employed;

5) strength calculations for the connection unit;

6) the development of a production process for the fabrication of the engine frame, with an eye to conditions required from the standpoint of mass production.

The procedure for the planning and design of the nozzle assembly:

1) calculation of basic nozzle dimensions in order to ensure the required ballistic characteristics of the engine;

2) the selection of the type of nozzle assembly (a single nozzle or a nozzle cover with several nozzles) and the justification for this selection;

3) geometrical planning of the nozzle cover for the missile and the selection of the type of connection to be used to link this cover with the combustion chamber;

4) strength calculations for the connection unit;

5) selection of the grid (trap) and the matching of its configuration with the selected grain (charge) and the nozzle cover;

6) thermal calculations for the elements of the nozzle assembly;

7) the working out of production techniques for the nozzle cover, geared to conditions of mass production.

The procedure for the planning and design of a missile stabilization system:

1) the selection of the type of stabilization system (finning, rotation, combined stabilization). An analysis and justification for the selection made;

2) calculation of stabilizer dimensions for the case of stabilization by means of finning;

3) calculation of the flare angle of the nozzle for turbojet missiles;

4) correction of stabilization elements on the basis of results obtained in windtunnel tests and test firings;

5) working out of production problems with respect to the stabilization elements of the missile;

6) estimate of anticipated firing-accuracy parameters for the missile being designed.

The procedure for the planning and design of the spacers and other auxiliary elements in the design:

1) the selection and justification for the type of connection unit (demountable, nondemountable, threaded, welded):

2) the selection of the structural diagram for the connection and shape of the component parts;

3) strength calculations for the component parts and the entire unit from the standpoint of hermetic sealing, rigidity, permenance of joints;

4) working out of production problems with respect to individual components and the assembly of the entire unit.

In the design of the solid-propellant grain (charge) of the engine, the selection and calculation of the igniter for the class of engines under consideration presents no particular difficulties and can be reduced to the selection of weighted portions of black powder which is used to bring the basic charge to a regime of stable com-

bustion. With respect to the design of the basic charge, however, it should be pointed out that this problem is extremely complex and is, in essence, basic to the design of the engine. The sequence of work to be carried out in the design of the working propellant charge can be as follows.

The procedure for the planning and design of the solid-propellant working charge is as follows:

1) the selection of the brand of powder (or other solid propellant), taking into consideration the basic tactical-technical requirement imposed on the parameters of interior ballistics and the operating conditions for the missile.

An analysis of the raw materials available for the selected composition of the solid propellant from the standpoint of fabricating it in great quantities under unfavorable conditions;

2) the selection of the working pressure in the combustion chamber, from the standpoint of providing the required thrust parameters and for stable solid-propellant combustion within a given interval of initial temperatures;

3) calculations of the parameters of interior engine ballistics (calculation of grain combustion);

4) the geometric design of the charge and the justification of the adopted grain shape;

5) the insertion of the grain into the combustion chamber;

6) correction of engine and charge in accordance with results of combustion and ignition tests on test engines.

In the designing of specific grain specimens, the sequence of solving individual design problems and the scope of the work being done can differ in individual cases (particularly, in the case of designing special grain shapes) from those cited in the procedures

above. Therefore, a creative approach is required for the above-mentioned procedures, and each should be adapted to agree with a specific missile design and the contents of the tactical-technical requirements for this missile.

[Footnotes]

Manuscript Page No.

27 A.S. Lokk, Upravleniye snaryadami [Missile Control], IL [Foreign Literature Press], 1958. G. Merill, G. Gol'dberg, R. Gel'mgol'ts [sic]. Issledovaniye operatsiy. Boyevyye chasti. Pusk snaryadov [Investigation of Operations. Combat Units. Missile Launchings], IL, 1959. E.A. Bonni, M.Dzh. Zakrou, K.U. Besserer. Aerodinamika. Reaktivnyye dvigateli. Praktika konstruirovaniya i rascheta, Fizmatgiz [Aerodynamics. Jet Engines. Construction Design Practice. Physics and Mathematics Press], 1960.

41 V.I. Feodos'yev and G.B. Sinyarev. Vvedeniye v raketenuyu tekhniku. Oborongiz [Introduction into Rocket Engineering. State Defense Industry Press], 1956.

[List of Transliterated Symbols]

30 $D_в = D_v = D_{voronka} = D_{funnel}$

30 $n_ф = n_f = n_{forma\ (voronki)} = n_{shape\ (of\ funnel)}$

32 $\eta_д = \eta_d = \eta_{dal'nost'} = \eta_{range}$

32 $\eta_б = \eta_b = \eta_{bokovoye\ (napravleniye)} = \eta_{lateral\ (direction)}$

38 $q_к = q_k = q_{konstruktsiya\ (dvigatelya)} = q_{engine}$

38 $q_п = q_p = q_{passivnyy} = q_{passive}$

38 $L_{оп} = L_{op} = L_{opereniye} = L_{tail\text{-}unit}$

39 $P^{б.ч} = P^{b.ch} = P^{boyevaya\ chast'} = P$ warhead

40 $k_c = k_s = k_{snaryad} = k_{missile}$

42 $k_{т.с} = k_{t.s} = k_{tip\ snaryada} = k_{type\ of\ missile}$

Chapter 3

DESIGN OF MISSILE WARHEAD

§ 1. DEMOLITION WARHEAD

Basic Design Characteristics of a Demolition Warhead

Demolition missiles belong to the class of basic-designation missiles and are intended for the destruction of various defensive structures.

The parameters of the combat effectiveness of a demolition missile are totally determined by the characteristics of the explosive employed, the weight of the explosive charge, and by certain structural elements of the warhead body.

It is the general practice to regard the basic missile force requirement as the disposition of the maximum quantity of effective explosive within the body of the warhead, so that it is possible to raise the force of the demolition warhead by using a more powerful explosive or by increasing the capacity of the explosive chamber.

The first method is, for all intents and purposes, a rather limited means of increasing effectiveness, since, first of all, the power of the explosive, i.e., the reserve of internal explosive energy liberated on detonation has a certain maximum and, secondly, with increased power the sensitivity of the explosive to external disturbances also increases, i.e., missile safety is affected (reduced), in operational handling.

The capacity of the warhead charge chamber can be increased – given a constant missile caliber – by reducing the thickness of the walls or increasing the length of the warhead. In this case, the minimum wall thickness must be such that the missile preserves structural strength on impact against an obstacle, and the maximum length is limited by the requirement of a compact demolition explosion and the considerations that are associated with the conditions of missile stability in flight (on the trajectory).

The basic structural characteristic of a demolition warhead, indicating the relative magnitude of the explosive weight content, is the missile warhead fill factor

$$\eta = \frac{P_*}{P_0^{b.ch}} 100\%,$$

which amounts to 50-60% for the most effective grains.

Other important structural characteristics of a demolition warhead are the following:

1) the relative wall thickness of the warhead frame (body)

$$\bar{\delta}_{st} \approx (8/300)\ d \text{ (M31, USSR)};$$

2) the relative warhead length

$$\bar{l}_{b.ch} \approx 1.5\ d \text{ (M31, USSR)};$$

3) the coefficients k_s and k_* of relative weight, whose numerical values are presented in Chapter 2, are the following:

$$k_s = P_0^{b.ch}/d^3 \text{ kg/dm}^3,$$

$$k_* = P_*/d^3 \text{ kg/dm}^3.$$

The above enumerated structural characteristics of the warhead are extremely important, since the average statistical values of these characteristics can be used successfully for tentative rough calculations in the pre-sketch design stage.

Of course, it should be borne in mind that the warhead parameters selected by means of these structural characteristics must

necessarily be refined during the subsequent stages of work on the missile.

Selection of Shape of Warhead Frame (Body)

The shape of the frame of a demolition warhead is selected on the basis of making provision for the optimum conditions of explosion development on the detonation of the grain against a given obstacle, as stipulated in the tactical-technical requirements. Moreover, in the selection of shape we must take into consideration the production-engineering requirements, and for standard missiles we must also consider the requirement of minimum aerodynamic warhead drag during flight.

The action of the demolition missile at the target is composed of two moments: the penetration of the grain (charge) into the obstacle and the detonation of the grain within the obstacle at a certain set depth. Consequently, the selected shape must provide primarily for ease of warhead penetration into the obstacle, on the one hand, and for maximum explosion shock-wave parameters, on the other hand.

Design practice and the utilization of demolition missiles has demonstrated that from the standpoint of facilitating missile penetration into a free-flowing obstacle such as conventional soils, the most suitable shape is a cone having an angle at the apex of the order of

$$2\beta_{b.ch} = 18\text{-}20^{\circ} \text{ (It may be } \sim 30^{\circ}).$$

A warhead with an ogive curve generatrix is somewhat worse in this respect.

From the standpoint of the maximum effect of the demolition explosion shock wave at the target, the most desirable warhead shape is that of a sphere, a short cylinder, or the like. These

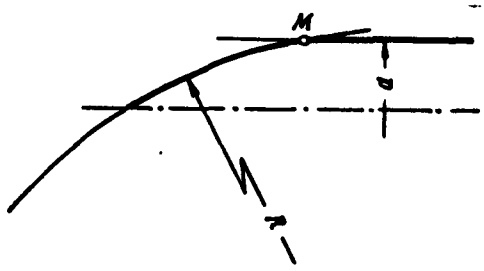

Fig. 3.1. Shape of warhead, resulting in minimum aerodynamic resistance (drag). R) ogive curve radius; d) cylinder diameter; M) point of intersection between cylindrical part and ogive curve.

shapes produce a high fill factor and allow for compact loading of explosives into the warhead chamber, thus making it possible to attain the highest parameters of demolition-explosion effectiveness. The warhead shapes that are optimum from the standpoint of effectiveness exhibit the shortcoming of difficulty in assembly, i.e., for missiles in which the warhead is situated at the front.

The minimum aerodynamic resistance (drag) is offered by a warhead shape which is comprised of an ogive curve and a cylinder, connected without exact merging of the edges (Fig. 3.1). A shape of this type makes it possible to reduce the coefficient of frontal missile-warhead resistance $C_{x\ b.ch}$ by 15 to 20% in comparison with even a shape exhibiting maximum generatrix contact, which at first seems to be more streamlined. However, a shape of this type does not lend itself to production and is virtually never employed in actual designs. The use of this shape on a tentative basis makes sense only in the design of turbojet missiles where

$$C_{x\ sn} \approx C_{x\ b.ch},$$

where $C_{x\ sn}$ is the coefficient of missile frontal resistance, whereas for finned missiles the basic portion of $C_{x\ sn}$ is composed of the resistance of the tail assembly (50-70%) and, consequently, the effect of warhead shape will be insignificant on the total $C_{x\ sn}$.

Thus if a cone is the best shape from the standpoint of obstacle penetrability, completely different shapes are optimum for purposes

of achieving maximum effectiveness of demolition at the target as well as from the standpoint of aerodynamics. As a result, the selection of shape in each specific design case can be reduced to the solution of the problem of determining the group of requirements whose fulfillment should receive preference. This solution must be based on an analysis of the tactical-technical requirements for the missile, taking into consideration the adopted structural diagram of the missile, which determines its over-all assembly.

Calculation of the Wall Thickness of the Demolition-Warhead Frame, on the Basis of Strength Conditions on Impact Against an Obstacle

Since a demolition missile is, as a rule, designed with the maximum possible fill factor, the body of the missile warhead in this case is a comparatively thin-walled structure. Naturally, the strength of this structure must be sufficient to withstand all possible external loads during the fabrication process, during storage, in transportation, and in the combat utilization of the missile; it is for this reason that the maximum warhead wall thickness is based on conditions of strength.

In an analysis of all possible external loads, it is easy to establish that the greatest loads are those which act on the missile at the instant that it strikes the obstacle. It is precisely this instant at which the missile strikes the obstacle that is taken as the calculation base for the determination of minimum permissible wall thickness. It should be borne in mind that the strength of the body must be adequate to withstand not only the initial instant of impact against the obstacle, but it must remain intact until the detonation of the explosive charge, since only in this case will the conditions for the complete utilization of the explosive charge at the target prevail, i.e., only in this case will maxi-

mum explosion effectiveness be achieved.

Selection of Critical Cross Section

Let us examine a missile at some arbitrary instant of missile penetration into an obstacle (Fig. 3.2). Neglecting the possible angle of attack α of the missile on the last segment of the trajectory, we will assume that the impact of the missile against the obstacle is normal; moreover, we will assume the impact to be symmetrical, which for angles of incidence close to the usual (40-50°), results in no basic errors in subsequent calculations, but substantially simplifies the computations.

We know that the internal stresses in the component parts and units of individual structures are produced by external forces and moments acting on these component parts. Therefore, before we consider the stresses acting on the wall of the warhead body, let us examine the external loads which result in these stresses. In the case of a direct strike, the external loads pertain only to forces, and here in accordance with Fig. 3.3, these forces for the part of the warhead body indicated by some arbitrary equatorial cross section MM are the following:

– the force of obstacle resistance to penetration, distributed over the part of the warhead frame penetrating the obstacle at the instant of time t and resulting in the appearance of a distributed load p_n on the outer surface of the body;

– the initial weight of the metal above the cross section MM, $p'_m n$, where n is the overload factor; P'_m is the weight of the above-mentioned metal, defined as the sum

$$P'_м = P'_{б.ч} + P_{дн} + P_{к.с} + P_{ст} + \ldots$$

$P'_{b.ch}$ is the weight of that part of the warhead frame above the cross section MM; P_{dn} is the weight of the bottom plate; $P_{k.s}$ is the

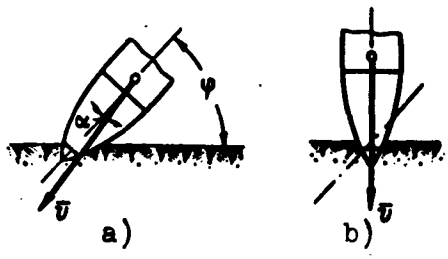

Fig. 3.2. Missile impact against an obstacle. a) actual diagram of impact; b) theoretical (calculation) diagram of impact; φ) angle of incidence; $\bar{v}$) velocity at instant of impact.

weight of the combustion chamber;

P_{st} is the weight of the stabilizer;

.....

– the pressure (pn) due to the equipment, acting on the inner wall of the warhead cavity.

As a result of the action of these loads, two basic types of stresses are developed: longitudinal compressive stresses $\sigma_z \approx f(P'_m n)$ and circumferential stresses $\sigma_\theta = f(pn)$.

If we assume that the weight characteristics of the missile are fully known, then in order to find the magnitudes of the active stresses we must also know:

– the magnitude and nature of change in overload with depth of penetration;

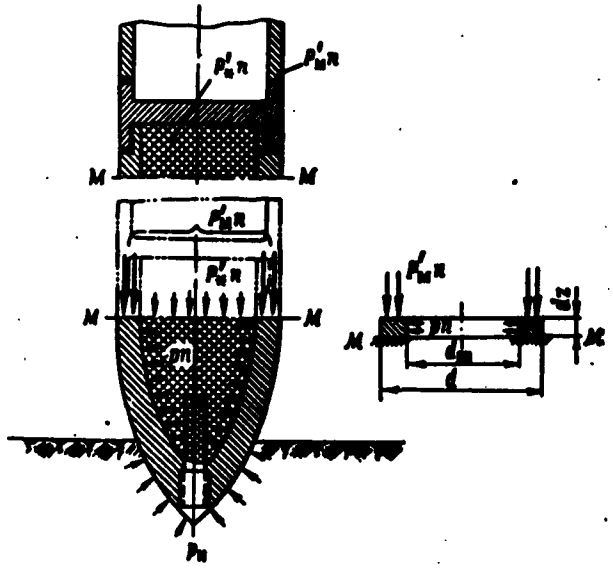

Fig. 3.3. Diagram of forces acting on the warhead in the case of missile impact against an obstacle.

– the counteraction of the obstacle to missile penetration.

It has been established experimentally that the magnitude of overload is a function of penetration depth; here, at the instant

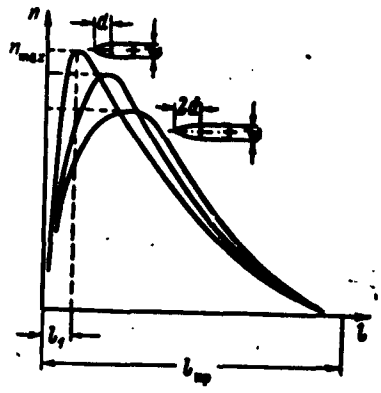

Fig. 3.4. Nature of change in overload n as a function of missile penetration into obstacle, for various warhead shapes. l_1) depth of penetration, corresponding to maximum overload; l_{pr}) total depth of penetration.

that the missile has penetrated approximately to a depth equal to the length of the ogive curve, the overload attains n_{max}. Along the remainder of the penetration course, the overload gradually diminishes to zero (Fig. 3.4). With respect to the countereffect of the obstacle, however, it can be taken into consideration in first approximation if it is assumed that the pressure due to the equipment remains constant in those sections of the warhead that have penetrated into the obstacle.

If we take all of the above into consideration, we can present the diagrams of active forces for various instants of time in the form of the curves shown in Fig. 3.5. By examining the curves we can satisfy ourselves that the "dangerous" [critical] cross section, i.e., loosely speaking, the cross section in which the greatest forces act, shifts with respect to the penetration of the grain (charge) into the obstacle, from the nose to the cylindrical part of the missile. However, a comparison of the absolute values of the forces acting at various instants of time (t_1, t_2, ...), will reveal that the true critical cross section AA should be sought at the instant of time t_3 at which the greatest inertial overload is acting on the missile, i.e., at the instant of time at which the active forces are at their maximum. In formal terms, the critical section in this case may be assumed to be any equatorial cross section. However, if we take into consideration the geometrical

features of the warhead and the fact that the deformations of the cross sections within the obstacle are limited by the counteraction of the very medium receiving a part of the load, it should be assumed that the actual critical cross section AA will be situated approximately at the point at which the ogive curve of the missile makes the transition to the cylindrical part of the missile, somewhat above the theoretical point of contact between the ogive curve and the cylinder.

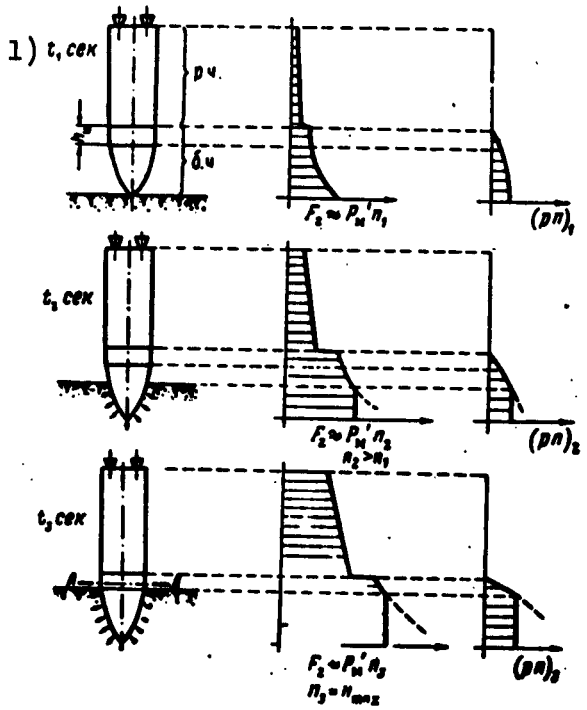

Fig. 3.5. Diagrams characterizing change in longitudinal force and pressure due to equipment, as functions of missile penetration into obstacle. n_1, n_2, and n_3) the overloads which correspond to the instants of time t_1, t_2, and t_3; 1) t, sec.

The cited justification for the selection of cross section AA as the critical cross section is not rigorous and is based primarily on intuitive concepts regarding the physics of this phenomenon; however, the final conclusion cannot be subject to any doubt and can be confirmed theoretically at any time by means of rather rigorous relationships.

Derivation of Tentative Formulas for Calculation of Stresses in the Critical Cross Section

In actual practice, it is expedient to isolate and examine separately two calculation cases: the case in which the stresses produced by the action of the forces of the inertial weight of the metal above the cross section AA are determining factors in warhead body strength, or the case in which

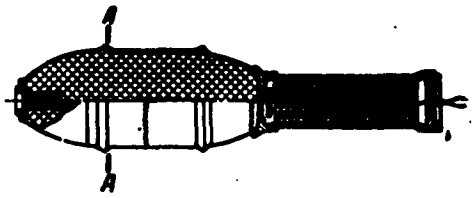

Fig. 3.6. A missile in whose warhead body the stresses due to the internal pressure of the equipment are critical (dangerous).

these stresses are the stresses from (pn).

The first case is found, for example, in long-range missiles of normal configuration and with a relatively low fill factor; the second case is found with a missile of the type shown in Fig. 3.6.

In the first case, a rather rigid cylindrical shell, compressed by a longitudinal force $P'_m n_{max}$, may be taken as the calculation diagram. For such a shell

$$\sigma_s = \frac{P'_m n_{max}}{\frac{\pi}{4}(d^2 - d_{vn}^2)} \qquad (3.1)$$

and the condition of strength will be

$$\frac{P'_m n_{max} \zeta}{\frac{\pi}{4}(d^2 - d_{vn}^2)} = \frac{\sigma_{szh}}{\zeta}, \qquad (3.2)$$

where $P'_m n_{max}$ is the inertial weight of the metal above the critical cross section; n_{max} is the maximum overload; d is the caliber of the warhead; d_{vn} is the diameter of the inner warhead cavity; σ_{szh} is the ultimate compressive strength of the material; ζ is the safety factor.

From (3.2) we can derive the relationship for an estimate of the limit wall thickness δ_{min}, for which it is sufficient to use the obvious relationship

$$d_{vn} = d - 2\delta,$$

by means of which it is easy to rearrange (3.2) to take the following form:

$$\frac{4P'_m n_{max} \zeta}{\pi \sigma_{szh}} = d^2 - (d - 2\delta)^2 = 2d\delta - 4\delta^2.$$

This expression is a quadratic equation for the sought δ:

$$\delta^2 - \frac{d}{2}\delta + \frac{P'_M n_{max} \zeta}{\pi \sigma_{cm}} = 0,$$

formally yielding two solutions

$$\delta_{1,2} = \frac{d}{2} \pm \sqrt{\frac{d^2}{4} - \frac{P'_M n_{max} \zeta}{\pi \sigma_{cm}}},$$

but which in essence uniquely defines the sought magnitude of the minimum permissible wall thickness

$$\delta_{min} = \frac{d}{2} - \sqrt{\frac{d^2}{4} - \frac{P'_M n_{max} \zeta}{\pi \sigma_{cm}}}. \qquad (3.3)$$

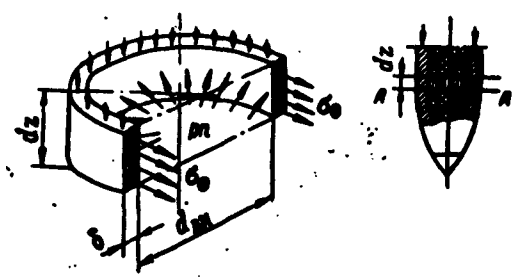

Fig. 3.7. For the determination of stresses due to pressure (pn).

The calculations that have been presented are quite tentative and make it possible to evaluate the magnitude of δ_{min} only in approximate terms.

In the second case, the calculation diagram is that of a thin-walled vessel under the action of internal pressure (pn). Under this pressure, circumferential stresses σ_θ are developed in the wall, and these are determined in accordance with Fig. 3.7 by the following relationship

$$\sigma_\theta = \frac{(pn) d_{sr} dz}{2\delta dz} = \frac{(pn) d_{sr}}{2\delta}. \qquad (3.4)$$

The condition of preservation of structural strength

$$\sigma_\theta = \frac{1}{\zeta} \sigma_b,$$

where σ_b is the ultimate strength, makes it possible to define the minimum wall thickness which will guarantee body strength with a safety factor ζ as

$$\delta_{min} = \frac{(pn) d_{sr}}{2 \frac{1}{\zeta} \sigma_b} \qquad (3.5)$$

or in terms of missile caliber

$$\delta_{min} = \frac{(pn)d}{2\left[(pn)+\frac{1}{\zeta}\sigma_b\right]}. \qquad (3.5')$$

In the more general case, it is not immediately clear which of the loads – the "pressing" weight of the metal or the pressure due to the equipment – may be the factor responsible for missile destruction. Here we must analyze the complex stressed state with active stresses, determined by the following relationships:

$$\left.\begin{aligned} \sigma_z &= \frac{P'_M n_{max}}{\frac{\pi}{4}(d^2-d_{in}^2)}, \\ \sigma_\theta &= \frac{(pn)d_{in}}{2\delta}, \\ \sigma_r^{max} &= -(pn), \end{aligned}\right\} \qquad (3.6)$$

where σ_r is the radial stress, and the minimum wall thickness must be determined on the basis of the so-called equivalent stress. However, the requirement which calls for the consideration of all three stresses in the tentative selection of δ_{min} occurs comparatively seldom, so that the problem need not be considered in greater detail.

We can see from Formulas (3.3) and (3.5) that we must know the magnitude of the rated (theoretical) overload for the calculation of δ_{min} and we must be able to calculate the pressure due to the equipment.

With respect to pn, the physical nature of this pressure is such that it represents the lateral component of the axial stress developed in the elastic-plastic column of explosives on missile impact against the obstacle. The magnitude of pn could be calculated as follows:

$$(pn) = -\frac{K_p}{1-\mu}(\sigma_z)_{in} = -\frac{K_p}{1-\mu}\frac{P'_0 n}{\frac{\pi d_{in}^2}{4}}, \qquad (3.7)$$

where $P_*^!$ is the weight of the column of explosives above the cross section under consideration; $P_*^!n$ is the inertial weight of this column of explosives; μ is the Poisson coefficient; K is the coefficient by means of which we take into consideration the dynamics of load applications on impact as well as certain secondary effects of the phenomenon.

However, there are no reliable values for the constant K, and in practical calculations it is impossible to employ Relationship (3.7). At the present time, the practice is to calculate pn by using the semi-empirical calculation relationships of the following type:

$$(pn)=k_1(h_{ts}^!+k_2\Delta h)n. \tag{3.8}$$

where $h_{ts}^!$ is the height of the cylindrical part of the body (frame) above the cross section AA; Δh is the height of the additional noncylindrical volumes in the upper part of the cavity containing the explosives; n is the overload factor; k_1, k_2 are the experimental coefficients.

Calculation of Maximum Overload Acting on Missile on Impact Against Obstacle

The overload is denoted by the number n which indicates the factor by which the mass forces are increased in the case of their dynamic application in comparison with their magnitude under static conditions.

$$n=\frac{P_{\text{дин}}}{P_{\text{ст}}}. \tag{3.9}$$

If we assume that the mass of the body remains constant in the phenomena under consideration, from (3.9) we will obtain

$$n=\frac{a}{g},$$

where a is the acceleration which, in this case, characterizes the

dynamics of force application; g is the acceleration of gravity.

Hence, it is absolutely necessary to know how the missile is decelerated in its penetration into the obstacle for purposes of calculating the overload, i.e., to determine the relationship $a = a(t)$ or at least to be able to calculate the quantity a_{max}.

If we hold that the entire kinetic energy

$$E_к = \frac{m_п v_к^2}{2} = \frac{q_п v_к^2}{2g},$$

where $m_p = q_p/g$, which the missile possesses at the instant of impact against the obstacle, is expended only on overcoming the resistance of the medium being penetrated, the energy balance can be determined in the following form

$$\frac{m_п v_к^2}{2} = A_{сопр},$$

where A_{sopr} is the total work of the forces of obstacle resistance.

We can assume in tentative calculations that the resistance force changes linearly from some R_{max} to zero as the missile penetrates deeper into the obstacle, so that

$$A_{сопр} = \frac{1}{2} R_{max} l_{пр} = \frac{1}{2} m_п a_{max} l_{пр}.$$

Now we will have

$$\frac{m_п v_к^2}{2} = \frac{1}{2} m_п a_{max} l_{пр}$$

or

$$a_{max} = \frac{v_к^2}{l_{пр}}, \tag{3.10}$$

after which n_{max} is defined as

$$n_{max} = \frac{v_к^2}{g l_{пр}}, \tag{3.10'}$$

where v_k is the missile velocity at the instant of impact against the obstacle; l_{pr} is the total depth to which the missile could penetrate into the obstacle, if all of the kinetic energy of the

missile were expended on the overcoming of the resistance forces.

The short-term effect of maximum overload produces a calculation factor

$$n_{расч} = \varepsilon_n n_{max}, \tag{3.11}$$

where $\varepsilon_p < 1$ is the coefficient by means of which we take into consideration the impact conditions and certain structural features of the warhead.

With respect to the quantity l_{pr} it should be stated that at the present time there are several empirical formulas which allow us to calculate this characteristic with sufficient accuracy for a preliminary analysis.

Of these formulas, the most widespread are the following.

1. The Berezanskiy formula

$$l_{пр} = \lambda k_п \frac{q_п}{d^2} v_к, \tag{3.12}$$

where l_{pr} is the depth of penetration, in m; q_p is the weight of the missile at the instant of impact against the obstacle (the passive weight of the missile), in kg; d is the caliber of the missile, in m; v_k is the velocity of the missile at the instant of impact, in m/sec; λ is the coefficient of missile shape; λ equals 1.0 for missiles exhibiting an ogive curve having a height of

$$h_{он} < 1{,}5d;$$

λ equals 1.3 for missiles exhibiting an ogive curve having a height of

$$h_{он} \approx 2{,}5d;$$

k_p is the coefficient of penetration whose magnitude is determined by the properties of the obstacle (see Table 3.1).

TABLE 3.1

The Berezanskiy Coefficients of Penetration (k_p)

1) Тип преграды	$k_п$
2) Плотный гранит и гранитные породы; очень крепкий песчаник и известняк	$1,6 \cdot 10^{-6}$
3) Обыкновенный песчаник и известняк; песчаный и глинистый сланцы	$3,0 \cdot 10^{-6}$
4) Мягкий сланец; известняк; мерзлый грунт	$4,5 \cdot 10^{-6}$
5) Щебенистый грунт; отвердевшая глина	$4,5 \cdot 10^{-6}$
6) Плотная глина; крепкий навос; земля, смешанная с камнем; песок влажный	$5,0 \cdot 10^{-6}$
7) Земля плотная; обыкновенный растительный грунт	$5,5 \cdot 10^{-6}$
8) Болотистая почва; мокрый глинистый грунт	$10,0 \cdot 10^{-6}$
9) Железобетон	$0,9 \cdot 10^{-6}$
10) Бетон (цементно-гранитный)	$1,3 \cdot 10^{-6}$
11) Кирпичная кладка на цементе; булыжная кладка	$2,5 \cdot 10^{-6}$

1) Type of obstacle; 2) dense granite and granite rocks; extremely strong sandstone and limestone; 3) conventional sandstone and limestone; sandy and argillaceous shales; 4) soft shale; limestone; frozen soil; 5) gravely soil; hardened clay; 6) thick clay; heavy alluvial deposits; dirt mixed with rock; moist sand; 7) packed earth; conventional planting soil; 8) swampy soil; wet clay soil; 9) reinforced concrete; 10) concrete (cement-granite); 11) stacked bricks on cement; cobblestone construction.

2. The Petri formula

$$l_{пр} = \frac{q_в}{d^2} \chi_п f(v_к). \qquad (3.13)$$

where l_{pr} is the depth of penetration, in m; q_p is the weight of the missile at the instant of impact against an obstacle, in kg; d is the caliber of the missile, in cm; χ_p is the coefficient of obstacle properties (see Table 3.2); $f(v_k)$ is the function of impact velocity (see Table 3.3).

In addition to Formulas (3.12) and (3.13), we may also encounter in the literature relationships that are of the same type as those proposed in his time by Ponsele [sic], Val'ye [sic], Vuich [sic], Zabudskiy, Peres [sic], Nobile [sic], and other investigators. There is no basic difference between these formulas,

TABLE 3.2

Coefficients χ_p of Obstacle Properties for the Petri Penetration Formulas

1) Тип преграды	χ_p
2) Скала известковая	0,43
3) Каменная кладка	0,94
4) Бетон среднего качества	0,64
5) Кирпичная кладка	1,63
6) Песчаный грунт	2,94
7) Земля с растительным покровом	3,86
8) Мягкий глинистый грунт	5,87

1) Type of obstacle; 2) limestone rock; 3) rock pile; 4) medium-quality concrete; 5) brick pile; 6) sandy soil; 7) ground with seed cover; 8) soft clay soil.

and the apparent difference only indicates the individual approach of each of the investigators to the solution of the posed problem. As an example, we will cite the Nobile formula.

$$l_{np} = \frac{P_s}{\lambda_0} k_N F_{m(e)} \text{ м}, \qquad (3.14)$$

where $P_s = q_p/(\pi d^2/4)$ is the lateral load, in kg/cm^2; λ is the coefficient of shape; $\lambda = 1$ for pointed missiles; $\lambda = 1.5$ for blunt missiles; k_N is the coefficient of medium properties; $F_{m(e)}$ is the coefficient of impact velocity for solid obstacles and soils (according to the subscripts).

TABLE 3.3

Values of the Velocity Function $f(v_k)$ for the Petri Penetration Formulas

1) Малые скорости удара										
$v_к$	40	60	80	100	120	140	160	180	200	220
$f(v_к)$	0,33	0,72	1,21	1,76	2,36	2,97	3,58	4,18	4,77	5,34
2) Средние скорости удара										
$v_к$	240	260	280	300	320	340	360	380	400	420
$f(v_к)$	5,89	6,41	6,92	7,40	7,87	8,31	8,74	9,15	9,54	9,92

1) Low impact velocities; 2) average impact velocities.

On the basis of the terms and coefficients, Formula (3.14) is similar to Relationships (3.12) and (3.13), which we examined in detail and which were selected as the basic relationships because the coefficients in these formulas were determined in greatest de-

tail and the greatest quantity of experimental material was generalized in their derivation.

Evaluation of Missile Effectiveness at the Target

The combat effectiveness of a demolition missile against an obstacle is measured in terms of the destruction of this obstacle by the gaseous products of the exploding charge and the fragments of the warhead shell. It has been established in practice that the basic destructive factors of a demolition explosion are the explosion shock wave, the stream of fragments, and the seismic effect of the explosion.

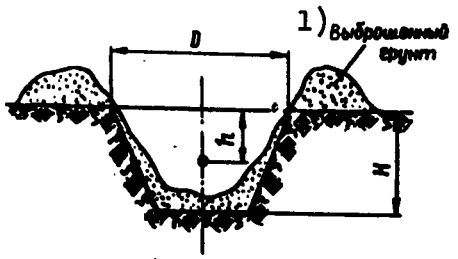

Fig. 3.8. Theoretical dimensions of the crater formed in the soil on the explosion of a missile at a depth h. 1) Soil thrown out.

Under combat conditions, the force of a demolition missile is evaluated in terms of the combined destructive effect of all three factors, and in this case the depth of the crater that is formed in the ground as a result of the explosion (Fig. 3.8) is generally taken as the standard measure of comparative explosion force.

In a tentative determination of the effectiveness of a demolition missile, the characteristic depth H (in m) can be evaluated in accordance with the following emperical formula:

$$H = k'_{VZ}\sqrt[3]{\frac{P_*}{C}}, \qquad (3.15)$$

where k'_{VZ} is some coefficient which characterizes the extent to which the obstacle yields to the action of the explosion; C is the coefficient which characterizes the effect of the depth h, in m, of missile explosion on the effectiveness of explosion; P_* is the

weight of the combat charge, or it is possible to use an even simpler relationship

$$H \approx \sqrt[3]{\frac{P_ф}{C'}}, \qquad (3.15')$$

where the coefficient C' is employed to take into consideration the features of the obstacle and the effect of charge explosion at various depths; the numerical values of this coefficient are presented in Table 3.4.

TABLE 3.4

Values of the Coefficient C'

1) Тип преграды	2) Значение коэффициента C'
3) Каменная кладка; бетон; скала; $h<0{,}9$ м	5,0
h до 1,5 м	4,0
h до 2,0 м	3,5
$h>2{,}0$ м	3,0
4) Щебни и несвязные насыпи	1,0 (среднее значение) 7)
5) Обычные грунты	0,7 (среднее значение)
6) Железобетон	8,0

1) Type of obstacle; 2) value of the coefficient C'; 3) rock pile; concrete; rock; 4) gravel and loose mounds; 5) conventional soils; 6) reinforced concrete; 7) average value.

If the explosion takes place directly at the surface of the obstacle, all other conditions being equal, the formed crater will be smaller; the depth of such a crater is generally estimated in accordance with the following formula:

$$H = k''_{vz} \sqrt[3]{P_ф} - h_{ц.т}, \qquad (3.16)$$

where k''_{vz} is some coefficient similar to the coefficient k'_{vz} in Formula (3.15) (see Table 3.5); $h_{ts.t}$ is the coordinate of the center of gravity of the missile warhead at the instant of explosion with respect to the surface of the obstacle (Fig. 3.9) (more exactly, this is not the coordinate of the center of warhead gravity, but the corresponding coordinate of the explosive charge).

TABLE 3.5

Values of the Coefficient k''_{vz}.

1) Тип преграды	2) Значение коэффициента k''_{vz}
3) Земля рыхлая	0,6
4) Земля с песком и гравием	0,56
5) Обыкновенный грунт	0,53
6) Плотный чистый песок	0,45
7) Земля, смешанная с камнем	0,5
8) Скала известняковая	0,23
9) Бетон	0,175
10) Железобетон	0,13

1) Type of obstacle; 2) value of the coefficient k''_{vz}; 3) mellow soil; 4) soil with sand and gravel; 5) conventional soil; 6) packed pure sand; 7) soil mixed with stones; 8) limestone rock; 9) concrete; 10) reinforced concrete.

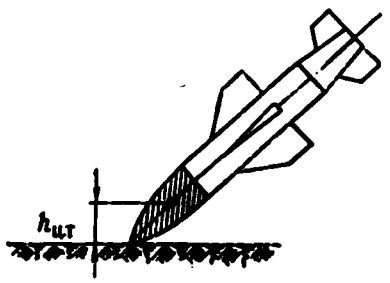

Fig. 3.9. Determination of the coordinates of $h_{ts.t}$ when using the calculation Formula (3.16).

It has been demonstrated in practice that the maximum explosive effect (the dimensions of the crater formed in the soil) are obtained if the explosion takes place at a depth, which for a missile carrying an explosive charge weighing P_* kg, amounts to approximately

$$h_{экг} = (0{,}85 \div 0{,}95)\sqrt[3]{P_*}\ \text{m}, \qquad (3.17)$$

With missile explosion at any depth, direct destruction due to the explosion is noted over a certain region with a limit radius R_r which originates at the point of explosion and is determined by the relationship

$$R_r = k_r \sqrt[3]{P_*},$$

where k_r is the coefficient whose numerical values for various obstacles are presented in Table 3.6.

This area is referred to as the region of destruction or the sphere of destruction. In addition to the sphere of destruction, there are also the so-called spheres of compression and percussion, in an explosion, which are characterized by the presence of certain characteristic deformations in the obstacle. If the missile penetrates into the obstacle to the following depth

$$h \geqslant R_p,$$

the explosion does not expose the entire thickness of the obstacle but rather a so-called camouflet is formed. In the case of a camouflet, the effect of the destructive shock wave and the fragments goes virtually unused, but the seismic effect of the explosion is at its maximum.

TABLE 3.6

Values of the Coefficient k_r.

1) Тип преграды	2) Значение коэффициента k_p
3) Земля рыхлая	1,4
4) Обыкновенный грунт	1,07
5) Песок	1,0—1,04
6) Глина с песком	0,96
7) Известняк и песчаник	0,92
8) Каменная кладка	0,84
9) Бетон	0,77
10) Железобетон	0,6—0,7

1) Type of obstacle; 2) value of the coefficient k_r; 3) mellow soil; 4) conventional soil; 5) sand; 6) clay with sand; 7) limestone and sandstone; 8) stone pile; 9) concrete; 10) reinforced concrete.

Selection of Explosive. Calculation of Time of Delayed Action Assuring Maximum Missile Effectiveness

Demolition warheads are made with two types of nose or side fuses — an impact (instantaneous) fuse and an inertial (delayed-

action) fuse, the latter delaying the explosion somewhat.

Impact (contact) fuses are used for thin-walled warheads, and these are characterized by the highest possible fill factors and relatively low strength. Causing the missile to detonate at the surface of the obstacle, such fuses predetermine the application of the effect of the explosion shock wave as the basic destructive factor of the explosion.

In the case of delayed-action fuses, the explosion takes place at some depth and its destructive effect is determined not only by the shock-wave parameters but by the seismic effect of the explosion as well. The basic problem that arises in the selection of a delayed-action fuse is the one relating to the matter of obtaining a delay in the explosion such that the effect of missile explosion will be the maximum. Bearing in mind the existence of an optimum depth of explosion h_{opt}, we have the problem of determining the optimum delay and this can be reduced to the calculation of the time required for the missile to penetrate to a depth h_{opt}. In this case, if we assume that the motion of the missile in the obstacle, in first approximation, is decelerated uniformly, we can use the following well-known relationship for uniformly decelerated motion for purposes of calculation:

$$l = v_0 t - \frac{a_{cp} t^2}{2},$$

from which it is easy to obtain $t = t(\underline{l})$ in the following form:

$$t_{1,2} = \frac{v_0}{a_{cp}} \pm \sqrt{\frac{v_0^2}{a_{cp}^2} - \frac{2l}{a_{cp}}}.$$

If we bear in mind that in our denotations

$$v_0 = v_m$$

and

$$l = \frac{h_{max}}{\sin \alpha},$$

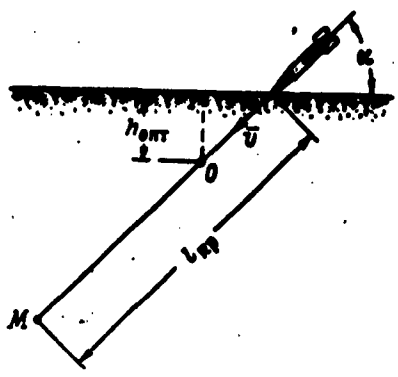

Fig. 3.10. For the determination of the optimum delay time for a delayed-action fuse.

and that in accordance with Formula (3.10) and the assumption of uniform missile deceleration, the following equation will be valid

$$a_{ср} = \frac{v_к^2}{2l_{пр}},$$

and we will obtain

$$t_{1,2} = \frac{2l_{пр}}{v_к} \pm \sqrt{\frac{4l_{пр}^2}{v_к^2} - \frac{4h_{опт}l_{пр}}{\sin\alpha v_к^2}},$$

whence the final calculation relationship for the estimation of optimum fuse delay time T_{opt} is determined as follows:

$$T_{опт} = \frac{2l_{пр}}{v_к}\left(1 \pm \sqrt{1 - \frac{h_{опт}}{l_{пр}\sin\alpha}}\right). \qquad (3.18)$$

Here $\underline{l}_{pr}$ is the total depth of penetration which is calculated for the given missile in accordance with Formulas (3.12) or (3.13); v_k is the velocity of the missile at the instant of impact with the obstacle; h_{opt} is the optimum depth at which the fuse of the given missile should be actuated; α is the angle at which the missile strikes the target.

The T_{opt} found in this manner is quite tentative and is refined finally in accordance with the results obtained in test firings of a control group of missiles.

If there is a discussion in the tactical-technical requirements of the type of fuse involving a certain definite delay or if the fuse type has been selected on the basis of some special considerations, then the depth $\underline{h}$ at which the initiation of the fuse and the explosion will take place under conditions of combat application of the missile against any given obstacle can be determined (estimated) on the basis of the relationships presented above. The

following will be the corresponding calculation relationship:

$$h=\left(v_{\text{к}}T-\frac{v_{\text{к}}^2T^2}{4l_{\text{ср}}}\right)\sin\alpha, \qquad (3.19)$$

where T is the delay time of the fuse being employed (the remaining denotations are the same as before).

It is precisely on the basis of the numerical value of this depth that we should seek in tables the coefficient C' of depth of explosion that is required for the application of the following formula

$$H=K_{\text{ш}}\sqrt[3]{\frac{P_{\text{в}}}{C'}},$$

by means of which we can estimate the comparative effectiveness of the warhead being designed.

It should be stressed that in order to obtain maximum combat effectiveness of the item being designed, the selection of the fuse must be without fault and, in particular, the fuse itself must assure a delay which will guarantee the initiation of the fuse at the optimum depth.

§ 2. FRAGMENTATION WARHEAD

Basic Structural Characteristics of Fragmentation and Fragmentation-Demolition Warheads

Fragmentation missiles are intended for firing against air and ground targets, including combat equipment and the enemy's combat forces. In accordance with the designation of fragmentation missiles, the basic requirements imposed on these can be reduced to the obtaining of the maximum quantity of lethal fragments and the maximum possible effective fragment (shrapnel) range.

As a rule, a fragmentation warhead must have a rather thick-walled shell and only sufficient explosive material in order to

fragment the shell into the lethal fragments as well as to impart the required initial velocity to these pieces of shrapnel.

A fragmentation warhead is characterized by the following structural parameters:

1) a relative warhead length which, for example, for the M8 missile amounts to

$$\bar{l}_{б.ч} \approx 2{,}1d;$$

2) a relative wall thickness for the warhead body

$$\bar{\delta}_{ст} = \frac{8}{82} d \qquad \text{(M8, USSR)};$$

3) the fill factor

$$\eta \approx 15\%;$$

4) the coefficients k_s and k_* of relative weight, where on the average

$$k_c = \frac{P_0^{б.ч}}{d^3} \approx 6{,}0 \ \text{kg/dm}^3,$$
$$k_\Phi = \frac{P_\Phi}{d^3} \approx 1{,}0 \ \text{kg/dm}^3.$$

Fragmentation-demolition missiles are intended to produce shell fragments in attacks against an enemy's combat forces and equipment, as well as to produce the destructive force of a shock wave whose action can be directed against defense installations. In terms of combat and design parameters, warheads of fragmentation-demolition missiles are classified in some intermediate position between fragmentation and demolition missiles.

The parameters of a typical fragmentation-demolition warhead of a solid-propellant rocket missile have the following values:

1) a relative warhead length

$$\bar{l}_{б.ч} = 3{,}5d \qquad \text{(M13, USSR)};$$

2) a relative wall thickness

$$\bar{\delta}_{ст} = \frac{13{,}5}{132} d \qquad \text{(M13, USSR)};$$

3) a fill factor $\eta = 25\%$;

4) coefficients of relative missile and equipment weight

$$k_c \approx 8{,}0 \text{ kg/dm}^3,$$
$$k_e \approx 2{,}0 \text{ kg/dm}^3.$$

Selection of Shape for Fragmentation Warhead

The body shape of a fragmentation warhead is selected on the basis of the conditions required to provide for uniform fragmentation of the entire shell into the smallest possible (minimum weight) lethal fragments. Fragments in this case are regarded lethal if they are capable at a given distance to take out of action some proposed target or to damage the vital parts of unarmored combat equipment.

On the basis of existing information it is possible, to regard as lethal a fragment which exhibits a kinetic energy of the order of 10 kg/m, weighing no less than 5-10 g, at the instant of contact with the target.

In addition to the basic requirement with respect to the shape of a fragmentation warhead – uniformity of shell fragmentation – it should also be borne in mind during the design stage that the shape must correspond to the adopted structural assembly of the missile and the shape must provide for convenient assembly of the individual missile units.

From the standpoint of fragmentation uniformity it is necessary to begin with a shape which will provide for symmetry in the stressed state over the entire warhead surface. The most suitable shape, from this standpoint, is the spherical or cylindrical shape given the condition that the initiation of the explosion takes place from the center of the warhead or along the warhead's axis of symmetry.

The requirements associated with the assembly of the missile are presented as optimum from the standpoint of the shape of the ogive curve or the cylinder.

It follows from what has been said above that, all other conditions being equal, the basic premise for the design of fragmentation armament (missiles) must be a cylindrical warhead made in the form of a fixed-thickness shell having a system of central axial initiation. On the one hand, in this case the fragmentation warhead is relatively simple and lends itself to production, and on the other hand, it is the most powerful warhead.

However, for example, missiles of standard configuration as a rule cannot be made with a warhead of this type. In fact, the need for a special ballistic cowling in the case of a cylindrical warhead on a missile of conventional configuration substantially increases the length of the foward part of the missile while virtually not changing the position of the missile center of gravity, thus reducing the stability of the missile in flight.

A spherical warhead has not yet come into practical use because of extreme difficulties in mounting such a shape on any of the possible structural missile configurations.

Designs for Fragmentation Warheads which will Provide for Shell Fragmentation into a Given Quantity of Fragments

In the explosion of conventional fragmentation warheads a certain quantity of nonuniform (with respect to weight) fragments are formed, and of these only some are capable of inflicting actual damage. It has been established that of the total weight of warhead body metal up to 30-40% is expended on the formation of small fragments which do not possess sufficient energy to damage the target, i.e., in actual fact these fragments are useless from the stand-

point of effectiveness in damaging the target. Moreover, a group of major fragments is formed in the explosion and these possess energy that is in excess of that required for the given target. As a result, only a comparatively small part of the metal of the missile shell is employed usefully.

The presence of fragments exhibiting inadequate or excessive energy for the damaging of a given target reduce the number of optimum lethal fragments, i.e., the combat effectiveness of the missile. The effectiveness of fragmentation warheads can be increased substantially by the forced fragmentation of the shell into a given quantity of fragments of required weight.

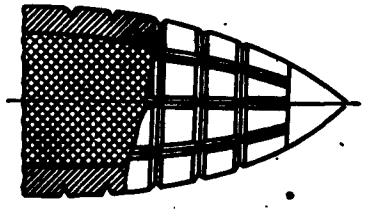

Fig. 3.11. Fragmentation warhead with rectangular notched grid.

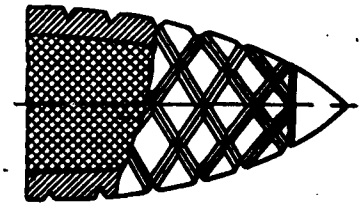

Fig. 3.12. Fragmentation warhead with rhombic notched grid.

The attempts to control the destruction of the warhead so as to obtain the greatest possible quantity of lethal fragments of minimum weight were undertaken as far back as the 1870's – 1880's. However, missile designs at that time were so cumbersome and unreliable that they found no practical application. The first suitable solutions to the problem of shell fragmentation into a given quantity of fragments of given weight appeared very much later.

Let us examine some of the warhead configurations which provide the given shell fragmentation.

Figure 3.11 shows a warhead which, generally speaking, can be fabricated in some other shape, depending on the assembly of the

units in the adopted structural configuration of the missile; this particular warhead is distinguished by the fact that a grid of special notches has been cut into its surface. These notches are stress concentrators and denote the sections into which the shell will be fragmented on explosion. Experimental explosions have shown, however, that the notched grid shown in Fig. 3.11 does not produce reliable shell fragmentation along the notch lines, since there is generally no explosion along the lateral notches.

The fragmentation can be stabilized if the notched grid is cut into the surface of the missile at a certain angle to the axis of the cylinder (a rhombic notched grid), as shown in Fig. 3.12. The angle of inclination of the notched lines is a function of certain structural parameters and the characteristics of the warhead material; this angle can be calculated in each specific case. The magnitude of this angle is a function of the diameter of the missile body and is constant therefore only for the cylindrical part of the warhead; in the case of the ogive-curve section, the angle of inclination of the notched line changes continuously so that the line itself becomes a complex helical curve of variable pitch.

If the warhead of a fragmentation missile is designed in the shape of a straight-line cylinder, the telescope assembly of two tubes with an assured tension will prove to be an extremely effective design. Rhombic notched grids are cut into the inner surface of the outer tube and the outer surface of the inner tube, the lines of these grids coinciding with each other. We can also cite, for example, such other highly effective missile designs as the prefabricated-cemented warheads and certain others.

Calculation of the Parameters of the Fragmentation Action of a Missile

The mechanism of warhead-shell fragmentation in the case of an

explosion is an extremely complex phenomenon whose theoretical study is made even more complicated by the fact that during the course of the basic processes there arise certain factors which have a substantial effect but do not lend themselves to rigorous examination. Nevertheless, as far back as the last century various investigators have made attempts to derive calculation formulas by means of which it would have been possible, for example, to calculate the number of fragments formed. Of these investigators we should mention, first of all, Yustrov and Yulovskiy. In their work on the problem of missile-shell fragmentation into a given number of fragments, and they did this work independently of each other, they came to the conclusion that the following missile parameters affect the process of fragmentation and determine, in the final analysis, the number of fragments formed:

– missile weight and caliber,

– weight of bursting charge and characteristics of explosive material,

– mechanical characteristics of the metal used in the shell,

– angle of missile impact against the obstacle,

– type and characteristics of fuse, etc.

Of all the calculation relationships the simplest and yet the most reliable is the formula proposed by Yustrov, which determines the relationship between the number of fragments and the basic parameters of the warhead in the following form:

$$N = \alpha_{BB} \frac{c_0}{c_{0\delta}} \frac{\gamma^2 + 0{,}5}{\gamma^2 - 1{,}0} \frac{P_*}{d}, \qquad (3.20)$$

where N is the number of fragments that are formed on the explosion of the warhead; α_{BB} is the coefficient whose magnitude is a function of the properties of the explosive (BB) used as the bursting charge (for TNT $\alpha = 46$); P_* is the weight of the explosive charge, in kg;

$\underline{d}$ is the caliber of the warhead in cm; σ_b is the ultimate strength of the material, in kg/mm^2; σ_* is the elasticity limit, in kg/mm^2; ε is the elongation on explosion, in %; χ is the total structural parameter which determines the fragmentation capacity of the missile, and has the following average values for warheads with various fill factors η:

$$\chi = 1.8 \qquad (\text{at } \eta = 7\%),$$
$$\chi = 1.5 \qquad (\text{at } \eta = 10\%),$$
$$\chi = 1.4 \qquad (\text{at } \eta = 15\%).$$

Formula (3.20) can be used to determine only the total number of fragments, without being able to determine the number of lethal fragments, and this is, for all intents and purposes, less significant.*

A more exact determination of the total quantity of fragments formed on the explosion of any given warhead, and the determination of the distribution spectrum with respect to mass, can be obtained only on the basis of statistical data produced in the explosion, in an explosion test pit, of a experimental models of the warhead being designed (see Chapter 7).

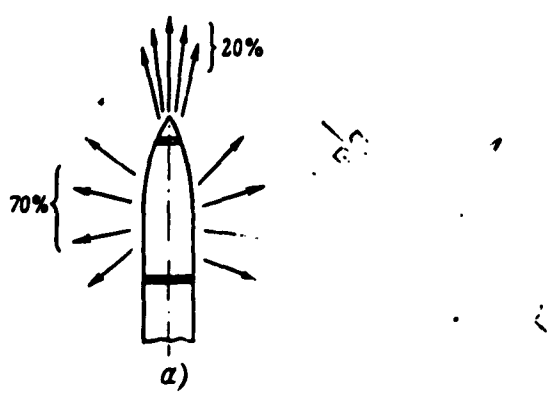

Fig. 3.13. Diagram of fragment scattering on warhead explosion. a) Plane diagram; b) three-dimensional diagram.

On the explosion of the missile, the fragments are scattered

in space in a nonuniform manner. The nature of this dispersion corresponds approximately to the diagram shown in Fig. 3.13. In the final analysis, the actual number of effective lethal fragments must be determined on the basis of a consideration of the features exhibited by the actual scattering of the fragments.

An important parameter which affects the lethal nature of a fragment and which determines the maximum distance over which the fragment preserves its lethal characteristics is the initial velocity of the fragment. This velocity is a function of a number of warhead parameters (the fill factor, the rate of explosive detonation, the shape of the warhead, etc.); on the average, this velocity amounts to 1000-2000 m/sec and is selected as a function of the specific conditions of missile application. It is possible, for example, to estimate the maximum velocity of the fragment at the point of explosion on the basis of the following formula:

$$w_0 \approx \frac{D\sqrt{6}}{4}\sqrt{\frac{4}{15}\frac{P_0^{b.ch}-P_*}{P_*}}, \qquad (3.21)$$

where D is the rate of explosive detonation, in m/sec; $(P_0^{b.ch} - P_*)$ is the weight of the missile shell, in kg; P_* is the weight of the explosives, in kg, or on the basis of other calculation relationships by means of which we can take into consideration the structural features of each warhead version through the use of a system of correction factors.

Effectiveness of Fragmentation Missile at the Target

Proximity tubes (fuses) of various designs, which initiate the warhead at some determined point along the trajectory, are the most expedient for fragmentation missiles, depending on the designation and the features of tactical application. Only with the use of such initiation devices at the target will it be possible to achieve the

effect of the maximum quantity of fragments formed at the instant of explosion, and only in this way will the greatest effectiveness of the warhead be obtained.

In addition to proximity fuses, fragmentation missiles frequently employ conventional impact fuses of instantaneous action. The utilization of such fuses reduces somewhat the effect of the fragmentation action, since some of the fragments penetrate, for example, into the surface of the earth on explosion. However, because of the simplicity of design in the case of conventional fuses and the difficulties encountered in the initiation of proximity fuses, in a number of countries impact fuses are still employed in the design of fragmentation missiles.

In recent times we have noted a tendency abroad to use such noncontact devices as radar fuses which are connected to the control equipment or the self-guidance apparatus of the missile; fuses of this type make it possible to initiate the missile at the most favorable missile position with respect to the target.

The quantitative measure of the effectiveness of a fragmentation missile is the so-called radius of continuous target damage and the magnitude of this radius is determined experimentally in each case by experimental explosions of warheads around targets. The assumption is that within the limits of the circle having the radius of continuous damage the probability of damaging the target must be 100%. In addition to this circle, the areas in which the probability of target damage amounts to 75, 50%, etc., are also examined, characterizing these areas with radii that correspond to the probability of damage. The radial values of the determined probability of target damage (destruction) serve as a detailed characteristic of the combat effectiveness of a fragmentation missile.

§ 3. HOLLOW-CHARGE WARHEAD

The Effect of a Hollow Charge and Its Application in the Case of Armor-Piercing Missiles

Among the field rocket missiles used for short-range purposes, the so-called hollow-charge reaction-thrust shells have become quite popular. The hollow-charge shells are an effective means of destroying armor-plated vehicles and tanks; in this case, an important advantage of missiles of this type is the fact that they exhibit not only high armor-piercing characteristics, but that the smallest combat units of an army, down to an individual infantryman, can be equipped with corresponding reaction-thrust systems.

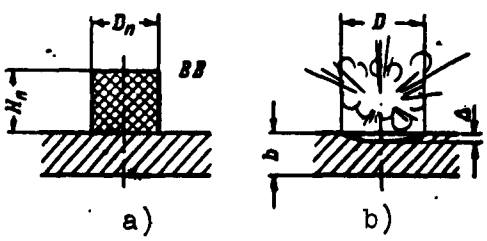

Fig. 3.14. The effect of an explosion of a charge on an armor plate of conventional shape. a) Prior to the explosion; b) after the explosion; D_p and H_p) the diameter and height of the detonating charge; Δ) the depth of the indentation (crater).

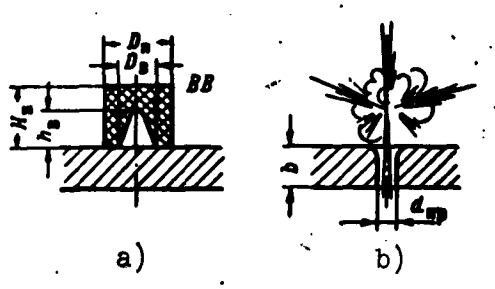

Fig. 3.15. The effect of an explosion of a hollow charge on an armor plate. a) Prior to the explosion; b) after the explosion; D_p and H_p) the diameter and height of the detonating charge; D_p and h_v) the diameter and depth of the funnel.

The effect of the hollow-charge shell at a target is based on the utilization of the so-called "cumulative" effect of an explosion, and this effect consists in the following.

If a conventional detonating charge is exploded at the surface of an armor plate, a shell-like (conchoidal) indentation is produced in the plate (Fig. 3.14). The depth of this indentation is a function of the quantity of charge and the brisance properties of the explosive; as a rule, the brisance is generally not too great. The

depth of the indentation can be increased substantially if the same detonation charge is exploded, but if a funnel of specified shape is drilled into the charge.

Finally, we can select the shape and dimensions of the funnel so as to penetrate the entire plate (Fig. 3.15) with the original quantity of explosive material.

In the latter case, as a result of the particular properties of the funnel in the grain, the energy of the explosion is redistributed so that the greater part of the energy is concentrated in the so-called "cumulative" stream and will be directed along the axis of the funnel to the surface of the obstacle. It is precisely in this that we find the "cumulative" effect of the explosion.

A study of the "cumulative" effect has shown that the basic factors which affect the effectiveness of armor piercing are the following:

– the dimensions and shape of the hollow-charge funnel,

– the material used for the facing of the inside of the hollow-charge funnel,

– the distance from the outer edge of the funnel to the obstacle at the instant of explosion, and certain other factors.

The optimum shapes of the hollow charge, as a rule, are quite complex from the standpoint of fabrication; therefore, it is but rarely that hollow-charge shells are used in actual models; the most popular practical funnel shapes are cones and spheres.

Experiments have demonstrated that, all other conditions being equal, the armor-piercing effect increases noticeably if the inner surface of the funnel is coated with a thin layer of some facing material; in this case, the increase in charge effectiveness is a function of the material selected for the facing and the thickness

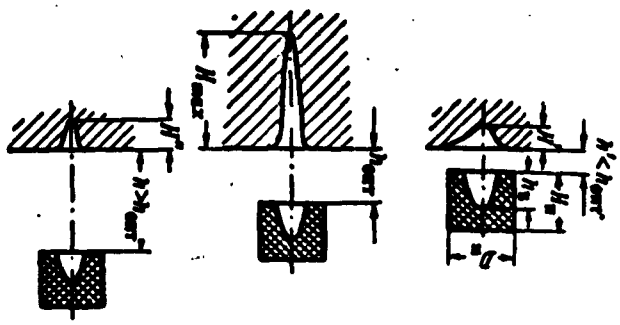

Fig. 3.16. The nature of the relationship between the "cumulative" effect and distance at the instant of explosion between the outer edge of the funnel and the obstacle. H', H_{max}, and H") the depths of the indentations; D_p and H_p) the diameter and height of the detonating charge; h, h', and h_{opt}) the distances between the outer edge of the funnel and the obstacle.

of the coating layer. Of all the tested facing materials, copper and zinc alloys proved to be the best; other metals (iron, aluminum) have less of an effect on the effectiveness of the "cumulative" explosion.

An investigation of the armor-piercing capability as a function of the distance (at the instant of explosion) between the outer edge of the funnel and the obstacle has shown that in each case there is some optimum distance which will produce the maximum effect, on initiation, at the target (Fig. 3.16). This distance is generally referred to as the focal distance and it is regarded as a basic parameter of the funnel.

Tentative Determination of the Dimensions of the Hollow Charge Which Will Ensure the Penetration of an Obstacle of Given Thickness

The "cumulative" effect in armament is used by imparting to the grain a certain configuration which includes the "cumulative" funnel as one of its elements. In all other respects, the hollow-charge warhead shows no differences from missiles of other classes.

The design of hollow grains is based on the conclusions drawn from the theory of the armor-piercing effect of the "cumulative" stream, said conclusions first derived by the Academician L.M. Lavrent'yev. He established, for example, that it is not the entire "cumulative" stream, but only some part of it, that exhibits armor-piercing capacity; that part of the "cumulative" stream is referred to as the effective length l_{ef} of the stream. The quantity l_{ef} is primarily a function of the dimensions and shape of the funnel and, moreover, of the material used to face the funnel and the parameters of the grain. The depth of armor piercing is essentially a function of the parameter l_{ef} of the "cumulative" stream.

In designing a hollow-charge warhead it becomes necessary to seek the optimum funnel with respect to the depth of complete obstacle penetration as stipulated in the tactical-technical requirements. This problem is resolved on the basis of extensive experimentation and the utilization of statistical data for the explosions of various hollow grains. The following extremely tentative relationships may be useful.

1. The diameter of the hollow-charge funnel is, on the average,

$$D_в \approx \frac{1}{n_ф} b_{max},$$

where b_{max} is the thickness of the given obstacle which must be penetrated; n_f is the coefficient that is a function of the funnel shape.

2. The diameter of the pierced hole generally does not exceed

$$d_{пр} = (0{,}05 \div 0{,}3)\, D_в.$$

3. For each type of funnel there exists a certain optimum height h_v of funnel cupola that is equal to 0.5 D_v for semispherical holes (1.0-1.5) and D_v for conic holes.

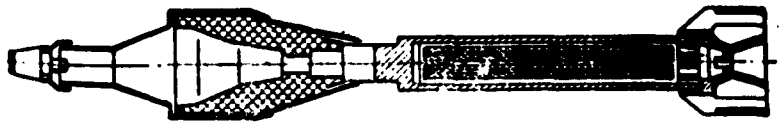

Fig. 3.17. An example of a design of a hollow-charge shell.

4. A layer of explosive, whose height does not exceed 0.5-0.8 D_v (above the apex of the funnel) participates in the shaping of the "cumulative" stream. In this case, any further increase in the height of the column, and consequently, in the weight of the explosive charge, without a corresponding change in the dimensions of the funnel, produces no increased effectiveness for the hollow grain and is therefore inexpedient.

Figure 3.17 shows an example of one of the designs of German hollow-charge shells used during the Great Fatherland War. We can see from the figure that the rocket part of the shell is basically like the rocket parts used in conventional finned field rocket missiles. However, the warhead is unique. It consists of a body of definite shape, stamped from sheet metal, and filled with explosive in addition to certain additional design elements which provide for the normal functioning of the shell – primarily an explosive train (chain) and the hollow of the charge. The sensing element of the fuse is extended beyond the outer edge of the grain to a special ballistic cowling so that the explosion, on contact with an obstacle, takes place at distances close to the optimum. It should be borne in mind that since the velocity of the hollow-charge shells in flight is, as a rule, not great (80-100 m/sec), the shape of the warhead has virtually no effect on the ballistic characteristics of the missile; this makes it possible to neglect the requirements of aerodynamics in the design of the warhead and to base the design exclusively

on the concepts that are associated with the required operating conditions of the explosive chain and the hollow charge.

As has already been pointed out, the rocket part of a hollow-charge shell is designed in the same manner as for other rocket missiles. We should mention the one interesting feature of manual hollow-charge cartridges having an effective range of up to 100 m. This feature consists in the fact that the rocket engine of such a cartridge generally functions on black powder. This is explained by the requirement of absolute reliability for this weapon and the need, in this connection, to provide for constancy of the physico-chemical and ballistic parameters of the powder, which is difficult to obtain when rocket solid propellants are used.

[Footnotes]

Manuscript Page No.

81 M.G. Yefimov. Kurs artilleriyskikh snaryadov. Oborongiz [Course in Artillery Missiles. State Defense Press], 1939;

G.M. Tret'yakov. Boyepripasy artillerii. Voyenizdat [Artillery Armament. Military Press], 1940.

[List of Transliterated Symbols]

52 $\overline{\delta}_{ст} = \overline{\delta}_{st} = \overline{\delta}_{stena} = \overline{\delta}_{wall}$

56 $P_{дн} = P_{dn} = P_{dno} = P_{bottom\ plate}$

56 $P_{к.с} = P_{k.s} = P_{kamera\ sgoraniya} = P_{combustion\ chamber}$

57 $P_{ст} = P_{st} = P_{stabilizator} = P_{stabilizer}$

60 $d_{вн} = d_{vn} = d_{vnutrennyy} = d_{inner}$

60 $\sigma_{сж} = \sigma_{szh} = \sigma_{szhatiye} = \sigma_{compression}$

63 $P_{дин} = P_{din} = P_{dinamicheskiy} = P_{dynamic}$

64 $E_{к} = E_{k} = E_{kineticheskaya} = E_{kinetic}$

64 $A_{сопр} = A_{sopr} = A_{soprotivleniye} = A_{resistance}$

Manu-
script
Page
No.

64 $l_{пр} = l_{pr} = l_{pronikaniye} = l_{penetration}$

65 $h_{ож} = h_{ozh} = h_{ozhival} = h_{ogive}$

66 $\chi_{п} = \chi_{p} = \chi_{pregrada} = \chi_{obstacle}$

68 $k_{вз} = k_{vz} = k_{vzryv} = k_{explosion}$

69 $h_{ц.т.} = h_{ts.t} = h_{tsentr\ tyazhesti} = h_{center\ of\ gravity}$

70 $h_{опт} = h_{opt} = h_{optimal'nyy} = h_{optimum}$

70 $k_{р} = k_{r} = k_{razrusheniye} = k_{destruction}$

72 $a_{ср} = a_{sr} = a_{srednyy} = a_{average}$

87 $D_{в} = D_{v} = D_{voronka} = D_{funnel}$

87 $n_{ф} = n_{f} = n_{forma} = n_{shape}$

87 $d_{пр} = d_{pr} = d_{proboina} = d_{pierced\ hole}$

Chapter 4

ELEMENTS OF THE INTERIOR BALLISTICS OF A SOLID-PROPELLANT ROCKET ENGINE

§1. SOME INFORMATION ON THE SOLID PROPELLANTS (POWDERS) USED IN ROCKET ENGINES

Composition of Rocket Powders

Smokeless (colloidal) powders. At the present time, the so-called smokeless or colloidal powders have become most popular for use as solid propellants for rocket engines. Colloidal powders are a solid solution of a fuel (combustible) based on an oxidizer, with special additives.

The fuel (combustible) base of the smokeless powders is a nitrocellulose of the pyroxylin type which is capable of being gelatinized in certain substances which contain a high percentage of active oxygen, thus producing a colloidal solution. On the cooling of such a solution, a plastic powder mass is obtained, and this mass lends itself easily to extrusion into grains that are then used as elements of the powder charge (grain) of the engine. In industrial production, nitrocellulose is obtained as a product in the treatment with concentrated nitric acid of cellulose contained in wood (50-60%), cotton (90-93%), flax, straw, and certain other forms of raw material. For the fabrication of rocket powders, the most important nitrogen contents of nitrocellulose are the following:

11.5-12.0% N – collodion

13.0-13.5% N – pyroxylin No. 1

12.0-12.5% N – pyroxylin No. 2.

Various materials may be used as the nitrocellulose solvent. In the adopted classification, these substances are generally divided into so-called volatile and nonvolatile solvents. In this case, volatile solvents are those which are almost completely removed from the powder during the production of the powder mass and the fabrication of the grain. Compositions using a volatile solvent are designated according to the type of nitrocellulose employed (for example, pyroxylin powder, etc.); as a rule, these are used comparatively rarely in rocket engineering. Nitroglycerine exhibits the best properties among the low-volatility solvents. However, because of its tendency to explosive decomposition, this material cannot be used in large quantities in a powder and it becomes necessary to use auxiliary solvents in order to achieve the complete solution of the nitrocellulose, thus making the powder mass explosion-proof. Dinitro diethylene glycol, for example, is used as an auxiliary solvent on a wide scale. The quantity of this auxiliary solvent may vary within a wide range and it may even exceed the amount of nitroglycerine used. Depending on the percentage content of solvent, powders using low-volatility solvents are referred to as nitroglycerine or diglycol, respectively.

In addition to the basic components, certain additives are included in the composition of the powder mass, making it possible to obtain a propellant with the desired physicochemical properties and ballistic parameters.

To obtain chemical stability for the powder, stabilizers are included in its composition; these are materials which retard the rate of the chemical decomposition reactions that take place within the powder mass during the storage of the grains, and the substances also pre-

vent the aging of the powder. The most widely used stabilizers are diphenylamines, ethylphenylurethane, various "centralites," and certain other compounds.

The chemical stability of the powders is of substantial significance in evaluating the operational suitability of the powders. The so-called litmus-paper and "brown-vapors" tests are used to determine the margin of chemical stability; the results of several other laboratory tests are also used for this purpose.

In addition to chemical stability, the physical stability of the grains is also of great significance in estimating the length of time that powder charges preserve their operational effectiveness. Experience has demonstrated that physical stability is a function of grain dimensions, powder composition, and the production techniques used in the fabrication of the powder mass and the grain. From the standpoint of physical stability, the basic defect of grains is their disintegration during storage. It is assumed that grain disintegration results not only from physical processes, but is due also to certain of the chemical reactions that take place within the powder mass during the storage of the grains. It has been established that the introduction of certain special admixtures into the powder composition has a favorable effect of the physical stability of the grains.

The properties of the powder mass, from the standpoint of grain fabrication techniques, are substantially improved if vaseline, wax, chalk, carbon black, and a certain other so-called industrial additives are included in the powder composition.

Finally, as a rule, the powder contains a great quantity of special additives for each composition, and these reduce the burning rate of the powder ("phlegmatizers"), increase the burning stability, reduce the temperature of powder burning, reduce the sensitivity of the burn-

ing of the powder to changes in the initial temperature of the charge, and the parameters of the interior ballistics of the engine, etc.

Thus smokeless rocket powder is a multicomponent solid solution of the colloidal type, based on nitrocellulose and a solvent. Powders based on a low-volatility solvent are generally used for the fabrication of rocket propellants.

The composition of several colloidal rocket powders is presented in Table 4.1. In American literature, smokeless powders are generally referred to as bipropellant solid rocket propellants.

Composite propellants. In connection with the development of engines operating on solid propellants, intensive work is being done abroad on seeking out and mastering new combinations and types of propellants which will exhibit greater ballistic and operational characteristics.

One of the trends in these new developments is the design of so-called composite propellant powders. Composite propellants are a fine mechanical mixture of the fuel (combustible) and the oxidizer, bonded by means of a plasticizer.

We have the following information on composite propellants from foreign literature.

The fuel components of composite propellants are usually rubber- or resin-like substances, and inorganic salts in whose molecules there is a great percentage of active oxygen are used as the oxidizers. Salts of the nitrate or ammonium perchlorate type are most frequently used as oxidizers since these are comparatively inexpensive and accessible while they exhibit high density and satisfactory energy characteristics. Of the fuel (combustible) constituents, asphalt-hydrocarbon resins, phenolfurfural, and formaldehyde rubber, as well as similar substances, are widely used.

There are also composite propellants which exceed the smokeless powders in terms of energy; however, their main advantage lies in the simplicity of grain fabrication and the convenience of operating engines using such propellants.

The most important feature of composite propellants is the fact that grains made of these powders can be obtained by casting, and here the powder can be poured directly into the engine chamber. As a result it becomes possible to fabricate solid-propellant grains of virtually any dimensions, whereas in the case of extruded grains made of smokeless powder, substantial production difficulties arise once diameters of 500 to 550 mm are attained and special extrusion equipment becomes necessary.

Composite propellants, as a rule, exhibit greater plastic properties, i.e., they do not disintegrate with fluctuations in temperature, and this distinguishes them from the smokeless powders which, as a rule, shatter during storage under conditions of variable temperature.

With the pouring of the composite propellant directly into the chamber, as the charge cools a strong bond is formed between the walls of the combustion chamber and the charge thus making it unnecessary to employ any special devices to receive the load acting on the charge during flight. Moreover, with an engine in which the combustion takes place along the surface of the inner channel it becomes unnecessary, in this case, to employ a restriction coating on the grains and the heating of the chamber walls is prevented throughout the greater part of the combustion, thus eliminating the need to apply a coating of a special thermal-insulation material to the wall or to use cooling systems. All of this makes it possible to use the maximum volume of the combustion chamber of the engine for propellant and to obtain an engine with increased weight characteristics.

TABLE 4.1

Chemical Composition of Several Smokeless Colloidal Solid Rocket Propellants

1 Название компонента / 2 Марка пороха	3 Германия				4 Англия			5 США						
	Z-167	R-61	17 H	105-5	SC	HSC	6 Медленно горящий	JP	JPN	M-7	MRN	R-61	BACA	JRN
7 Нитроклетчатка	55,8	67,8	63,7	60,0	49,5	49,5	56,5	52,2	51,5	54,5	56,51	61,5	59,9	51,5
8 Динитродиэтиленгликоль	16,35	35,3	16,0	39,66	—	—	—	—	—	—	—	35,0	—	—
9 Динитротриэтиленгликоль	16,35	—	16,0	—	—	—	—	—	—	—	—	—	—	—
10 Нитроглицерин	—	—	—	—	41,5	47,0	28,0	48,0	43,0	35,5	28,0	—	26,9	43,0
11 Динитротолуол	9,0	—	—	—	—	—	11,0	—	—	—	11,0	—	—	—
12 Тринитротолуол	12,5	—	—	—	—	—	—	—	—	—	—	—	—	—
13 Централит	—	—	2,0	—	9,0	3,5	4,4	—	1,0	0,9	4,5	—	2,9	1,0
14 Диэтилфталат	—	—	—	—	—	—	—	3,0	3,0	—	—	—	—	—
15 Дифениламин	—	0,8	—	—	—	—	—	0,6	—	—	—	—	—	—
16 Дифенилуретан	—	—	1,0	—	—	—	—	—	—	—	—	2,1	—	—
17 Этилфенилуретан	—	1,1	—	—	—	—	—	—	—	—	—	1,4	—	—
18 Гидроцеллюлоза	—	1,5	—	—	—	—	—	—	—	—	—	—	—	—
19 Акардит	—	0,3	—	—	—	—	—	—	—	—	—	—	—	—
20 Стабилит	0,5	—	—	0,74	—	—	—	—	—	—	—	—	—	—
21 ТЭН	6,0	—	—	—	—	—	—	—	—	—	—	—	—	—
22 Нитрозин	—	—	—	—	—	—	—	0,1	—	—	—	—	—	—
23 α-нитронафталин	—	—	—	—	—	—	—	—	—	—	—	—	6,1	—
24 Диметилфталат	—	—	—	—	—	—	—	—	—	—	—	—	—	3,25
KNO_3	—	0,6	—	—	—	—	—	1,1	—	—	—	—	—	—
K_2SO_4	—	—	—	—	—	—	—	—	1,25	—	1,5	—	2,0	1,25
$BaSO_4$; TiO	—	—	0,5	—	—	—	—	—	—	—	—	—	—	—
MgO	—	0,25	—	0,4	—	—	—	—	—	1,0	—	—	—	—
TiO_2	—	—	—	—	—	—	—	—	—	—	—	—	0,9	—
25 Сажа	—	—	0,3	0,1	—	—	—	—	0,2	1,2	0,5	—	—	0,2
26 Воск	—	0,35	—	—	0,07	0,07	0,1	—	0,05	—	0,08	—	—	0,08
$CaCO_3$	—	—	—	—	0,35	0,35	—	—	—	—	—	—	—	—
$KClO_4$	—	—	—	—	—	—	—	—	—	7,8	—	—	—	—

1) Component; 2) brand of powder; 3) Germany; 4) Great Britain; 5) USA; 6) slow burning; 7) nitrocellulose; 8) dinitro diethylene glycol; 9) dinitro triethylene glycol; 10) nitroglycerine; 11) dinitrotoluene; 12) trinitrotoluene; 13) centralite; 14) diethylphthalate; 15) diphenylamine; 16) diphenylurethane; 17) ethylphenylurethane; 18) hydrocellulose; 19) acardite; 20) stabilite; 21) TEN; 22) nitrosine; 23) α-nitronaphthalene; 24) dimethylphthalate; 25) carbon black; 26) wax.

The ratio between the fuel (combustible) and oxidizer in the composite solid propellant may vary within a rather wide range. This makes it possible to obtain the desired magnitude of oxygen balance in the propellant mixture, whereas in the case of smokeless powders the ratio between fuel and oxidizer is determined by the chemical composition of the components and the quantitative relationships governing the formation of colloidal solutions; in this case, this is a fully determined quantity which, as a rule, is less than unity. Finally, the catalog of initial products used for composite solid propellants is

almost unlimited, whereas for the fabrication of smokeless powder only certain nitrocellulose products and a restricted number of solvents can be used.

Among the basic shortcomings of composite solid propellants we should include the strong relationship between the parameters of the solid-propellant combustion and the dimensions of the particles that go to make up the powder, hygroscopicity, and danger of explosion.

The combustion parameters as a function of particle dimensions (of the components) and particularly of the particle dimensions of the oxidizer determine the increased instability of combustion for composite solid propellants.

In terms of a margin of internal energy, composite solid propellants exceed smokeless powders and, in certain cases, even some regular explosives; in view of this, they represent a danger of explosion. The normal combustion of these powders may result in detonation. Composite solid propellants may also be detonated by reaction to various external impact. Special experiments, carried out by the Thiokol Chemical Corporation (USA), have demonstrated that the sensitivity of composite solid propellants to external impact is a function primarily of the volumetric relationship between the fuel (combustible) and the oxidizer. The lower the volumetric ratio (given one and the same weight ratio), the more sensitive the powders.

For the most widely used ammonium perchlorate-based compositions, the maximum volumetric ratio of oxidizer to fuel (combustible) amounts to 2.85:1.0 (Fig. 4.1).*

Intensive work on seeking new rocket propellants and, in particular, on the testing of composite solid propellants is being carried on in America. For example, one USA firm developed an effective propellant which uses an inexpensive ammonium nitrate and a special com-

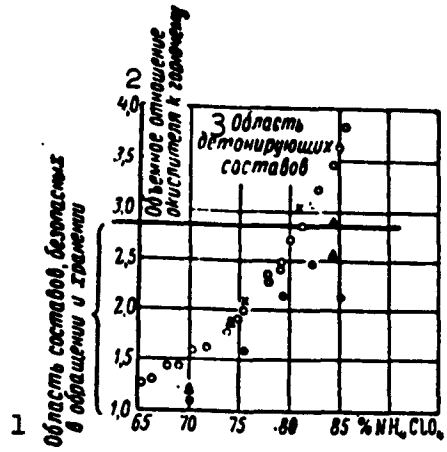

Fig. 4.1. Sensitivity of composite rocket solid propellants based on ammonium perchlorate to external impact as a function of the ratio of the volumetric content of fuel (combustible) and oxidizer in the propellant. O, ▲, ●) The points which correspond to various propellants tested for sensitivity to external impact; 1) region of compositions safe in handling and storage; 2) volumetric ratio of oxidizer to fuel (combustible); 3) region of detonating compositions.

bustible base. The fuel (combustible) base consists of a special material which polymerizes well with butadiene and yields a material exhibiting satisfactory bonding properties. Carbon black (2%) and a plasticizer (2%) are introduced into the composition in the form of admixtures.

The composite solid propellant produced by the Thiokol Chemical Corporation consists primarily of a polymer, an inorganic salt as the oxidizer, and a small quantity of certain chemical additives. It is assumed that polymers of butadiene and primarily polysulfide elastic materials are used as bonders in the solid propellants produced by this firm.

The Aerojet-General Firm developed a solid propellant, in 1957,

which uses polyurethanes as binders. On the basis of statements made by representatives of this company, the specific impulse of this propellant is assumed to be 240 kg·sec/kg. However, experience in working with polyurethane solid propellants has demonstrated that these exhibit a series of substantial shortcomings (instability in the rate of the oxidation reaction during combustion, rapid solidification with significant shrinkage, etc.), and they can therefore be recommended for use in engines only after appropriate finishing operations. Polyurethane solid propellants have not found any widespread application to this time. The firm has obtained patents on a series of solid composite propellants. One of these consists in the following:

trinitrocyclohexylamine..... 85%

plasticizer (wax)..... 15%

and in the other we use

ammonium perchlorate..... 50%

trinitrotoluene (TNT)..... 25%

thermoplastic binder (for example, asphalt)... 25%

The Aerojet-General Company and certain others (Hercules, Rohm and Haas) are working on solid monopropellants like nitropolymers and nitrated plastics. The Rohm and Haas Company recently announced the successful test of a new solid propellant of this type — "netrinacrylate" — for which we do not as yet have any data. It is assumed that the specific impulse of this propellant may be approximately 300 kg·sec/kg.

The British firm Imperial Chemical Industries developed an experimental solid propellant which is composed of:

ammonium nitrate..... 55-75%

calcium formate..... 45-25%

calcium stearate..... 0.5%

The solid propellant produced by the Grand Central Rocket Company consists of ammonium perchlorate, a polysulfide, and additives, producing a specific impulse of up to 250 kg·sec/kg.

The work being done on the development of composite solid propellants have been begun relatively recently, but the first specimens of such propellants have already been tested successfully in rocket engines of various designations. Examples of the compositions of such composite solid propellants are presented in Table 4.2.

TABLE 4.2

Chemical Composition of Some Composite Solid Rocket Propellants

1 Название компонента \ 2 Марка	3 Англия		4 США				
	ALt-161	5 Перхлоратный порох	GALSIT	NDRS	6 топливо фирмы Thiokol Chemical	7 состав на основе GALSIT	8 состав с пониженной температурой горения
9 Хлорнокислый калий	76,0	—	75,0	—	—	80,0	50,0
10 Перхлорат аммония	—	81,0	—	—	—	—	—
11 Пикрат аммония	—	—	—	45,0	—	—	—
12 Пикрат натрия	—	—	—	45,0	—	—	—
13 Нитрат аммония	—	—	—	—	80,0	—	—
14 Асфальтонефтепродукт	16,8	—	25,0	—	18,0	10,0	49,0
15 Смолистая связка	7,0	13,0	—	10,0	—	8,0	—
16 Специальные добавки	0,2	6,0	—	—	2,0	2,0	1,0

1) Component; 2) brand; 3) Great Britain; 4) USA; 5) perchlorate powder; 6) the propellant produced by the Thiokol Chemical Company; 7) a composition using GALCIT base; 8) a composition with a reduced combustion temperature; 9) potassium perchlorate; 10) ammonium perchlorate; 11) ammonium picrate; 12) sodium picrate; 13) ammonium nitrate; 14) asphalt-petroleum product; 15) resin binder; 16) special additives.

It is interesting to point out that composite rocket solid propellants were developed by the Germans as early as during the Second World War. However, the development of these propellants during that period was necessitated by the serious shortage of raw materials for

colloidal powers rather than the effort to obtain a powder (solid propellant) with increased characteristics. As an example of a composite solid propellant, developed in Germany toward the end of the Second World War, we can cite the Z-36 composition (in %):

tetranitrocarbonal	52.0
KNO_3	41.0
sawdust	3.0
polyvinyl acetate	2.0
carbon black	2.0

The heating value of the Z-36 powder amounted only to 650 kcal/kg, i.e., it was substantially lower than the regular colloidal powders.

Basic trends in the development of promising future solid propellants.* Of other trends in promising investigations which are receiving particular attention abroad at the present time we should make mention of the work being done on propellants exhibiting increased heating values, a low burning rate, a reduced sensitivity of the rate to changes in the initial temperature of the charge and to pressure fluctuations within the engine, as well as on powders which have an expanded range of stable combustion and a low combustion temperature. Work along these lines is being done both in order to develop new powders as well as to modify the propellants and powders that have already been adopted for armament purposes. Apparently, these developments are far from having been perfected, since no reports have appeared in the literature, which would permit us to draw any final conclusions nor to make any recommendations as to any operating compositions.

One of the trends in promising developments is the increase of the power characteristics of the propellants. With this purpose in mind, attempts have been made to use lithium, fluoride, boron-contain-

ing substances, and several others, as components for solid rocket propellants.

At the present time, much experimentation is being done on compositions which use nitrate and lithium perchlorate. Lithium perchlorate has an extremely high oxygen potential and may be used for the production of propellants exhibiting an extremely high specific impulse. In America, the American Potash Company, and others, are working on the development of lithium propellants.

Particular attention is being devoted to the propellants containing boron.* Boron has a high heating value (14,400 kcal/kg) and is capable, in combination with hydrogen, to form substances – boron hydrides – which have even greater heating values. A general shortcoming of the boron hydrides, in their application as fuels (combustibles) for rocket engines, is their toxicity, thermal instability, and several other properties which make it difficult to operate engines on propellants containing boron. Investigations which sought to improve the physicochemical properties of the boron hydrides resulted in the development of borohydrocarbons which exhibit satisfactory stability and toxicity parameters, but a somewhat reduced heating value. It is assumed that the solid propellant advertised by the Olin Mathieson Chemical Corporation is an alkylated pentaborane or decaborane.

Fluorine-containing solid propellants are quite effective, since fluorine is one of the most powerful of the known oxidizers; however, these propellants are extremely toxic and have not found any practical application to the present time.

Basic Rocket Solid Propellant Characteristics

In accordance with the requirements imposed on rocket solid propellants, the most important propellant characteristics are the following:

specific impulse..... j_1 kg·sec/kg

heating value..... $Q_{w(zh)}$ kcal/kg

referred force..... f_p kg-m/kg

specific weight..... γ g/cm^3

combustion temperature..... T_p °K

heat capacities of products of combustion, per unit mass..... C_pC_v kcal/kg°C

index of combustion process..... $k = C_p/C_v$

gas constant of products of combustion..... R kg-m/kg°K

boundary of anomalous combustion..... p^*_{min} kg/cm^2

The parameter which characterizes the effectiveness of the rocket engine from the standpoint of an increment in the momentum of the rocket as a result of the combustion of 1 kg of propellant is referred to as specific impulse. For contemporary propellants, the magnitude of specific impulse is equal, on the average, to

$$j_1 \approx 200 \text{ kg·sec/kg}.$$

Strictly speaking, j_1 is a characteristic not only of the propellant but of the entire rocket engine; it is therefore more proper to speak of the specific impulse of the engine. However, to make the comparative evaluation of various propellants more convenient it is the practice to employ this characteristic, determining its magnitude by burning the propellant charge in some standard test engine.

Much work is being done on increasing the specific impulse of propellants and engines. Data is available on the successful testing of engines having a specific impulse of up to 250-280 kg·sec/kg.*

The heating value of the propellant determines the reserve of thermal energy that is liberated in the engine on the combustion of the charge, and for various compositions averages 800 to 1250 kcal/kg. It should be borne in mind that because of the negative oxygen balance

in the solid-propellant compositions, i.e., because of a shortage of oxygen in conventional smokeless powders, as these are burned in a rocket engine only a part of the total reserve of internal heat energy is liberated (20-40%), whereas the remaining energy is liberated in the final oxidation of the products of combustion in the flame of the gas stream beyond the nozzle. The total heating value of smokeless powders is 3000-4000 kcal/kg. We can use the lost heating-value percentage by developing various engine combinations with complete combustion or by shifting the oxygen balance of the composition. The heating value of the powder is generally determined by carrying out experimental combustion tests. The magnitude of the heating value is equal to the quantity of heat liberated per 1 kg of powder burning in a closed volume, given the condition that the products of combustion are cooled by water to a temperature of +18°C. In first approximation, the magnitude of the heating value may be estimated by calculation, using the so-called β_i coefficients that have been determined experimentally. The change in the heating value of the powder is referred to as the coefficient β_i for the powder component; this change is brought about by the introduction of 1% of this component. It is conventionally maintained that β = const, i.e., the given quantity of any component, with some arbitrary powder composition, liberates a constant quantity of heat. This makes it possible to calculate the heating value in accordance with the following formula:

$$Q_{в(м)} \approx \sum_{i=1}^{s_p} p_i \beta_i. \qquad (4.1)$$

where β_i is the coefficient, in kcal/kg%; p_i is the content of the ith component in the powder, in %; s_p is the number of components in the powder composition.

The specific weight of the propellants for those compositions

that are already in production is found within the following range: $\gamma = 1.4\text{-}1.8$ g/cm^3. In order to obtain high engine characteristics, it is desirable to obtain a propellant with higher specific weight, since in this case it will be possible to concentrate a greater reserve of energy per unit volume of combustion chamber, or with a given magnitude of required energy reserve it will be possible to obtain smaller engine dimensions and weight.

With the combustion of a powder charge in the combustion chamber of an engine, temperatures of 2000-2500°C are developed. At such temperatures, almost all of the structural materials melt, and special heat-resistant compositions and alloys begin to lose their strength properties. However, because conventional solid-propellant rocket engines generally operate for only short periods of time, no dangerous overheating of the structure is, as a rule, observed; special cooling measures must therefore be implemented only in the region of the critical section of the nozzle. Nevertheless, it is recommended that propellants with lower combustion temperatures be selected. The high combustion temperature becomes a problem in the design of engines in which combustion lasts for 30 to 50 seconds or more. Such engines can function normally only if extensive use is made of special heat-insulation coatings or if forced-cooling systems are developed.

If we contend that the combustion process in a solid-propellant engine is isobaric, we will have

$$Q_{w(x)} = C_p T_p, \qquad (4.2)$$

i.e., the propellants with a high heat capacity C_p for the products of combustion (kcal/kg°C) will be characterized by low combustion temperature. On the other hand, if we use the well-known thermodynamic relationship

$$C_p = \frac{k}{k-1} AR, \qquad (4.3)$$

where k is the index of the process; R is the gas constant of the products of combustion; A is the thermal equivalent of work, and if we express R in terms of the universal gas constant

$$R = 848/\mu_\Sigma \text{ kg-m/kg}^\circ\text{K}, \qquad (4.4)$$

we will obtain

$$C_p = \frac{k}{k-1} A \frac{848}{\mu_\Sigma},$$

i.e., the products of combustion exhibiting low molecular weight will have greater specific heat capacity. Thus, all other conditions being equal, it would be desirable to use propellants whose products of combustion have low molecular weight and a high gas constant. The molecular weight of the gas mixture of the products of combustion is determined by the composition of the mixture and is calculated in accordance with the following formula:

$$\mu_\Sigma = \sum_{i=1}^{n} \mu_i r_i, \qquad (4.5)$$

where μ_i is the molecular weight of each of the products of gas combustion entering into the composition; r_i is the volumetric fraction of this gas in the mixture; μ_Σ is the so-called apparent molecular weight of the mixture.

The quantity that is conventionally referred to as the force of the powder is an extremely important characteristic for rocket propellants:

$$f_p = RT_p \text{ kg-m/kg}. \qquad (4.6)$$

The force of the powder is a complex characterization of the composition of the products of combustion and their temperature, and determines the specific operating capacity of the powder. In addition to the heating value, the force of the powder is a basic power character-

TABLE 4.3

Some Ballistic Characteristics of Rocket Propellants

1 Марка	2 $Q_{w(ж)}$ ккал/кг	3 γ г/см³	T_p °K	C_p[1]	k	4 f_p кгм/кг	5 j_1[2] кгсек/кг	6 p^*_{min} кг/см²
Z-167	830	1,58	2250	0,376	1,23	84 000	—	—
7 R-61 (Германия)	890	1,60	2390	0,382	1,24	87 400	—	—
17-H	790	1,62	2160	0,360	1,21	82 000	—	—
105-5	890	1,59	2390	—	—	86 900	—	—
JP	1230	1,60	3160	0,437	1,22	103 400	230	—
JPN	1230	1,61	3160	0,424	1,21	103 400	230	—
M-7	1250	—	3210	—	—	104 000	220	—
MPN	880	—	2310	0,398	—	86 800	—	—
8 R-61 (США)	—	1,62	—	—	1,23	—	240	20,0
JRN	895	—	2390	0,381	—	87 400	195	—
SC	955	—	2535	—	1,22	90 700	190	—
HSC	1170	1,64	3030	—	1,22	100 600	200	—
9 Экспериментальный английский порох	—	1,57	1700	0,367	1,24	—	160	—
ALt-161	—	1,77	1750	—	1,27	—	185	—
10 Английский перхлоратный порох	—	—	2400	0,367	1,26	—	—	—
11 GALSIT	—	1,74	1970	—	1,25	—	195	15,0
12 Состав фирмы Thiokol Chemical	—	1,55	1460	—	1,26	—	190	—
NDRS	—	1,77	1750	—	1,25	—	200	—
13 Низкотемпературный состав	—	1,65	1520	—	1,24	—	165	—
14 Состав, полученный на основе GALSIT	—	1,94	2700	—	1,27	—	210	—

*The quantity C_p is a function of temperature and pressure. The table presents the value of C_p (and correspondingly of k) at p = 100 kg/cm² and temperature T_p for each propellant.

**The magnitude of the specific impulse is presented for the standard test engine at a pressure of 70 atm and a nozzle expansion of d_a/d_k = = 2.24.

1) Brand; 2) $Q_{w(zh)}$, kcal/kg; 3) γ, g/cm³; 4) f_p, kg-m/kg; 5) j_1,** kg·sec/kg; 6) p^*_{min}, kg/cm²; 7) R-61 (Germany); 8) R-61 (USA); 9) experimental British powder; 10) British perchlorate powder; 11) GALCIT; 12) composition produced by the Thiokol Chemical Company; 13) low-temperature composition; 14) composition based on GALCIT.

istic of the propellant.

With respect to the quantity p^*_{min} which determines the lower boundary of pressures at which the propellant will burn without anomalies, it should be pointed out that the boundary of permissible pressure values must be as low as possible. In this case, it will be possible to design an engine for low operating pressures, i.e., with minimum wall thicknesses and correspondingly low structural weight. Contemporary foreign propellants exhibit a limit pressure boundary of the order of 15 to 35 kg/cm^2.

It has been established that the quantity p^*_{min} is determined not only by the properties of the propellant, but by the structural features of each individual engine; therefore, under certain conditions p^*_{min} increases to higher values. The problems of anomalous combustion and the selection of the operating pressure are examined in greater detail below; here we must concern ourselves only with the fact that the best propellants are those which under comparable conditions burn normally at lower pressures.

Some characteristics of various propellants are presented in Table 4.3. It should be pointed out that with respect to individual propellants, contradictory data are encountered in the literature, and therefore the corresponding characteristics are not presented because of their doubtful reliability.

§2. APPROXIMATE CALCULATION OF THE COMPOSITION OF THE PRODUCTS OF COMBUSTION

Many of the processes that take place within a solid-propellant rocket engine, and some of the parameters of interior ballistics, are strong functions of the composition and the properties of the products of propellant combustion; therefore the determination of the composition of the products of combustion is an extremely important matter.

In first approximation, the calculation of the composition of the products of combustion can be reduced to finding and solving a system of equations for the coefficients of the propellant-combustion reaction, and this system of equations, in general form, is written as follows:

$$C_aH_bO_cN_d \rightarrow x\,CO_2 + y\,CO + z\,H_2 + u\,H_2O + \frac{d}{2}N_2.$$

where $C_aH_bO_cN_d$ is the so-called conventional formula for the propellant; a, b, c, and d are the number of gram-atoms of the corresponding elements in a conventional molecule of propellant; x, y, z, u, and d/2 are the number of gram-molecules of the corresponding substances in the products of propellant combustion (the coefficients of the reaction).

The notation which enumerates all of the above chemical elements that enter into the composition of the propellant components is referred to as the conventional formula; this formula indicates the total gram-atoms of these elements for all components. The conventional formula is found on the basis of the chemical composition of the propellant and is derived for 1 kg of propellant.

The procedure employed for the derivation of the conventional formula is best demonstrated in a specific example. Let us examine a propellant having the following composition (in %):

nitrocellulose (12.2% N)	56.6
nitroglycerine	28.0
dinitrotoluene	11.0
centralite	4.4
industrial wax	0.1

and the known chemical formulas of the individual components:

nitrocellulose (12.2% N)..... $C_{22.5}O_{36.16}H_{28.8}N_{8.7}$

nitroglycerine..... $C_3H_5(ONO_2)_3$

dinitrotoluene..... $C_6H_6(CH_3)(NO_2)_2$

centralite..... $CON_2C_2H_5(C_6H_5)_2$

industrial wax..... $C_{20}H_{42}$,

where the formula for nitrocellulose is derived through the utilization of the following relationships:

$$\left.\begin{aligned} C_{n.c} &= 21{,}85 - 1{,}180\,(N\% - 12{,}75);\\ O_{n.c} &= 36{,}40 + 0{,}444\,(N\% - 12{,}75);\\ H_{n.c} &= 27{,}32 - 2{,}690\,(N\% - 12{,}75);\\ N_{n.c} &= 9{,}10 + 0{,}722\,(N\% - 12{,}75) \end{aligned}\right\} \qquad (4.7)$$

(N is the nitrogen content, in %, in the nitrocellulose of the powder).

According to definition, the conventional powder formula will take the following form:

$$C_{\sum_{j=1}^{5} C_j}\ H_{\sum_{j=1}^{5} H_j}\ O_{\sum_{j=1}^{5} O_j}\ N_{\sum_{j=1}^{5} N_j}$$

where, for example, $\sum_{j=1}^{5} C_j$ is the sum of the gram-atoms of carbon in each of the five components of the given composition, per 1 kg of powder.

We will find C_j for one of the powder components; for example, we will find this quantity for dinitrotoluene. In accordance with the chemical formula, there are seven atoms of carbon in the molecule of this substance; on the other hand, if the powder contains 11% dinitrotoluene, there will be 110 g of the substance in 1 kg of the powder. Hence the number of gram-atoms of carbon in the total of the subscripts in the conventional powder formula will be

$$C_j = 7\frac{110}{182} = 4{,}23.$$

or, in general form

$$C_j = n_j \frac{g_j}{\mu_j} \qquad (4.8)$$

where n_j is the number of carbon atoms in a molecule of the jth component of the powder; g_j is the weight fraction of the jth component, in 1 kg of powder; μ_j is the molecular weight of the jth component.

As a result, the subscript of the conventional formula is defined as the sum

$$a=\sum_{j=1}^{s} C_j=\sum_{j=1}^{s} n_j \frac{g_j}{\mu_j}, \qquad (4.9)$$

where s is the number of components entering into the composition of the given powder.

The subscripts for the other elements in the conventional formula are determined in much the same manner.

Without dwelling in detail on the calculation, we will present the calculation results in special form (Table 4.4).

After the conventional formula for the powder has been formed, we determine three relationships for the calculation of the combustion-reaction coefficients, and these relationships are equations of the material balance of the reacting substances:

$$a=x+y,$$
$$b=2z+2u,$$
$$c=2x+y+u.$$

It should be borne in mind that in addition to the basic combustion reaction

$$C_aH_bO_cN_d \rightarrow x\,CO_2+y\,CO+z\,H_2+u\,H_2O+\frac{d}{2}N_2,$$

secondary reversible reactions take place in the gaseous products, and of these the following are the basic reactions:

$$2CO \rightleftarrows CO_2+C,$$
$$H_2O+CO \rightleftarrows CO_2+H_2$$

and the dissociation reactions:

$$CO_2 \rightleftarrows CO+O,$$
$$H_2O \rightleftarrows H+OH.$$

It has been demonstrated by special analysis that for the pressures and temperatures characteristic of the combustion chambers in a solid-propellant rocket engine, the equilibrium constant of the reaction

$$2CO \rightleftarrows CO_2 + C$$

is so great that this reaction may be regarded as shifted as far as possible to the left, i.e., it need not be considered in practical calculations. The dissociation reactions also play no significant role, so that we must take into consideration only the following reaction:

$$H_2O + CO \rightleftarrows CO_2 + H_2,$$

which is written in the following form for the products of propellant combustion:

$$u\,H_2O + y\,CO \rightleftarrows x\,CO_2 + z\,H_2.$$

The equilibrium constant of this reaction

$$K = \frac{[H_2O]\,[CO]}{[CO_2]\,[H_2]}$$

yields the additional equation

$$K = \frac{uy}{xz};$$

which when taken into consideration serves to close the system of equations employed for the determination of the combustion-reaction coefficients:

$$\left.\begin{aligned} a &= x + y \\ b &= 2z + 2u, \\ c &= 2x + y + u, \\ K &= \frac{uy}{xz}. \end{aligned}\right\} \qquad (4.10)$$

The quantity K is a function of the temperature of the products of combustion; therefore, the solution of the system can be found only if the temperature of powder combustion is known. If the combustion temperature is not given, we proceed in the following manner. We assume

TABLE 4.4

Data for the Calculation of the Conventional Propellant Formula

1 Название компонента	2 Химическая формула компонента	3 Молекулярный вес компонента	4 Содержание в 1 кг пороха	5 Содержание отдельных элементов на 1 кг пороха в г-ат			
				$C_j = n_j \frac{g_j}{\mu_j}$	$H_j = k_j \frac{g_j}{\mu_j}$	$O_j = m_j \frac{g_j}{\mu_j}$	$N_j = f_j \frac{g_j}{\mu_j}$
6 Нитроклетчатка	$C_{22.5}H_{28.5}O_{36.16}N_{9.7}$	1000	565	12,70	16,25	20,40	4,91
7 Нитроглицерин	$C_3H_5(ONO_2)_3$	227	280	3,70	6,18	11,10	3,70
8 Динитротолуол	$C_6H_3(CH_3)(NO_2)_2$	182	110	4,23	3,63	2,42	1,21
9 Централит	$CON_2C_2H_5(C_6H_5)_2$	302	44	2,18	2,18	0,14	0,29
10 Воск технический	$C_{20}H_{42}$	282	1	0,07	0,15	—	—
11 Итого в 1 кг топлива будет,				22,88	28,39	34,06	10,11
12 т. е. условная формула запишется так: $C_{22.88}H_{28.39}O_{34.06}N_{10.11}$							

Note. k_j, m_j, and f_j are the number of hydrogen, oxygen, and nitrogen atoms in a molecule of the jth component of the propellant.

1) Component; 2) chemical formula for component; 3) molecular weight of component; 4) content in 1 kg of powder; 5) content of individual elements in 1 kg of powder, in gram-atoms; 6) nitrocellulose; 7) nitroglycerine; 8) dinitrotoluene; 9) centralite; 10) industrial wax; 11) the total for 1 kg of propellant will be; 12) i.e., the conventional formula is written as follows: $C_{22.88}H_{28.39}O_{34.06}N_{10.11}$.

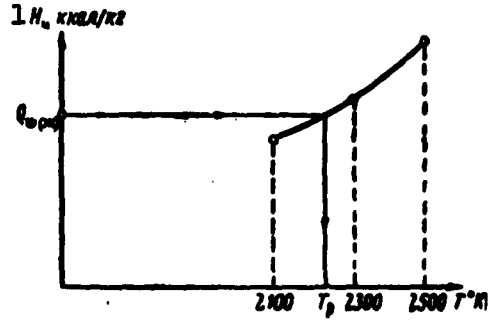

Fig. 4.2. Graph for the determination of true temperature of the products of powder combustion. H_1 is the heat content (enthalpy) of the powder; 1) H_1, kcal/kg.

three tentative values of T_p and the composition of the products of combustion for each temperature is determined. On the basis of the composition of the products of combustion and the heat content of the components of the gas mixture, the total heat content of the products of combustion is determined; a comparison of the heat contents against the heating value of the powder makes it possible to find the temperature of the products of combustion (Fig. 4.2), on the basis of which we can refine the composition of the products of combustion.

A more detailed calculation of the temperature of the products of combustion was presented in the book by G.B. Sinyarev and M.V. Dobrovol'skiy: "Zhidkostnyye raketnyye dvigateli" (Oborongiz, 1957) ["Liquid Rocket Engines" (State Defense Industry Press, 1957)].

If we know the composition of the products of combustion, we can easily calculate the basic quantities which characterize the properties of the gas mixture. For example, in accordance with the laws governing gas mixtures, partial pressures of individual components of the mixture can be calculated according to the following formula:

$$p_i = p_\Sigma r_i, \qquad (4.11)$$

where p_i is the partial pressure of the ith component of the gas mixture; p_Σ is the total pressure in the gas mixture, said pressure equal to the pressure within the combustion chamber; r_i is the volumetric fraction of the gas in the mixture.

The apparent molecular weight μ_Σ of the mixture will be

$$\mu_\Sigma = \sum_{i=1}^{s_r} \mu_i r_i, \qquad (4.12)$$

where μ_i is the molecular weight of the ith gas in the composition of the mixture; s_r is the number of components in the mixture.

If we know these quantities, we can determine the heat capacity of the products of combustion, their gas constant, and certain other

parameters which are of great significance for the interior-ballistic and thermal calculations for the engine. The composition of the products of complete combustion of certain solid propellants is presented in Table 4.5.

TABLE 4.5

Composition of the Products of Combustion of Certain Brands of Solid Rocket Propellants

1 Компоненты продуктов сгорания / 2 Марка	JPN	JP	M-7	ALt-161	BACA	HSC	Английский перхлортный порох 3
CO_2	25,1	27,1	24,8	3,3	26,3	25,3	
CO	26,0	25,0	24,7	44,0	24,9	25,7	
H_2O	28,3	28,0	28,5	9,9	27,7	27,9	
H_2	5,0	3,9	4,1	27,4	3,8	4,7	
N_2	15,1	16,5	14,9	0,1	15,9	15,4	
OH	0,5	0,4	0,4	—	0,6	—	
4 Твердые частицы	—	—	0,9	—	1,1	0,4	
KCl	—	—	1,7	15,1	—	—	
SO_2	—	—	—	0,2	0,3	—	
5 Молекулярный вес μ_Σ	27,8	28,0	28,7	30,0	27,9	25,0	25,0

Note. Composition of the products of propellant combustion is presented in molecular percentages for p = 70 atm.

1) Components of the products of combustion; 2) brand; 3) British perchlorate powder; 4) solid particles; 5) molecular weight μ_Σ.

§3. BASIC QUANTITATIVE RELATIONSHIPS GOVERNING COMBUSTION OF SOLID ROCKET PROPELLANTS

Mechanism of Combustion of Solid Rocket Propellants

On the basis of published works, we would come to the conclusion that only the combustion of colloidal powders has been studied in sufficient detail up to the present time. It is for this reason that all that follows is of direct significance only with respect to the combustion of smokeless rocket powders of this class. With respect to composite propellants it has been established experimentally that, in

first approximation, the basic quantitative relationships governing the combustion of these propellants can be assumed to be the same as in the case of the colloidal powders.

As a rule, a great quantity of various components are included in the composition of the powder; these components form complex physical and chemical bonds between one another and, therefore, the powder combustion is a complex multistage process.

The earliest experiments and the first theoretical generalizations of the observation results made it possible to establish that the powder, as a rule, burns in parallel layers, and it was also established that the basic reactions of the combustion process occur in the gas phase; in addition, it was determined that the combustion of the powder precedes the thermal decomposition of the surface layer of the powder grain. Since nitrocellulose, the base of the rocket powder, is nonvolatile, it was not possible to explain the mechanism of the formation of the gas phase until 1942; it was at this time that the hypotheses as to the gasification of the products of the thermal decomposition of the surface layer of the powder was offered; in addition, it was impossible to offer an explanation for the above until we were able to obtain theoretical results that were in good agreement with experimental data.*

By gasification we mean the process of the primary decomposition of the solid propellant which results in the disruption of certain chemical bonds and produces gaseous products and solid particles that are suspended in the gas phase. These products enter into final chemical reactions of combustion within the confines of the gas phase.

In the opinion of many specialists and investigators, the disruption of the solid phase is the stage of combustion which determines the rate of the entire process and this, in the general case, is not

equal to the rate of the formation of the primary gaseous products, said rate calculated in accordance with the following formula:

$$m_r = k_m e^{-\frac{E}{RT_z}}, \qquad (4.13)$$

where m_r is the mass rate of gas formation; k_m is some constant of the process; E is the total energy of activation; R is the gas constant; T_z is the gas temperature at the boundary of separation between the solid and gas phases.

We can present, in the following form, a more complete picture of the successive processes taking place in the powder during combustion in the chamber of the rocket engine.

As the outer layer of the powder grain is heated to temperatures of 100-120°C, the molecular bonds of the nitrocellulose in the powder grain are depolymerized and the solvate-hydrate complexes of the molecules are destroyed.

With continued increase in temperature, the stronger chemical and physical bonds are destroyed, and by t = 200-220°C a liquid-viscous layer of melted powder is formed at the surface of the grains.

The volatile components of the powder are vaporized at the surface of the liquid-viscous layer and the nitrocellulose is gasified; as a result, a layer of so-called vapor-gas is formed at the surface of the grain. The region in which the gas phase is formed is referred to as the zone of powder gasification. Here, in the immediate vicinity of the burning surface, the products of the gasification virtually do not interact, and only certain exothermic reactions take place; these are of no particular significance. The stream of particles in the gasification zone is normal to the surface of the grain. The products of the gasification, entrained by this stream, are carried into the vapor-gas cloud where the combustible mixture of the gases is prepared.

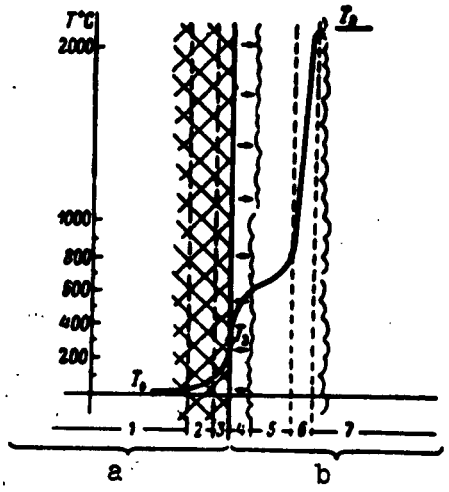

Fig. 4.3. Diagram of the combustion of a colloidal rocket solid propellant. T_z) gas temperature at the boundary of separation between the solid and gas phases; T_0) initial charge temperature; a) solid powder phase; b) gaseous products; 1) cupola of grain with initial powder parameter; 2) zone of primary decomposition of powder components; 3) liquid-viscous layer; 4) gasification zone; 5) zone of combustible mixture preparation; 6) zone of combustion; 7) products of powder combustion.

The final combustion reactions which take place intensively in the so-called zone of combustion are initiated in the layer of the vapor-gas cloud where a corresponding concentration of active products is achieved. At the end of the combustion zone, the gas temperature attains the isobaric combustion temperature.

Figure 4.3 shows a diagram of the combustion of a colloidal powder. A detailed study of the reactions taking place within the combustion zone has demonstrated that these take place successively, in two stages. At the end of the first stage, the products of incomplete oxidation predominate in the products of combustion and these contain ox-

ides of unreduced nitrogen. In this case, approximately one half of the enthalpy of the powder is liberated. During the second stage, the complete reduction of the nitrogen from its oxides takes place, and the remaining substances are oxidized. The reactions of this phase liberate the remaining 50% of the energy of powder combustion.

It has been established that as the combustion terminates on the completion of the reactions of the first stage alone, low-frequency pressure fluctuations are observed in the engine, combustion becomes unstable in nature, and there is a tendency to anomalous attenuation. On the other hand, the reactions of the second stage may take place only under definite conditions within the engine, and we have reference here particularly to pressures not below some definite operating pressure for the given powder composition. Thus the nature of the phases of the powder-combustion mechanism is a function of the parameters of the interior ballistics of the engine and the engine design; in order to liberate a greater quantity of energy within the combustion chamber and to achieve stable combustion, we require conditions which guarantee the occurrence of the chemical reactions of the second combustion stage.

On completion of the combustion reaction, the gaseous products that have been formed move through open passages in the engine to the nozzle and are ejected. As a result of the discharge of the products of combustion, a reactive force is developed and this force is the reaction of the exhaust stream of the products of combustion.

It should be pointed out that the sequence of processes (examined in detail) that takes place in the combustion of solid rocket propellants is not absolutely reliable. However, it may be used as an operating diagram of the combustion, since it yields results that are, for the most part, in good agreement with experimental data.

Burning Rate Function

One of the basic features of a solid-propellant rocket engine is the fact that the burning rate of the powder in the engine is a strong function of the magnitude of the pressure in the combustion chamber. The linear burning rate of the powder as a function of pressure is generally referred to as the powder-combustion function, and here by linear (mechanical) burning rate for the powder grains we mean the rate at which the burning surface of the charge shifts in the direction of the inside normal:

$$u_1 = \frac{de}{dt},$$

where u_1 is the linear burning rate; e is the so-called cupola of the grain (the minimum distance covered by the burning front during the time of engine operation).

The physical nature of the burning rate as a function of pressure is obvious. In fact, the burning rate is defined as the rate at which the chemical reactions take place in the zone of combustion and it is determined by the quantity of gases entering into this zone of combustion from the grain.

The quantity of these gases is directly proportional to the mass rate of formation of the gaseous products of primary powder decomposition, which in accordance with (4.13) increases as the temperature in the vicinity of the charge surface rises. Thus, the combustion (burning) rate in the final analysis increases as the temperature in the vicinity of the charge surface rises. The characteristic curve of this function is presented in Fig. 4.4. On the other hand, the grain is heated as a result of the transfer of heat between the upper layer of the grain and the high-temperature zone of combustion. The heat flow to the grain may be regarded as inversely proportional to the distance

Burning Rate Function

One of the basic features of a solid-propellant rocket engine is the fact that the burning rate of the powder in the engine is a strong function of the magnitude of the pressure in the combustion chamber. The linear burning rate of the powder as a function of pressure is generally referred to as the powder-combustion function, and here by linear (mechanical) burning rate for the powder grains we mean the rate at which the burning surface of the charge shifts in the direction of the inside normal:

$$u_1 = \frac{de}{dt},$$

where u_1 is the linear burning rate; e is the so-called cupola of the grain (the minimum distance covered by the burning front during the time of engine operation).

The physical nature of the burning rate as a function of pressure is obvious. In fact, the burning rate is defined as the rate at which the chemical reactions take place in the zone of combustion and it is determined by the quantity of gases entering into this zone of combustion from the grain.

The quantity of these gases is directly proportional to the mass rate of formation of the gaseous products of primary powder decomposition, which in accordance with (4.13) increases as the temperature in the vicinity of the charge surface rises. Thus, the combustion (burning) rate in the final analysis increases as the temperature in the vicinity of the charge surface rises. The characteristic curve of this function is presented in Fig. 4.4. On the other hand, the grain is heated as a result of the transfer of heat between the upper layer of the grain and the high-temperature zone of combustion. The heat flow to the grain may be regarded as inversely proportional to the distance

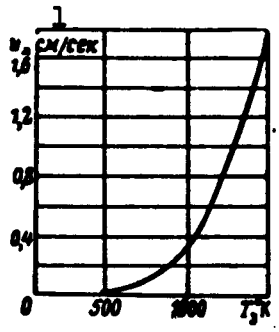

Fig. 4.4. The curve showing the burning rate of a colloidal powder as a function of the temperature near the surface of the burning grain. 1) u_1, cm/sec.

Fig. 4.5. Diagram clarifying the burning rate as a function of the magnitude of pressure in the engine.

$$q_1 = k/\delta(p)\ (T_p - T_z) = f(p)\ [\text{kcal/m}^2\text{hr}].$$

k) a powder constant; $\delta(p)$ the distance from the zone of combustion to the surface of the grain; T_p) the temperature of the products of combustion; T_z) the temperature close to the surface of the charge; 1) the flow of the products of combustion; 2) p, kg/cm^2; 3) reverse heat flow; 4) powder grain.

between the surface of the grain and the combustion zone, i.e., the

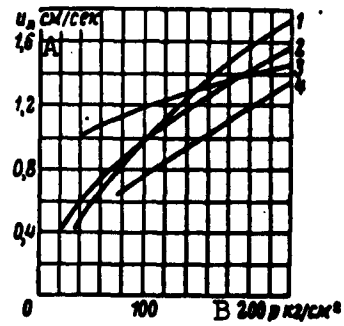

Fig. 4.6. Characteristic curves of the relationship between the burning rate u and the pressure p for colloidal powders of various compositions. 1-4) Powder compositions; A) u_1, cm/sec; B) 200 p, kg/cm^2.

burning rate, all other conditions being equal, is all the greater, the smaller the distance between the combustion zone and the surface of the grain (Fig. 4.5).

What takes place in the engine as the pressure within the engine is increased? With an increase in pressure, the vapor-gas cloud is compressed against the surface of the grain and the transfer of heat between the grain and the combustion zone is intensified. As a result, the temperature close to the surface of the charge rises and, consequently, the rate of gas formation increases, i.e., the mass of products entering the combustion zone increases. All of this results in a situation in which the rate of powder burning increases. Conversely, with a drop in pressure in the engine, the vapor-gas cloud moves away from the surface of the grain and the intensity of heat transfer between the cloud and the grain diminishes, thus resulting in a reduction in the burning rate.

It should be pointed out that in the case of an unlimited increase in pressure there is a certain minimum distance between the surface of the grain and the combustion zone (of the order of the mean molecular

free path), i.e., there must exist some maximum burning rate. On the other hand, with a reduction in pressure, the burning rate can be reduced to zero (the damping of the combustion process), if the heat transferred to the grain from the zone of combustion is inadequate to permit vaporization processes and the gasification of the liquid-viscous powder layer.

As has already been indicated, in first approximation the combustion rate may be regarded as constant at any point on the surface of the grain. The hypotheses as to the burning in parallel layers become invalid only in the case of engines exhibiting a high ratio of burning surface to free combustion-chamber cross section, where the burning rate increases along the surface of the grain; however, this case may be regarded as special.

The theoretical determination of the relationship between the burning rate and the pressure involves certain difficulties because of the features encountered in the chemical kinetics of the reactions taking place in the various zones of the vapor-gas cloud, and because the basic quantitative relationships governing diffusion and heat transfer in the gaseous products are extremely complex. Moreover, the very structure of the vapor-gas cloud remains essentially uninvestigated. Therefore, it is the general practice to seek the laws governing burning in the form of certain empirical relationships which will generalize the experimental data from a statistical standpoint.

The evaluation of the results obtained in experimental burning of powders has shown that it is impossible to represent the function of the burning $u_1 = u_1(p)$ by a single function for the various powders and the wide range of possible values for the operating pressures. Therefore, the burning functions for various powders are expressed in various ways.

In this case, the so-called power burning functions have become the most commonly used:

$$u_1 = A + Bp^{\nu},$$
$$u_1 = u_1 p^{\nu},$$

which approximate the relationship between the burning rate of colloidal powders and the pressure in a range from 100 to 150 kg/cm^2 comparatively well. Given higher pressures (up to 300 kg/cm^2) the burning function for the powders generally approaches a linear function:

$$u_1 = Ap + B,$$
$$u_1 = u_1 p.$$

In the formulas for the burning functions that have been presented above, u_1 is the linear burning rate, in cm/sec; p is the operating pressure in the combustion chamber, in kg/cm^2; A, B, ν, and u_1 are certain experimental coefficients that are functions of the powder composition, the initial temperature of the charge, the operating pressure, and certain similar parameters.

Table 4.6 presents, as an example, the burning functions of certain powders. These functions have been averaged over the entire pressure interval and must therefore be regarded as approximate functions, yielding only a general qualitative characteristic for the relationship between the burning rate and pressure. In practical calculations it becomes necessary to bear in mind that the coefficients of the burning function are themselves functions of the magnitude of pressure.

Figure 4.6 shows characteristic curves of the relationship between the burning rate and pressure for several colloidal powders.

As a result of the fact that the burning rate is a function of pressure, the engine characteristics are unstable, and we also have the fact that the actual combustion process exhibits tendencies to oscillation in the case of pressure fluctuations appearing within the

TABLE 4.6

Burning-Rate Function for Several Rocket Solid Propellants

1 Марка / 2 Диапазон давлений и начальная температура заряда	3 $p^*_{min} < p < 150$ кг/см²			4 150 кг/см² $< p <$ 300 кг/см²		
	$t_0 = -20°$ C	$t_0 = +20°$ C	$t_0 = +60°$ C	$t_0 = -20°$ C	$t_0 = +20°$ C	$t_0 = +60°$ C
JP	$0{,}0683p^{0.71}$	$0{,}0632p^{0.71}$	$0{,}1011p^{0.71}$	—	$0{,}0049p+0{,}32$	$0{,}006p+0{,}41$
JPN	$0{,}0762p^{0.69}$	$0{,}0879p^{0.69}$	$0{,}1016p^{0.69}$	—	$0{,}0043p+0{,}51$	—
5 Медленно горящий английский состав	$0{,}0323p^{0.70}$	$0{,}0375p^{0.67}$	$0{,}0436p^{0.70}$	—	$0{,}0029p+0{,}22$	—
17-H	$0{,}0233p^{0.72}$	$0{,}0270p^{0.72}$	$0{,}0315p^{0.72}$	—	—	—
ALt-161	—	$0{,}0297p^{0.70}$	—	—	—	—
6 Английский перхлоратный порох	—	$0{,}0045p^{0.4}$	—	—	—	—

1) Brand; 2) range of pressures and initial temperature of charge; 3) $p^*_{min} \leq p \leq 150$ kg/cm^2; 4) 150 kg/cm$^2 \leq p \leq 300$ kg/cm^2; 5) slow burning British composition; 6) British perchlorate powder.

engine. In this connection, there is some interest in the work being done to find powder compositions whose burning rate is independent or virtually independent of changes in pressure within the engine.

The Burning Rate as a Function of the Initial Charge Temperature t_0

As has already been stated, the physicochemical decomposition processes involving the components of the powder precede the actual combustion of the powder; here, the powder components enter the solid phase and, as a rule, the decomposition processes are accompanied by absorption of heat. The intensity of these processes is a function of the intensity of heat transfer to the surface of the grain. The lower the initial temperature of the powder charge, the greater the quantity

of heat that must be supplied in order for the primary reactions of the destruction of the solid powder phase and the formation of the vapor gas to take place. If we maintain that the magnitude of the reverse heat flow from the zone of combustion to the solid phase of the propellant is approximately constant (this is what is observed in a solid-propellant rocket engine), it is easy to understand that for low initial charge temperatures a correspondingly large heating-time interval is required for the surface layer of the grain, as a result of which the relative rate of the chemical processes resulting in the formation of the gas phase will be low and, consequently, the burning rate of the powder will also be low.

The thermal conductivity of the powder is comparatively low (in comparison with the burning rate), so that during the burning time the grain is not heated up, i.e., the temperature in the main part of the grain remains virtually unchanged. Thus the relationship between the burning rate and the initial charge temperature is preserved throughout the entire burning time and it is for this reason that the second basic characteristic of powder combustion appears.

In first approximation we may assume that a change in the burning rate with a change in pressure in the engine and the initial charge temperature are mutually independent. In this case, in order to take into consideration the effect of these two factors on the burning rate, we can use two various functions, so that

$$u_1 = u(p) f(t_0),$$

where u_1 is the burning rate; u(p) is the burning-rate function for the powder; $f(t_0)$ is a dimensionless function by means of which we take into consideration the effect of initial charge temperature on the burning rate; this function is generally referred to as the temperature function of combustion.

It is most convenient to introduce $f(t_0)$ as the quantity which indicates the extent to which the burning rate undergoes change at any given temperature in comparison with some established rate such as, for example, the rate at $t_0 = +20^\circ C$ (at p = const). In this case

$$f(t_0) = \frac{u_z(p, t_0)}{u_z(p, t_0 = +20^\circ)}. \qquad (4.15)$$

In the general practice of calculations $f(t_0)$ is calculated in terms of the temperature coefficient β_t of the burning rate in accordance with the following formula:

$$f(t_0) = 1 + \beta_t (t_0 - 20^\circ), \qquad (4.16)$$

where β_t indicates the change in powder burning rate with a change in charge temperature by 1° (from a temperature of $+20^\circ C$),

$$\beta_t = \frac{u_z(p, t_0) - u_z(p, t_0 = +20^\circ)}{u_z(p, t_0 = +20^\circ)} \frac{1}{t_0 - 20^\circ}. \qquad (4.17)$$

In differential form, more suitable for the subsequent mathematical transformations,

$$\beta_t = \frac{1}{u_{+20}} \frac{du}{dt_0}, \qquad (4.18)$$

where t_z is the variable temperature of the charge.

Experiments have demonstrated that the temperature coefficient of the burning rate is not an absolute constant and changes somewhat with a change in the temperature of the charge and the pressure within the combustion chamber; however, this need not be taken into consideration in the tentative calculations.

The relationship $\beta_t = \beta(p)$ is important only in the case of low pressures; if we neglect $\beta_t = \beta(p)$ for pressures in excess of 50-70 kg/cm^2, this will have virtually no effect on the accuracy of the calculation results. With respect to the relationship $\beta_t = \beta(t_z)$, this will have an effect on the temperature function of the burning rate throughout the entire possible temperature interval of rocket engine

application. The relationship $\beta_t = \beta(t_z)$ is generally presented in the following form:

$$\beta_T = \frac{1}{B_T - (t_0 - 20^\circ)}, \qquad (4.19)$$

where B_t is some constant of the powder whose magnitude is inversely proportional to the temperature coefficient of the burning rate at 20°C.

If we take (4.19) into consideration, the temperature function of the combustion can be presented in the following form:

$$f(t_0) = 1 + \beta_T (t_0 - 20^\circ) = \frac{B_T}{B_T - (t_0 - 20^\circ)} = \frac{1}{1 - \frac{t_0 - 20^\circ}{B_T}}. \qquad (4.20)$$

TABLE 4.7

1 Температурный интервал °C	2 Средняя температура интервала $t_{ср}$	3 Среднее значение температурного коэффициента
−100÷ −40	−70	$2{,}2 \cdot 10^{-3}$
− 40÷0	−20	$2{,}16 \cdot 10^{-3}$
−10÷+10	0	$4{,}6 \cdot 10^{-3}$
0÷+20	+10	$7{,}0 \cdot 10^{-3}$
+20÷+40	+30	$10{,}3 \cdot 10^{-3}$
+40÷+80	+60	$14{,}0 \cdot 10^{-3}$

1) Temperature interval, °C; 2) mean temperature interval, t_{sr}; 3) mean value of the temperature coefficient.

Experiments have shown that at atmospheric pressure the relationship $\beta_t = \beta(t_z)$ can be characterized by the indicated values of the temperature coefficient, as presented in Table 4.7.

In tentative calculations, it may be maintained that for the majority of colloidal powders the change in the temperature of the charge by 1°C for the operating pressures characteristic for solid-propellant engines changes the burning rate on the average by 0.1-0.5% (in the

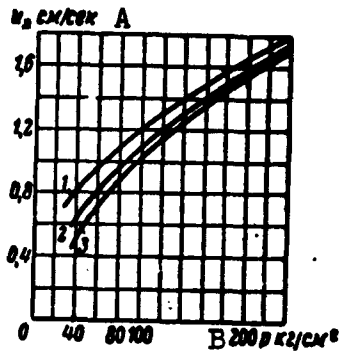

Fig. 4.7. Curves for the burning rate of colloidal powder for various conditions of ignition. 1) $t_0 = +60^\circ C$; 2) $t_0 = +20^\circ C$; 3) $t_0 = -20^\circ C$. A) u_1, cm/sec; B) 200 p, kg/cm^2.

same direction).

Figure 4.7 shows a family of combustion curves for various initial charge temperatures for a colloidal rocket powder.

Relationship between the Burning Rate and the Structural Features of the Engine (Combustion Anomalies)

An extremely important feature of the operation of a rocket solid-propellant engine is the relationship between the parameters of the combustion process and, in particular, the magnitude of the burning rate and the structural features of each specific engine and the relationship between certain geometric characteristics of the powder charge and the dimensions of the combustion chamber.

From this standpoint it is interesting to point to two basic phenomena which are observed in solid-propellant engines: erosive burning and vibration burning (referred to as resonant burning ["chugging" or "screaming"] in American literature).

Erosive burning. Erosive burning is observed, as a rule, at the initial instant of engine operation and primarily in structures in which the magnitude of the free combustion-chamber cross section is

somewhat greater than the area of the critical section of the nozzle. With this relationship between the dimensions of the flowthrough sections, the velocity of the motion of the products of combustion along the surface of the grain can increase noticeably and attain substantial magnitudes in the sections of the nozzle. With sufficiently high velocities, a local increase in burning intensity is observed, and this acceleration of burning is referred to as erosive burning.

The magnitude of the linear burning rate in the cross sections in which erosive burning u_1^v takes place is proportional to the local velocity of the flow

$$u_1^v = u_1(1 + k_v w_r), \qquad (4.21)$$

where u_1 is the rated (calculated) linear burning rate, without any consideration of the effect of the flow of products of combustion; k_v is the erosive-burning coefficient; w_g is the velocity of the stream (flow) of the products of combustion in the given cross section.

The physical nature of the appearance of erosive burning can be presented in the following form. Given a sufficiently high rate of gas flow from the burning surface and comparatively small dimensions for the flowthrough sections, a local increase in static pressure in the stream of the products of combustion and an increase in the velocity of the flow is observed at the nozzle end of the grain. A substantial increase in velocity results in the appearance of a nonsteady-state turbulent boundary layer on the outer surface of the vapor-gas cloud. An increase in static pressure and more intensive heat transfer in the zone of combustion as a result of the turbulent mixing of the vapor-gas layers results, in the final analysis, in an increase in the local burning rate. A quantitative increase in the burning rate is determined by the sensitivity of the kinetics of the reactions taking place in the vapor-gas and the powder grain to a change in pressure and in

the heat flows in the corresponding phases of the system.

The nature of erosive burning is not yet sufficiently clear, and various attempts at simplified calculations have not produced any satisfactory results. It has, nevertheless, been confirmed that the determining factors resulting in erosive burning are the parameters of the stream of products of combustion and the intensity of heat transfer; in addition, it has been established that erosive burning becomes noticeable only for $w_g > w^*_g$, so that more exactly

$$u_a^* = u_a[1 + k_v(w_r - w_r^*)], \qquad (4.22)$$

where w^*_g is the maximum velocity of the products-of-combustion flow, at which the erosion effect is not observed.

Wimpress* and Green** found that for a powder of the JPN type the quantity k_v is

$$k_v = 0.00219 \text{ sec/m}.$$

Geckler*** recommends that k_v be assumed equal to

$$k_v = 0.00163 \text{ sec/m}.$$

Later investigations**** showed that the coefficient k_v is a function of the velocity of the flow; the following numerical values of k_v were obtained here:

$k_v = 0.00245$ sec/m at $w_g = 200$ m/sec

$k_v = 0.00225$ sec/m at $w_g = 250$ m/sec

$k_v = 0.00214$ sec/m at $w_g = 350$ m/sec

(for engine pressures up to 80 kg/cm^2).

At pressures somewhat in excess of 80 kg/cm^2, the coefficient k_v increases approximately to $k_v \approx 0.003$ sec/m for the same velocities.

Figure 4.8 shows the curve of the relative increase in burning rate in the case of erosive burning as a function of the velocity of the flow. The curve was obtained for a powder that was similar in composition and properties to the JPN powder.

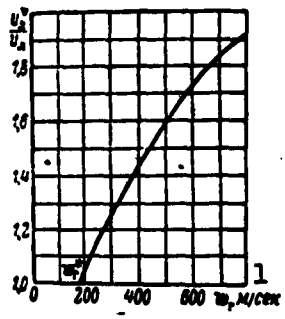

Fig. 4.8. Curve of relative increase in burning rate due to erosion for various velocities of the stream of the products of combustion. 1) w_g, m/sec.

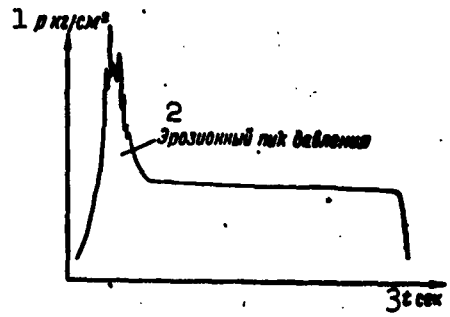

Fig. 4.9. Curve of pressure in engine with intensive erosion at initiation of combustion. 1) p, kg/cm^2; 2) erosion peak of pressure; 3) t, sec.

Figure 4.9 shows a characteristic curve for the change in pressure in an engine in the case of intensive erosion at the initial instant of burning.

An experimental investigation of erosive burning has shown that it takes place only at the beginning of the burning process and comes to a rapid conclusion, since the free cross section quickly increases as the burning continues. Nevertheless, erosive-burning regimes, as a rule, are regarded as intolerable for rocket engines. This is explained by the fact that the appearance of an extended pressure peak which ac-

companies the erosive burning regime results in the need for an unjustified increase in the thickness of the combustion-chamber walls, i.e., it results in the need to increase the weight of the engine, and this reduces the structural and operational characteristics of the power plant.

Erosive burning can be eliminated or its effect can be substantially reduced by increasing the initial free cross section of the combustion chamber, or by making possible an intervening outflow of the products of combustion through the sides of the combustion chamber. A pronounced increase in the free cross section would not be desirable in this case, since this would result in a reduction of charge density and an increase in engine length, whereas a method of side outflow is associated with additional losses. Another means of eliminating the effect of erosive burning is the restriction of the initial burning surface so that the calculated (theoretical) pressure does not immediately rise to its operating values after ignition. In this case, an increase in pressure as a result of erosive burning only offsets the pressure, without resulting in the appearance of any significant peak.*

Vibration burning (the American term is resonant burning). The phenomenon of vibration burning is more complex in its physical nature and conceals great dangers. The possibility of the appearance of combustion vibrations determines the degree of engine reliability, as well as the degree of reliability for the entire rocket.

Vibration combustion (combustion vibration) in a solid-propellant rocket engine occurs as a result of the dynamic action of the flow of the products of combustion on the process of the burning of the operating charge. As a result of this interaction within the combustion chamber intensive pressure pulses may occur, and their amplitudes sometimes become commensurate with the nominal values of the operating

pressure. The presence of the above-mentioned pressure pulses is the primary indication of a resonant-burning regime.

Despite the extensive investigations, the theoretical statements with respect to the quantitative relationships governing resonant (vibration) burning have not been reliably verified to the present time because of the difficulties that arise in setting up the corresponding experiments. Moreover, the very diagram of the mechanism of the excitation and development of unstable combustion vibrations, said diagram serving as the basis for the theoretical investigations, is essentially hypothetical.

The clearest picture of the development of vibration burning at some arbitrary point M of the grain surface can be given in the following form (Fig. 4.10). The random pressure disturbance whose appearance is associated with the dynamics of the nonsteady-state flow of the products of combustion extends to the zone of solid-propellant combustion. Let the pressure pulse due to this disturbance be represented by the curve A. The adiabatic compression of the combustion zone takes place under the action of this pulse and as a result the temperature and density of the layer of reacting gases increase. This, in turn, results in more intensive heat transfer and an increase in the rate of diffusion between the volumes of reacting and nonreacting gases. In summation, the chemical rate of the combustion reaction and the pressure in the zone of combustion exhibits pronounced increases, at least temporarily. Under certain conditions, this can result in the movement, opposite to the direction of the flow of the products of combustion, of a reinforced pressure wave consisting of the initial wave reflected from the surface of the grain and the excess pressure developed in the combustion zone as a result of the action of the initial wave (curve B).

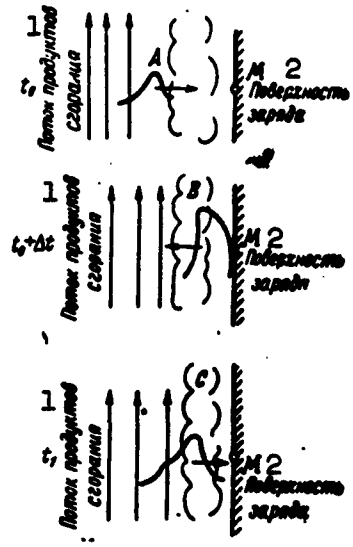

Fig. 4.10. Evolution of pressure pulse as it interacts with the burning surface of a solid propellant in the case of an engine tendency to vibration (resonant) burning. 1) Flow of products of combustion; 2) surface of grain.

The pressure wave B is propagated within the cavity of the combustion chamber, it is reflected from the other surfaces, and returns to the initial point. In this case, if the returned wave C is less intense than the initial wave, the pressure oscillations at the point under consideration will gradually be attenuated. If, however, the parameters of the returned (reflected) wave prove to be higher than those of the initial disturbance A, the oscillations will begin to increase. In this case, the system will be nonstable for those frequencies corresponding to the frequency of the return (reflection) of the reinforced reflected waves. The pressure oscillations will increase until the damping or nonlinearity of the increase in burning intensity prevent any further increase in vibration amplitude or until the combustion chamber blows up.

Local changes in the linear burning rate of the grain are the ex-

ternal indications of the effect of resonant burning; these result in phenomena such as the so-called grain "burnouts." The nature of the change in the linear burning rate in the case of vibrations is a function of the nature of the propellant and certain parameters of interior engine ballistics.

In accordance with experimental data, the burning rate for colloidal powders, in the case of vibration, on the average diminishes with low operating pressures and increases with high operating pressures.*

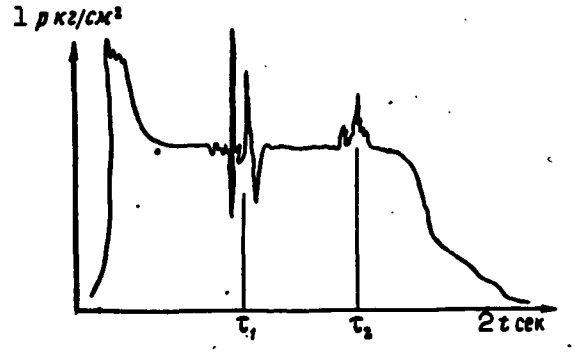

Fig. 4.11. Curve of pressure in engine, with pressure vibrations at instants τ_1 and τ_2.
1) p, kg/cm^2; 2) t, sec.

Of the remaining factors which affect the nature of the change in the burning rate on the appearance of vibrations within the engine we should make mention of the operating pressure in the engine, the frequency of the excited vibrations, the temperature of the powder charge, the heating value of the powder, etc.

It is impossible to verify the quantitative relationships governing the effect that the above-enumerated factors have on the linear burning rate, although it has been established, for example, that low-heating-value powders and powders with metallic additives stand out

because of their increased burning-rate stability in the case of random pressure vibrations within the engine.

It is interesting to point out that pressure vibrations can appear in a solid-propellant rocket engine only, as a rule, at certain identical and completely determined instants of burning time for the given engine, and these are functions of the dimensions of the inner cavity of the combustion chamber and the ballistic parameters of the engine (Fig. 4.11). The nature of the vibrations in this case can change from experiment to experiment.

An experimental investigation of the phenomena associated with the vibration (resonant) burning regimes demonstrated* that the pressure oscillations observed within the chamber generally correspond to a certain spectrum of sonic frequencies. In this case, as a rule, it becomes possible to record low frequencies. However, the appearance of frequencies of the order of 50,000 cps and above in individual experiments indicates that frequencies up to 10,000 cps, the frequencies most frequently encountered in practice, by no means encompass the entire spectrum of probable pulsation frequencies. The spectrum of standing pressure waves corresponds to the spectrum of observed vibration frequencies; the nodes of the loops of these standing pressure waves may either be stationary or they may wander and, as a rule, they do not coincide for waves of various tones. In this case, the amplitudes of the oscillations may be nonidentical in various parts of the chamber, even in the case of waves of one and the same tone. Vibrations are excited generally in those cross sections of the combustion chamber in which pressure-wave loops occur (and correspondingly, in which temperature-wave loops occur, etc.).

If the combustion vibrations release heat and an additional quantity of gases in exact phase with the pressure oscillations, no addi-

tional work need be done during the cycle. If, however, the combustion-vibration cycle is delayed with respect to the pressure vibrations, additional work is carried out each time on the oscillating gas column and the vibration amplitude increases particularly intensively. In this case, the wave front becomes steeper and under certain conditions within the engine the pressure wave may even degenerate into a detonation wave. In all probability, the phase shift is a function simultaneously of the characteristics of several processes taking place both within the gaseous products as well as within the solid mass of the charge, and various processes may play the most important role depending on the type of propellant used and the parameters of the engine.

Neglecting the possibility that the engine might be destroyed, some of the energy liberated during the burning of powder in the case of resonant-burning regimes is expended on the oscillation of the column of products of combustion and is virtually lost in the combustion chamber. It is for this reason that the development of effective methods of combating unstable vibration regimes is of such important practical significance.

No uniform method of eliminating the appearance of vibrations in an engine has been found since the very nature of the phenomenon has not been studied too thoroughly. Nevertheless, as a result of experimental investigations certain measures have been discovered, and these can stabilize the burning process with comparative reliability in individual cases. Among these measures, in the opinion of foreign specialists, the following are the most effective.

1. The design of a combustion-chamber cavity for an engine, in which the natural frequencies would correspond to energy excitation levels substantially in excess of the magnitude of energy liberated per unit time in the engine as a result of the burning of the powder.

All random pressure vibrations are quickly damped in a combustion chamber of this type and do not result in substantial disruption of the engine operating regime.

This method did not find widespread application in the practice of the design of solid-propellant rocket engines, since the utilization of this method, as a rule, results in the reduction of the structural indices for the engine.

2. The design of an engine in accordance with a diagram in which antinodes of standing pressure waves may appear in the random development of vibrations only in those sections in which there is no burning.

3. The design of an engine in which provision has been made for the damping of the possible vibrations.

For example, viscous friction and heat removal may be employed in order to damp the vibrations that can arise within an engine. In fact, the intensity of the vibrations drops markedly if it becomes possible to produce turbulence in the stream of products of combustion, and also if there is a sufficiently large heat-removal surface in the region of the antinodes of the pressure waves. The turbulent viscous friction, which absorbs energy, and heat removal eliminate the source of increased vibrations. Naturally, in this case there is a pronounced increase in the internal losses within the combustion chamber.

The results of certain gasdynamic investigations have shown that the presence of suspended particles in the products of combustion may be an effective means of damping the oscillations. These conclusions were confirmed in practice. Thus, for example, it was established* that such inclusions as carbon (carbon black), aluminum, and its oxides, and similar admixtures, introduced into the composition of the grain in the form of a fine powder, are sufficiently effective in blocking the development of powerful vibrations within the engine. Unfortunately,

contemporary concepts of the mechanism of burning and its interrelationship with pressure vibrations makes it impossible to find any general principles for the selection of these "blocking" additives, and such additives are being sought only through tedious experimentation.

4. If the burning takes place only at the surface of the inner grain channel, an extremely effective means of stabilizing the burning process is achieved by positioning a central longitudinal rod made of a noncombustible material in the channel or by fabricating the channel to have a burning surface with a noncircular perimeter.

The mechanism of the damping of the oscillations through the introduction of a central rod is not yet completely clear; however, it is apparent that the observed effect can be reduced to the absorption of the vibration energy of the gas column as a result of the resonance vibrations of the rod itself.

With the introduction of a central rod, the structural weight of the engine is increased and so are the heat losses within the combustion chamber.

5. We were able to establish that in the case of grains burning along the surface of the channel and along the outer surface (in particular, for single-channel cylindrical grains), combustion stability increases if small-bore radial holes have been cut into the grain cupola. It has been established experimentally* that the optimum diameter of these stabilization openings is approximately 0.30-0.45 of the diameter of the grain channel, and the maximum distance between these is determined by the geometric dimensions of the lateral cross section of the grain and the ballistic characteristics of the powder being used. It has also been established that the system of radial holes must be positioned along the grain, approximately along a helical line, so that adjacent openings exhibit an average shift of 120° with respect

to one another. In the case of powders exhibiting a heating value ranging from 950 to 1200 kcal/kg, the optimum distance between two adjacent holes ranges from 20 to 100 mm for grains of various dimensions.

The introduction of radial holes introduces virtually no change in the engine characteristic and produces only some additional degression of the curve $p = p(t)$.

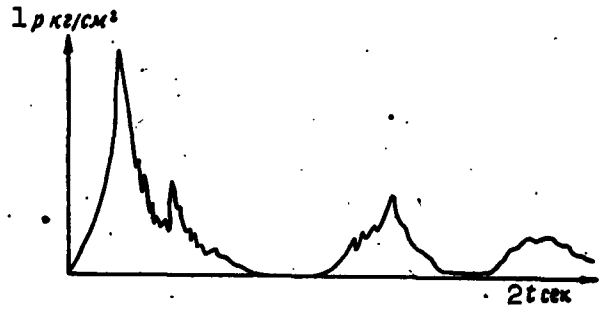

Fig. 4.12. Curve of pressure in the case of intermittent burning, in an engine with an operating pressure of $p < p^*_{min}$. 1) p, kg/cm^2; 2) t, sec.

Intermittent (anomalous) burning. Finally, there is another anomalous burning phenomenon which is observed in certain solid-propellant engine designs and this is the so-called intermittent unstable burning. Here we are dealing with operating pressures that are below a certain critical value of p^*_{min} for the given engine design at which the burning concludes as the chemical reactions of the first stage of the gas-phase oxidation processes alone come to a conclusion. As has already been stated, in this case only a part of the thermal energy (corresponding to the heating value of the given powder) is liberated. This energy may not be adequate to support continuous burning, and the burning ceases. However, if the engine had an opportunity to warm up during the time of the first ignition and if the igniter gases remained in the combustion chamber, the burning may resume after a certain period of time has elapsed. As a result, we observe some characteristic

"chugging," after which either final damping takes place or an unstable burning regime involving powerful low-frequency vibrations is established (Fig. 4.12).

In order to eliminate intermittent burning it becomes necessary to increase the operating pressure in the combustion chamber or to change the design of the engine. If such changes are undesirable, on the basis of any considerations, it becomes necessary to select a new powder composition which would provide for normal burning in the engine at the selected operating pressure.

§4. THEORETICAL BASES FOR THE CALCULATION OF PRESSURE IN A SOLID-PROPELLANT ROCKET ENGINE

Curve of Pressure Change in Engine on Combustion of Powder Charge

During the process of the burning of the powder gaseous products are formed and these fill the combustion chamber, producing pressure. The time change for pressure in the combustion chamber is one of the basic operating characteristics of the engine and is obtained in the form of the so-called pressure curve (Fig. 4.13).

Several characteristic sections can be isolated on the pressure curve and these characterize the various periods of engine operation. The initial pressure required for reliable burning of the operating powder charge is built up in the engine during a period of time τ_n sec through the action of a special igniter consisting of a pyrocartridge and weighed portions of a fast-burning black powder. After a period of τ_n sec the pressure in the engine attains its theoretical value; however, as a rule, afterwards it continues to increase for some time and only after $\tau_{p\ max}$ sec, having attained maximum values (ejection pressure), does it begin to drop to its operating level. The time required for the final establishment of the pressure is referred to as the time of engine entry into regime. At the end of the engine operation, upon

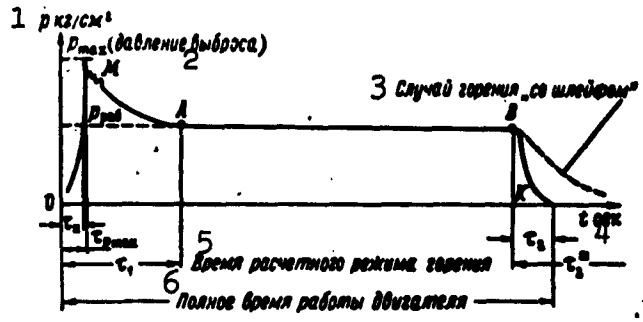

Fig. 4.13. Characteristic pressure curve for a solid-propellant rocket engine. τ_n) The time required to build up to the operating pressure; τ_1) total time of transient response (entry into regime); τ_2 (τ_2^{sh})) time required for complete combustion and free outflow of gases from engine; p_{rab}) operating pressure in combustion chamber; 1) p, kg/cm^2; 2) ejection pressure; 3) the case of combustion "with loop"; 4) t, sec; 5) time of theoretical burning regime; 6) total time of engine operation.

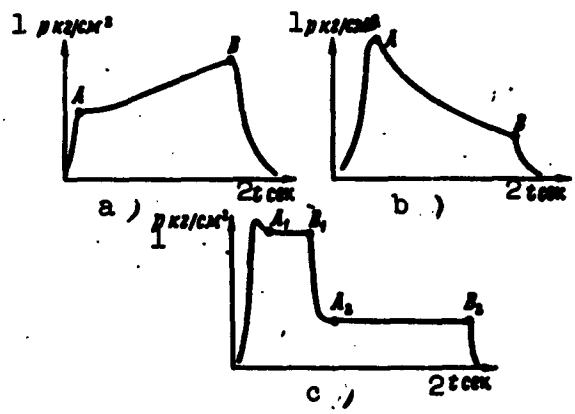

Fig. 4.14. Some types of pressure curves, encountered in solid-propellant rocket engines of various designations. a) Progressive-burning curve; b) degressive-burning curve; c) curve of burning with two stages of thrust. A, A_1, A_2, B, B_1, and B_2) characteristic points on the curve; 1) p, kg/cm^2; 2) t, sec.

cessation of burning, the pressure is rapidly reduced through the nozzle and passed into the atmosphere. Sometimes, when for some reason solid grain residue remains in the engine upon completion of the burning process, the so-called burning "with loop" is observed, and here the pressure behind the point B drops comparatively slowly and follows no particular quantitative relationship.

The phenomenon of burning "with loop," generally speaking, is undesirable, since it results in great variation in velocity at the end of the active phase.

In addition to the curves shown in Fig. 4.13, some engines yield curves of another type (Fig. 4.14). However, there is no basic difference between all of the various types of possible burning curves.

The Concept of the Equation of Balance and its Application to the Calculation of Maximum Pressure

The pressure produced by powder gases in an engine and the nature of the change in pressure, in time, are determined by the balance between the influx of gases from the burning charge and the flow rate of the products of combustion through the nozzle.

In general form, the equation of balance for some arbitrary time t can be expressed by the following relationship:

$$M_0 + M_+ = M_- + \Delta M,$$

where M_+ is the per-second influx of gases into the engine; M_- is the per-second flow rate of gases from the engine; ΔM is the quantity of gases remaining in the engine in addition to that quantity found in the engine during the preceding instant of time; M_0 is the gas mass in the combustion chamber at the instant of time t.

If we assume that the powder burns in parallel layers and that the grain is physically uniform, we will have

$$M_+ = \gamma u_r S_r, \qquad (4.23)$$

where γ is the specific weight of the powder; S_Σ is the total burning surface; $u_1 S_\Sigma$ is the volume of grain burned within 1 sec.

Completely analogously, for the flow rate of the gases through the nozzle

$$M_- = \rho_{kp} w_{kp} \sigma_{kp},$$

where ρ_{kr} is the gas density in the critical section of the nozzle (throat); w_{kr} is the velocity of the gases in the critical section of the nozzle; σ_{kr} is the area of the critical section of the nozzle.

The gas parameters in the critical section (throat) can be expressed in terms of certain gas-mixture constants and in terms of the parameters of the products of combustion in the combustion chamber of the engine. For example, for ρ_{kr} we will have

$$\rho_{kp} = \rho_0 \left(\frac{2}{k+1}\right)^{\frac{k}{k-1}}. \qquad (4.24)$$

where ρ_0 is the gas density in the combustion chamber of the engine; $k = c_p/c_v$ is the index of the combustion process.

If we assume that the state of the gases in the engine can be described by the following equation

$$p_0 v_0 = RT_0,$$

and if we bear in mind that

$$v_0 = \frac{1}{\rho_0},$$

we will obtain

$$\rho_{kp} = \frac{p_0}{RT_0}\left(\frac{2}{k+1}\right)^{\frac{k}{k-1}}. \qquad (4.25)$$

where p_0 is the pressure in the combustion chamber; R is the gas constant of the products of powder combustion; T_0 is the temperature in the combustion chamber.

The critical velocity is determined by the following relationship:

$$w_{кр} = \sqrt{\frac{2k}{k+1} gRT_0}. \qquad (4.26)$$

If we substitute (4.25) and (4.26) into the expression for the per-second flow rate of the gases through the nozzle, we will find

$$M_- = \rho_{кр} w_{кр} \sigma_{кр} = \frac{p_0}{RT_0} \left(\frac{2}{k+1}\right)^{\frac{k}{k-1}} \sqrt{\frac{2k}{k+1} gRT_0}\, \sigma_{кр}$$

or after transformation

$$M_- = \frac{\left(\frac{2}{k+1}\right)^{\frac{k}{k-1}} \sqrt{\frac{2k}{k+1} g}}{\sqrt{RT_0}} p_0 \sigma_{кр}. \qquad (4.27)$$

The coefficient

$$A = \frac{\left(\frac{2}{k+1}\right)^{\frac{k}{k-1}} \sqrt{\frac{2k}{k+1} g}}{\sqrt{RT_0}}$$

is approximately constant and is referred to as the coefficient of exhaust discharge (outflow) and for various flows averages

$$A = 6\text{-}10 \text{ g/kg·sec.}$$

If we neglect the mass M_0 of the gases, which was found in the combustion chamber of the engine prior to initiation of combustion, the equation of the balance of the gases in the engine during the time Δt will be found in the following form if we take into consideration (4.23) and (4.27):

$$\gamma u_x S_\Sigma \Delta t = A p_0 \sigma_{кр} \Delta t + \Delta M.$$

Let us express the mass ΔM in terms of the parameters of the interior ballistics of the engine. For this purpose, let us examine the equation of state written for the entire volume of the combustion chamber:

$$p_0 v'_{к.с} = MRT_0,$$

where $v'_{к.с}$ is the free volume of the combustion chamber; M is the gas mass within the volume $v'_{к.с}$ at an arbitrary instant of time t.

In accordance with this equation, the change in the mass of the gases in time is determined by the derivative

$$\frac{dM}{dt}=\frac{d}{dt}\left(\frac{p_0 v'_{k.c}}{RT_0}\right)=\frac{p_0}{RT_0}\frac{dv'_{k.c}}{dt}+\frac{v'_{k.c}}{RT_0}\frac{dp_0}{dt},$$

i.e., for Δt it amounts to

$$\Delta M=\left(\frac{p_0}{RT_0}\frac{dv'_{k.c}}{dt}+\frac{v'_{k.c}}{RT_0}\frac{dp_0}{dt}\right)\Delta t. \qquad (4.28)$$

Now, the balance equation will be

$$\gamma u_a S_\Sigma \Delta t = A p_0 \sigma_{kp} \Delta t+\left(\frac{p_0}{RT_0}\frac{dv'_{k.c}}{dt}+\frac{v'_{k.c}}{RT_0}\frac{dp_0}{dt}\right)\Delta t$$

or

$$\gamma u_a S_\Sigma = A p_0 \sigma_{kp}+\frac{p_0}{RT_0}\frac{dv'_{k.c}}{dt}+\frac{v'_{k.c}}{RT_0}\frac{dp_0}{dt}, \qquad (4.29)$$

where $(p_0/RT_0)(dv'_{k.s}/dt)$ accounts for the quantity of gases used to fill the volume of combustion chamber which becomes free as the grain is consumed; $(v'_{k.s}/RT_0)(dp_0/dt)$ accounts for the quantity of gases used to increase the pressure within the volume of the combustion chamber.

Generally, Eq. (4.29) is transformed as follows:

$$\frac{dp_0}{dt}=\frac{RT_0}{v'_{k.c}}\left[\gamma u_a S_\Sigma\left(1-\frac{p_0}{\gamma RT_0}\right)-A p_0 \sigma_{kp}\right], \qquad (4.30)$$

for which it is enough to use

$$\frac{dv'_{k.c}}{dt}=u_a S_\Sigma,$$

which is valid, since a change in volume is determined only by the burning up of the powder grain.

In the form of (4.30), the balance equation is a differential equation for $p = p(t)$. This equation is solved most simply by the methods of numerical integration, for which it is convenient to present it in the following form

$$\Delta p=\frac{RT_0}{v'_{k.c}(t)}\left[\gamma u_a(t) S_\Sigma(t)\left(1-\frac{p(t)}{\gamma RT_0}\right)-A p(t)\sigma_{kp}\right]\Delta t \qquad (4.31)$$

and to assume the following as the initial data: $(p)_0$ is some initial pressure; $(S_\Sigma)_0$ is the initial total burning surface; A, γ, $f_p = RT_0$, $u_1 = u(p)$ are characteristics of the powder used in the engine; $(v_{k.s})_0$, σ_{kr} are the structural parameters of the engine.

The pressure at any kth instant of engine operation is determined in accordance with the following formula

$$p_k = p_{k-1} + \Delta p_k,$$

where

$$p_1 = (p)_0 + \Delta p_1.$$

Equation (4.30) may be used not only for the derivation of the curve for the change in pressure in the engine, but for the calculation of the magnitude of the maximum pressure p_{max}. In fact, the condition for the maximum of the function p = p(t) will be

$$\frac{dp}{dt} = 0,$$

which for $RT_0 \neq 0$ and $v'_{k.s} \neq 0$ yields

$$\gamma u_1 S_\Sigma \left(1 - \frac{p_{max}}{\gamma RT_0}\right) - A p_{max} \sigma_{kp} = 0. \qquad (4.32)$$

If we bear in mind that for conventional powders $\gamma \approx 1.6$ g/cm^3, $RT_0 \approx 85{,}000$ kg-m/kg, the term $p_{max}/\gamma RT_0 \approx p_{max}/136{,}000$ of Relationship (4.32) at pressures ranging from 100 to 150 atm can be neglected and can be used in simplified form:

$$u_1 \gamma S_\Sigma = A p_{max} \sigma_{kp}. \qquad (4.33)$$

From (4.33) the quantity p_{max} for the power function of burning $u_1 = u_1 p^\nu f(t_0)$ is defined as follows:

$$p_{max} = \left[\frac{u_1 \gamma f(t_0) S_\Sigma}{A \sigma_{kp}}\right]^{\frac{1}{1-\nu}} \qquad (4.34')$$

and for the linear burning function $u(ap + b)f(t_0)$

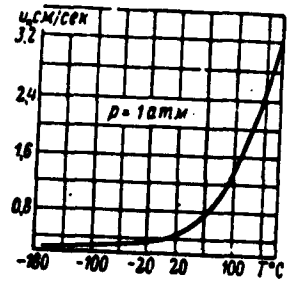

Fig. 4.15a. The nature of the relationship between the burning rate of nitroglycerine powder and the initial charge temperature at p = const.

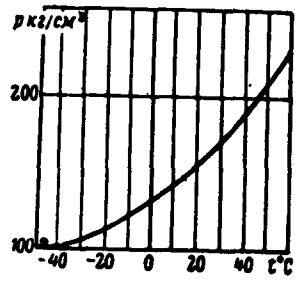

Fig. 4.15b. The nature of the relationship between the operating pressure in the engine and the initial temperature of the powder charge.

$$p_{max} = \frac{\frac{b}{a}}{\frac{A}{a_1}\frac{1}{S_\Sigma/\sigma_{kp} f(t_0)} - 1}. \qquad (4.34'')$$

Since the expressions for the calculation of p_{max} were obtained by using the empirical formulas for the burning rate, a mathematical analysis of the relationships (4.34") and (4.34') is difficult. Nevertheless, we may arrive at the conclusion that one of the significant parameters of the engine, which affects the quantity p_{max}, is the ratio of the burning surface to σ_{kr}. With an increase in (S_Σ/σ_{kr}) the pressure maximum in the engine increases and Relationship (4.34") indicates directly the existence of some limit value of (S_Σ/σ_{kr}) at which the pressure $p_{max} \to \infty$. The maximum value of (S_Σ/σ_{kr}) is deter-

mined from the following condition

$$\frac{A}{a\gamma}\frac{1}{S_\Sigma/\sigma_{кр}f(t_0)}-1=0,$$

i.e., it amounts to

$$\left(\frac{S_\Sigma}{\sigma_{кр}}\right)_{пред}=\frac{A}{a\gamma f(t_0)}. \qquad (4.35)$$

Magnitude of Pressure in Combustion Chamber as a Function of Initial Charge Temperature

An important feature and a basic serious shortcoming of a solid-propellant rocket engine is the strong relationship between the operating pressure and the initial charge temperature. This relationship is explained by the effect that the initial temperature of the charge has on the burning rate of the powder (Fig. 4.15a) and which at σ_{kr} = const results in significant variations in thrust, burning rate, etc., for various temperature conditions of engine operation.

Figure 4.15b presents a characteristic curve which illustrates the operating pressure in the combustion chamber of the engine (operating on solid propellants) as a function of the initial temperature of the powder charge. We can see from the curve that in the temperature interval of $\pm 40^{\circ}C$ the pressure in the engine, and consequently, the magnitude of thrust, can change by a factor of almost two, and this will, of course, result in a reduction of the combat and operational characteristics of the weapon.

Formulas (4.34') and (4.34") make it possible to obtain the relationship between the pressure and the temperature of the charge in explicit form.

In fact, with a power burning function for a certain charge temperature we will have

$$p_{t_0}=\left[\frac{u_1\gamma f(t_0)S_\Sigma}{A\varkappa_{кр}}\right]^{\frac{1}{1-\nu}},$$

and for t = +20°C

$$p_{+20^\circ} = \left[\frac{u_1 \gamma S_3}{A z_{\text{exp}}}\right]^{\frac{1}{1-\nu}},$$

whence

$$\frac{p_{t_0}}{p_{+20^\circ}} = \left[\frac{\frac{u_1 \gamma f(t_0) S_3}{A z_{\text{exp}}}}{\frac{u_1 \gamma S_3}{A z_{\text{exp}}}}\right]^{\frac{1}{1-\nu}} = [f(t_0)]^{\frac{1}{1-\nu}},$$

i.e., taking into consideration (4.20)

$$p_{t_0} = p_{+20^\circ}\left[\frac{B_\tau}{B_\tau - (t_0 - 20^\circ)}\right]^{\frac{1}{1-\nu}}. \qquad (4.36')$$

Accordingly, for the case of a linear burning function

$$p_{t_0} = \frac{\frac{b}{a}}{\frac{A}{a\gamma}\frac{1}{S_3/e_{\text{exp}} f(t_0)} - 1} = \frac{1}{\frac{A}{b\gamma}\frac{1}{S_3/e_{\text{exp}} f(t_0)} - \frac{a}{b}},$$

$$p_{+20^\circ} = \frac{1}{\frac{A}{b\gamma}\frac{1}{S_3/e_{\text{exp}}} - \frac{a}{b}}.$$

From the last we will determine

$$\frac{A}{b\gamma}\frac{1}{S_3/e_{\text{exp}}} = \frac{1}{p_{+20^\circ}} + \frac{a}{b} = \frac{1 + \frac{a}{b} p_{+20^\circ}}{p_{+20^\circ}}$$

and, substituting this expression into the formula for p_{t_0}, we will obtain

$$p_{t_0} = \frac{1}{\frac{1 + \frac{a}{b} p_{+20^\circ}}{p_{+20^\circ}}\frac{1}{f(t_0)} - \frac{a}{b}} = \frac{p_{+20^\circ} f(t_0)}{1 + \frac{a}{b} p_{+20^\circ}[1 - f(t_0)]},$$

which yields the following, if we take into consideration (4.20)

$$p_{t_0} = \frac{B_\tau p_{+20^\circ}}{B_\tau - (t_0 - 20^\circ) - \frac{a}{b} p_{+20^\circ}(t_0 - 20^\circ)}. \qquad (4.36'')$$

It sometimes becomes necessary to assume the pressure for a certain temperature t_0, but not in accordance with its value at $t_0 = +20^\circ C$, but in accordance with its value at the lowest extreme temperature,

i.e., $t_0 = -40^\circ C$. Corresponding calculation relationships are easily obtained from the relationships presented above. We will present these without drawing any conclusions:

$$p_{t_0} = p_{-40^\circ}\left[\frac{B_\tau + 60^\circ}{B_\tau - (t_0 - 20^\circ)}\right]^{\frac{1}{1-\nu}}. \qquad (4.37')$$

$$p_{t_0} = p_{-40^\circ}\frac{B_\tau + 60^\circ}{B_\tau (t_0 - 20^\circ) + \frac{a}{b} p_{-40^\circ}(t_0 - 40^\circ)}. \qquad (4.37'')$$

In analogy with the relationship between the initial temperature of the charge and the linear burning rate of the powder, the relationship between temperature and pressure is frequently given by means of the so-called temperature pressure gradient, which is introduced in the following form

$$\frac{1}{p_0}\frac{dp}{dt_0}$$

using this to characterize the relative intensity of the pressure increase in the engine with some change in the initial temperature of the charge. If we use (4.36') and (4.36"), we will obtain the following for the corresponding burning functions:

$$\frac{1}{p_{+20^\circ}}\frac{dp}{dt_0} = \frac{1}{1-\nu}\frac{1}{B_\tau - (t_0 - 20^\circ)}, \qquad (4.38')$$

$$\frac{1}{p_{+20^\circ}}\frac{dp}{dt_0} = \frac{1 + \frac{a}{b} p_{+20^\circ}}{B_\tau - (t_0 - 20^\circ) + \frac{a}{b} p_{+20^\circ}(t - 20^\circ)}. \qquad (4.38")$$

We can see from these formulas that the sensitivity of pressure to changes in temperature is all the greater the higher the temperature and the greater the pressure in the engine.

Formula (4.38') makes it possible to establish a direct link between the temperature pressure gradient and a change in the burning rate:

$$\frac{1}{p_{+20^\circ}}\frac{dp}{dt_0} = \frac{1}{1-\nu}\left(\frac{1}{u_{+20^\circ}}\frac{du}{dt_0}\right). \qquad (4.39)$$

where use is made of

$$\frac{1}{u_{+20^\circ}}\frac{du}{dt_z}=\frac{1}{B_T-(t_0-20^\circ)}.$$

If we bear in mind that $\nu = 2/3\text{-}3/4$, we will see that

$$\frac{1}{p_{+20^\circ}}\frac{dp}{dt_z}=(3+4)\frac{1}{u_{+20^\circ}}\frac{du}{dt_z},$$

i.e., with a change in the initial temperature of the charge, pressure changes substantially more intensively than does the burning rate of the powder.

The temperature pressure gradient $d(\ln p)/dt_z$ for certain powders amounts to:

for JP powder – 0.0126;

for JPN powder – 0.0162;

for ALt-161 composite powder (propellant) – 0.0036;

for British perchlorate powder – 0.0038.

The development of variable (controlled) nozzles or the utilization of demountable nozzle assemblies are the only ways of stabilizing the parameters of interior ballistics in the given temperature interval of rocket operation. Consequently, a reduction or an increase in the area of the critical section of the nozzle (throat) with minus or plus temperatures, demountable or variable nozzles make it possible to maintain the approximate constancy of pressure within the given temperature interval.*

The limited utilization of these two methods is explained by the fact that the design of variable, and particularly of automatically variable, nozzles is associated with certain difficulties, and the utilization of demountable nozzles reduces the mobility of the weapon.

Sensitivity of Maximum Pressure to Changes in Charge and Engine Parameters

The following expression is referred to, in mathematics, as the

sensitivity of the function y = f(x) to its argument (the logarithmic derivative)

$$\varepsilon = \frac{\frac{dy}{y}}{\frac{dx}{x}}.$$

The quantity ε characterizes the relative change of the function for some relative change in the argument. It is easy to check that the sensitivity of the exponential function $y = x^n$ is equal to the exponent:

$$\varepsilon = \frac{\frac{d(x^n)}{x^n}}{\frac{dx}{x}} = \frac{\frac{nx^{n-1}dx}{x^n}}{\frac{dx}{x}} = n.$$

Let us use the concept of the sensitivity of the function to its argument to investigate the features of engines operating on solid propellants.

In accordance with (4.34') the maximum pressure in the combustion chamber of the engine, for a given powder, is the function having the following parameters

$$p_{max} = p(S_\Sigma, \sigma_{kp}, t_0),$$

where S_Σ and t_0 are the parameters of the powder charge; σ_{kr} is the structural parameter of the combustion chamber.

Since this function is exponential

$$p_{max} = \left[\frac{u_1 \gamma S_\Sigma f(t_0)}{A \sigma_{kp}}\right]^{\frac{1}{1-\nu}},$$

its sensitivity to a change in the corresponding parameters in the charge in the engine will be equal to the exponent, i.e.,

$$\frac{dp_{max}}{p_{max}} = \frac{1}{1-\nu}\left[\frac{dS_\Sigma}{S_\Sigma} - \frac{d\sigma_{kp}}{\sigma_{kp}} + \frac{d[f(t_0)]}{f(t_0)}\right].$$

or, in finite differences

$$\frac{\Delta p_{max}}{p_{max}} = \frac{1}{1-\nu}\left[\frac{\Delta S_\Sigma}{S_\Sigma} - \frac{\Delta \sigma_{kp}}{\sigma_{kp}} + \frac{\Delta [f(t_0)]}{f(t_0)}\right]. \qquad (4.40')$$

One of the features of the operation of a solid-propellant rocket

engine is the high sensitivity of the maximum pressure within this engine to changes in the parameters for the charge and the engine. In fact, since for contemporary powders $\nu = 2/3\text{-}3/4$,

$$\frac{\Delta p_{max}}{p_{max}} = (3 \div 4)\left[\frac{\Delta S_1}{S_1} - \frac{\Delta e_{xp}}{e_{xp}} + \frac{\Delta [f(t_0)]}{f(t_0)}\right].$$

For a linear burning function the sensitivity of pressure to a change in the corresponding parameters is most easily found if we approximate the linear function of some power function in accordance with

$$ap + b = u_1 p^{\tilde{\nu}},$$

$$\frac{d}{dp}(ap + b) = \frac{d}{dp}\left(u_1 p^{\tilde{\nu}}\right).$$

From the last equation

$$a = u_1 \tilde{\nu} p^{\tilde{\nu}-1} = u_1 \tilde{\nu} \frac{p^{\tilde{\nu}}}{p},$$

after which it is easy to obtain

$$\frac{a}{ap + b} = \frac{u_1 \tilde{\nu} \frac{p^{\tilde{\nu}}}{p}}{u_1 p^{\tilde{\nu}}} = \frac{\tilde{\nu}}{p},$$

whence $\tilde{\nu}$ is determined in the following form:

$$\tilde{\nu} = \frac{ap}{ap + b}.$$

Thus over a small interval of changes in pressure the linear burning function

$$u = ap + b,$$

can be replaced by the power function of the following form

$$u = u_1 p^{\frac{ap}{ap+b}}.$$

For the approximate function, the sensitivity of pressure is defined as

$$\frac{1}{1 - \tilde{\nu}},$$

i.e., it amounts to

$$\frac{1}{1-\tilde{\nu}}=\frac{1}{1-\frac{ap}{ap+b}}=\frac{ap+b}{b}.$$

Thus, for the linear burning-rate function of the powder

$$\frac{\Delta p_{max}}{p_{max}}=\frac{ap+b}{b}\left[\frac{\Delta S_{\Sigma}}{S_{\Sigma}}-\frac{\Delta \alpha_{sp}}{\alpha_{sp}}+\frac{\Delta[f(\ell_0)]}{f(\ell_0)}\right]. \qquad (4.40")$$

It follows from (4.40") that the sensitivity of the maximum pressure to changes in the parameters of the charge and the engine is a function not only of the properties of the powder but of the absolute pressure in the engine as well.

In actual practice it is desirable to have an engine exhibiting low sensitivity of pressure within the combustion chamber to changes in the charge and engine parameters, since in this case the engine characteristics would be more stable. Relationships (4.40') and (4.40") indicate that in order to achieve this situation it is necessary to operate at low pressures and to have powders exhibiting minimum coefficients ν and burning-rate functions a/b.

Stability of Steady-State Pressure in the Combustion Chamber

Under certain conditions, steady-state pressure p_{st} in the combustion chamber of a solid-propellant rocket engine exhibits the property of stability, i.e., pressure is maintained constant for the case of random pressure oscillations.

The mechanism of stability for steady-state pressure is obvious from Fig. 4.16. From the curves shown in this figure we can see that at pressures $p < p_{st}$, the influx of gases from the powder grain exceeds the flow rate (outflow), whereas in the case of $p > p_{st}$, $M_{-} > M_{+}$. This results in the fact that in the case of a random pressure drop in the engine, the excess influx of gases again raises the pressure to p_{st}, and vice versa, in the case of a random pressure rise, the flow rate (outflow) increases substantially more intensively than does the

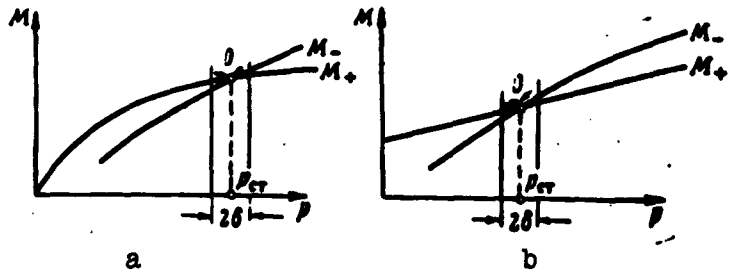

Fig. 4.16. Curves which explain the mechanism of the stability of steady-state pressure in the combustion chamber of a solid-propellant rocket engine. a) In the case of the power burning-rate function $u_1 = u_1 p$; b) in the case of the linear burning-rate function $u_1 = ap + b$; 2δ) the interval of possible pressure oscillations.

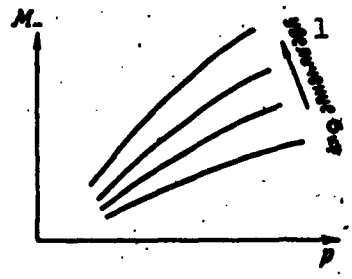

Fig. 4.17. Relationship $M_- = M(p)$ for engines with various σ_{kr}. 1) Increase in σ_{kr}.

inflow, and the excess pressure is dissipated, so that an operating pressure equal to p_{st} is established.

As we can see, the existence of steady-state pressure and its stability is wholly determined by the nature of the relationship between pressure and M_+ and M_-.

In accordance with (4.27) and the remarks made with respect to the outflow coefficient

$$M_- = (6\text{-}10)\ 10^{-3}\ p_0 \sigma_{kr}\ \text{kg/sec},$$

i.e., the character of $M_-(p)$ is virtually a function only of the dimension of the critical section of the engine nozzle (throat); for various σ_{kr}, this equation is satisfied by the family of curves shown in Fig. 4.17

The inflow of gases is determined by the following relationship:

$$M_+ = \gamma u S_\Sigma,$$

i.e., it will be $M_+ = \gamma S_\Sigma u_1 p^\nu$ for the power burning-rate function and $M_+ = \gamma S_\Sigma (ap + b)$ for the linear burning-rate function.

In both cases, the form of the functional relationship $M_+ = M(p)$ is determined by the relationships between the coefficients in the burning-rate function for the powder.

Two families of curves correspond to the equation

$$M_+ = \gamma S_\Sigma u_1 p^\nu = k p^\nu;$$

the first family for $\nu < 1$, and the second family, for $\nu > 1$ (Fig. 4.18). A comparison of the curves $M_+ = M(p)$ for the power burning-rate function of the powder with the outflow characteristic $M_- = M(p)$ for the given engine indicates that in the case of either $\nu < 1$ or $\nu > 1$ there exists a point which corresponds to a steady-state regime of engine operation. However, this point exhibits the property of stability only in the case of $\nu < 1$. In fact, we can see from Fig. 4.19 that when $\nu > 1$, the mutual relationship between $M_+(p)$ and $M_-(p)$ is such that in the case of a random change in pressure, the system will tend to increase the difference so that in the final analysis the pressure will either fall or increase without limit.

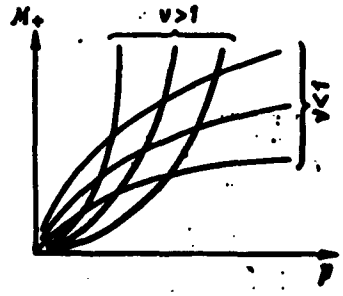

Fig. 4.18. Relationship $M_+ = M(p)$ for powders with a power burning-rate function.

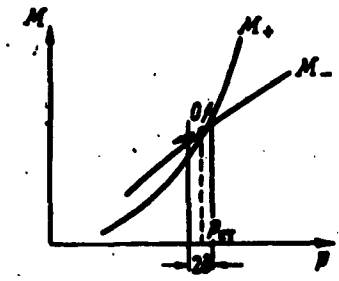

Fig. 4.19. Instability of steady-state pressure in an engine, for $\nu > 1$.

Thus the steady-state pressure in the combustion chamber of a solid-propellant rocket engine exhibits the property of stability if the exponent ν in the burning-rate function of the powder is less than one ($\nu < 1$).

We can see from Fig. 4.20 that, all other conditions being equal, the absolute magnitude of the steady-state pressure is all the lower the lower the absolute value of ν.

In the case of a linear burning-rate function, the curves for the inflow of gases form the family shown in Fig. 4.21. Only the curves with $a > 0$, in this family, have any real meaning. In the case of $a = 0$ we will be dealing with an ideal powder whose burning rate is not a function of pressure, whereas in the case of $a < 0$ we will be dealing with a powder whose burning rate must be diminished as pressure increases, and this is in poor agreement with the adopted hypotheses on the mechanism of the burning rate as a function of pressure, and moreover this is never observed in practice.

It follows from Fig. 4.22 that steady-state pressure in the combustion chamber is lower, the lower the coefficient a (or the ratio a/b) in the burning-rate function of the powder, and that there exists a certain limit steady-state pressure p^*_{st} such that for $p > p^*_{st}$ engine operation is impossible. With a given brand of powder, steady-

state pressure is a function of the shape of the flow-rate (outflow) engine characteristic; there exists a certain limit steady-state pressure at which it corresponds, even in this case, to conditions under which

$$\frac{S_3}{\omega_{кр}} = \frac{A}{\alpha_1 f(t_0)},$$

and this has already been obtained earlier (4.35).

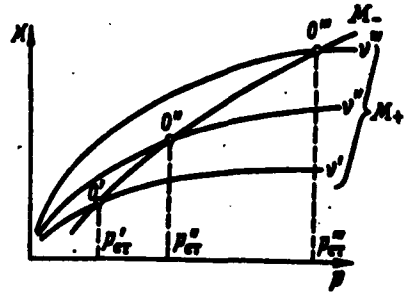

Fig. 4.20. Magnitude of steady-state pressure as a function of the exponent in the burning-rate function for the powder. ν, ν", ν'") are the values of the exponent in the burning-rate function; p'_{st}, p''_{st}, and p'''_{st}) are the corresponding steady-state pressures.

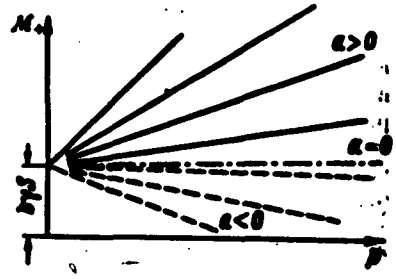

Fig. 4.21. Relationship $M_+ = M(p)$ for powders having a linear burning-rate function. a and b) coefficients of the linear burning-rate function.

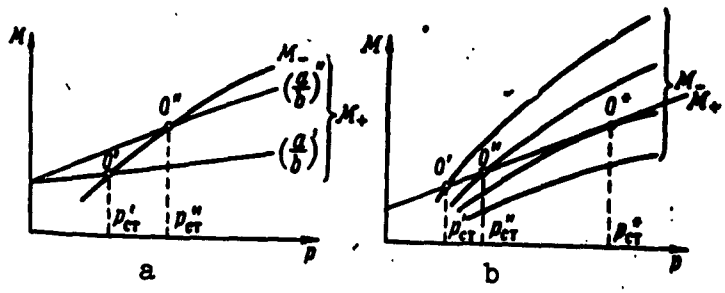

Fig. 4.22. Magnitude of steady-state pressure as a function of the coefficients of the linear burning-rate function and the structural features of the engine. a) The case in which various powders are utilized; b) the case of burning in engines exhibiting various flow-rate characteristics.

In the final analysis, we come to the conclusion that stability of steady-state pressure in the engine is a function of the relationship of several charge and engine parameters and of the properties of the brand of powder selected. For stability of steady-state pressure p_{st} the ratio between the magnitude of the total burning surface of the charge and the area of the critical section of the nozzle should not exceed a certain limit value and the coefficients ν and a/b of the burning-rate function for the powder should be as small as possible, and that in any event the following conditions should be satisfied:

$$\nu < 1,$$

$$a/b < 1.$$

Selection of Operating Pressure in Engine

The relationship between the nature of combustion and the burning rate of the working charge and the pressure within the combustion chamber indicates that essentially pressure within the combustion chamber is a parameter which wholly determines the operation of a solid-propellant rocket engine, since the burning of the powder may be regarded as a basic process within the engine. Therefore, the designation of a magnitude for the operating pressure in the combustion chamber is

one of the most important points in the design of a solid-propellant rocket engine. In the selection of the operating pressure we encounter a great many, frequently contradictory, requirements, so that it is virtually impossible to propose some general method for the selection of the optimum operating pressure. The magnitude of the operating pressure must be selected each time for specific conditions as given by the tactical-technical requirements, isolating the group of requirements which is most important for the given case. The basic concepts for the selection of the operating pressure can be formulated in the following form:

1) the operating pressure must exceed some maximum value of p^*_{min} in order to guarantee stable and uniform combustion of the working powder charge at given charge temperatures;

2) the operating pressure must be sufficiently high if the engine is to attain a comparatively high specific impulse;

3) with an increase in operating pressure the required structural weight of the power plant also increases, and this reduces the efficiency of the engine, even if the ballistic characteristics are great;

4) if it is necessary to provide for a definite time of burning in the case of limited engine dimensions, the pressure is selected so as to have a burning rate that corresponds to this pressure, thus making it possible to attain the given engine operating time;

5) the thrust of the rocket engine is directly proportional to the pressure in the combustion chamber; therefore, if the magnitude of thrust is uniquely defined, it becomes necessary to select a pressure for which consideration has been given to its effect on the thrust.

The lower boundary of permissible pressure. The tendency of a solid-propellant engine to anomalous intermittent burning in the region of low pressures requires that an operating pressure be designated in

excess of a certain p^*_{min}, determined experimentally for each powder composition. As has already been indicated, for the majority of rocket colloidal powders, the quantity p^*_{min} averages 15-35 atm.

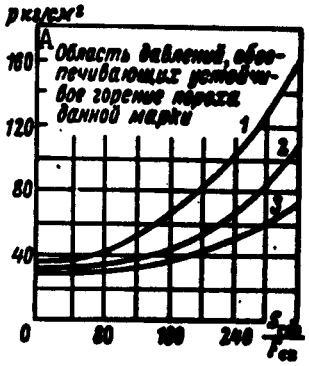

Fig. 4.23. Lower boundary of permissible pressure in an engine for one of the colloidal-type powder compositions. 1) $t_0 = -20^\circ C$; 2) $t_0 = +20^\circ C$; 3) $t_0 = +60^\circ C$; A) region of pressures providing for stable burning of a powder of a given brand.

In design practice and the testing of solid-propellant rocket engines we observe cases in which intermittent burning took place even at pressures in excess of p^*_{min}. These facts proved mysterious for a long period of time and were regarded as chance occurrences. However, a more careful examination of the cases of anomalous burning at pressures of $p > p^*_{min}$ made it possible to establish that the lower boundary of operating pressures is a strong function of the conditions of powder ignition and the structural features of the charge in the engine. The basic factors which determine the true $p^*_{min} = f$ (the operating conditions of an actual engine), were the initial temperature of the charge and the ratio between the total burning surface of a working charge and the magnitude of the free cross section of the combus-

tion chamber. It was established that at low charge temperatures, higher operating pressures are needed for normal burning in an engine and for engines exhibiting high values of the parameter S_{gor}/F_{sv} the permissible p^*_{min} increases sharply (S_{gor} is the burning surface, F_{sv} is the free cross section of the combustion chamber).

Thus for the given brand of powder the lower boundary of permissible operating pressures must be determined by taking into consideration the given temperature interval of engine operation and the structural features of the engine:

$$p^*_{min} = f\left(\begin{matrix}\text{powder}\\ \text{brand}\end{matrix} \quad t_0, \frac{S_{rop}}{F_{cs}}\right).$$

For practical calculations it is convenient to make use of special curves which delineate the region of pressures which guarantee the continuous burning of a powder of a certain brand in a specific engine for various relationships between the dimensions of the charge and the combustion chamber. These curves are constructed on the basis of data obtained in special tests of powder for various t_0 and S_{gor}/F_{sv}, said curves being parabolic in shape as shown in Fig. 4.23.

We can see from Fig. 4.23 that if the designs of the charge and the engine are known, i.e., if the ratio S_{gor}/F_{sv} is known, then for the given temperature interval ($t_{0\ min}$–$t_{0\ max}$) the pressure p^*_{min} is uniquely defined as the point of intersection between the ordinates corresponding to the given S_{gor}/F_{sv} and the curve for $t_{0\ min}$. It should be borne in mind that the ratio S_{gor}/F_{sv} changes with time and here, as a rule, it also diminishes. This results in a situation in which, if a certain pressure p has been selected so as to assure continuous burning for $(S_{gor}/F_{sv})_{t=0}$, as the burning of the charge continues the stability conditions are not disrupted.

A more general case for the design process of a solid-propellant

rocket engine is the case in which the quantity S_{gor}/F_{sv} can be made to vary. In this case, as can be seen from Fig. 4.23, there exists a multiplicity of points which provide for conditions of stable burning. If no additional requirements are imposed on the magnitude of the operating pressure, then of these points it is expedient to examine those points along the boundary of the region of stable burning, said points corresponding to the minimum temperature of the given temperature range of engine operation. In this case, the problem is to select a certain optimum pair (p^*_{min}, S_{gor}/F_{sv}).

For field reaction-thrust armament, one of the basic characteristics of efficiency is the maximum range of missile flight, which for a certain given weight is determined by the velocity of the missile at the end of the active phase of the trajectory and by some secondary parameters.

An analysis of Tsiokovskiy's formula

$$v_{max} = u_e \ln\left(1 + \frac{\omega}{q_p}\right),$$

where u_e is the gas-exhaust velocity; q_p is the passive weight of the rocket, shows that the maximum velocity of the missile, which determines its effective range, is the greater the smaller the structural weight of the missile (at ω = const). On the other hand, we can see from the design of a solid-propellant reaction-thrust missile that the basic part of the structural weight is the weight of the rocket combustion chamber, and the latter in turn is determined by the thickness of the combustion-chamber walls and the length of the chamber itself. Consequently, in order to increase the maximum velocity of the missile it is necessary to make the combustion chamber so as to have a minimum wall thickness and a minimum length.

The thickness of the walls in the combustion chamber are selected

on the basis of combustion-chamber strength under the action of a given pressure within the engine; in this case, to make an engine with walls of minimum thickness it is necessary for the working pressure in the engine to be at a minimum.

The length of the combustion chamber is determined primarily by the length l_{sh} of the powder grains. The latter, with a given total powder weight ω, amounts to

$$l_{sh} = \frac{\omega}{\gamma n_{sh} s_t},$$

where γ is the specific weight of the powder; $n_{sh}s_t$ is the area of the lateral cross section of the charge consisting of n_{sh} grains, with a butt-end area of s_t for each grain.

It is evident that for a combustion chamber with an inside diameter D_k

$$n_{sh}s_t = \frac{\pi D_k^2}{4} - F_{sv},$$

i.e.,

$$l_{sh} = \frac{\omega}{\gamma} \frac{1}{\frac{\pi D_k^2}{4} - F_{sv}}.$$

We can see from the formula that at ω = const and a given diameter for the inner cavity of the combustion chamber, the length of the powder grain is all the smaller the lower the magnitude of F_{sv}, i.e., the greater the ratio S_{gor}/F_{sv}. Therefore, in order to obtain an engine of minimum length it is necessary to assume a high value for the ratio S_{gor}/F_{sv} in the design stage.

Thus the greatest velocity at the end of the active phase would be exhibited by missiles designed so as to have the lowest possible operating pressures, and further designed so as to exhibit the highest possible parameter S_{gor}/F_{sv}.

However, in the case of such a missile, as can be seen from Fig.

4.23, the process of the burning of the propellant would be unstable, since the operating point M of the process would be situated in the unstable region.

It follows from what has been said above that with the selected brand of powder (or the brand of powder stipulated in the tactical-technical requirements) the minimum possible pressure in the combustion chamber is estimated on the basis of the conditions which specify that the missile exhibit adequate velocity at the end of the active phase of the trajectory and, consequently, exhibit the required flight range.

A practical evaluation of the minimum permissible pressure can be reduced to the following. Several pairs (p^*_{min}, S_{gor}/F_{sv}) are assumed on the curve which delineates the region of unstable burning for the given brand of powder:

$$(p^*_{min};\ S_{rop}/F_{cs})_1,$$
$$(p^*_{min};\ S_{rop}/F_{cs})_2.$$
. . . . . .
. . . . . .

For each of these pairs of parameters the required wall thickness δ of the engine is calculated (according to pressure) and the required length of grain and engine is determined (in accordance with the ratio S_{gor}/F_{sv}).

In conclusion, some pair of dimensions (δ,$\underline{l}$) will correspond to each pair (p^*_{min}, S_{gor}/F_{sv}), and these dimensions will determine the weight of the combustion chamber. Those values of p^*_{min} and S_{gor}/F_{sv} are selected for which the weight of the engine will be at its minimum. The p^*_{min} and S_{gor}/F_{sv} selected in this manner can be corrected later on; in this case, the pressure can be increased somewhat, if p^*_{min} fails to provide the required magnitude of engine thrust or specific impulse, or S_{gor}/F_{sv} can be changed in order to obtain the required over-all missile parameters.

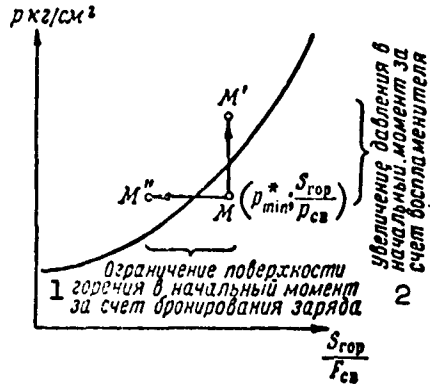

Fig. 4.24. Means of stabilizing burning at the initial instant of engine operation. 1) Restriction of burning surface at initial instant, by coating the charge; 2) increase of pressure at initial instant, by means of igniter.

We should devote attention to the fact that if the final selection of the initial operating point M exceeds somewhat the boundary of stable burning, the burning of the powder charge in certain cases can nevertheless be stabilized; in this case, the following methods have proved to be the most effective:

1) increasing the weighed portions of the igniter in order to develop a pressure greater than p^*_{min} at the initial instant and so as to have the point M enter the region of unstable burning;

2) the coating of a part of the grain surface, said coating to cover the initial burning surface, which will also serve to shift the point M into the region of unstable burning (Fig. 4.24).

The upper limit of pressure in the engine. One of the considerations which restricts the magnitude of the upper limit of the operating pressure is (from the standpoint of the interior ballistics of the engine) the requirement to provide for a given burning time of a charge (grain) of some selected configuration, i.e., the required time of engine operation.

The engine-operating time as a function of the operating pressure is governed by the fact that the burning rate of the powder is a function of pressure. In fact, a grain weighing ω burns in the engine during the time

$$\tau = \frac{\omega}{\omega_{sec}},$$

where ω_{sec} is the per-second mass flow rate of propellant.

For any powder grain configuration, in first approximation, we may assume that

$$\omega_{sec} = u_1 S_\Sigma \gamma,$$

where u_1 is the burning rate; S_Σ is the total burning surface of the grain; γ is the specific weight of the propellant, i.e.,

$$\tau = \frac{\omega}{u S_\Sigma \gamma},$$

and since

$$u = u(p),$$

the burning time of the grain will be a strong function of pressure. Let

$$u(p) = u_1 p^\nu.$$

The maximum upper pressure in the engine, whose operating time is given as being equal to τ, will be

$$p^\circ_{max} = \left[\frac{\omega}{u_1 \gamma S_\Sigma \tau}\right]^{\frac{1}{\nu}},$$

or if we take into consideration that the engine is functioning under conditions of various temperatures,

$$p^\circ_{max} = \left[\frac{\omega}{u_1 \gamma S_\Sigma \varphi(t_{0\,max})}\right]^{\frac{1}{\nu}}. \qquad (4.41')$$

With a linear burning-rate function

$$\tau = \frac{\omega}{u S_\Sigma \gamma} = \frac{\omega}{(ap + b) f(t_{0\,max}) S_\Sigma \gamma}$$

and

$$p^{\circ}_{max} = \frac{1}{\alpha}\left(\frac{\omega}{\gamma S_{\Sigma} \tau f(\ell_{\theta max})} - b\right). \qquad (4.41'')$$

It is natural, of course, that if both the working pressure p_{rab} and the time τ are either given or selected for the engine, then the above relationships will make it possible to evaluate the required magnitude of burning surface which is defined as follows for the two burning-rate functions:

$$S_{\Sigma} = \frac{\omega}{\varkappa(p_{pab}) f(\ell_{max}) \gamma \tau}. \qquad (4.42)$$

The final selection of the operating pressure on the basis of the limiting range of its extreme values

$$p^{\circ}_{min} < p < p^{\circ}_{max}$$

is carried out at a much later stage of the engine design and, as a rule, here we take into consideration the results obtained in test-stand firings of experimental engine models.

§5. BASIC RELATIONSHIPS FOR THE THEORY OF GAS OUTFLOW FROM AN ENGINE

The operation of a solid-propellant rocket engine can be presented schematically as a combination of two interrelated processes — the burning of the powder and the movement (outflow) of the products of combustion from the combustion chamber. In this case, the reaction force that results in the motion of the rocket or of some other special installation comes about directly as a result of the outflow of the products of powder combustion.

We know from the theory of jet engines that the effectiveness (thrust) of an engine of this type is a function of a great many factors, but is determined primarily by the parameters of the exhaust gas stream and certain structural characteristics of the rocket. It has also been established that of all the parameters of the stream the most important are the velocity of the products of combustion at the outlet

from the engine, and in this case the engine is all the more effective the higher this exhaust velocity.

To increase the exhaust velocity at the outlet from the combustion chamber, special fittings are installed, and these are called nozzles. They make it possible to increase the velocity of the flow of the products of combustion to 1500-2500 m/sec.

Elements of the Theory of an Ideal Supersonic Nozzle

The study of the quantitative relationships governing the motion of gases and gaseous mixtures indicates that there exist two types of flows which exhibit basic differences between one another.

With low velocities of motion, gases behave virtually like an ideal incompressible fluid and are subject to the basic quantitative relationships of hydrodynamics. However, as soon as the velocity of the gas motion begins to increase and exceed a certain maximum limit, the effect of compressibility introduces such unique features into the nature of the gas flow — such basic qualitative changes of the flow — that the corresponding flow must be regarded as a special flow which is subject to specific laws which are different from the laws of hydromechanics.

It turned out that the maximum velocity which separates these two types of flows is the velocity of sound propagation in the given gas or gaseous mixture. The respective flows are generally referred to as subsonic or supersonic.

Without dwelling in detail on an examination of the features of subsonic or supersonic flows, we will point out only that with respect to the problem of interest to us, i.e., the acceleration of the flow, the following has been established: in order to increase the velocity of the flow in the case of subsonic flow, it is necessary to compress the stream, whereas in the case of supersonic flow the stream must,

conversely, be expanded. In this case, the mathematical relationship between the velocity of gas motion and the area of the flow cross section takes the following form:

$$\frac{F}{F_{kp}}=\frac{\left(1+\frac{k-1}{2}M^2\right)^{\frac{k+1}{2(k-1)}}}{M\left(\frac{k+1}{2}\right)^{\frac{k+1}{2(k-1)}}}, \qquad (4.43')$$

where F is the area of the flow in some section of the gas stream; F_{kr} is the area of the stream section in which the velocity of the gas motion is equal to the critical velocity, i.e., the velocity of sound propagation in this gas; M is the dimensionless gas velocity in the cross section of the stream having a flow area F (the M(ach) number of the flow);

$$M=\frac{w}{a_{zv}};$$

w is the velocity of gas motion in the cross section under consideration; a_{zv} is the speed of sound in this same cross section; k is the exponent for the process of the expansion of the gas flow.

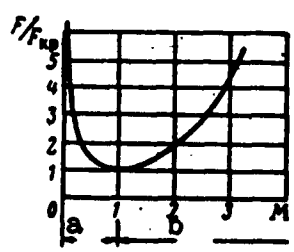

Fig. 4.25. Dimensionless area of the lateral cross section of the flow as a function of the dimensionless velocity M of the flow. a) Range of subsonic flows; b) supersonic flows.

Relationship (4.43) is expediently presented graphically (Fig. 4.25) for purposes of analysis. From the graph we can see that in the

cross section $F/F_{kr} = 1$, i.e., $F = F_{kr}$, a critical flow regime is established ($M = 1$), i.e., $w = a_{zv}$. At velocities $w < a_{zv}$, lower ratios of F/F_{kr} correspond to greater velocities (greater M(ach) numbers), i.e., to accelerate the stream in this range of velocities it is necessary to compress the flow in accordance with the left-hand branch of the curve. On the other hand, when $w > a_{zv}$ greater ratios of F/F_{kr} correspond to higher M(ach) numbers, i.e., to accelerate the flow in the case of velocities greater than the speed of sound it is necessary to expand the flow, in accordance with the right-hand branch of the curve.

In accordance with this, a supersonic nozzle intended to accelerate the flow of the products of combustion from velocities of the order of several tens of meters per second to supersonic velocities, is given a complex shape (profile) which can conditionally be divided into three sections:

— the inlet section of the nozzle, with a converging channel;

— the outlet section of the nozzle, with a diverging channel;

— the critical section of the nozzle (throat), with a channel of minimum cross section.

Relationship (4.43) makes it possible to calculate the velocity of the gas flow in any section of the nozzle, if the configuration of the nozzle is known. This same relationship can be used to determine the shape (dimensions) of the nozzle, said information necessary in order to obtain the required flow velocities in the corresponding sections of the nozzle. Strictly speaking, Relationship (4.43) is valid only in the absence of losses in the stream, i.e., with a change in the state of the gas in accordance with an ideal adiabatic curve. It is for this reason that this curve describes the process of gas acceleration only for an ideal nozzle.

Gas-Flow Parameters in the Critical Cross Section of the Nozzle

In the theory of gasdynamics, in which we study supersonic flows of gases, it is demonstrated that the parameters of the gas stream in the critical section of a supersonic nozzle depend only on the gas parameters in the combustion chamber and the exponent for the process of gas expansion:

$$\left.\begin{aligned} \frac{p_0}{p_{кр}} &= \left(\frac{k+1}{2}\right)^{\frac{k}{k-1}}, \\ \frac{\rho_0}{\rho_{кр}} &= \left(\frac{k+1}{2}\right)^{\frac{1}{k-1}}, \\ \frac{T_0}{T_{кр}} &= \frac{k+1}{2}, \\ \frac{a_0}{a_{кр}} &= \left(\frac{k+1}{2}\right)^{\frac{1}{2}}, \end{aligned}\right\} \qquad (4.44)$$

where p_0, ρ_0, T_0, and a_0 are the parameters of the gas mixture of the products of combustion; p_{kr}, ρ_{kr}, and T_{kr} are the parameters of the flow of the products of combustion in the critical section of the nozzle; $a_{kr}(w_{kr})$ is the critical speed of sound.

Using (4.44) and bearing in mind that for an adiabatic process the speed of sound $a_{zv} = \sqrt{kgRT}$, we can easily obtain a calculation formula of the following form for the critical velocity of the flow:

$$a_{кр} = w_{кр} = \sqrt{\frac{2k}{k+1} gRT_0}. \qquad (4.45)$$

In addition to the dimensionless flow velocity $M = w/a_{zv}$ it is convenient to introduce the relative magnitude

$$\frac{w}{w_{кр}} \left(\text{or } \frac{w}{a_{кр}}\right),$$

which indicates by how many times the velocity of the stream in some section differs from the velocity of the stream in the critical section. This magnitude is referred to as the velocity factor and is denoted by

$$\lambda = \frac{w}{w_{кр}}.$$

It is evident that the parameters M and λ are interrelated; we can show that the relationship can be described as follows:

$$\left.\begin{aligned} M^2 &= \frac{\frac{2}{k+1}\lambda^2}{1-\frac{k-1}{k+1}\lambda^2}, \\ \lambda^2 &= \frac{\frac{k+1}{2}M^2}{1+\frac{k-1}{2}M^2}. \end{aligned}\right\} \qquad (4.46)$$

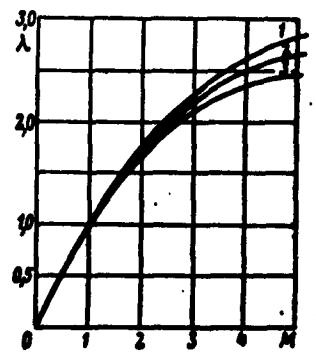

Fig. 4.26. Curves showing the interrelationship between the M(ach) number and the velocity factor λ. 1) k = 1.20; 2) k = = 1.25; 3) k = 1.30.

In the theory of jet engines we use both the dimensionless velocity M as well as the coefficient λ; in this case, some simpler relationships can be obtained through the use of the M(ach) numbers, whereas in other cases simpler relationships are obtained through the use of the coefficient λ. Figure 4.26 shows the curves which illustrate the interrelationship between the dimensionless velocity of the stream and the velocity coefficient; these curves can be employed in the calculations.

The dimensionless area of the nozzle as a function of the velocity of the flow (4.43) is expressed as follows in terms of the veloc-

ity coefficient λ:

$$\frac{F}{F_{кр}}=\frac{1}{\lambda}\left[\frac{\frac{2}{k+1}}{1-\frac{k-1}{k+1}\lambda^2}\right]^{\frac{1}{k-1}}. \qquad (4.43'')$$

This formula can also be used in addition to (4.43'), when it is necessary to determine the velocity of the flow in various cross sections of the nozzle or when it is necessary to select the dimensions of characteristic nozzle sections.

Calculation of Gas-Stream Parameters in Any Nozzle Cross Section

The parameters of the gas flow in any cross section of the nozzle are functions not only of the gas parameters in the combustion chamber and the exponent k, but also of the local velocity of the flow.

The calculation relationships for the determination of the flow parameters at any cross section take the following form:

$$\left.\begin{aligned}
\frac{p_0}{p}&=\left(1+\frac{k-1}{2}M^2\right)^{\frac{k}{k-1}},\\
\frac{\rho_0}{\rho}&=\left(1+\frac{k-1}{2}M^2\right)^{\frac{1}{k-1}},\\
\frac{T_0}{T}&=\left(1+\frac{k-1}{2}M^2\right),\\
\frac{a_0}{a}&=\left(1+\frac{k-1}{2}M^2\right)^{\frac{1}{2}}.
\end{aligned}\right\} \qquad (4.47)$$

In calculating the flow not in accordance with the M(ach) number but in accordance with the velocity coefficient λ, it is convenient to use the so-called gasdynamic flow functions:

$$\left.\begin{aligned}
\pi(\lambda)&=\frac{p}{p_0}=\left(1+\frac{k-1}{k+1}\lambda^2\right)^{\frac{k}{k-1}},\\
\varepsilon(\lambda)&=\frac{\rho}{\rho_0}=\left(1-\frac{k-1}{k+1}\lambda^2\right)^{\frac{1}{k-1}},\\
\tau(\lambda)&=\frac{T}{T_0}=\left(1-\frac{k-1}{k+1}\lambda^2\right).
\end{aligned}\right\} \qquad (4.48)$$

The values of the gasdynamic functions $\pi(\lambda)$, $\varepsilon(\lambda)$, and $\tau(\lambda)$ for

various $\underline{k}$ and λ are presented in special tables, and this substantially facilitates the carrying out of the required calculations. Figure 4.27 presents the curves for $\pi(\lambda)$, $\varepsilon(\lambda)$, and $\tau(\lambda)$, which can be used in practical computations.

Formulas (4.47) or (4.48) make it possible to calculate the parameters of an ideal flow at the outlet section of the nozzle of an engine, and for this purpose it is sufficient to substitute M_a or λ_a into the formulas; these quantities, determined in accordance with (4.43) or (4.43') by the relative dimensions of the nozzle alone, characterize the velocity of the flow at the outlet section of the nozzle. In this case, the following will be the calculation relationships:

$$\left.\begin{aligned} \frac{p_0}{p_a} &= \left(1+\frac{k-1}{2}M_a^2\right)^{\frac{k}{k-1}}, \\ \frac{\rho_0}{\rho_a} &= \left(1+\frac{k-1}{2}M_a^2\right)^{\frac{1}{k-1}}, \\ \frac{T_0}{T_a} &= \left(1+\frac{k-1}{2}M_a^2\right) \end{aligned}\right\} \qquad (4.49)$$

or

$$\left.\begin{aligned} p_a/p_0 &= \pi(\lambda_a), \\ \rho_a/\rho_0 &= \varepsilon(\lambda_a), \\ T_a/T_0 &= \tau(\lambda_a). \end{aligned}\right\} \qquad (4.50)$$

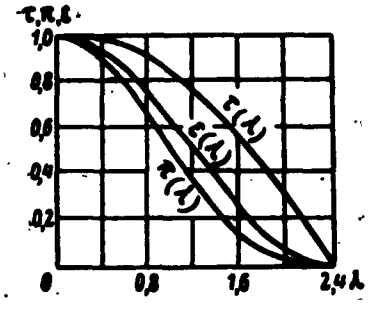

Fig. 4.27. Curves of the gas-dynamic functions.

Figure 4.28 presents tentative curves which illustrate the nature

of the change in the parameters of the gas flow along the length of the engine; for these curves p_a, ρ_a, and T_a are the parameters of the flow of the products of combustion at the outlet section of the nozzle; M_a is the M(ach) number of the flow at the outlet section of the nozzle; λ_a is the velocity coefficient of the flow at the outlet section of the nozzle; w_a is the flow velocity of the products of combustion at the outlet section of the nozzle; d_{kr} and d_a are the diameters of the critical and outlet sections of the nozzle, respectively.

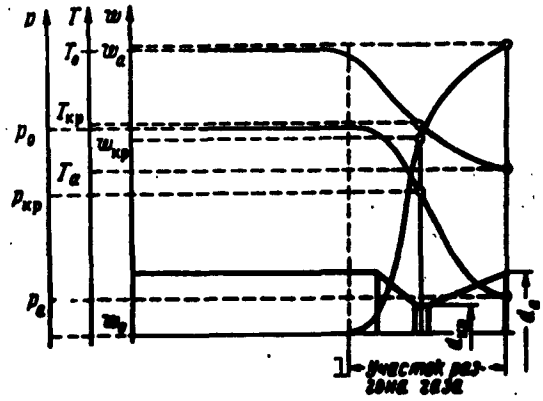

Fig. 4.28. The nature of the change in the parameters p, w, and T of the products of combustion along the combustion chamber of a solid-propellant rocket engine. 1) Gas-acceleration section.

Concept of Rated and Nonrated Exhaust Regimes

The regime of the outflow of the products of combustion through the nozzle is referred to as the rated regime, if the gases are expanded during the exhaust process to a pressure equal to the pressure of the ambient medium, i.e., if the pressure p_a in the stream at the outlet section of the nozzle is equal to the pressure p_H of the ambient medium:

$$p_a = p_H.$$

In practice, we frequently encounter cases in which $p_a \neq p_H$, in which case $p_a > p_H$ (an operating regime with underexpansion) or $p_a < p_H$ (an operating regime with overexpansion).

An engine operating regime with underexpansion appears when the area of the outlet section of the nozzle for some reason must be made smaller than the theoretical (calculated) dimensions. In the case of underexpanded outflow, the engine functions rather stably, and only some loss of engine thrust, due to incomplete expansion of the stream of products of combustion, is observed. Underexpansion may take place when the area of the outlet section of the nozzle is equal to the calculated dimension, if the pressure changes during the flight of the object so that it drops noticeably below p_a at some instant of time (climb to great altitudes with pronounced rarefaction of the atmosphere).

In an overexpansion regime, the gas expands to a pressure below that of the ambient medium. This results in a flow that is actually moving from a region of reduced pressure to a region of greater pressure. Experiments with nozzles which overexpand the gas stream have demonstrated* that such motion, at first glance contradictory to physical concepts, can actually take place. However, the possibility of the existence of such motion is restricted by comparatively low "super differences," and the motion of the gas in an overexpansion nozzle is itself distinguished by great instability. With significant overexpansion, when $p_a/p_H \leq 0.3\text{-}0.5$, intensive jumps may arise within the nozzle, and these disrupt significantly the regime of the normal acceleration of the flow of products, so that in certain cases not even the critical velocity will be attained.

In the case of overexpansion, engine thrust may also diminish in comparison to the calculated thrust, and in this case the drop in thrust will take place as a result of the action of the excessive coun-

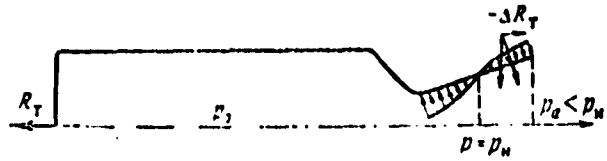

Fig. 4.29. Reduction in engine thrust R_t in the case of operations with an overexpansion regime.

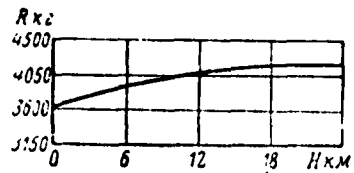

Fig. 4.30. Curve of relative measurement of engine thrust (engine operating on solid propellant) as function of altitude H of rocket flight.

terpressure exerted on a part of the nozzle contour (Fig. 4.29). In the general case, the nature of the change in engine thrust in the case of overexpanded gas outflow, in comparison with thrust in the case of theoretical outflow, depends on the degree of overexpansion and the configuration of the nozzle; in this case, with overexpansion increased outflow velocity will serve to increase engine thrust somewhat, whereas engine thrust will drop as a result of $p_a < p_H$ and the effect of the counterpressure on the wall of the nozzle. It is generally quite difficult to predict in advance what the final total change in thrust will be, since this change is determined by the geometry and ballistic parameters of each specific engine.

If the nozzle is functioning under a regime of underexpansion, with a decline in external pressure (p_H), for example, because of a change in flight altitude, engine thrust generally increases somewhat (Fig. 4.30).

§6. REACTION FORCE AND SPECIFIC IMPULSE OF A SOLID-PROPELLANT ROCKET ENGINE

Derivation of Reaction-Force Formulas

For the derivation of the formulas of reaction force we will use the theorem for the mechanics of momentum. In accordance with this theorem, a change in momentum of any isolated mechanical system is equal to the impulse acting on this system.

In our case (Fig. 4.31), at any arbitrary instant of time t the isolated system consisting of a rocket and a certain volume of ambient air surrounding the rocket will be characterized by momentum.

$$K_t = m\bar{v},$$

where m is the rocket mass; $\bar{v}$ is the flight velocity of the rocket (vector).

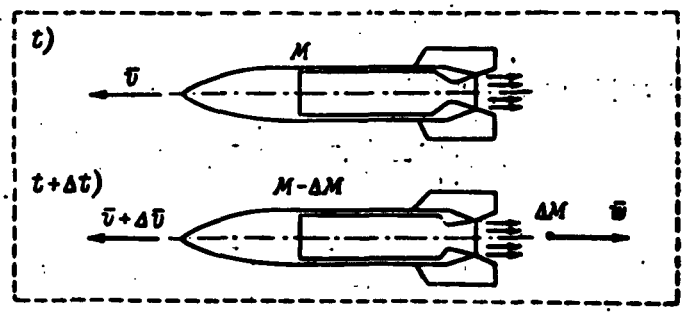

Fig. 4.31. For the derivation of the equation of motion for the rocket.

After an interval of time Δt, the system under consideration will consist of the rocket, the ambient air, and the mass of the products of combustion ejected from the nozzle of the rocket during the time period Δt. In this case, the mass of the rocket has been reduced by Δm, and the velocity has increased by $\Delta\bar{v}$. If the velocity of the products of combustion is denoted by $\bar{w}$, the total momentum of the system in the latter case will be

$$K_{t+\Delta t} = (m-\Delta m)(\bar{v}+\Delta\bar{v}) + \Delta m(\bar{v}-\bar{w}).$$

In accordance with the momentum theorem

$$\Delta K_t = \left(\sum_{i=1}^{n} \bar{F}_i\right) \Delta t,$$

where $\left(\sum_{i=1}^{n} \bar{F}_i\right) \Delta t$ is the impulse acting on the system of forces; $\sum_{i=1}^{n} \bar{R}_i$ – is the sum of all forces appearing in the system under consideration; ΔK_t is the change in the momentum of the system.

In our case

$$\Delta K_t = K_{t+\Delta t} - K_t = (m - \Delta m)(\bar{v} + \Delta \bar{v}) + \Delta m (\bar{v} - \bar{w}) - m\bar{v} =$$
$$= m\bar{v} - \Delta m \bar{v} + m\Delta \bar{v} - \Delta m \Delta \bar{v} + \Delta m \bar{v} - \Delta m \bar{w} - m\bar{v}$$

or, neglecting the quantities of a higher order of smallness,

$$\Delta K_t \approx m\Delta \bar{v} - \Delta m \bar{w}.$$

In accordance with the theorem we will have

$$m\Delta \bar{v} - \Delta m \bar{w} = \left(\sum_{i=1}^{n} \bar{R}_i\right) \Delta t,$$

$$m \frac{\Delta \bar{v}}{\Delta t} - \frac{\Delta m}{\Delta t} \bar{w} = \sum_{i=1}^{n} \bar{R}_i$$

or, in differential form,

$$m \frac{d\bar{v}}{dt} - \frac{dm}{dt} \bar{w} = \sum_{i=1}^{n} \bar{R}_i,$$

$$m \frac{d\bar{v}}{dt} = \frac{dm}{dt} \bar{w} + \sum_{i=1}^{n} \bar{R}_i. \qquad (4.51)$$

Expression (4.51) is a differential equation for the motion of a body of variable mass. This equation was first derived by the Russian scientist I.V. Meshcherskiy and published in his works on the dynamics of a point of variable mass (1897). We can see from (4.51) that the equation for the motion of a body of variable mass is unlike the equation for the motion of conventional solids only in that the number of external forces includes yet another additional force ($(dm/dt)\bar{w}$), which characterizes the nature of the change in the mass of the body

and the parameters of the relative motion of the ejected mass.

Let us examine $\sum_1^n \bar{R}_i$ in greater detail. For the selected system, this total includes: the force of gravity $m\bar{g}$, the thrust R_t, and the forces that are due to the action of the rocket in the face of the approaching stream of air (the aerodynamic forces R_{aerd}):

$$\sum_{i=1}^{n} \bar{R}_i = m\bar{g} + \bar{R}_t + \bar{R}_{аэрд}.$$

Presenting the aerodynamic force in the following form:

$$\bar{R}_{аэрд} = \bar{R}_p + \bar{R}_{тр} + \Delta\bar{R}_{проч},$$

where $\bar{R}_r$ is the equivalent force of pressure distributed over the body of the rocket; $\bar{R}_{tr}$ is the equivalent force of aerodynamic friction; $\Delta\bar{R}_{proch}$ is the equivalent force of all other aerodynamic forces, we will obtain the following equation of rocket motion:

$$m\frac{d\bar{v}}{dt} = \frac{dm}{dt}\bar{w} + m\bar{g} + \bar{R}_r + \bar{R}_p + \bar{R}_{тр} + \Delta\bar{R}_{проч}. \qquad (4.51')$$

Now let an operating rocket be made immobile (firmly held fast on a test stand). It is evident that in this case v = 0; $m\bar{g}$ is offset by the reaction of the stand supports; and $\bar{R}_{tr}$, $\Delta\bar{R}_{proch} = 0$, i.e., (4.51') will take the following form:

$$\frac{dm}{dt}\bar{w} + \bar{R}_r + \bar{R}_p = 0.$$

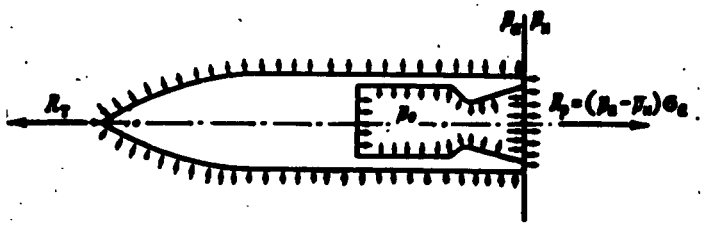

Fig. 4.32. Diagram of forces acting on a rocket fastened on a test stand, with engine in operation.

We can see from Fig. 4.32 that as a result of the symmetry of the rocket body, pressure is offset almost completely along the entire con-

tour (outline) of the rocket and it is only at the outlet of the nozzle that some difference in pressure occurs, so that

$$R_p = (p_a - p_н)\,\sigma_a,$$

where p_a is the pressure of the outflow products at the outlet section of the nozzle; p_H is the counterpressure of the ambient medium at the outlet section of the nozzle; σ_a is the area of the outlet section of the nozzle.

If we take into consideration the mutual direction of the vectors $\bar{w}$, $\bar{R}_t$, and the component $(p_a - p_H)\,\sigma_a$, and assuming a positive direction of rocket motion, we will obtain

$$-\frac{dm}{dt}w + R_т - (p_a - p_н)\,\sigma_a = 0,$$

whence the formula which determines the thrust of the rocket engine will be:

$$R_т = \frac{dm}{dt}w + (p_a - p_н)\,\sigma_a$$

or

$$R_т = m_{сек}w + (p_a - p_н)\,\sigma_a, \qquad (4.52)$$

where $m_{sec} = dm/dt$ is the per-second flow rate of gases from the engine.

In the case of a theoretical outflow regime $p_a = p_H$, and the formula for thrust takes the following form:

$$R_т = m_{сек}w. \qquad (4.52')$$

If we denote

$$w_{эф} = w + \frac{\sigma_a}{m_{сек}}(p_a - p_н),$$

then for any outflow regime the thrust can be presented in the following single form:

$$R_т = m_{сек}w_{эф}, \qquad (4.52'')$$

where w_{ef} is the effective outflow velocity.

In calculation practice it is convenient to use a formula to cal-

culate R_t in terms of the pressure p_0 in the combustion chamber of the engine. The corresponding relationship is easily obtained if we take into consideration that according to (4.27)

$$m_{sec} = A p_0 \sigma_{kp}.$$

In fact, if we substitute this expression for m_{sec} into (4.52), we will obtain

$$R_T = m_{sec} w_a + (p_a - p_n) \sigma_a = A p_0 \sigma_{kp} w_a + p_a \sigma_a - p_n \sigma_a =$$
$$= \left(A w_a + \frac{p_a}{p_0} \frac{\sigma_a}{\sigma_{kp}} \right) p_0 \sigma_{kp} - p_n \sigma_a.$$

Let us examine the sum in the brackets of the last relationship. Here

$$A = \frac{\left(\frac{2}{k+1}\right)^{\frac{k}{k-1}} \sqrt{\frac{2k}{k+1} g}}{\sqrt{RT_0}} = A(k);$$

$$w_a = \sqrt{\frac{2k}{k+1} g R T_a} = \sqrt{\frac{2k}{k+1} g R T_0 \left[1 - \left(\frac{p_a}{p_0} \right)^{\frac{k-1}{k}} \right]}.$$

According to (4.49)

$$\frac{p_a}{p_0} = \frac{1}{\left(1 + \frac{k-1}{2} M_a^2\right)^{\frac{k}{k-1}}} = \frac{p_a}{p_0}(k, M_a),$$

but from (4.43) it follows that

$$M_a = M\left(k, \frac{\sigma_a}{\sigma_{kp}}\right),$$

i.e.,

$$\frac{p_a}{p_0} = f\left(k, \frac{\sigma_a}{\sigma_{kp}}\right),$$

so that Aw_a is a function only of $\underline{k}$ and σ_a/σ_{kr}. In the final analysis, we will see that

$$A w_a + \frac{p_a}{p_0} \frac{\sigma_a}{\sigma_{kp}} = \xi\left(k, \frac{\sigma_a}{\sigma_{kp}}\right),$$

i.e.,

$$R_T = \xi\left(k, \frac{\sigma_a}{\sigma_{kp}}\right) p_0 \sigma_{kp} - p_n \sigma_a.$$

or, neglecting the quantity $p_H\sigma_a$ in view of the smallness of atmospheric pressure in comparison with the operating pressures in the combustion chamber,

$$R_\tau = \xi\left(k, \frac{\sigma_a}{\sigma_{kp}}\right) p_0 \sigma_{kp}. \qquad (4.53)$$

The coefficient $\xi(k, \sigma_a/\sigma_{kr})$ is referred to as the coefficient of reaction force or the Lanzheven [sic] coefficient. The numerical values of this coefficient for $k = 1.25$ and various nozzle expansions d_a/d_{kr} are presented in Table 4.8.

TABLE 4.8

Numerical Values of the Theoretical Magnitude of the Coefficient of Reaction Force

1) Расширение $d_a/d_{кр}$	1,0	1,2	1,4	1,6	1,8	2,0	2,2	2,4	2,6	2,8	3,0
$\xi = \xi(d_a/d_{кр})$	1,25	1,38	1,46	1,51	1,56	1,60	1,62	1,64	1,67	1,68	1,70

1) Expansion, d_a/d_{kr}.

Total Reaction-Force Impulse and Specific Impulse of Engine

The total impulse J of the reaction force is referred to as the integral characteristic of the curve for engine thrust R_t with respect to time:

$$J = \int_0^\tau R_\tau \, dt,$$

where τ is the operating time of the rocket engine.

If engine thrust is approximately constant throughout the entire period of engine operation,

$$J = \overline{R}_\tau \tau. \qquad (4.54)$$

The magnitude of the total impulse is a complex characterization of the effectiveness of the operation of a solid-propellant rocket engine, and here the level of thrust developed by the engine and the

period of time that the thrust acts on the rocket are both taken into consideration.

It is the general practice to regard the magnitude which indicates the impulse imparted to the rocket in the burning of 1 kg of powder in the engine as the most important characteristic of a solid-propellant rocket engine. This quantity is referred to as specific impulse:

$$J_1 = \frac{J}{\omega}, \tag{4.55}$$

where ω is the total weight of the working powder charge.

If we express ω in terms of the per-second flow rate of the powder gases $\omega = m_{sec} g \tau$ and if we take into consideration (4.54), we will find

$$J_1 = \frac{J}{\omega} = \frac{\bar{R}\tau}{g m_{cek} \tau} = \frac{\bar{R}}{m_{cek} g}. \tag{4.56}$$

Substituting the value of R and m_{sec} into this equation, we will obtain this formula in expanded form:

$$J_1 = \frac{R}{g m_{cek}} = \frac{1}{A p_0 \varphi_1} (k p_0 \varphi_{sp} - p_a \varphi_a)$$

or

$$J_1 = \frac{k}{A} - \frac{1}{A} \frac{p_a}{p_0} \frac{\varphi_a}{\varphi_{sp}}. \tag{4.56'}$$

Using this expression and some of the relationships presented above, we can show that

$$J_1 = \frac{w_{ef}}{g}. \tag{4.57}$$

The specific impulse should be regarded as the basic criterion for the evaluation of the effectiveness of a solid-propellant rocket engine. The greater the value of the specific impulse, the more effective the corresponding engine.

Derivation of the K.E. Tsiolkovskiy Formula

It is easy to derive the K.E. Tsiolkovskiy formula from the equa-

tion of rocket motion, if we assume that the flight is accomplished in the absence of any resistance to the motion of the rocket and if we neglect the action of mass forces on the flight. Given these assumptions, the equation of rocket motion is simplified to the following form:

$$m\frac{d\bar{v}}{dt}=\frac{dm}{dt}\bar{w}_{эф}$$

or if we take into consideration the directions of the vectors $\bar{v}$ and $\bar{w}_{ef}$

$$m\frac{dv}{dt}=-\frac{dm}{dt}w_{эф}.$$

and the equation can easily be integrated.

In fact, dividing the variables, we will obtain

$$dv=-w_{эф}\frac{dm}{m},$$

whence

$$\int_{v_0}^{v_t}dv=\int_{m_0}^{m_t}-w_{эф}\frac{dm}{m},$$

$$\Delta v_t=v_t-v_0=-w_{эф}\ln\frac{m_t}{m_0}, \qquad (4.58')$$

where Δv_t is the increment in velocity as a result of the operation of the rocket engine (in comparison with the initial velocity); m_t is the rocket mass remaining from the initial mass m_0 at some instant of time.

The maximum velocity increment in this case is

$$\Delta v_{max}=-w_{эф}\ln\frac{m_к}{m_0}, \qquad (4.58'')$$

where m_k is the final weight of the rocket, i.e., the passive weight q_p; m_0 is the initial weight of the rocket (launching weight).

The ratio m_k/m_0 characterizes the perfection of the structural fabrication of the rocket and is referred to as the coefficient μ_k of the rocket:

$$\Delta v_{max}=-w_{эф}\ln\mu_к.$$

It can be demonstrated that for a multistage rocket, in which the stages are successively jettisoned,

$$\Delta v_{max} = -w_{эф} \ln (\mu_{к1}\mu_{к2} \cdots \mu_{к\, n_{ст}}),$$

where n_{st} is the number of operating stages.

For solid-propellant rocket engines, the K.E. Tsiolkovskiy formula is generally written somewhat differently, using

$$m_к = q_т,$$
$$m_0 = q_т + \omega,$$

i.e., in the following form

$$v_{max} = w_{эф} \ln \frac{q_т + \omega}{q_т} = w_{эф} \ln \left(1 + \frac{\omega}{q_т}\right) \qquad (4.58''')$$

or taking into consideration (4.57)

$$v_{max} = j_1 g \ln \left(1 + \frac{\omega}{q_т}\right). \qquad (4.59)$$

Thrust and Specific Impulse as Functions of the Structural Features and Ballistic Characteristics of the Engine

In the most general form, the thrust of a rocket engine is determined by the following relationship

$$R_т = \left(A w_a + \frac{f_a}{f_0} \frac{c_a}{c_{ид}}\right) p_0 \varphi_{ид} - p_н f_a,$$

for which it has been demonstrated that

$$\left(A w_a + \frac{f_a}{f_0} \frac{c_a}{c_{ид}}\right) = \xi\left(k, \frac{c_a}{c_{ид}}\right).$$

Thus thrust is completely determined by the magnitude of the operating pressure in the combustion chamber of the engine, the composition, and the properties of the gaseous products of powder combustion ($\underline{k}$), and the structural features of the engine, particularly the relationship between the areas of the outlet and critical sections of the nozzle; the parameters of the ambient medium (p_H) also have some effect on thrust. However, if the ambient medium is the atmosphere,

$$(p_H)_{max} = 1 \text{ kg/cm}^2$$

and at pressures of $p_0 \approx 50\text{-}100$ kg/cm^2 in the combustion chamber of a

solid-propellant rocket engine their effect can be neglected.

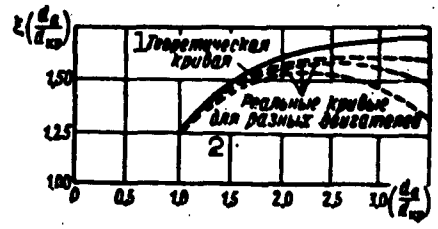

Fig. 4.33. The nature of the actual relationship $\xi = \xi(d_a/d_{kr})$. 1) Theoretical curve; 2) actual curves for various engines.

For a selected operating pressure established by σ_{kr} and a definite powder, the thrust of a solid-propellant rocket engine is a single-valued function of σ_a/σ_{kr}. In design practice, instead of the area ratio σ_a/σ_{kr} we more frequently use the ratio of the diameters of the corresponding cross sections, referring to this ratio as the expansion of the nozzle:

$$\xi = \frac{d_a}{d_{kr}},$$

i.e., for the conditions mentioned above engine thrust is wholly determined by the expansion of the nozzle.

The theoretical relationship $R = R(d_a/d_{kr})$, determined by the relationship $\xi = \xi(d_a/d_{kr})$ (see Table 4.7), is achieved in practice only in the case of small expansion. In the case of great expansion, a less intensive increase in thrust (in comparison with the theoretical increase) is observed with an increase in d_a/d_{kr} because of losses in the nozzle and certain secondary outflow effects; in fact, there may be some drop in the magnitude of thrust for $(d_a/d_{kr}) > (d_a/d_{kr})_{pred}$. The tentative relationship between the Lanzheven [sic] coefficient and the expansion of the nozzle for conditions of actual outflow is presented in Fig. 4.33. We can see from the curve presented in this figure

that

$$\left(\frac{d_a}{d_{kp}}\right)_{опт} = 2 \div 3$$

and the maximum magnitude of the Lanzheven coefficient does not exceed

$$\xi_{max} = 1{,}4 \div 1{,}55.$$

Of the factors affecting the magnitude of specific impulse, the first that should be mentioned are the following:

1) expansion of nozzle, d_a/d_{kr};

2) pressure p_0 in the combustion chamber of the engine;

3) the initial temperature of the powder charge and the temperature of the products of combustion;

4) the heating value $Q_{w(zh)}$ of the powder;

5) the presence of various kinds of losses in the engine and primarily in the nozzle, as well as the heat losses in the combustion chamber.

Let us examine the successive effect on j_1 of each of the above-enumerated factors.

In accordance with (4.56)

$$j_1 = \frac{R_t}{g m_{sec}},$$

and since m_{sec} is not a function of nozzle expansion, $j_1 = j_1(d_a/d_{kr})$ is similar to $R_t = R(d_a/d_{kr})$. The above-presented considerations with respect to the existence of certain maximum expansion values remain in force, and if these values are exceeded a drop in the theoretical parameters of thrust and specific impulse is observed in practice. Specific impulse as a function of expansion varies for various values of operating pressure in the combustion chamber. With an increase in the operating pressure the increment in impulse as a result of the increased expansion becomes more pronounced. As an example, in Table 4.9 we have presented the relative increment in specific engine impulse

for various pressures due to increased nozzle expansion from σ_a/σ_{kr} = = 1.0 to σ_a/σ_{kr} = 5.0 in one case and from σ_a/σ_{kr} = 1.0 to the theoretical value (for each pressure) in the other case.

TABLE 4.9

Relative Increment in Specific Impulse as a Function of Nozzle Expansion for Various Pressures within the Combustion Chamber

1 Давление в камере сгорания	100	150	200
	2 кг/см²		
$\frac{\Delta J_1}{J_1}$ % 3 при $\frac{\sigma_a}{\sigma_{кр}}=1 \rightarrow \frac{\sigma_a}{\sigma_{кр}}=5{,}0$	26,8	27,8	28,2
$\frac{\Delta J_1}{J_1}$ % при $\frac{\sigma_a}{\sigma_{кр}}=1 \rightarrow \frac{\sigma_a}{\sigma_{кр}}=\left(\frac{\sigma_a}{\sigma_{кр}}\right)_{расч}$	29,0	32,1	33,6

1) Pressure in the combustion chamber; 2) kg/cm^2; 3) at.

We can see from Table 4.9 that with great expansion, pressure has a relatively weak effect on the magnitude of the specific impulse. For example, for $d_a/d_{kr} \approx 2.24$ an increase in operating pressure from 100 to 200 kg/cm^2 (i.e., by a factor of two) increases the value of the specific impulse by only 1.4%. This increment in impulse virtually fails to offset even the increase in engine weight resulting from the need to provide for strength with this increased pressure.

On the other hand, increased nozzle expansion from d_a/d_{kr} = 2.24 to the theoretical value increases the specific impulse by 2.2% at p_0 = 100 kg/cm^2; by 4.3%, at p_0 = 150 kg/cm^2; and by 5.4%, at p_0 = 200 kg/cm^2.

If we take into consideration that because of the limited flare angle of the outlet cone it becomes necessary to increase the length of the nozzle in the case of nozzle expansion, the weight of the engine (its nozzle assembly) will increase as the expansion becomes

greater. In this case, the effective impulse increment will be reduced accordingly.

Thus with an increase in nozzle expansion, specific engine impulse increases only up to some limit expansion values which are equal approximately to

$$\left(\frac{d_a}{d_{кр}}\right)_{пред} = 2 \div 3.$$

Further expansion can result in the reduction of the specific impulse of the engine. With increased nozzle expansion the weight of the nozzle assembly of the engine increases, so that it is always necessary to estimate the effective impulse increment in the calculations, rather than the absolute increment.

Let us dwell in some detail on specific impulse as a function of pressure. In accordance with (4.56'), at $\sigma_a/\sigma_{kr} = \text{const}$

$$j_1 = \text{const}_1 + \frac{\text{const}_2}{p_0},$$

i.e., with an increase in the pressure in the combustion chamber, the impulse j_1 increases, attaining its maximum value at $p_0 \to \infty$:

$$(j_1)_{max} = \frac{k}{\lambda}.$$

For one of the engines, the values of j_1 for various operating pressures, calculated according to (4.56'), amounted to:

$j_1 = 215$ kg·sec/kg at $p_0 = 50$ kg/cm^2

$j_1 = 220$ " at $p_0 = 100$ "

$j_1 = 223$ " at $p_0 = 200$ "

$j_1 = 225$ " at $p_0 = 500$ "

however, test firings of this engine demonstrated that the true dependence of specific impulse on pressure is somewhat weaker, and the average values of the impulses measured during the experiment were as follows:

$$\left.\begin{array}{ll} j_1 = 196 \text{ kg·sec/kg} & \text{at } p_0 = 70 \text{ kg/cm}^2 \\ j_1 = 200 \quad " & \text{at } p_0 = 100 \quad " \\ j_1 = 202.4 \quad " & \text{at } p_0 = 200 \quad " \\ j_1 = 202.5 \quad " & \text{at } p_0 = 250 \quad " \end{array}\right\} d_a/d_k = 1.42.$$

Hence we can see that beginning with $p_0 = 150$ kg/cm^2, the engine exhibited a specific impulse that was virtually independent of the operating pressure in the combustion chamber.

Thus with an increase in the operating pressure in the combustion chamber, the specific impulse of a solid-propellant rocket engine increases. It has been established in practice that for each engine design there exists a certain maximum value of $(j_1)_{max}$ such that no changes in pressure can result in

$$j_1 > (j_1)_{max}.$$

Again we must devote our attention to the fact that with an increase in the pressure in the combustion chamber there is an increase in the structural weight of the engine because of the increased wall thickness of the combustion chamber; thus it becomes necessary each time to take into consideration not the theoretical, but the effective, increment in impulse, and the losses due to the additional weight must also be taken into consideration.

With an increase in the initial temperature t_0 of the charge, the specific impulse of the engine increases, since in this case there is an increase in the reserve of physical heat contained in the powder and liberated as the grain burns; in addition, changes are observed in the remaining parameters of the interior engine ballistics, which result in an increase in specific impulse (increase in engine pressure, reduction in operating time, etc.).

The nature of the effect that the initial temperature of the charge has on specific impulse can be seen from the example presented

in Table 4.10.

TABLE 4.10

Specific Engine Impulse as a Function of Initial Charge Pressure in the Interval $\pm 50^{\circ}C$

t_0 °C	+50	+30	+15	0	−30	−40	−50
j_1 кг сек/кг [1]	205,9	202,8	201,3	199,6	199,2	196,6	196,6

1) j_1, kg·sec/kg.

As can be seen from the above-mentioned data, in the temperature interval $\pm 50^{\circ}C$ the specific impulse can change by approximately 5% with respect to its value at $t_0 = +15^{\circ}C$.

The gas temperature has an effect on the specific impulse insofar as it determines the outflow coefficient

$$A = \frac{\varphi(k)}{\sqrt{RT_0}},$$

and the specific impulse

$$j_1 = \frac{1}{A}\left(\xi - \frac{p_a}{p_0}\frac{\omega_a}{\omega_{ep}}\right),$$

i.e.,

$$j_1 = \frac{\sqrt{RT_0}}{\varphi(k)}\left(\xi - \frac{p_a}{p_0}\frac{\omega_a}{\omega_{ep}}\right).$$

The difficulty encountered in the thermal shielding of an engine having a high temperature in the combustion chamber and the reduction of the strength characteristics of the structural materials with an increase in temperature limit the permissible temperature of the products of combustion. Therefore, an increase in the temperature of the gases as a means of increasing the specific impulse of the engine is undesirable and the problem as to the quantitative relationship $\Delta j_1 = f(\Delta T)$ is not considered here.

Since

$$Q_{w(x)} = c_p T_0$$

and

$$J_1 = \frac{\sqrt{RT_0}}{\varphi(k)}\left(\xi - \frac{p_a}{p_0}\frac{\sigma_a}{\sigma_{sp}}\right),$$

the specific impulse is formally proportional to $\sqrt{Q_{w(zh)}}$. In practice, this relationship has a weaker effect and is expressed by the proportionality to the root $\sqrt[3]{Q_{w(zh)}}$ and even to $\sqrt[4]{Q_{w(zh)}}$.

[Footnotes]

Manuscript Page No.

96 EI VINITI AN SSSR, seriya "Raketnaya tekhnika" [Scientific-Research Technical Institute of the Academy of Sciences USSSR- not identified in standard references – series of "Rocket Engineering"], 1959, No. 2, No. RT-4 [Rocket Engineering No. 4]. Jet Propulsion, 1958, Vol. 28, No. 7.

100 EI VINITI AN SSSR, seriya "Raketnaya tekhnika," 1959, No. 29, No. RT-87; No. 41, No. RT-123. Aviation Week, 1953, Vol. 68, No. 25.

101 EI VINITI AN SSSR, seriya "Raketnaya tekhnika," 1959, No. 25, No. RT-73, 74.

102 Missiles and Rockets, 1958, 3, No. 1.

115 ZhETF [Journal of Experimental and Theoretical Physics], 1942, Vol. 12, Nos. 11-12.

130 *R.N. Wimpress, Internal. Ballistics of the Solid-Fuel Rockets, McGraw-Hill, New York, 1950.

130 **Jet Propulsion, 1954, Vol. 24, No. 1.

130 ***Combustion Colloquium, Cambridge University, England, Butterworths Scientific Publications, 1954.

130 ****Jet Propulsion, 1958, Vol. 28, No. 9.

132 Journal of the British Interplanetary Society, Oct.–Dec. 1957

135 Astronautica Acta, 1959, Vol. 5, No. 1; EI VINITI AN SSSR, seriya "Raketnaya tekhnika," No. 18, No. RT-51.

136 EI VINITI AN SSSR, seriya "Raketnaya tekhnika," 1959, No. 5, No. RT-13.

Manuscript Page No.

138 Astronautica Acta, 1959, Vol. 5, No.1.

139 R.N. Wimpress, Internal. Ballistics of the Solid-Fuel Rockets, McGraw-Hill, New York, 1950.

152 D. Satton., Raketnyye dvigateli, IL [Rocket Engines, Foreign Literature Press], 1952.

178 G.B. Sinyarev, M.V. Dobrovol'skiy, Zhidkostnyye raketnyye dvigateli, Oborongiz [Liquid Rocket Engines, State Defense Industry Press], 1957.

[List of Transliterated Symbols]

109 $C_{нкл} = C_{nkl} = C_{nitrokletchatka} = C_{nitrocellulose}$

119 $u_{л} = u_{l} = u_{lineynaya\ (skorost')} = u_{linear\ (rate)}$

120 $T_{з} = T_{z} = T_{zaryad} = T_{grain\ (charge)}$

126 $\beta_{т} = \beta_{t} = \beta_{temperatura} = \beta_{temperature}$

127 $t_{ср} = t_{sr} = t_{srednyaya\ (temperatura)} = t_{mean\ (temperature)}$

130 $w_{г} = w_{g} = w_{gaz} = w_{gas}$

141 $\tau_{н} = \tau_{n} = \tau_{nabor} = \tau_{build\ up}$

142 $\tau^{ш} = \tau^{sh} = \tau^{shashka} = \tau^{grain}$

142 $p_{раб} = p_{rab} = p_{rabocheye\ (davleniye)} = p_{operating\ (pressure)}$

144 $\rho_{кр} = \rho_{kr} = \rho_{kriticheskoye} = \rho_{critical}$

145 $v'_{к.с} = v'_{k.s} = v'_{kamera\ sgoraniya} = v'_{combustion\ chamber}$

149 пред = pred = predel'noye = limit

159 $p'_{ст} = p'_{st} = p'_{statsionarnyye\ (davleniya)} = p'_{steady\text{-}state\ pressures}$

163 $S_{гор} = S_{gor} = S_{goreniye} = S_{burning}$

163 $F_{св} = F_{sv} = F_{svobodnoye\ (secheniye)} = F_{free\ (cross\ section)}$

168 $\omega_{сек} = \omega_{sec} = \omega_{per\ second}$

171 $a_{зв} = a_{zv} = a_{zvuk} = a_{sound}$

182 $R_{аерд} = R_{aerd} = R_{aerodinamicheskaya} = R_{aerodynamic}$

182 $R_{р} = R_{r} = R_{ravnodeystvuyushchaya} = R_{equivalent}$

182 $R_{тр} = R_{tr} = R_{treniye} = R_{friction}$

182 $R_{проч} = R_{proch} = R_{prochiye} = R_{all\ other}$

183 $w_{эф} = w_{ef} = w_{effektivnaya} = w_{effective}$

187 $m_{к} = m_{k} = m_{konechnyy\ (ves)} = m_{final\ (weight)}$

Chapter V

THE DESIGN OF AN ENGINE FOR A SOLID-PROPELLANT MISSILE

§1. SELECTION OF STRUCTURAL DIAGRAM FOR COMBUSTION CHAMBER AND MATERIAL FOR TUBE

As a rule, the engine for a solid-propellant rocket missile consists of a frame of a combustion chamber and several additional elements, the basic among which are the nozzle assembly and the forward

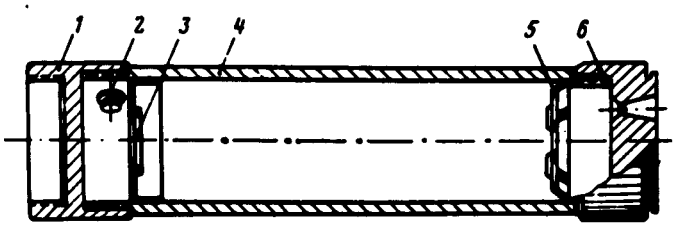

Fig. 5.1. Design of engine for solid-propellant rocket missile. 1) Forward connection device; 2) frame of igniter cartridge; 3) grain trap (spacer); 4) tube of combustion chamber; 5) diaphragm; 6) nozzle assembly.

spacer which connects the combustion chamber with the warhead of the missile (Fig. 5.1). The combustion chamber is designed to house the solid-propellant charge, the igniter, the ignition system, etc., as well as to provide for normal conditions of propellant burning during the time of engine operation.

Structurally the frame of the combustion chamber is generally made in the form of a cylindrical tube. At times we encounter designs of different types; however, the fabrication and assembly of combustion chambers involves, as a rule, considerable difficulties and it is for this reason that such chambers are employed comparatively rarely.

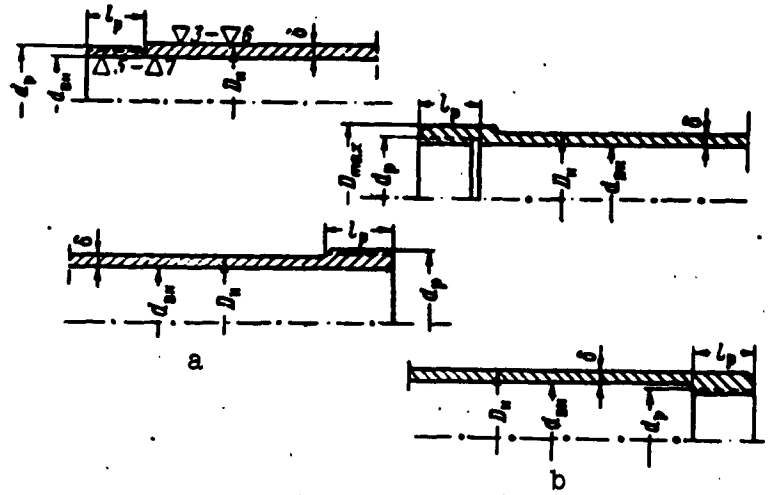

Fig. 5.2. Typical structural diagrams for the combustion chamber of an engine. l_p) The length of the threaded portion; δ) thickness of the wall; D_n and d_{vn}) outside and inside diameter, respectively; d_r) thread diameter; D_{max}) maximum diameter.

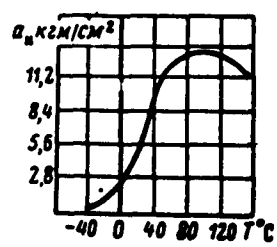

Fig. 5.3. Impact strength a_n, kg-m/cm^2 as a function of temperature T°C for steel, with failure at low temperatures.

Some of the structural versions of combustion chambers are presented in Fig. 5.2. A comparative evaluation of the typical combustion-chamber designs shown in Fig. 5.2 demonstrates that there are no basic differences between them; the chambers differ from one another only by the location of the connecting thread (on the outside – Fig. 5.2a; on the inside – 5.2b) and in the design of the threaded section. It should be pointed out that if a missile is not fabricated with threaded con-

nections, but is designed to employ some other connection method (welding, gluing, pressure fitting, etc.), the design of the combustion chamber remains as before and only the threaded section is replaced by another, corresponding to the given connection.

The tube of the combustion chamber must be selected on the basis of the consideration that a firm connection be achieved with the two above-mentioned component parts in contact with the tube, and the connection must provide for the permanence of the joint and the hermetic sealing of the combustion-chamber cavity under conditions of high pressures and temperatures which occur within a solid-propellant rocket engine that is in operation. An important criterion for the evaluation of the structural diagram of a combustion chamber is the requirement for technological adaptability to fabrication, said requirement geared to conditions of fabricating these component parts on a mass-production basis. From this standpoint, for example, tubes with an inside thread are less desirable, since for these:

– the processing of the chamber from within presents certain difficulties, especially in the case of undercutting;

– it is difficult to obtain a high-quality thread on component parts of small calibers.

Finally, we should also point out that the configuration of the inner cavity of the combustion chamber has an effect on the parameter κ of the engine, of which more will be said in greater detail below.

In addition to the selection of the structural diagram, an extremely important stage in the design of the combustion chamber is the resolution of the problem relating to the material employed in the frame of the engine. In selecting the material, we should bear in mind that instantaneous pressure pulses at the beginning and the end of the burning of the powder are possible during engine operation, especially

during the missile-testing stage. Hence one of the most important characteristics of the material used for the walls of the combustion chamber is the impact strength which must be sufficiently great over the entire temperature interval set for the engine.

Missiles that were used during the period of the Second World War were fabricated, as a rule, of unalloyed structural steels. With respect to their characteristics, these steels satisfy all of the requirements imposed on the material used in the construction of a combustion chamber, but these steels exhibit comparatively low mechanical properties. In this connection, the requirements for strength demand the fabrication of comparatively thick-walled combustion chambers, and this increased the structural weight of the missile, thus reducing the maximum velocity and flight range of the missile.

It is more expedient to use low-alloyed steels of increased strength for combustion chambers. These steels make it possible substantially to lighten a rocket engine without introducing any significant increase in cost.

In the case of steels involving more complex alloying, reductions in impact strength at low temperatures may be observed (Fig. 5.3), and moreover, the fabrication techniques for component parts made of such steels is generally comparatively complex and these steels are therefore rarely employed.

In the case of engines operating on high heating-value powders or if the engines are subjected to extended operation, the walls of the combustion chamber are coated with special heat-insulating compositions. Sometimes these heat-insulating coatings are introduced simply in order to reduce the structural weight of the missile, since by insulating the wall against the effects of high temperatures it becomes possible to reduce the temperature stresses within the combustion cham-

ber thus simultaneously reducing the necessary wall thickness. The well-known German antiaircraft missile "Tayfun-P" operated on a powder of conventional heating value $Q_{w(zh)}$ = 800-850 kcal/kg for 1.5 sec. However, the walls of the combustion chamber in this missile were coated with two heat-insulation layers, thus making it possible to reduce the thickness of the walls to δ = 2.0 mm and to guarantee with this thickness a preservation of combustion-chamber strength for the operating pressure of p_{max} = 130 atm. Test firings of the engines used in the "Tayfun-P" missile, when no heat-insulation coatings were employed, resulted in the destruction of the combustion chambers. To preserve the strength of the combustion chamber it became necessary to increase the thickness of the walls by a factor of more than two. In this case, the weight of the engine also almost doubled, thus reducing the maximum velocity of the missile to 870-920 m/sec, whereas a missile with a heat-insulation coating and δ = 2.0 mm exhibited a velocity of v_{max} = 1500 m/sec.

At the present time, the new structural materials such as plastics have found widespread application in rocket engineering, including the field of rocket engine construction; among the plastics, we refer primarily to various types of glass-filled plastics.

Glass-filled plastics are compositions consisting of a reinforcing high-strength filler and a polymerized binder through which this filler is distributed. Fiberglass or glass cloth is used most frequently in structural glass-filled plastics. Various synthetic resins such as, for example, the epoxies, the phenols, special polyesters, etc., are used as the basic binder depending on the requirements imposed on the material and the operating conditions for the component parts.

Structural glass-filled plastics are characterized by extremely

high tensile stresses. For example, with a glass-cloth and epoxy-resin base it is possible to obtain materials exhibiting σ_b = 4000-4500 kg/cm^2 and $a_n \approx 150$ kg·cm/cm^2, for a specific weight of γ = 1.7-1.8 g/cm^3. The comparative tensile strength of glass-filled plastics with respect to certain other structural materials can be shown by the following figures*:

alloyed steel.....	900 ($\sigma_b \approx 7{,}000$ kg/cm^2)
heat-treated alloyed steel.....	1800 ($\sigma_b \approx 14{,}000$ kg/cm^2)
high-strength alloyed steel.....	2000 ($\sigma_r \approx 16{,}000$ kg/cm^2)
high-strength aluminum-based alloy.....	2100 ($\sigma_r \approx 6{,}000$ kg/cm^2)
titanium alloy.....	2800 ($\sigma_r \approx 13{,}000$ kg/cm^2)
fiberglass plastic with conventional impregnation.....	2150 ($\sigma_r \approx 3{,}850$ kg/cm^2)
fiberglass plastic with special impregnation	2950 ($\sigma_r \approx 5{,}250$ kg/cm^2)

(σ_r is the breaking strength)

While exhibiting high tensile strength, glass-filled plastics also exhibit low thermal conductivity $\alpha \approx 0.002$ cal/cm·deg·sec ($\alpha_{stali} \approx 0.1$ cal/cm·deg·sec; $\alpha_{alyum} = 0.4$ cal/cm·deg·sec) and are therefore simultaneously both structural and heat-insulation materials which function satisfactorily under conditions involving temperatures of the order of 2000-2500°C for short periods of time.

Let us cite several examples of the application of plastics in the designs of rocket missiles:

— on the "Nike-Hercules" missiles and on certain other missile-interceptors (USA) warheads have been installed and their frames (bodies) are made of glass-filled textolite [a resin-impregnated laminated cloth] (by the Aerojet-General Company);

— the cross-shaped wing of the antitank rocket missile "Vickers 891" (Great Britain) is made of glass-filled plastic material;

— stabilizers made of glass-filled textolite are mounted on the U.S. Navy air missile "Talos";

— the Contravers Company, in cooperation with the Erlicon B Company (Switzerland), developed model 56 of the RSC-1 "ground-to-air" missile class, whose engine frame is made of fiberglass impregnated with a special organic adhesive composition;

— the Reinhold Company (USA) designed, developed, and undertook a test production run of an artillery rocket missile with a solid-propellant engine made entirely of plastics;

— finally, the inner heat-insulation of the frame of the solid-propellant engine used in the anti-missile "Nike-Zeus" missile, which operates for a period of 60 sec, is a lining made of glass-filled textolite.

The component parts of a rocket missile can be fabricated out of glass-filled plastics by means of a wrapping method (the nose spinner, the body of the combustion chamber, a nozzle) or by means of extrusion (spacers, the grid, the nozzle, stabilizers).

With the wrapping method, the glass cloth (or a strip of glass threads), impregnated with a binder, is wound in several layers on a special rigid mandrel. The mandrel is placed into a thermostat together with the material wound on the mandrel, and the binder is polymerized in the thermostat where the material hardens. After the required length of time in the thermostat, the mandrel is removed and the finished product taken off.

Plastics are extruded in special heated die-casting molds. The polymerization of the binder takes place during the time that the component part is kept in the closed die-casting mold.

In the design of component parts made of glass-filled plastics it should be borne in mind that individual critical cross sections of com-

ponent parts can be reinforced by the introduction of steel fittings into the structure of these component parts.

On the other hand, ways have been found of increasing substantially the strength of the glass-filled plastics themselves in the near future. One of these means is the attempt to increase the adhesion of the binder to the fiberglass by, for example, the preliminary treatment of the filler by means of special silicon-organic compounds. These compounds are capable of forming chemical bonds both with the glass as well as with the resins in the composition of the binder. In the final analysis, the glass-filled plastics become more monolithic and their strength increases.

Another method is the attempt to use a stronger filler — quartz fibers, etc. Here, strength is increased only in those structures in which the basic load is transmitted to the filler.

Examples of structural glass-filled plastics are such materials as "roketon [sic]," "missaylon [sic]," "orbiton [sic]," and some others,* which have found widespread application in rocket building in the USA.

§2. SELECTION OF DIAGRAM FOR CONNECTION OF ROCKET PART OF MISSILE TO THE WARHEAD AND NOZZLE ASSEMBLY

It is possible to connect the rocket part of the missile with the warhead either directly or by means of a transition element, i.e., a connection plate.

Direct connection is possible if either the warhead has a bottom plate (Fig. 5.4a), or the tube of the combustion chamber has a blind end (Fig. 5.4b). Of the two possible methods for the case in which the missile warhead has a bottom plate, all other conditions being equal, it is best to select the first version. This method provides for permanence of joints under the action of the high pressures within the combustion chamber, which expand the combustion chamber circumferen-

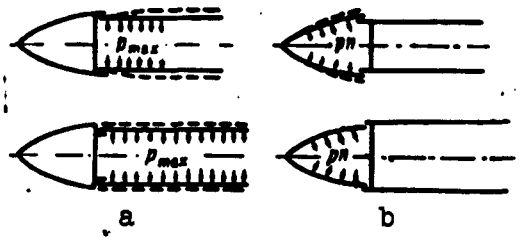

Fig. 5.4. Structural means of connecting the warhead and the rocket part of the missile without using a connection plate.
pn is the pressure due to the fittings.

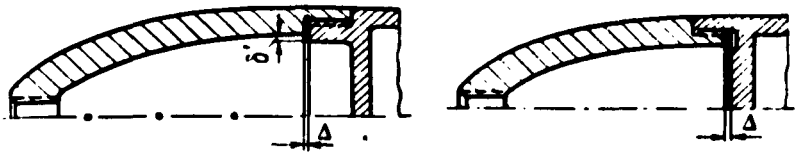

Fig. 5.5. Comparison of two methods of connecting the warhead of the missile to the rocket part.

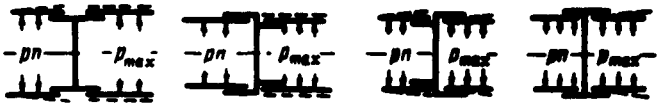

Fig. 5.6. Structural methods of connecting the warhead and rocket parts of the missile by means of a connecting plate.

tially, since the bulging forces at the end of the tube are borne by the rigid element of the warhead. Generally speaking, the fabrication of a warhead with a blind bottom plate exhibits a number of substantial shortcomings in and of itself (difficulty in the mechanical processing of the inside cavity of the combustion chamber, the impossibility of utilizing advanced methods of outfitting, etc.) and this method is therefore used only where absolutely necessary.

Of the two remaining methods, it is most expedient to use the second. The shortcomings of the first method in comparison with the

second method in this case are the following:

– the pressure (pn) due to the fittings, said pressure arising at the instant of missile impact against an obstacle and expanding the walls of the warhead is borne, in the second case, by the rigid collar of the combustion-chamber frame, so that the possibility of the joint opening at the instant of impact or premature explosion is completely eliminated;

– it is extremely difficult to attain complete agreement between the outline of the inner contour of the combustion chamber and the head, from a production standpoint, during the fabrication (production processing) of the component parts. In practice, we will always have an error δ' in component-part dimensions (Fig. 5.5), and this makes high-grade fitting out of the warhead difficult nor does it make it possible to make use, for example, of the liner method of outfitting, said method exhibiting great advantages;

– the spacer which provides for the selection of the clearance Δ between the bottom plate and the head part has the shape, in the first case, of a narrow ring (Fig. 5.5). In mounting (screwing on) the component parts, we find that this spacer is easily deformed and fails to carry out its functions.

An analysis of the possible types of connection devices for the warhead and rocket parts allow us to draw the conclusion that in connecting these parts by means of a connection plate, from the standpoint of strength and permanence of joint, the best version of all possible structural versions (Fig. 5.6) is the one in which the component parts being connected are encompassed by the structural elements of the connecting plate (Fig. 5.6d). Other connections may be used only when they are made necessary for some specific reason and only if the strength of the joint and the hermetic sealing of the joint

will be assured in each particular case.

All that has been said about the connection of the warhead to the rocket part pertains in equal measure to the second joint between the rocket part and the nozzle assembly. And here, the most advantageous connection version is the one in which the combustion chamber is covered by a nozzle cover. We must bear in mind only that there are increased requirements imposed on this type of connection, since the nozzle part of the engine is subject to greater temperature stresses.

§3. STRENGTH CALCULATIONS FOR THE BASIC COMPONENTS OF THE COMBUSTION CHAMBER

The body of the combustion chamber. The basic stress-bearing component part of the combustion chamber is its cylindrical frame. The frame (body) of the combustion chamber is subjected to a pressure p_{rasch} that is uniformly distributed over the inner surface, and it is also subjected to axial forces of elongation which appear as a result of the pressure against the side covers of the combustion chamber.

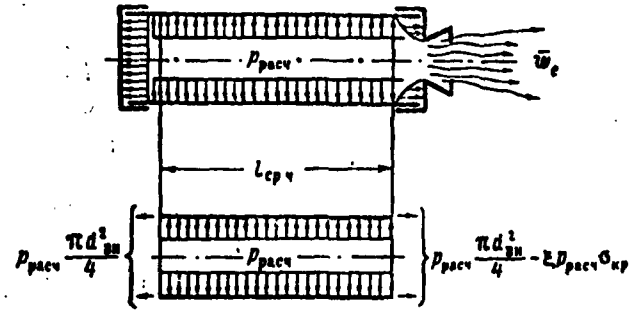

Fig. 5.7. Design diagram of loads, for verification of strength of middle section of combustion-chamber tube.

For the design of the middle part of the frame cylinder we can use the relationships of the momentless theory of shells, neglecting the effect of the bending at the edges, and we can make use of the design diagram of the loads presented in Fig. 5.7.

A stress field is produced by the action of this load in the wall of the combustion chamber, and each point in this field is characterized, in the general case, by three stresses (Fig. 5.8): a circumferential stress σ_θ, a radial stress σ_r, and an axial stress σ_z.

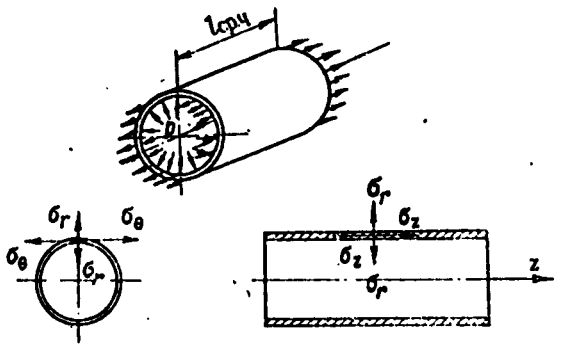

Fig. 5.8. Diagram indicating distribution of main stresses acting on the wall of the combustion-chamber tube.

Let us find the relationships which determine these stresses in terms of the structural dimensions of the combustion chamber and let us also determine the characteristics of the material used in building the frame.

For the determination of σ_θ let us examine the equilibrium of that part of the cylinder cut by two meridional and equatorial sections (Fig. 5.9). Since the wall of the combustion chamber may be regarded as thin, we will assume that the stress σ_θ is constant throughout the thickness of the wall and distributed uniformly within the wall. Given this assumption, the equation of the equilibrium of the cut-out part, in its projection onto KK, will be

$$\sigma_\theta 2\delta l - p_{\text{расч}} d_{\text{вн}} l = 0, \quad (\underline{l} \text{ is the length of the engine}) \quad (5.1)$$

where the resultant of the pressure forces is found by the familiar theorem on the resultant of pressure forces in a given direction: the resultant of pressure forces, uniformly distributed over some contour, in a given direction is equal to the product of the pressure

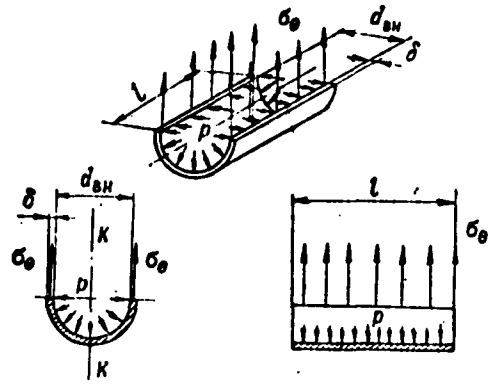

Fig. 5.9. Stresses σ_θ in the wall of the combustion chamber.

onto the projection of the closing line of this contour by the given direction (Fig. 5.10):

$$F_{k+k} = p^*(AB)_{kk} = p^*,\ AB\sin\alpha = p^*CB.$$

From Eq. (5.1) we will obtain

$$\sigma_\theta = p_{\text{расч}}\frac{d_{вн}}{2\delta} \qquad (5.1')$$

or from the caliber d of the missile

$$\sigma_\theta = p_{\text{расч}}\frac{d-2\delta}{2\delta}, \qquad (5.1'')$$

since

$$d = d_{вн} + 2\delta.$$

The stresses σ_z arise in the lateral cross section of the tube as a result of the axial elongation force. We can see from the force-distribution pattern (see Fig. 5.7) that two forces are acting on the chamber in a longitudinal direction: $p_{rasch}(\pi d^2_{vn}/4)$, acting on the forward connecting device; $(p_{rasch}(\pi d^2_{vn}/4) - \xi p_{rasch}\sigma_{kr})$, is the force acting on the nozzle cover (the Lanzheven coefficient ξ is employed to take into consideration the redistribution of pressure over the nozzle cover during the outflow of gases through the nozzle).

If two unequal forces act on the body in the opposite direction, the body will shift and be elongated. In this case, the elongation

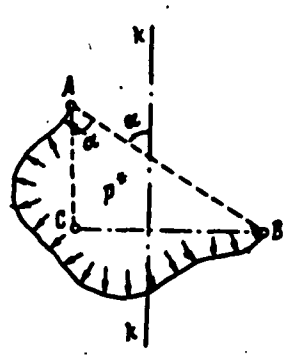

Fig. 5.10. For the calculation of the resultant produced by the forces of internal pressure p_{rasch}. p*) The pressure acting on the contour AB; α) angle between the closing lines of the contour and the given direction KK.

force will be the smaller of the active forces, and the force causing the body to move will be given by the difference between the active forces. With respect to our case, it will turn out that the combustion chamber will be subject to elongation by the following force:

$$p_1 = p_{pacч}\left(\frac{\pi d_{вн}^2}{4} - \xi\sigma_{кр}\right) \qquad (5.2)$$

and it will move under the action of the following force:

$$\left[p_{pacч}\frac{\pi d_{вн}^2}{4} - \left(p_{pacч}\frac{\pi d_{вн}^2}{4} - \xi p_{pacч}\sigma_{кр}\right)\right] = \xi p_{pacч}\sigma_{кр} = R_т,$$

where R_t is the force of thrust.

Under the action of the force p_1 in the lateral cross section of the chamber, there will arise stresses that are equal to the following (in accordance with the definition of the stresses)

$$\sigma_в = \frac{p_1}{\frac{\pi}{4}(d^2 - d_{вн}^2)} = \frac{p_{pacч}\left(\frac{\pi d_{вн}^2}{4} - \xi\sigma_{кр}\right)}{\frac{\pi}{4}(d^2 - d_{вн}^2)} =$$

$$= p_{pacч}\frac{d_{вн}^2 - \xi d_{кр}^2}{d^2 - d_{вн}^2}, \qquad (5.3)$$

where $\underline{d}$ is the outer diameter of the combustion-chamber tube; d_{kr} is the diameter of the critical cross section of the nozzle.

Finally, with respect to the stress σ_r it is not difficult to see that this stress will have its greatest value on the inner surface of the chamber:

$$\sigma_r^{max} = -p_{расч} \qquad (5.4)$$

and this stress diminishes to

$$\sigma_r = 0 \text{ (more exactly to } \sigma_r = p_H)$$

on the outer (free) surface of the tube (p_H is the external pressure).

Thus all three of the main stresses that arise within the wall of a combustion chamber under the action of the inside pressure have been found:

$$\left.\begin{aligned} \sigma_\theta &= \frac{p_{расч} d_{вн}}{2\delta}, \\ \sigma_z &= p_{расч} \frac{d_{вн}^2 - b d_{нр}^2}{d^2 - d_{вн}^2}, \\ \sigma_r^{max} &= -p_{расч}. \end{aligned}\right\} \qquad (5.5)$$

A comparison of the algebraic magnitudes of the stresses σ_θ, σ_z, and σ_v shows that in terms of the main stresses the greatest of these – σ_1 – is, as a rule, the stress σ_θ, and the smallest – σ_3 – is the stress σ_r, even if it attains its maximum value.

The strength calculation involves the successive solution of two basic problems. The first of these problems – the structural calculation – can be reduced to a tentative determination of the wall thickness δ which for the selected component-part material (with σ_b known) must provide for the preservation of the structural strength with a margin ζ, under a load of pressure $p_{расч}$. In the solution of this problem we generally take into consideration only the greatest of the active stresses (in our case, σ_θ) and we determine the required thickness from the following condition:

$$\sigma_\theta < \frac{1}{\zeta} \sigma_b.$$

Substituting into this equation the values of σ_θ from (5.1")

$$p_{расч} \frac{d - 2\delta}{2\delta} < \frac{1}{\zeta} \sigma_b,$$

we will find δ to be equal to

$$\delta \geq \frac{p_{расч} d}{2\left(p_{расч} + \frac{1}{\zeta} \sigma_в\right)}. \qquad (5.6)$$

The quantity p_{rasch}, entering into this formula, is calculated as follows:

$$p_{расч} = k_1 k_2 p^{max}_{+t^\circ_{max}}, \qquad (5.7)$$

where the coefficients k_1 and k_2 are employed to take into consideration the regulated tolerances for the scattering of pressure in the case of various batches of powders and the elimination of pressure on the ignition of the charge; $p^{max}_{+t^\circ_{max}}$ is the maximum pressure calculated according to the balance equation for the extreme positive temperature from the temperature interval stipulated in the tactical-technical requirement.

The determination of the thickness of the wall according to (5.6) will make it possible to estimate the weight q_k of the engine In this case, we may use the tentative relationship:

$$q_к \approx 1{,}3 \frac{\pi}{4}(d^2 - d^2_{вн}) l \gamma = 1{,}3 \frac{\pi}{4}[d^2 - (d - 2\delta)^2] l \gamma$$

or after rearrangement

$$q_к \approx 4 \gamma (d\delta - \delta^2) l, \qquad (5.8)$$

where γ is the specific weight of the tube material; d is the caliber of the missile; δ is the thickness of the engine wall.

If q_k (in kg) does not fall within the limits permitted according to the tactical-technical requirements for the weight of the engine, it becomes necessary to replace the material with a stronger material or it is necessary to reexamine the interior ballistics of the engine, so as to bring the weight of the engine within the required limits.

After the correction of the quantity δ the second strength-cal-

culation problem is solved, i.e., the verification calculation. In the verification calculation the true stressed state at the critical point of the chamber wall is estimated and the true strength margin of the structure is determined. With the adopted assumptions with respect to the nature of stress distribution through the thickness of the wall, we will find that the critical point will be the one that lies on the inner surface of the tube and has the main stresses:

$$\sigma_1 = \sigma_\theta = p_{расч} \frac{d - 2\delta}{2\delta},$$

$$\sigma_2 = \sigma_z = p_{расч} \frac{d_{вн}^2 - 4d_{ср}^2}{d^2 - d_{вн}^2},$$

$$\sigma_3 = \sigma_r^{max} = -p_{расч}.$$

In the case of a multiaxial stressed state, the concept of equivalent stress σ_{ekv} is employed in order to determine the strength of the component part at the critical point. By equivalent stress we mean the conditional tensile stress whose effect at this point produces the same stressed state as the effect of the true main stresses. This definition of equivalent stress makes it possible to write the conditions of component-part strength in the case of a complex stressed state in the following form

$$\sigma_{экв} < \frac{1}{\zeta} \sigma_b,$$

and the true strength margin ζ^* can be defined as the ratio of these stresses:

$$\zeta^* = \frac{\sigma_b}{\sigma_{экв}}.$$

For the calculation of equivalent stress it is necessary for us to know which factor of the stressed or strained state is the determining factor for the destruction of the component part. To this time, the nature of the destruction of various materials and component parts made of these materials has not been studied with suf-

ficient adequacy to enable us reliably to seek some equivalent state and the conditional equivalent stress which corresponds to this state. There are only individual hypotheses in this regard and these are referred to as strength theories.

For materials such as tough steels we obtain good agreement between theory and experiment through the use of the so-called theory of the strength of maximum tangential stresses, according to which

$$\sigma_{экв} = \sigma_1 - \nu\sigma_3, \qquad (5.9')$$

or through the theory of the strength of the maximum energy of shape change, according to which

$$\sigma_{экв} = \frac{1}{\sqrt{2}}\sqrt{(\sigma_1-\sigma_2)^2+(\sigma_2-\sigma_3)^2+(\sigma_1-\sigma_3)^2}, \qquad (5.9'')$$

where σ_1, σ_2, and σ_3 are the main stresses; ν is the coefficient by means of which we take into consideration certain properties of the material, and which for steel is equal to unity.

The questions related to the various theories of strength and the calculation of equivalent stresses are considered in greater detail in special literature on this problem as well as in textbooks dealing with the resistance of materials.

The verification calculation will make it possible finally to refine the unit δ, which provides for the required margin of structural strength.

If the walls of the combustion chamber are not coated with a heat-insulating material, we must take into consideration the effect of temperature on the strength of the engine. This effect makes itself felt primarily in the appearance of auxiliary stresses within the walls of the combustion chamber, said stresses proportional to the magnitude of the temperature difference across the wall. These stresses are referred to as temperature stresses. In first approximation, it may be maintained that the temperature stresses and the stresses due

to pressure are independent of each other, so that the total stresses can be sought in the following manner:

$$\sigma_i^{\Sigma} = \sigma_i^{p} + \sigma_i^{T},$$

where σ_i^{Σ} is the total stress determined by the effects of temperature and pressure; σ_i^{p} is the stress component by means of which we take into consideration the effect of pressure alone; and σ_i^{T} is the stress component by means of which we take into consideration the effect of temperature alone.

The components σ_i^{p} can be calculated in accordance with Formulas (5.5).

The temperature stresses σ_i^{T} are functions primarily of the temperature difference across the wall of the engine and the geometric characteristics of the lateral cross section of the tube. The formulas for the calculation of the temperature stresses have the following form:

$$\left.\begin{aligned} \sigma_0^T &= \frac{E\alpha\Delta T_{max}}{1-\mu} f_1(d, \delta), \\ \sigma_z^T &= \frac{E\alpha\Delta T_{max}}{1-\mu} f_2(\mu, d, \delta), \\ \sigma_r^T &= E\alpha\Delta T_{max} f_3(\mu, d, \delta), \end{aligned}\right\} \qquad (5.10)$$

where E is the modulus of elasticity for the wall material; α is the thermal conductivity of the wall material; μ is the Poisson ratio; $f_1(d, \delta)$, $f_2(\mu, d, \delta)$ and $f_3(\mu, d, \delta)$ are certain functions by means of which we take into consideration the effect of the geometric characteristics of the tube cross section on the temperature stresses; ΔT_{max} is the theoretical temperature difference across the engine wall.

One of the most complex problems associated with the calculation of the temperature stresses is the determination of the temperature difference

$$\Delta T_{max} = (T_{ст} - T_{ж})_{max},$$

where $T_{vn} = T(t)$ is the time-varying temperature of the metal at the inner surface of the tube; $T_n = T(t)$ is the time-varying temperature of the metal at the outer (external) surface of the tube.

In order to select the rated ΔT_{max}, we must know how the temperature changes, with respect to time, at the boundaries of the wall. The nature of the change $T_{vn} = T(t)$ and $T_n = T(t)$ is a function of the temperature in the combustion chamber and of certain physical characteristics of the stream of the products of combustion, moving along the inner wall of the engine, as well as of the thickness and the heat-conduction properties of the wall and, finally, of the parameters of the stream flowing past the outer wall of the tube. At the initial instant of rocket-engine operation, let the temperature of the engine wall be T_0^{st}. Then, during the powder-burning process a fraction of the heat due to radiation and convection will be transmitted from the hot products of combustion ($T^{p.s} = 2200^{\circ}K$) to the "cold" ($T_0^{st} \ll T^{p.s}$) wall. The flow of heat will be received by the inner surface of the engine wall. The heat absorbed by the wall will in part accumulate in the layers of metal adjacent to the inner boundary of the tube and in part be transmitted to the outer layers of the metal. As a result of the accumulation of heat, the temperature of the inner layers will increase rapidly, tending at the maximum to the temperature $T^{p.s}$ of the products of combustion. The transfer of heat to the outer layers of the metal will in turn result in the increased temperature of these layers. With an increase in the temperature of the outer boundary of the wall, a fraction of the heat will be radiated into the external flow which flushes the engine. The rate of temperature increase for the inner and outer walls, as well as the distribution of the temperatures in the wall cross section, are determined by the relationship between the processes of heat ab-

sorption and heat conduction, the properties of the wall material, the radiation of heat to the external medium, and certain other factors.

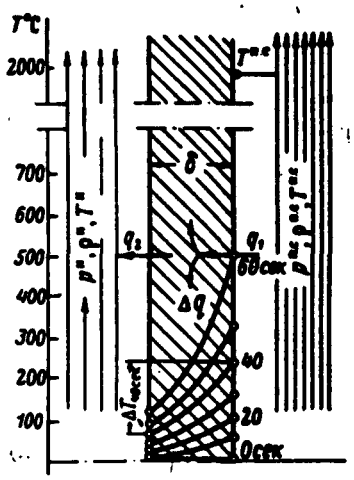

Fig. 5.11. Change in the temperature field in the case of nonsteady-state heating of the combustion-chamber wall of a solid-propellant rocket engine p^n, ρ^n, T^n) pressure, density, and temperature, respectively, of the external medium; $p^{p.s}$, $\rho^{p.s}$, $T^{p.s}$) pressure, density, and temperature, respectively, of the products of combustion; q_1) flow of heat to the wall of the combustion chamber; q_2) flow of heat to the ambient medium; Δq) heat accumulated by the wall.

The solution of the problem relating to the nonsteady-state heating of the wall is comparatively complex and is therefore not presented here. The nature of the change of the temperature field of the wall, with respect to time, is illustrated in Fig. 5.11.

If we take into consideration the temperature stresses, the stressed state of the critical tube point will be characterized by the total stresses:

$$\left.\begin{aligned}
\sigma_\theta^\Sigma &= p_{расч}\frac{d_{вн}}{2\delta}+\frac{E\cdot\Delta T_{max}}{1-\mu}f_1(d,\delta),\\
\sigma_z^\Sigma &= p_{расч}\frac{d_{вн}^2-\delta d_{кр}^2}{d^2-d_{вн}^2}+\frac{E\cdot\Delta T_{max}}{1-\mu}f_2(p,d,\delta),\\
\sigma_r^\Sigma &= -p_{расч}+E\alpha\Delta T_{max}f_3(p,d,\delta),
\end{aligned}\right\} \quad (5.11)$$

where σ_θ^Σ, σ_z^Σ, and σ_r^Σ are the total stresses, and the subscripts to the stresses are distributed in the following manner, as before:

$$\sigma_1=\sigma_\theta^\Sigma,$$
$$\sigma_2=\sigma_z^\Sigma,$$
$$\sigma_3=\sigma_r^\Sigma.$$

The heating of the wall results not only in the appearance of additional stresses, but it is also important to bear in mind that with a change in the temperature of the wall there is a change in the permissible stress for the given material. In this connection, it is

necessary to introduce into the calculation the quantity $(\sigma_b)_T$ rather than the standard value of σ_b; the first quantity is determined for some mean temperature of the engine wall.

If we take into consideration the temperature stresses and the reduction of the permissible stress in the heating of the wall, the formula for the structural calculation takes the following form:

$$\delta \geqslant \frac{p_{расч} d}{2\left[p_{расч} + \frac{1}{\zeta}(\sigma_b)_T - \sigma_0^T\right]}, \qquad (5.12)$$

in which case, given comparatively low temperature differences ΔT_{max} (given uniform heating of the wall), we can use the simplified relationship

$$\delta \geqslant \frac{p_{расч} d}{2\left[p_{расч} + \frac{1}{\zeta}(\sigma_b)_T\right]}. \qquad (5.12')$$

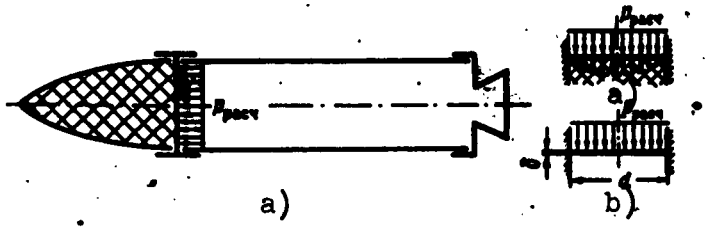

Fig. 5.12. Selection of diagram for verification of the strength of the forward connection plate of the combustion chamber.

The condition for the verification calculation takes the following form:

$$\sigma_{экв} < (\sigma_b)_T.$$

Given uniform heating of the wall, the temperature components of stress can, in first approximation, be neglected in the calculation of σ_{ekv}.

The connection plate. The connection plate connects the combustion chamber with the warhead of the missile. The basic load acting on this component part is the pressure p_{rasch} distributed uniformly

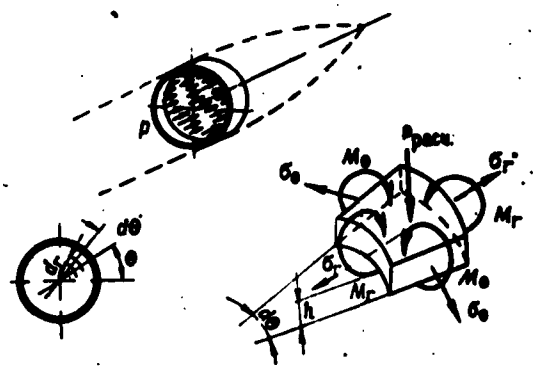

Fig. 5.13. Load diagram for a circular-plate element. θ) Instantaneous section angle; dr, dθ) dimensions of the elementary surface in the plane of the connection plate; h) height of the surface (thickness of the wall); M_r, M_θ) bending moments; σ_r, σ_θ)normal stresses at the sides of the surface.

over the plate. Strictly speaking, the contour employed to test the strength of this component part should be the round plate (pinched along its contour) which lies on an elastic base, i.e., the fittings of the missile warhead (Fig. 5.12a). However, in practical calculations we most frequently use the simplified diagram shown in Fig. 5.12b), neglecting the presence of this elastic base.

Figure 5.13 shows a diagram of the forces and moments acting on an element of the round plate as well as the determining stresses at the sides of this element.

We will not attempt a conclusion at this point, but will present the final formula for the calculation of the stresses which determine the strength of the component part. These formulas (for those points lying on the outer contour of the plate) take the following form:

$$\left.\begin{aligned} \sigma_r^{max} &= \frac{3}{16} p_{расч} \frac{d_{вн}^2}{h^2}, \\ \sigma_\theta &= \frac{3\mu}{16} p_{расч} \frac{d_{вн}^2}{h^2}. \end{aligned}\right\} \qquad (5.13)$$

The structural design of the component part is carried out on the basis of the stresses σ_r^{max}. In this case, the thickness of the wall is determined by the caliber of the missile in accordance with the following relationship

$$\frac{3}{16} p_{расч} \frac{(d-2\delta)^2}{\delta^2} = \frac{1}{\zeta} \sigma_b$$

in the form

$$\delta_{1,2} = \frac{d}{2} \cdot \frac{1}{1 \pm \sqrt{\frac{4 \frac{1}{\zeta} \sigma_b}{3 p_{расч}}}}. \qquad (5.14)$$

Since the presence of an elastic pad BB in an actual structure reduces a portion of the active load, the thickness δ of the plate wall, determined from (5.14), will assure the strength of the component part. In this connection, the verification calculation for the plate, as a rule, is not carried out. Moreover, we can select a coefficient $k < 1$ such that

$$\delta = k \frac{d}{2} \cdot \frac{1}{1 \pm \sqrt{\frac{4 \frac{1}{\zeta} \sigma_b}{3 p_{расч}}}}$$

will provide for the strength of the connection plate.

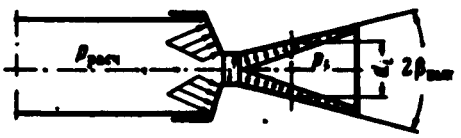

Fig. 5.14. Diagram of distribution of rated load on the wall of a rocket nozzle. $2\beta_{vykh}$) flare angle of the outlet funnel of the nozzle.

For a preliminary evaluation of the magnitude of δ, we can use the following relationship:

$$\delta = 0{,}45 d \sqrt{\frac{p_{расч}}{\frac{1}{\zeta} \sigma_b}}. \qquad (5.15)$$

In the practice of designing reaction-thrust armament we may encounter cases in which a convex shape is imparted to the connection plate in order to increase the rigidity of the connection plate or for certain other purposes (the improvement of the fragmentation of

the combustion chamber on the explosion of the warhead, etc.). In this case, the strength calculation for the component part becomes even more cumbersome. In first approximation, it is possible to calculate the required thickness of the wall of the convex connection plate by means of Formulas (5.14) and (5.15), bearing in mind that the quantity δ will, in this case, be determined with some excess.

The nozzle assembly of the combustion chamber. The nozzle assembly can be made in the form of a nozzle cover or in the form of a single central nozzle.

Figure 5.14 shows a diagram of the load acting on the walls of a single nozzle. Under the action of the component of this load, the nozzle walls become elongated in the radial direction, as a result of which stresses arise within the wall;

$$\sigma_t = \frac{p_i (d_m)_i}{2\delta_i} \cos\alpha,$$

where p_i is the static pressure in the i^{th} section of the nozzle (diameter d_i).

In accordance with the elementary theory of nozzles, this pressure is determined from the following relationship:

$$\frac{p_0}{p_i} = \left(1 + \frac{k-1}{2} M_i^2\right)^{\frac{k}{k-1}},$$

where p_0 is the pressure in the combustion chamber; M_i is the M(ach) number of the flow in the i^{th} section, said number determined in turn by the magnitude of the area F_i of the i^{th} section,

$$\frac{F_i}{F_{kr}} = \frac{\left(1 + \frac{k-1}{2} M_i^2\right)^{\frac{k+1}{2(k-1)}}}{M_i \left(\frac{k+1}{2}\right)^{\frac{k+1}{2(k-1)}}};$$

F_{kr} is the area of the critical cross section of the nozzle.

Finally, for some i^{th} section of the nozzle the minimum wall

thickness which will ensure the strength of the component part with a strength margin ζ is determined as follows:

$$\delta_i = \frac{(d_{вн})_i}{2} \frac{p_{расч}}{\left(1+\frac{k-1}{2}M_i^2\right)^{\frac{k}{k-1}}} \frac{1}{\frac{1}{\zeta}\sigma_в}. \qquad (5.16)$$

The stressed temperature conditions in the nozzle, and particularly in the region of the critical cross section, make it necessary to fabricate thicker nozzle walls than would be required in accordance with (5.16). The additional mass of the metal increases the quantity of heat removed from the inner surface of the nozzle profile thus preventing overheating and metal erosion, caused by the action of a high-velocity stream of gas against the overheated wall. In the case of large flow rates and operating times, special graphite, molybdenum, or other heat-resistant liners are employed in the throat (the critical cross section) to prevent the formation of scale on the nozzles. The temperature drops rapidly in the diverging part of the nozzle and the temperature effect on nozzle wall strength can be neglected.*

In fabrication of the nozzle assembly in the form of a nozzle cover, the thickness of the component part is determined by the linear dimensions of the nozzle, and this thickness, as a rule, ensures the strength of the connection plate with multiple margin (Fig. 5.15a). The strength of such a component part need not be checked again. Even in the case of a prefabricated multinozzle assembly (Fig. 5.15b) the thickness is after all determined on the basis of structural and production considerations, rather than on the basis of strength. For purposes of control it might be borne in mind that the connection plate will be strong in the case of a multinozzle assembly if the minimum thickness of the component part is not

made smaller than the thickness of the forward connection plate, said thickness calculated on the basis of the formulas cited above.

Threaded joints of combustion-chamber units. The most common joint for the combustion chamber of a missile with the warhead and the nozzle cover is one involving threading. The thread may turn out to be a weak point in the construction of the missile, especially in the case of turbojet missiles in which great rpm produce additional load, markedly reducing the effectiveness of the threaded joint.

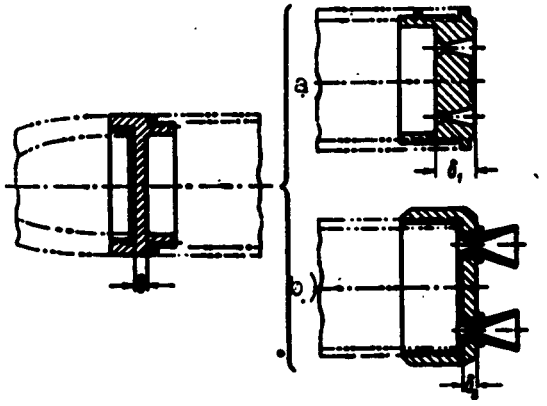

Fig. 5.15. With respect to the problem of checking the strength of the nozzle cover made in the form of a multinozzle assembly. $\delta < \delta_1, \delta_2$; $\delta_1\delta_2$ were determined on the basis of structural and production considerations.

Figure 5.16 shows the load diagram for a threaded joint that is characteristic for thread operating conditions in a rocket missile. The basic load on the turns of the thread is produced by the longitudinal force p_1 which is equal, as has already been shown, to

$$p_1 = \frac{\pi}{4}(d_{ш}^2 - td_{ср}^2)p_{расч}.$$

The bulging load p_2 produces no stresses in the thread; however, as a result of this force the magnitude of the contact surface of the turns is reduced and the hermetic sealing of the joint is disrupted; all of this results in a reduction in the strength of the joint, so

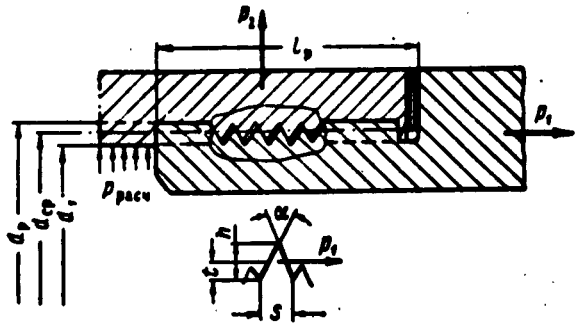

Fig. 5.16. Load diagram of threaded joint between combustion chamber and nozzle assembly. p_1) longitudinal load; d_1) inside diameter of the thread; d_r) thread diameter; d_{sr}) average diameter of the thread; p_2) outward force which separates the joint; s, α, h, t) elements of the thread profile.

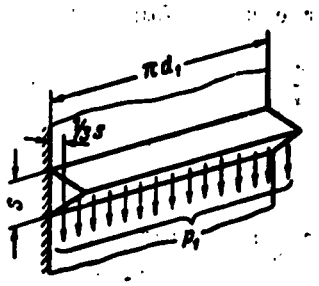

Fig. 5.17. Theoretical diagram for tests of thread functioning in the case of bending.

that we can state that the presence of p_2 is equivalent to some increase in the theoretical load p_1, and this must be taken into consideration in the calculations. To reduce the undesirable effect of the impairment of the strength characteristics of the joint as a result of the action of p_2, the component parts of the two prefabricated units are frequently screwed on with a red lead putty or with special lead monoxide compounds. With this type of assembly, the tightness of the joint increases markedly, and it may be stated that the presence of p_2 does not reduce the strength of the threaded joint.

The effect of load p_1 is such as to produce bending, crumpling, and shearing of the working turns of the thread. Calculations show that the bending stresses are determining in this case.

In designing a thread to withstand bending it is assumed that the work of a thread turn is equivalent to the bending of a beam which

coincides in shape with the profile of the thread and is embedded along the base of the profile (Fig. 5.17). Then, using the familiar relationships for the bending of a beam, we will obtain

$$\sigma_1 = \frac{M_1}{W} \frac{1}{z},$$

where σ_1 is the bending stress; M_1 is the bending moment; W is the moment of cross-section resistance to bending; sz = l_r is the working length of the thread; z is the number of working turns in the thread; s is the pitch of the thread, or after substitition of M_1 and W

$$\sigma_1 = \frac{p_1 \frac{1}{3} s}{\frac{\pi d_1 (0{,}85\, s)^2}{6}} \frac{1}{z} \approx 0{,}88 \frac{p_1}{d_1 l_p}. \qquad (5.17)$$

Here the factor 0.85 is used to take into consideration the features of an actual thread profile in comparison against a theoretical profile.

The required working length of the thread is hence determined in the following form

$$l_p = 0{,}88 \frac{p_1}{d_1 \frac{1}{\zeta} \sigma_b},$$

where ζ is the strength margin, or by taking into consideration the expression which determines p_1

$$l_p = 0{,}88 \frac{\pi}{4} \frac{(d_{sm}^2 - t d_{cp}^2)}{d_1 \frac{1}{\zeta} \sigma_b} p_{pacч} \approx 0{,}7 \frac{d_{sm}^2 - t d_{cp}^2}{d_1 \frac{1}{\zeta} \sigma_b} p_{pacч},$$

i.e., in terms of the nominal diameter of the thread:

$$l_p \approx 0{,}7 \frac{d_{sm}^2 - t d_{cp}^2}{(d_p - 2s)} \frac{p_{pacч}}{\frac{1}{\zeta} \sigma_b}. \qquad (5.18)$$

The total length of the threaded section can be determined if we hold that

$$L_p = (1{,}4 \div 1{,}5)\, l_p$$

i.e., according to the following formula

$$L_p \approx \frac{d_{вн}^2 - \xi d_{ср}^2}{(d_p - 2s)} \frac{p_{расч}}{\frac{1}{\zeta} \sigma_b}. \qquad (5.18')$$

The condition of thread strength against shearing, apparently, is written in the following form

$$p_1 = \pi d_1 (0{,}85s) z \frac{1}{\zeta} \tau_s,$$

where τ_s is the destructive shearing stress, whence the shearing stresses, which appear in the thread turns under the action of the calculated load, are determined as follows:

$$\tau_s \approx 0{,}3 \frac{d_{вн}^2 - \xi d_{ср}^2}{(d_p - 2s) l_p} p_{расч}. \qquad (5.19)$$

We will see that this stress is smaller by a factor of more than two than the stresses σ_i due to bending, which are determined according to (5.18) for this very same section as being equal to

$$\sigma_u \approx 0{,}7 \frac{d_{вн}^2 - \xi d_{ср}^2}{(d_p - 2s) l_p} p_{расч}. \qquad (5.20)$$

We will assume, without proof, that the equivalent stress for testing thread strength will be

$$\sigma_{экв} = \sqrt{\sigma_u^2 + 4\tau_s^2},$$

which, if we take into consideration (5.19) and (5.20), yields

$$\sigma_{экв} = \sqrt{0{,}7^2 + 4 \cdot 0{,}3^2} \frac{d_{вн}^2 - \xi d_{ср}^2}{(d_p - 2s) l_p} p_{расч} \approx \qquad (5.21)$$

$$\approx 0{,}92 \frac{d_{вн}^2 - \xi d_{ср}^2}{(d_p - 2s) l_p} p_{расч}.$$

For test-stand chambers and engines capable of being started repeatedly, it would be expedient to evaluate the possibility of thread crumpling. Thread crumpling will not occur if

$$p_1 < \pi d_{ср} (0{,}64s) z \sigma_{см}, \qquad (5.22)$$

where 0.64 is employed to take into consideration that part of the profile height engaged in the crumpling; $sz = l_r$ is the length of the working section of the thread; σ_{sm} is the permissible specific crumpling load.

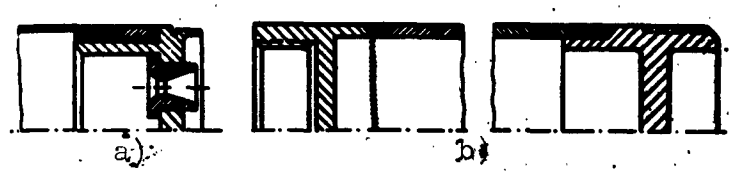

Fig. 5.18. Examples of welded joints in the construction of a rocket missile.

The relationships presented here can be used not only for the design of the threaded joints between combustion chambers and warheads and nozzle covers, but for the design of other threads encountered in the design of a rocket missile (threaded [screwed in] nozzles, sparkplugs, etc.).

Connection of combustion-chamber units by means of welding. Threaded joints exhibit a number of structural inadequacies, of which the most substantial are the need to make the component parts substantially thicker at the joint and the comparatively great fit area.

More promising from this point of view are connections made by means of welding – contact welding (Fig. 5.18a) or arc welding (Fig. 5.18b).

When arc welding is used, the component parts, as a rule, are connected into a joint with a V-shaped spreading of the edges. The rated load for verification of the strength of a joint seam is the tensile stress, and assuming a continuous seam for the entire length of the weld, the conditions of joint strength can be written in the following form:

$$p_1 < \sigma' h 2\pi d, \qquad (5.23)$$

whence the required height h of the weld seam (the thickness of the

wall at the weld) is defined as

$$h = \frac{p_1}{2\pi d \frac{1}{\zeta}\sigma'}$$

or after substitution

$$p_1 = \frac{\pi}{4}(d_{вн}^2 - \zeta d_{вр}^2) p_{расч},$$

$$h \approx 0{,}125 \frac{d_{вн}^2 - \zeta d_{вр}^2}{d} \frac{p_{расч}}{\frac{1}{\zeta}\sigma'}, \qquad (5.24)$$

where σ' is the permissible tensile stress for the weld seam of the joint. The magnitude of this stress is primarily a function of the type of welding employed and amounts to 0.6-0.9 of the permissible stress for the basic metal (0.6 for manual welding, and 0.9 for automatic welding with a layer of flux).

In refined calculations, it should be borne in mind that in addition to the tensile force p_1, an outer bending moment acts on the weld seam, and the magnitude of this moment is a function of the relationship between the pressure in the combustion chamber and the rigidity of the tube.

If the component parts being welded are not too thick, contact, seam, or even point welding are generally employed. The strength of the joint in this case is determined by the possibility of shearing the weld points and is written in the following form:

$$p_1 < \tau_s' \frac{\pi d_{т.т}^2}{4} n_{т.т}, \qquad (5.25)$$

where τ_s' is the permissible shear stress for the weld point $d_{s.t}$ is the diameter of the weld point; $n_{s.t}$ is the number of points, whence the required number of weld points is determined as follows:

$$n_{т.т} = \frac{p_1}{\frac{\pi d_{т.т}^2}{4} \frac{1}{\zeta}\tau_s'}$$

or after substitution of the expression for p_1

$$n_{c.т} = \frac{d_{ш}^2 - 6d_{т.р}^2}{d_{c.т}^2} \frac{p_{раст}}{\frac{1}{\zeta}\tau_s'}. \qquad (5.26)$$

Here, for the various types of welding, the values of τ_s' should be set at 0.5-0.65 of the σ_b of the basic metal, and the optimum magnitude of the weld-point diameter should be regarded as equal to

$$d_{c.т} = 1{,}5h_{min} + 5 \text{ мм},$$

where h_{min} is the minimum thickness of the component parts being welded.

§4. DESIGN OF MISSILE NOZZLE ASSEMBLY

The diaphragm, the volume of the combustion chamber behind the diaphragm, and the nozzle cover make up the so-called nozzle assembly of the engine. This assembly serves to shape the stream of the products of combustion at the outlet from the chamber of the engine and to set up the calculated outflow. The design of a nozzle assembly is one of the most important stages in the development of a missile design.

Selection of Type of Nozzle Cover

The nozzle cover may be made in the form of a single central nozzle or in the form of a multinozzle assembly (nozzle cover). The choice between these two versions of nozzle assembly depends on a number of factors, among which, first of all, we should point out the following:

- the structural diagram of the missile;
- the type of missile stabilization;
- missile caliber;
- tactical-technical requirements with respect to flight range and firing accuracy.

It is quite evident that the nozzle-cover version with a single central nozzle is possible only in the case of a normal missile design or, for example, in the case of designs in which the rocket portion is contained on the inside, just as it is initially assumed in the design of a turbojet missile that a nozzle cover is to be employed. The influence of missile caliber on the selection of the type of nozzle cover for the missile is a less determining factor. We can say only that missiles having calibers between 80 and 100 mm are made, as a rule, with a single central nozzle, although the well-known Germany missile "Taifun-P" (d = 100 mm) nevertheless had a multinozzle cover. With missiles having calibers of d > 100 mm, the nozzle assembly can be fashioned as a multinozzle cover, as well as with a single central nozzle. All other conditions being equal, the fabrication of the nozzle assembly in the nozzle-cover version is characterized by a number of substantial advantages, among which the following are particularly important:

1) the possibility of achieving some gain in the weight of the unit, particularly for missiles of medium and large calibers (Fig. 5.19);

2) the increase in missile firing accuracy by reducing virtually to zero the possible excentricity of the reaction force;

3) improvement of the gasdynamic gas-discharge regime from the combustion chamber and the reduction of losses attributable to the formation of the stream at the inlet to the nozzle;

4) reduction of the dimensions of missile length, etc.

Individual nozzles, particularly nozzles of large dimensions, are generally stamped and welded constructions (Fig. 5.20). Sometimes casting is employed in the fabrication of such nozzles.

A nozzle cover can be made in the form of a single component part

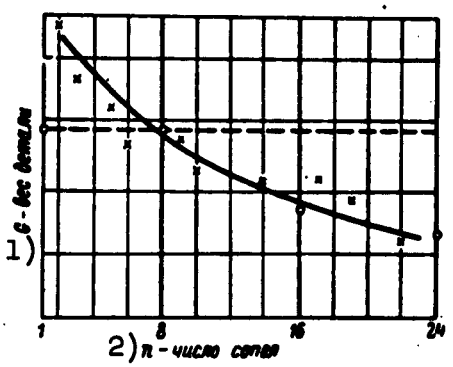

Fig. 5.19. Diagram of change in weight of nozzle assembly for various versions of covers with n bored nozzles. o) weight of actual component parts; x) calculation points; 1) G, weight of component part; 2) n, number of nozzles.

with bored (drilled) nozzles, either in the form of an assembly into which the individual nozzles are drilled (less frequently, welded, rolled, extruded) into a bottom plate carrying a corresponding grouping of preset holes (see Fig. 5.15). The version for the structural outline of the nozzle cover is selected on the basis of a weight analysis of the assemblies and a comparative evaluation of their adaptability to production. Individual small nozzles of prefabricated multinozzle covers are made in the form of a single component part, turned from a rod, or in the form of a welded construction (Fig. 5.21).

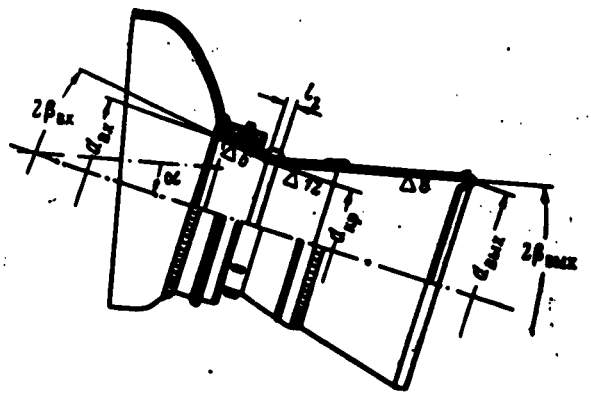

Fig. 5.20. Example of structural design of central nozzle. $2\beta_{vkh}$ and β_{vykh} are the flare angles of the inlet and outlet nozzle cones; α is the angle of nozzle-axis inclination to the engine axis.

Nozzles employed in engines exhibiting a burning time of between 5 and 10 seconds can be made of conventional low-carbon steel and need not be cooled during operation. In the case of longer burning time,

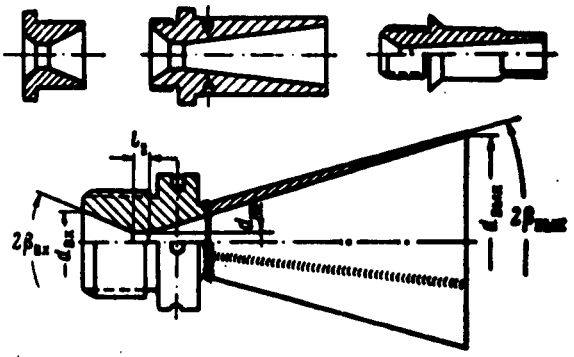

Fig. 5.21. Various nozzles for prefabricated multinozzle covers. d_{vkh} and d_{vykh} are the inlet and outlet nozzle diameters, respectively.

special measures must be implemented in order to prevent the overheating or burning out of the nozzle walls. Since the external forced cooling of a solid-propellant engine introduces undesirable complications from the standpoint of design and substantially increases the weight of the engine as a result of the ballast mass of the coolant, these measures must be reduced to the selection of special materials whose utilization in the nozzle construction will avert any excessive overheating of the component part. Various ceramics, specially processed graphite, and similar heat-resistant materials are employed for such purposes on a wide scale. Component parts of these materials are extruded or produced by powder-metallurgy techniques.

Calculation of Flowthrough and Linear Nozzle Dimensions

The contour of the inner nozzle cavity is defined by three flowthrough (d_{vkh}, d_{kr}, and d_a) and three linear (l_1, l_2, and l_3) dimensions, where d_{vkh} is the diameter of the inlet section; d_{kr} is the diameter of the critical section (throat); d_a is the diameter of the outlet section; l_1 is the length of the inlet cone; l_2 is the length of the critical nozzle section; l_3 is the length of the outlet funnel.

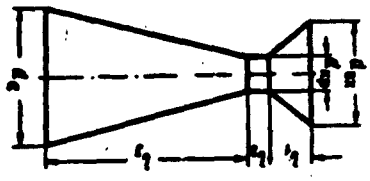

Fig. 5.22. Diagram of flowthrough and linear nozzle dimensions.

A diagram of the basic nozzle dimensions is presented in Fig. 5.22.

The flowthrough sections of the nozzle determine the most important parameters of a rocket engine. For example, the formula for the reaction force R, written in a form containing the Lanzheven [Langevin] coefficient, shows that the magnitude of this force is wholly determined by the pressure in the combustion chamber and the dimensions of the flowthrough sections of the nozzle.

$$R = \xi p_0 \sigma_{kp},$$

where σ_{kr} is the area of the critical nozzle section; ξ is the Langevin coefficient whose numerical value is a function of the ratio between the diameters of the outlet and critical sections of the nozzle (a function of nozzle divergence).

The most important of the above-enumerated dimensions is the diameter d_{kr} of the critical section of the nozzle (the throat). The magnitude of this diameter, in first approximation, can be found from the equation of balance

$$u_1 \gamma S_\Sigma = A p_0 \sigma_{kp},$$

in accordance with which

$$d_{kp} = \sqrt{\frac{4 u_1 \gamma S_\Sigma}{\pi A p_0}},$$

or by taking into consideration the average values of the constants $\gamma = 1.6$ g/cm^3 and $A \approx 8$ g/kg·sec

$$d_{kp} \approx 0{,}5 \sqrt{\frac{u_1 S_\Sigma}{p_0}}. \qquad (5.27)$$

where u_1 is the linear powder (grain) burning rate for the conditions given for the particular engine, in cm/sec; S_Σ is the total burning

surface of the grain, in cm^2; p_0 is the working pressure in the combustion chamber, in kg/cm^2.

Experience in the testing of solid-propellant rocket engines has demonstrated that the calculated throat diameter must always be corrected on the basis of the results obtained in hot-firing tests, since the outflow of the products of combustion is a strong function of the structural features of each specific engine.

If the purpose of the experiments is to determine the coefficient φ by means of which we take into consideration the difference between the actual gas flow rate through the nozzle and that calculated on the basis of theory, the dimension d_{kr} can be determined more exactly in accordance with the following formula:

$$d_{кр} = 0{,}5\sqrt{\frac{u_a S_\Sigma}{\varphi p_0}}, \qquad (5.28)$$

where φ is the discharge correction factor, i.e., the ratio of the actual mass flow (gas flow rate) from the given engine to the theoretical mass flow (gas flow rate):

$$\varphi = \frac{M_{-}^{ист}}{w_{кр}\rho_{кр}\omega_{кр}} = \frac{M_{-}^{ист}}{A p_0 \sigma_{кр}};$$

w_{kr} and ρ_{kr} are, respectively, velocity and density of the gases in the nozzle throat; M_{-}^{ist} is the actual gas flow rate from the engine.

For engines with various nozzle-assembly versions and parameters of interior ballistics, the factor φ has an average value of φ = = 0.85-0.98.

There are other methods of calculating the magnitude of d_{kr}; however, not a single one of these methods can guarantee a dimension d_{kr} which will not require subsequent correction.

The second important nozzle dimensions is d_a. Its magnitude for a given d_{kr} is selected in dependence on the proposed divergence of

the nozzle which is adopted in the planning stage. Nozzle divergence is the ratio of the outlet diameter of the nozzle to the diameter of the throat (critical cross section):

$$\varepsilon = d_a/d_{kr} \text{ (less frequently } \sigma_a/\sigma_{kr}).$$

This ratio is an extremely important structural characteristic of an engine, since it determines such engine parameters as thrust and specific impulse. With constant parameters of interior ballistics, the thrust of a rocket engine and its specific impulse can be increased only by changing the nozzle exit angle. In practice, nozzles with great divergence are used comparatively rarely, since gasdynamic losses in such nozzles reduce the effect of increasing R and j_1 with an increase in $\varepsilon = d_a/d_{kr}$. A reduction in the ballistic characteristics of an engine can be observed in nozzles with $d_a/d_{kr} > 3\text{-}4$, since the increment in thrust in such nozzles sometimes fails to offset the increased weight of the engine structure.

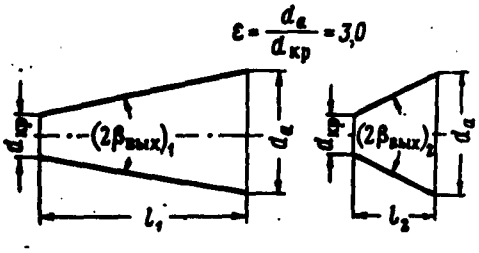

Fig. 5.23. Diagram of nozzles exhibiting $\varepsilon = d_a/d_{kr}$ = const for various pairs of dimensions $2\beta_{vykh}$ and $\underline{l}$.

It should be borne in mind that some nozzle expansion (divergence) can be achieved through nozzle length or the flare angle of the outlet funnel (Fig. 5.23). The condition of continuous gas flow through the nozzle limits the permissible angle of conic flare to the following quantity:

$$2\beta_{вых} = 20 \div 30^\circ.$$

In this case, the following angle is regarded as optimum:

$$(2\beta_{вых})_{опт} \approx 18^\circ,$$

here, however, on the basis of calculation data, with a change in $2\beta_{vykh}$ from 10 to 30°, the specific impulse of the engine changes only by 2-3%.

The dimension $\underline{l}$ is chosen on the basis of results obtained in a weight analysis of the various nozzle versions.

Nozzles exhibiting the following divergence are most widely used in practice:

$$\varepsilon = 1{,}5 \div 2{,}5.$$

With the selected nozzle divergence and the calculated d_{kr}, the diameter of the outlet section of the nozzle is defined as

$$d_a = \varepsilon d_{кр}, \tag{5.29}$$

in which case, generally,

$$d_a = (1{,}5—2{,}5)\, d_{кр}.$$

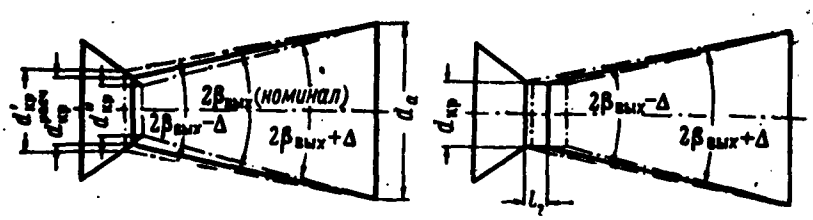

Fig. 5.24. Stability (technological) of dimension d_{kr} as a function of the area $\underline{l}_2$ with an outlet-cone flare-angle tolerance of $\pm\Delta$. Δ) Tolerance for magnitude of angle $2\beta_{vykh}$; d_{kr}^{rasch}) calculated magnitude of critical cross section; d'_{kr} and d''_{kr}) diameters of throat (critical cross section), corresponding to limit values of the angle $2\beta_{vykh}$.

The third flowthrough nozzle dimension (d_{vkh}) is not a theoretical (calculated) dimension and is selected on the basis of structural considerations. The linear nozzle dimensions $\underline{l}_1$ and $\underline{l}_2$ are also not calculated and are selected during the design stage. Upon designation of these dimensions, the following recommendations can be kept in mind:

1. $\underline{l}_1 \approx (3\text{-}4)d_{kr}$ must not be less than 10-20 mm with an inlet cone flare angle of $2\beta_{vkh} = 90^\circ$.

This relationship between the elements of the geometry of the

inlet cone provides for the formation of a stream at the inlet to the nozzle with the smallest losses, and a comparatively short length for the inlet cone.

2. $l_2 \leq d_{kr}$ must not be less than 3-5 mm.

This dimension is set on the basis of two basic requirements – the production-technological requirements and the operating requirements. From the standpoint of production, the need for the area l_2 can be explained by the fact that only with such an area is it possible to hold the dimension d_{kr} to a high precision class in the case of comparatively nonrigid tolerances for the dimensions of the inlet and outlet cones (Fig. 5.24). Moreover, the cylindrical surface of the critical cross section may be used as a reliable control and production base for the processing (machining) of the profile of the inner nozzle channel. The operational requirements with respect to the quantity l_2 are determined by the fact that the stability of the dimensions d_{kr} depends to some extent on the quantity l_2 during engine operation. Phenomena such as nozzle-wall erosion result in a situation in which, for small l_2, substantial "erosion" of the nozzle is observed, and this leads to a drop in pressure in the combustion chamber, as a result of which the engine is no longer operating at the theoretical regime.

With definite d_{kr} and d_a and the selected nozzle exit angle, the quantity l_3 is determined on the basis of the following relationship:

$$\tan \beta_{max} = \frac{\frac{d_a - d_{kp}}{2}}{l_3},$$

and the calculation formula is conveniently presented in the following form:

$$l_3 = \frac{d_{kp}}{2 \operatorname{tg} \beta_{max}} (\varepsilon - 1), \qquad (5.30)$$

where β_{vykh} is half the flare angle of the outlet cone of the nozzle.

Selection of Grids

In almost all contemporary solid-propellant rocket engines there is a diaphragm (grid) that is a structural part of the nozzle assembly of the missile. The grid is designed to support reliably the powder charge (grain) in the combustion chamber and serves simultaneously to ensure the best possible burning conditions for the grain and the complete combustion of its particles in the chamber without ejection of said particles from the engine. It should be borne in mind that a certain quantity of the powder particles are nevertheless ejected with the stream of the products of combustion, so that the grid helps only to reduce the number of such particles. From the standpoint of the gasdynamic operating regime of a rocket engine, the presence of a grid reduces engine characteristics, since the grid is a source of additional internal resistance which throttles the stream of the products of combustion.

Numerous experiments with grids of various shapes have shown that the magnitude of the free cross section $F_{d.sv}$ or even the ratio $F_{d.sv}/(\pi d_{kr}^2/4)$ are inadequate characteristics of the actual role played by the grid in the engine. To evaluate the properties of the grid, the configuration of the component part is extremely important, as is the relationship between the shape of the grid and the shape of the selected powder grain, and the mutual position of the flowthrough sections of the grid and the engine nozzles. The butt ends of powder grains must not cover the free cross section of the grid, since otherwise the effective free cross section of the grid is reduced and the pressure losses increase. The gasdynamic characteristics of the grid are noticeably improved if the grains do not rest on the plane of the

*tg = tan

grid but on special protuberances of the grid, generally fashioned in the shape of fins. The presence of such fins ensures a fixed clearance between the butt ends of the burning grains and the surface of the grid, which improves the conditions of gas flow to the nozzle and reduces the losses due to grid resistance. The height of the centering ribs is generally 5-10 mm (for missiles of medium caliber). The shape of the grid is selected so that the nozzle orifices of the combustion chamber are projected onto the free spaces of the grid. Of the remaining factors whose consideration makes possible the design of a grid with high characteristics, we should mention the following.

1. The shape of the grid must be such as to provide for a clearance of the order of 10 mm between the inner surface of the chamber and the outer contour of the grid. From this standpoint, a ring with a diameter equal to d_{vn} cannot be tolerated as the outer contour.

The above-mentioned requirement pertains to the case in which a charge (a single-grain or multigrain charge) is used in an engine, and the charge burns both along the outer and inner surfaces. In the case of single-grain charges burning only in a channel, the shape of the outer contour of the grid is not of great significance.

2. It is desirable that the outlines of the grid elements be streamlined in the direction of the gas flow. In order to avoid complex mechanical processing, grids with streamlined elements are most expediently produced by casting.

3. The strength calculations for the grid is a difficult problem in practice. The fin thickness for grids is, as a rule, selected by experimentation. In evaluating the strength characteristics of a grid, it should be borne in mind that the deformation of this component part during the process of engine operation is intolerable.

4. The design of the grid for turbojet missiles should be selected with consideration of the centrifugal loads produced by the rotation of the missile. In selecting the shape for the grid, it becomes necessary in this case to select such shapes in which strength and rigidity are greater in the radial direction (star, tubular, etc). Experience shows that the improper selection of a grid or the inappropriate selection of the "grain-grid" unit may result in a pressure pulse at the initial instant of burning, and this is of course undesirable.

Generally speaking, a solid-propellant rocket engine can be designed without a grid. The grains can be securely fixed in such an engine by means of special devices mounted on the forward connection plate, and the ejection of powder particles can be prevented by the appropriate design of the nozzle cover. All other conditions being equal, an engine without a grid is more promising, since it provides for better operating missile parameters.

Experiments have shown that it is expedient to have a so-called free space behind the grid in an engine, i.e., a space between the grid and nozzle cover. The length $l_{sv.d}$ of this space is a function of the features of a specific engine and, for example, for the M13 missile, is

$$l_{св.д} \approx 0{,}25\, d_{вн}, \qquad (5.31)$$

where d_{vn} is the inside diameter of the combustion chamber of the engine.

The engine-operating parameters improve as the space behind the grid increases; however, the structural weight of the missile increases in this case, and this is intolerable.

It would be desirable for the space behind the grid to be a solid of revolution with a smooth transition to the outlines of the nozzle

cover; however, this is not an absolute must. Examples of grid designs are presented in Fig. 5.25.

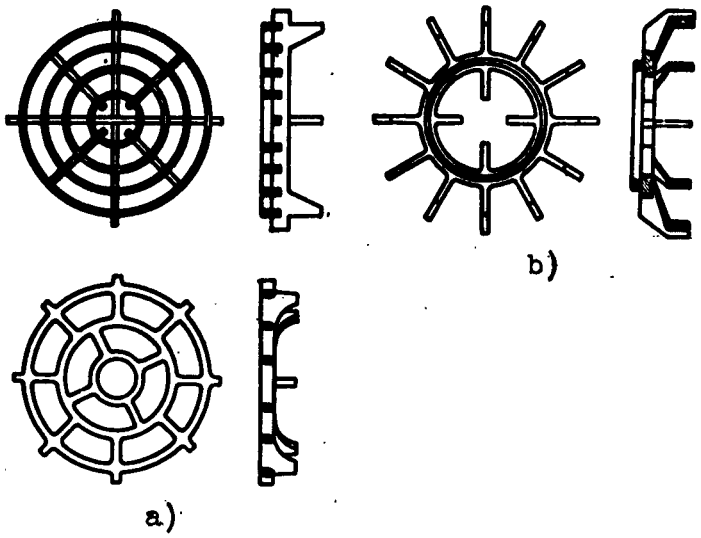

Fig. 5.25. Examples of grid designs employed in solid-propellant rocket engines. a) Grids for multigrain charges (stamped-and-welded and cast versions); b) grid for single-grain charge.

The Concept of Variable and Demountable Nozzles and Nozzles with Controlled Gas Streams*

As has already been pointed out, one of the features encountered in the burning of rocket powders is the relationship between the burning rate and the initial temperature of the charge:

$$u_{t_0} = u_{+20^\circ C} f(t_0),$$

where $u_{+20^\circ C}$ is the burning rate of the powder at a charge temperature of $t_0 = +20^\circ C$; $f(t_0)$ is the temperature burning-rate function,

$$f(t_0) > 1 \text{ for } t_0 > 20^\circ C;$$

$$f(t_0) < 1 \text{ for } t_0 < 20^\circ C.$$

The change in the burning rate with a change in t_0, at $d_{kr} = \text{const}$, causes the pressure in the combustion chamber to change as a function of the charge-ignition conditions, and given identical structural charge parameters, it will be low in the case of low (minus) temperatures, and high in the case of high temperatures. Since the magnitude

of pressure determines the basic characteristics of the rocket engine (thrust, specific impulse), the scattering of the pressure for various initial charge temperatures produces instability of the characteristics, substantially reducing the combat and operational characteristics of the weapon. Here it should be borne in mind that the sensitivity of pressure to changes in the burning rate is quite great and, for example, for the case of a power burning-rate function for the powder, it amounts to

$$\frac{\Delta p}{p}=\frac{1}{1-\nu}\left(\frac{\Delta u_{t_0}}{u_{t_0}}\right)=3\div 4\left(\frac{\Delta u_{t_0}}{u_{t_0}}\right),$$

since for present-day powders

$$\nu=\frac{2}{3}\div\frac{3}{4}.$$

For certain brands of powder, the burning rate at various ignition temperatures varies so markedly that the corresponding range of pressures in the combustion chamber is quite simply intolerable.

If we bear in mind that for a certain definite powder charge, the pressure in the combustion chamber, given a fixed burning rate, is a function only of the magnitude of the critical nozzle section (throat) of the engine

$$p=\frac{\gamma S_3}{A}u_3\frac{1}{\sigma_{\text{кр}}},$$

then it is natural to undertake two means of stabilizing the pressure in the engine for a given temperature interval of engine operation:

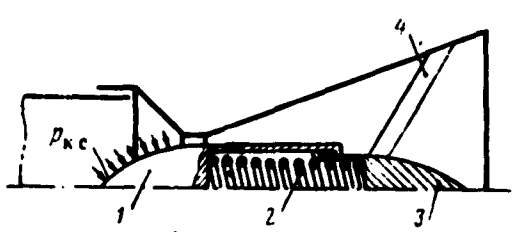

Fig. 5.26. Elementary diagram of self-regulating nozzle.

1) to use a powder that exhibits a weak relationship between the burning rate and the initial charge temperature and for which the magnitude of the pressure in the combustion chamber exhibits low sensitivity to the param-

eters of the charge;

2) to use special nozzles whose throat (critical cross section) would change with a change in pressure so as to leave pressure approximately constant.

Since there are virtually no powders that are not sensitive to the initial charge temperature, the first method is one for future investigation. However, the second method is quite realistic and there are many engines for which the magnitude of the critical cross section is regulated for the purpose of pressure stabilization over the wide temperature interval encountered in the operation of a rocket missile.

It is most efficient to employ a variable-nozzle design which would monitor automatically the pressure in the combustion chamber and react continuously to pressure fluctuations. Such nozzles are referred to as autocontrollable-area nozzles. An elementary diagram of a nozzle with smooth pressure control is presented in Fig. 5.26. We can see from the diagram that the autocontrollable nozzle differs from an uncontrollable conventional nozzle in that a special device is mounted in the former to monitor the pressure in the combustion chamber and to vary the flowthrough section of the nozzle in accordance with the changes in this pressure.

The device consists of a floating plug 1, guide springs 2, and supports 3; the plug is held by three supports 4 in the divergent section of the nozzle. The floating plug is under the action of two forces at any given instant of time; these forces are represented by the resultant of the pressure $p_{k.s}$ (in the combustion chamber) distributed over the frontal surface of the plug, and the resistance force of the spring, causing the plug to assume a certain position along the axis of the nozzle, depending on the relationship between these forces.

The spring 2 is selected so that at the rated pressure in the combustion chamber, the plug will assume a position on the axis of the nozzle at which the area of the flowthrough section of the nozzle ensures a balance of gases in the engine, i.e., at which

$$\mu_T S_2 = A p_0 \sigma_{kp}.$$

With an increase in $p_{k.s}$ the force acting on the plug as a result of this pressure increases, and the plug shifts to the right increasing the flowthrough section of the nozzle. Pressure begins to diminish in this case, and the plug gradually returns to a position corresponding to the rated pressure in the combustion chamber. With a drop in pressure, the plug is moved to the left by the springs and covers the critical cross section of the nozzle (the throat) thus producing a rise in pressure.

For the control diagram shown in Fig. 5.26 p_0 = const cannot be achieved and it is possible only to reduce substantially the magnitude of pressure scattering. This can be explained by the fact that the counter force p_{pr} of the spring is not constant and is itself a function of the area of the critical cross section, since

$$p_{pr} = cx = ck\sigma_{kp},$$

since the quantity σ_{kr} is determined by the coordinate $\underline{x}$ of the plug's position on the axis of the nozzle. Here $\underline{c}$ is the rigidity of the spring; $\underline{k}$ is some coefficient which determines the relationship between the coordinate $\underline{x}$ of the plug's position on the axis of the nozzle and the area of the open cross section of the nozzle.

Figure 5.27 presents curves for $p_0 = f(\sigma_{kr})$ which are solutions for the equation of balance for the extreme temperatures of the given interval ($\pm$ 50°C), and the characteristic of the spring p_{pr} = cx. We can see from the figure that if the nozzle is of the uncontrollable kind (σ = const = σ_2), a change in initial charge temperature in a

range from – 50 to + 50°C will cause the pressure in the engine to vary within limits of $\Delta p_{\sigma = const}$, corresponding to the BC ordinate segment on the graph. The plug-regulator shifts as a result of the introduction of the autocontrol system shown in the diagram in Fig. 5.26 in the case of a change in combustion-chamber pressure, thus producing a corresponding change in the area of the flowthrough section. If the spring characteristic is represented by the straight line AB, the maximum scattering of pressure in the temperature interval of ± 50°C is determined by the quantity $\Delta p' < \Delta p_{\sigma = const}$, and the critical cross section of the engine changes from σ_2 to σ_1.

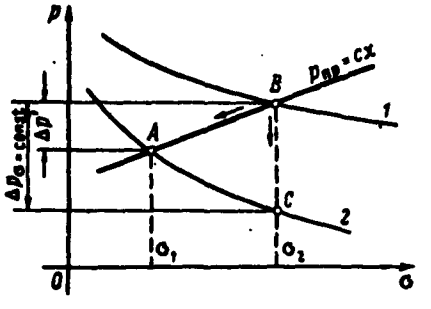

Fig. 5.27. Diagram characterizing drop in maximum pressure scattering in combustion chamber as a result of the utilization of the simplest method of controlling the magnitude of the critical cross section σ_{kr}. 1) $t_0 = + 50°C$; 2) $t_0 = - 50°C$.

The regulation device shown in Fig. 5.26 is the simplest possible. More advanced control schemes make it possible to maintain a virtually constant pressure within the combustion chamber over the entire temperature interval encountered in missile utilization. Naturally, these more advanced methods are more complex.

It should be borne in mind that it is necessary to control a nozzle not only for the purpose of stabilizing pressure during missile operation under various temperature conditions, but to provide for constancy of pressure within the combustion chamber at some fixed initial charge temperature, when the configuration of the grain is such that the burning surface is not constant during the time in which the propellant burns.

The design and testing of a selfcontrollable-area nozzle are connected with great difficulties. One of the basic problems en-

countered in the design of a nozzle with a control device is the matter of providing for the normal functioning of the design under conditions in which a high-temperature flow of the products of combustion flows past the regulation device (the plug). In this case, it is absolutely necessary to take into consideration not only the change occurring in the properties of the structural material situated in the area of the high operating temperatures, but it is also necessary to take into consideration the distortion of the working characteristics of the springs used, as a rule, in the design of a plug device. The development of nozzles with automatically controlled σ_{kr} is permissible only in those cases in which the utilization of such nozzles is justified by the imposition of high requirements with respect to the objects and by the small tolerance for the magnitude of the working pressure.

It is sometimes expedient to employ step control of σ_{kr}, since this is structurally a simpler solution involving the utilization of a complex of demountable nozzles. A diagram showing the application of such nozzles is presented in Fig. 5.28. Let the pressure p_{sr} be the rated pressure at σ = const = σ_{zimn}, and the scattering of this pressure at the extreme temperatures will be $\Delta p_{\sigma = \text{const}}$. We can see from the curves presented in Fig. 5.28 that the quantity $\Delta p_{\sigma = \text{const}}$ may be approximately the same as the average operating pressure, so that the extreme pressures will diverge from p_{sr} by a factor of almost one and a half. Such a scattering of pressures is intolerable. Let us divide the set temperature interval of $\pm$ 50°C for missile operation by:

summer (+ 50- +20°);

interseasonal (+ 20- – 20°);

winter (– 20- – 50°)

and let us select three various nozzles, each of which will make it

possible, in its own temperature range, to maintain an approximate constancy of engine thrust with a relatively small scattering of the operating pressure. These nozzles are conveniently designated as summer σ_{letn}, interseasonal σ, and winter σ_{zimn}.

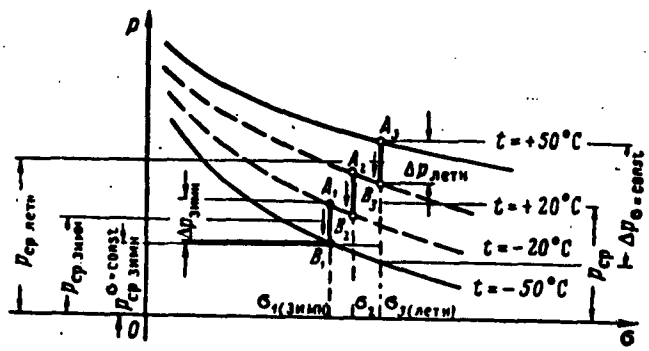

Fig. 5.28. Diagram illustrating possibility of reducing scattering of pressure p in the combustion chamber of a rocket engine with a large interval of operating temperatures t by using demountable nozzles.

Figure 5.28 shows that for each of these nozzles the scattering of pressure is substantially lower than in the case of σ = const, and the average pressure levels are correspondingly somewhat higher ($p_{sr.\ zimn} > p_{sr.zimn}^{\sigma=const}$). To summarize, for the approximate constancy of the characteristics of a rocket engine, several demountable (seasonal) nozzles may be chosen and one of these is to be used for each corresponding initial charge temperature.

In the design of demountable nozzles, we proceed from the basic requirement of R = const, which when we take into consideration

$$R = \xi p_0 \sigma_k$$

yields

$$p_0 \sigma_k = \text{const}$$

or

$$p_{t_1} \sigma_{t_1} = p_{t_2} \sigma_{t_2}, \qquad (5.32)$$

whence for the special case of $t_1 = +20^\circ$ we will have

$$\frac{e_{+20^\circ}}{e_t} = 1 + \frac{1 + kp_{+20^\circ}}{kp_{+20^\circ}} \frac{t - 20^\circ}{B_T}, \qquad (5.33)$$

where $\underline{k}$ is the ratio of the coefficients of the powder burning-rate function; B_t is the thermochemical powder constant, and it is assumed that $u_{\underline{1}} = u(ap + b)f(t_0)$, and that all of the denotations correspond to those adopted in interior ballistics.

Relationship (5.33) makes it possible to select demountable nozzles graphically. The sequence of the selection is clear from Fig. 5.29. It is desirable that the operating range for each nozzle over-

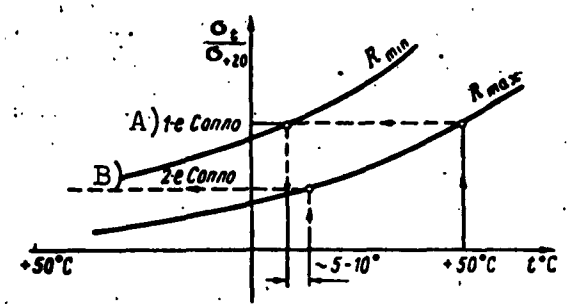

Fig. 5.29. Diagram for the selection of demountable nozzles which provide for constancy of engine thrust (within the limits of the given scattering of thrust). R_{min}) minimal required thrust; R_{max}) maximum required thrust; A) first nozzle; B) second nozzle.

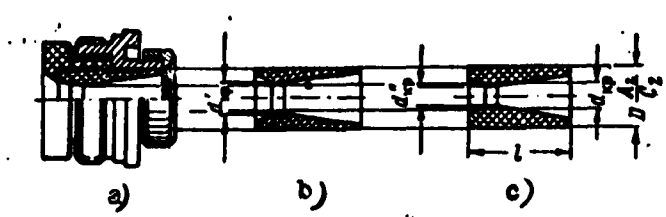

Fig. 5. 0. Nozzle with demountable liners. a) Interseasonal liner (for medium initial charge temperatures); b) summer liner; c) winter liner; d_{kr}, d'_{kr}, d''_{kr}) critical cross section of interseasonal, summer and winter liners, respectively; $D(A_2/C_2)$) fit diameter of liner assembly with nozzle frame.

laps that of the others by 5-10°. In designing an engine with demountable nozzles, it should be borne in mind that the number of

such nozzles must be kept to a minimum. In order to eliminate the cumbersome operation of nozzle reinstallation, particularly during the work at the starting position, it is expedient to employ demountable central liners rather than demountable nozzles. The replacement of such liners does not require subsequent tedious adjustment of the nozzles, and thus a significant reduction is achieved in the time spent on adjustment operations.

Figure 5.30 shows a nozzle with various demountable liners. In the fabrication of such nozzles, the complex of liners for each nozzle is generally put through its final processing during the assembly stage. This makes it possible to satisfy the requirements imposed with respect to the surface of the inner channel of the nozzle as well as to achieve exact correspondence of dimensions during the fitting stage.

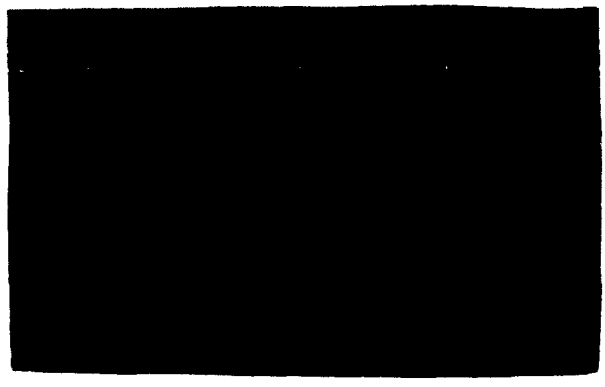

Fig. 5.31. Warm-up of "Honest John" rocket engine prior to start.

One of the methods employed to stabilize the characteristics of a solid-propellant rocket engine in the temperature interval set for this engine involves the prestart warming up of the engine. American periodical literature has presented several photographs of the Army "Honest John" rocket being preheated before launch (Fig. 5.31). The Americans use a metallic net as the heat source for this warm-up stage

i.e., a cover through which an electric current is passed for a specified period of time. At first glance, this method seems to be convenient; however, because of the low heat (temperature) conductivity of the powder, this method may be employed only in comparatively few cases.

In recent times engine designs have appeared with nozzles making it possible to change the direction of the exhaust gas stream according to a definite program or on the basis of a specific command. Such turning of the stream results in the appearance of a lateral reaction-force component (with respect to the axis of the engine), and this component is generally used to guide the flight of the object Nozzles with controllable gas streams have been developed for sustainer rocket engines as well as for booster assemblies.

As an example we can cite the booster unit for the aircraft-missile "Snark" (USA). The utilization of sensitive electronic devices in the control system of this missile makes intolerable any great acceleration of the object on launch. As a result, the missile acquires velocity comparatively slowly and, since the aerodynamic control surfaces become effective only at relatively great flight velocities, the missile is in fact unguided during the launch phase. This may result in pronounced deviation of the missile at the initial instant of flight from the calculated trajectory, which in turn results in the subsequent reduction of firing accuracy. The only means of guiding the flight of an aircraft-missile during the launching phase involves the utilization of the effect produced by the regulation (turning) of the stream of the products of combustion produced by the missile during the launch phase; this stream must be turned so as to offset the deviation of the object. A diagram of the "Snark" booster assembly is shown in Fig. 5.32. The command for the turning

of the deflection device in the nozzle is issued from the autopilot of the object to a servomechanism.*

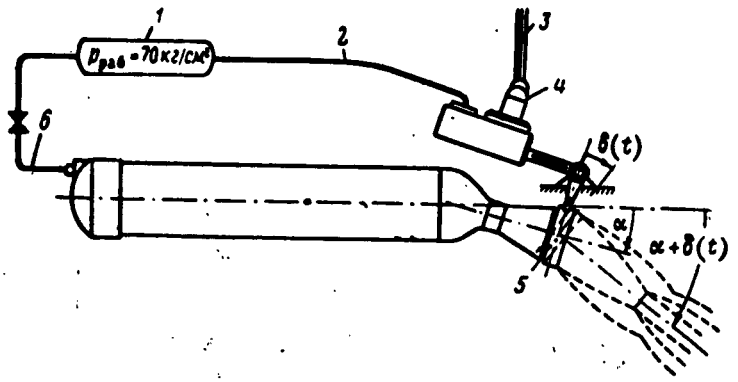

Fig. 5.32. Diagram of construction of booster assembly with controllable device to deflect the axis of the stream [of the products of combustion] (aircraft-missile "Snark" (USA). δ(t)) angle of turn for special device, on command; α) angle between axes of nozzle and engine; α+δ(t)) total angle of stream deflection; 1) hydraulic pressure accumulator; 2) pressure feed pipe; 3) to autonomous control system of object; 4) operating servocylinder; 5) rotating ring; 6) tubing for removal of powder gases.

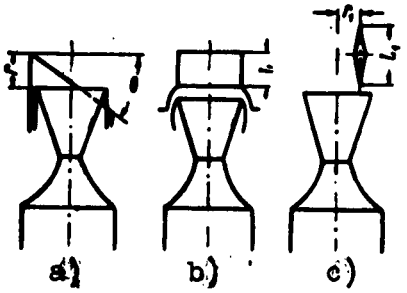

Fig. 5.33. Diagrams of nozzles with controllable gas stream. a) Nozzle with canted controllable (turnable) outlet; b) nozzle with controllable deflection device; c) nozzle with gas (jet) vane.

The development of controllable nozzles for sustainer engines would be expedient, for example, for rocket missiles with great operating flight altitudes, where the rarefaction of the air makes it impossible to use aerodynamic control, and where gas (jet) vanes are undesirable from a structural standpoint; the use of such a nozzle is also advisable for certain similar reasons. For example, it is well known that nozzles with controllable deflection devices are used in the sustainer engine of one

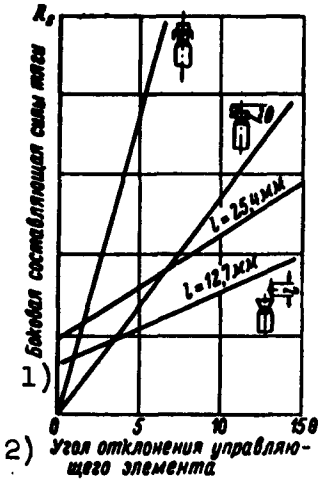

Fig. 5.34. Operating characteristics for nozzles with controllable gas stream. 1) Lateral component of thrust; 2) angle of deflection of control element.

of the stages of the ballistic "Polaris" rocket.

Nozzles with a controllable exhaust (gas) stream may be produced in a number of versions, and these are presented schematically in Fig. 5.33. The most effective of these verions, on the basis of data gathered in special investigations,* is the nozzle with a telescoping controllable deflection device. However, it should be borne in mind that the testing of such a nozzle is associated with great difficulties.

Figure 5.34 shows the operating characteristics of the above-mentioned nozzle versions for purposes of comparison, and here we can see clearly the advantages of the nozzles with telescoping deflection fittings.

§5. SEVERAL TYPES OF ROCKET POWDER CHARGES USED IN SOLID-PROPELLANT ROCKET ENGINES

The working charge of a solid-propellant rocket engine consists, as a rule, of a single or several independent elements, referred to as grains. The powder grains are made from a specially prepared initial mixture by extrusion into long bars of given lateral cross section, or by casting. These bars, after cooling and quality inspection, are cut into the required lengths and then machined.

The geometric dimensions and shapes of the powder grains which go to make up the working charge of the engine have a significant effect on the basic characteristics and operating regime of a solid-propellant rocket engine. The shape of the powder grains is of particu-

larly great significance in terms of the burning curve p = p(t), which determines the progressive, neutral, and regressive burning of the charge.

The curve which corresponds to the engine operating regime at which the pressure in the combustion chamber increases as the charge burns is referred to as a progressive curve. By analogy, the regressive curve is characteristic of an operating regime in which the pressure in the combustion chamber drops monotonically during the operation of the engine, and the neutral curve pertains to the case in which the pressure remains constant (or approximately constant).

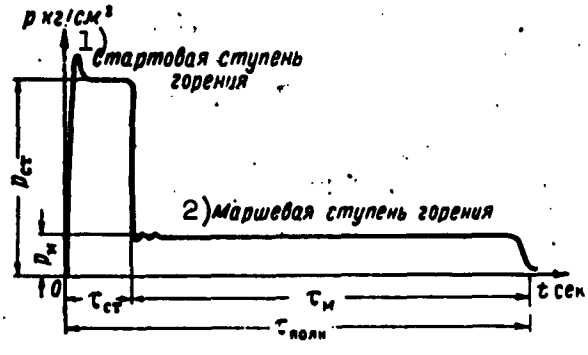

Fig. 5.35. Burning curve with two thrust stages providing for maximum speed for entry of missile into the controlled-flight phase. r_{st} and r_m) pressure in combustion chamber during launch and cruising regimes, respectively; τ_{st} and τ_m) engine operating time during launch and cruising regimes, respectively; τ_{poln}) total engine operating time; 1) starting stage of burning; 2) cruising stage of burning.

For the majority of missiles employed by the field rocket artillery, the thrust of the engine must remain constant throughout the entire period of engine operation. This means that in the case of uncontrollable nozzles, the configuration of the powder charge must provide for approximate constancy of pressure magnitude in the combustion chamber throughout the entire period of the burning of the powder

However, this requirement is not a general requirement, since for certain types of rockets it is more expedient to employ, for example, a progressive burning characteristic which ensures low thrust at the beginning and high thrust at the end of engine operation. In this case, the rocket passes through the lower denser layers of the air (atmosphere) at a relatively slow speed and accelerates primarily in the rarefied layers of the atmosphere.

As a result, the mean effective resistance and velocity losses produced by overcoming the resistance are substantially reduced in comparison with those encountered when engine thrust is constant. It is desirable in the case of other rocket missiles to achieve maximum speed of missile entry into the controlled-flight phase, with the missile moving at a slower speed during this phase, enabling it to react to the commands of the control system. In this case, a regressive or, perhaps even a step, burning characteristic would be preferable (Fig. 5.35).

In certain cases, to attain the required velocity rapidly, the missile is designed as a two-stage assembly, in which case the first stage is the booster which is jettisoned upon completion of the burning stage.

Among all possible cross-sectional shapes of grains, of which the most frequently employed are presented in Fig. 5.36, relative constancy of pressure is provided by grains with specially shaped channels (for example, star-shaped grains) and grains which burn simultaneously along the outer surface and the surface of the inner channels (tubular cylindrical, elliptical, and triangular, seven-channel and three-channel three-petal grains). It is possible to select a relationship between the geometrical elements of the cross section for these grains at which the total burning surface will be

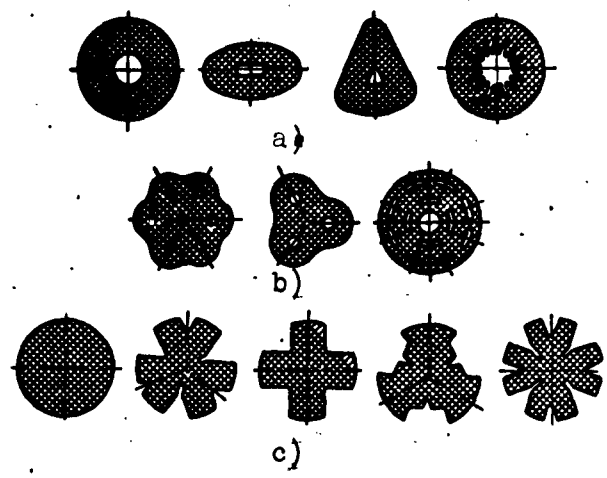

Fig. 5.36. Several cross-sectional shapes of grains frequently encountered in solid-propellant engines. 1) Tubular grains; b) multitubular grains; c) grains without channels.

kept approximately constant throughout the entire period of engine operation, and at σ_k = const determines the constancy of pressure.

As an example, let us examine a single-channel cylindrical grain. Let the cross-sectional dimensions of the grain at the initial instant be the following: R_0 is the circumferential radius of the outer surface; r_0 is the radius of the inside channel; L_0 = const(t) is the length of the grain (and this may be attained, for example, by armoring the side ends of the grain).

The total burning surface S_0 for this instant will be

$$S_0 = 2\pi R_0 L_0 + 2\pi r_0 L_0 = 2\pi (R_0 + r_0) L_0;$$

after $\underline{t}$ sec, a part of the grain will have burnt up, and if the burning rate during this period of time was $\underline{u}$ mm/sec, then the dimensions of the grain will become the following:

$$R_t = R_0 - 2ut,$$
$$r_t = r_0 + 2ut,$$

and the total burning surface S_t will be

$$S_t = 2\pi R_t L_0 + 2\pi r_t L_0 = 2\pi (R_t + r_t) L_0 =$$
$$= 2\pi (R_0 - 2ut + r_0 + 2ut) L_0 = 2\pi (R_0 + r_0) L_0 \equiv S_0.$$

If the grain burns both along the side surface and the end surfaces, the total burning surface changes somewhat; however, this change is comparatively small, particularly in the case of grains of great length. Let us estimate the value of ΔS_{max}. It is clear that when the ends of the grain participate in the combustion,

$$S_0 = 2\pi (R_0 + r_0) L_0 + 2\pi (R_0^2 - r_0^2),$$
$$S_t = 2\pi (R_0 + r_0) L_t + 2\pi [(R_0^2 - r_0^2) - 4ut (R_0 + r_0)],$$

where

$$L_t = L_0 - 2ut.$$

Hence it is easy to determine ΔS_t in the following form:

$$\Delta S_t = S_t - S_0 = -12\pi ut (R_0 + r_0).$$

The minus sign indicates that the burning surface is diminishing gradually. From a geometrical standpoint

$$(ut)_{max} < R_0,$$

so that the maximum change in the burning surface will not exceed

$$|\Delta S_{max}| < 12\pi (R_0 + r_0) R_0. \qquad (5.34)$$

and since the length of the powder grain, as a rule, is generally 8-12 calibers of the grain, i.e.,

$$R_0 = \frac{L}{16 \div 24},$$

$$|\Delta S_{max}| < (0{,}5 \div 0{,}75)(R_0 + r_0) L_0.$$

Comparing this quantity with the first term of the expression determining S_0, we will find that ΔS_{max} will not exceed $(0.25\text{-}0.35)S_0$ even in the case of such comparatively short grains.

In actual fact ΔS_{max} is even smaller and, therefore, the utilization of single-channel cylindrical grains, as a rule, ensures constancy of pressure in the engine, with a possible deviation of the order of 5% toward the end of combustion.

We must point out that in certain engines it may be completely unnecessary for the total burning surface of the charge to remain con-

stant throughout the entire period of engine operation in order to attain p = const. The situation here is that as the working charge burns up, certain engine and charge characteristics and parameters undergo change, and these quantities determine the magnitude of pressure in the combustion chamber, so that in order to stabilize the pressure this change in engine operating conditions must be compensated. The most convenient method to achieve this is the control of the burning surface of the charge. For example, according to data from Wimpress, in order to achieve a rigorous p = const in one of the engines employing JPN-powder charges, it would be necessary gradually to reduce the burning surface, with an approximate reduction of 25% of the burning surface toward the end of combustion.

Grains which burn only on the outer surface (cylindrical grains without channels, cruciform, etc.) as a rule exhibit regressive burning, whereas grains burning from within exhibit progressive burning (if the channels of such grains are not given special shapes).

In order for the powder grain to burn only along a certain limited and predetermined surface, a restriction coating is applied. The restriction coating applied to a grain involves the application of a special coating to those surface areas of the grain which are not to participate in the combustion process, and this coating is cemented or similarly attached to the powder mass of the grain, thus eliminating the possibility of the appearance of a flame along the surfaces. For example, in order for the grain to burn only along the surface of the channel, the outer and end surfaces of the grain are covered with the restriction coating. As an example of a restriction coating we can cite, for example, the composition of the restriction coating so widely used in the USA, which is based on standard rubber S (USA standard) with admixtures of gas black, a plasticizer, and special vulcanization

187

additives. For the application of the restriction coating of the charges, the above-indicated mixture is prepared in specific proportions and rolled into sheets of required thickness. The grains are rolled into these sheets and kept under high pressure in special thermostats ($t \approx 100^{\circ}C$) for specific periods of time. The rubber is vulcanized in the thermostat, and as a result a reliable restriction coating for the treated surface of the grain is formed. Various polymerizing tars and synthetic materials may be employed as bases for the restriction-coating composition in addition to rubber.

In selecting the composition of the restriction coating it should be borne in mind that the basic requirements imposed here are the following:

– the need to provide for good adhesion with the surface of the powder grains;

– instablity to the action of the flame and the stream of the products of combustion along the restriction coating;

– preservation of properties over the wide temperature interval of missile operation.

If the required nature of the curve $p = p(t)$ can be achieved by selecting a particular cross-sectional grain shape and the partial restriction of the charge surface, then the second basic characteristic of engine operation – the burning time of the charge – is completely determined by grain dimensions and primarily by the magnitude of the so-called combustion cupola. The combustion cupola can be defined as the minimum distance between the initial burning surface and the position of the flame front at the final instant of combustion. For example, in the case of a single-channel cylindrical grain, where combustion is observed both along the other surface as well as in the channel, the magnitude of the cupola $\underline{e}$ is determined by the following

expression:

$$e' = \frac{R_0 - r_0}{2},$$

since the position of the flame front at the end of the combustion process corresponds approximately to the center of the grain surface. If one of the surfaces of such a grain is restricted and combustion takes place only along the surface of the inside channel (or, conversely, only along the outer surface), the magnitude of the cupola will be

$$e'' = R_0 - r_0.$$

We can see from this example that, all other conditions being equal, grains burning from without and along the surface of the channel have a thinner cupola, i.e., a shorter operating time than do grains burning only along the channel surface or only along the outside surface. If the burning surface is the butt-end surface of the grain, then

$$e''' = L_0$$

and, since generally $L_0 \gg R_0$, the time of engine operation in this case is at its maximum.

The detailed properties of charges of various configurations are presented in Table 5.1.

With a reduction in the over-all dimensions of the grain, the thickness of the cupola in terms of absolute magnitude also diminishes and, therefore, in order to attain minimum combustion times multi-grain charges are employed. For example, let a single-grain charge of a single-channel cylindrical grain having the dimensions R_{01}, r_{01}, and L_{01} for the previous missile caliber be replaced by a charge consisting of seven grains and a geometrical cross section similar to the initial grain (R_{02}, r_{02}, and L_{02}). Let us see how the burning time for the charge will change in this case. In the first case, the magni-

tude of the combustion cupola wholly determined the duration of grain combustion, and in this case will be

$$e_{1sh}=\frac{R_{01}-r_{01}}{2}=\frac{R_{01}}{2}\left(1-\frac{r_{01}}{R_{01}}\right)$$

and, correspondingly, in the second case it will be

$$e_{7sh}=\frac{R_{02}-r_{02}}{2}=\frac{R_{02}}{2}\left(1-\frac{r_{02}}{R_{02}}\right)$$

(e_{7sh} is the cupola of a seven-grain charge).

TABLE 5.1.

Properties of Some of the Simplest Types of Grains for the Case of Comparable Charge Dimensions (R_0, r_0 = const)

Характер кривой горения 1) \ Сравнительное время горения 2)	3) Малое	4) Среднее	5) Наибольшее
Прогрессивная 6)		7) Шашки с горением по поверхности цилиндрического канала	
p=const	8) Шашки, горящие снаружи и по поверхности канала	9) Шашки, горящие по поверхности канала, имеющего сложную форму; шашки с пропилами	10) Шашки, горящие с торца
Дегрессивная 11)		12) Шашки с горением по наружной поверхности	

1) Nature of the combustion curve; 2) comparative combustion time; 3) small; 4) average; 5) greatest; 6) progressive; 7) grains with combustion along the surface of a cylindrical channel; 8) grains burning on the outside and along the surface of the channel; 9) grains burning along the surface of a channel of complex shape; grains with grooves; 10) grains burning at the butt-end surfaces; 11) regressive burning; 12) grains burning along the outside surface.

If we assume that

$$2R_{01}\approx d_{vn}$$

and that if the seven grains are tightly packed into the combustion chamber, having an inside diameter of d_{vn},

$$2R_{02}=\frac{d_{вн}}{3},$$

we will obtain the following for grains with similar cross sections

$$\frac{e_{2в}}{e_{1в}}=\frac{R_{02}\left(1-\frac{r_{02}}{R_{02}}\right)}{R_{01}\left(1-\frac{r_{01}}{R_{01}}\right)}\approx\frac{1}{3},$$

i.e., in the second case the burning time for the charge diminishes by a factor of three in comparison with the very fastest burning version of a single-grain charge.

In making the transition to a multigrain charge, the charge density characterized by the weight of a unit of charge length, as a rule, diminishes (see Table 5.2) and the length of the combustion chamber increases in order to hold the earlier quantity of powder within the engine. This results in an impairment of the weight characteristics of the engine and, in particular, leads to a reduction in the value of the ratio ω/q_p which, according to the formula of K.E. Tsiolkovskiy, determines the magnitude of the velocity acquired by the missile as a result of the functioning of the rocket engine.

TABLE 5.2.

Comparative Charge Density Characteristic for Powder Rocket Charges Having Various Cross-Sectional Shapes

Форма поперечного сечения 1) шашки	2) Количество шашек в заряде	3) Плотность заряжания
4) Одноканальная цилиндрическая шашка	1	1,000
5) То же	5	0,834
	7	0,916
6) Телескопическая шашка	1	0,984
7) Семиканальная шашка Уолша	1	~1,000
8) Трехканальная трехлепестковая шашка	7	0,967
9) Крестообразная шашка	1	0,909

1) Shape of grain cross section; 2) number of grains in charge; 3) charge density; 4) single-channel cylindrical grain; 5) the same; 6) telescoping grain; 7) seven-channel Walsh grain; 8) three-channel three-petal grain; 9) cruciform grain.

Let us take note of the fact that in the case of constant grain-cupola thickness, the burning time can be changed by altering the pressure magnitude which determines the powder burning rate; however, in this case, the time of engine operation can be changed only within comparatively narrow limits.

Thus the following applies with respect to a preliminary recommendation on the selection of the type of powder charge for the engine being designed.

1. If thrust must be kept at a constant level throughout the entire period of engine operation, the grain selected should be taken from among those burning from within and having a complex channel configuration or burning from without and along the surface of the channel; for extremely long periods of engine operation, we must select a charge which burns at the butt-end surfaces.

2. For regression burning, grains burning from without should be selected, or the engine should be designed for two thrust stages.

3. Progressive combustion is achieved by grain shapes providing for combustion within the channel.

4. For pronounced reduction of operating time in all three cases, multigrain charges should be employed. In this case, it may be assumed that in first approximation burning time is reduced in direct proportion to the increase in the number of grains in the charge.

Let us examine in greater detail the problem involved in the selection of a charge for engines with medium burning time. With an engine operating time of 20-30 seconds and higher, the basic problem encountered in the achievement of a functioning design is the matter of preventing the overheating of the lift components and the combustion-chamber units, and primarily of the engine walls. From this standpoint, the charge version in which burning takes place along the sur-

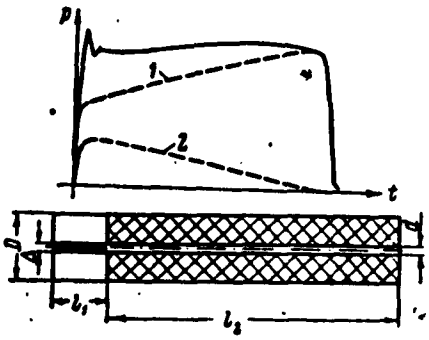

Fig. 5.37. Diagram of charge with slit grooves, providing for approximate neutrality of the curve p = p(t) with combustion along the surface of the inside channel. 1) Combustion curve for simple single-channel grain; 2) combustion curve for compensating surface.

face of the inner channel is optimum, since when densly packed into the combustion chamber this charge reliably insulates the walls of the chamber with a layer of powder mass which, because of its low thermal conductivity, is almost an ideal insulating material. The progressive-burning curve (p = p(t)) for a grain with a simple channel (cylindrical), not always desirable for an engine, may be eliminated or, at least, substantially reduced by the introduction of auxiliary regressive burning surfaces in the grain or through the utilization of so-called compensating grains.

Figure 5.37 shows a grain in which burning takes place along the surface of the channel, and this grain has been processed in such a fashion as to keep the burning surface approximately constant, i.e., the combustion characteristics of the grain may be regarded as virtually neutral.

The final touches on the shape of the grain involve the introduction of grooves, Δ mm wide, into the thickness of the grain at its end surface. Combustion takes place not only along the surface of the grain channel but along the surface of the grooves as well. As a result, at the initial instant the total burning surface can be markedly increased. As combustion progresses, the surface of the grooves diminishes as a result of the increase in the dimension d, since

$$S_\Delta = (D-d)\, l_1\, n.$$

The regressive nature of the combustion surfaces of the grooves and the progressive nature of the basic combustion surfaces make it possible, for a given selection of the geometrical elements of the grain, to attain approximate neutrality of the charge-combustion characteristic.

While in order to satisfy the tactical-technical requirements with respect to thrust parameters, the combustion surface must be equal to S cm^2, the relationship between the geometrical elements of the powder grain of this type are determined in first approximation from the following conditions:

$$\left.\begin{aligned} S_{нач} &\approx \pi D l_2 \\ S_{кон} &\approx \pi d l_2 + n(D-d) l_1, \end{aligned}\right\} \quad S_{нач} = S_{кон} = S,$$

(n is the number of grooves in the charge), whence

$$\left.\begin{aligned} l_2 &\approx \frac{S}{\pi D}, \\ l_1 &\approx \frac{S - \pi d l_2}{n(D-d)} = \frac{S}{\pi D}, \end{aligned}\right\} \tag{5.35}$$

where l_1 is the length of the groove; D is the outside diameter of the grain; d is the inside diameter of the grain; S_{nach} and S_{kon} are, respectively, the initial and final combustion surfaces, or if the grooves are made symmetrical with the two ends of the grain:

$$l_1 \approx \frac{S}{2\pi D}. \tag{5.35'}$$

Compensating surfaces can be made not only in the form of grooves at the ends of the grain. Of the other versions of such surfaces we can cite, for example, the inverse inside cone and certain similar versions (Fig. 5.38).

In conclusion, let us dwell in some detail on the problem of selecting the charge for rocket engines with step characteristics of combustion, to whose development particularly great attention has been devoted in recent times. If we do not consider the possible versions

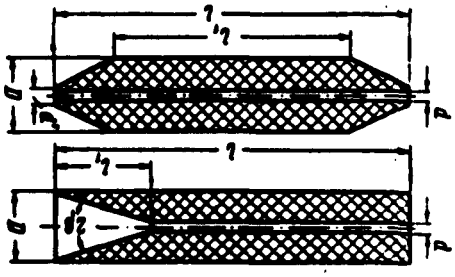

Fig. 5.38. Examples of charges burning along the surface of the inside channel with reduced progressive-burning curve $p = p(t)$. l_1, l, d, D, 2β, and d') characteristic grain dimensions.

of an engine with dual thrust, in which the programming of thrust is determined by the structural features of the engine (a design with successively positioned chambers forming a single structural whole, and certain similar features), the step combustion characteristic can be attained:

1) for a limited combustion time

– by using conventional single-channel cylindrical grains with intermediate restriction coating (Fig. 5.39). In this case, the grain may be made of a powder of one and the same brand or of two various powders. In the latter case, the production techniques for the charge are substantially more complex and it becomes quite difficult to obtain a reliably functioning charge;

2) for medium combustion time

– by producing a composite grain using two powder preparations; a fast burning preparation – for launch, and a slow burning preparation for the cruising phases of the flight (Fig. 5.40);

– by using two various powder preparations in accordance with the rate of combustion for the required program;

3) for long operating times

– by using two various powder preparations for butt-end combustion. As an example we can cite the charge employed by the US Navy drone XKDT-1 "Til' - [sic]", shown in Fig. 5.41. The charge is made entirely of a powder mixture having the following composition (in %):

ammonium nitrate	80
synthetic rubber	10
admixtures (combustion catalysts, carbon black, a plasticizer, vulcanization additives)	10

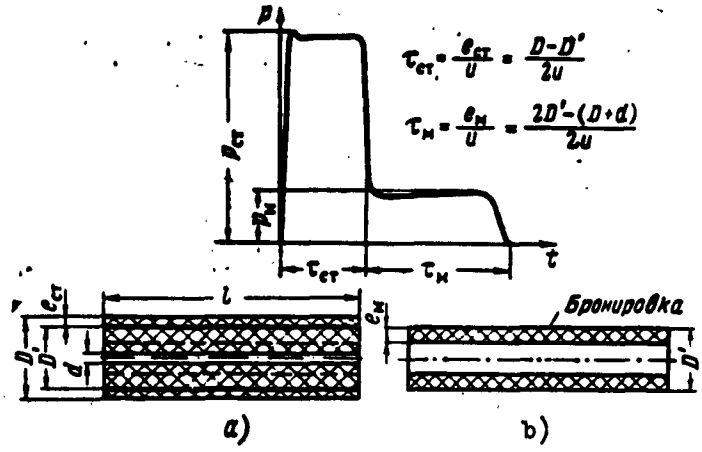

Fig. 5.39. Example of charge providing for dual thrust for small period of engine operation. e_{st}) grain cupola burning during first stage of engine operation; e_m) grain cupola burning during the cruising regime of engine operation; 1) restriction coating.

A greater combustion rate for the starting portion of the charge can be obtained by changing the composition of the catalytic admixtures somewhat as well as by changing the production techniques involved in the fabrication of the propellant mixture.

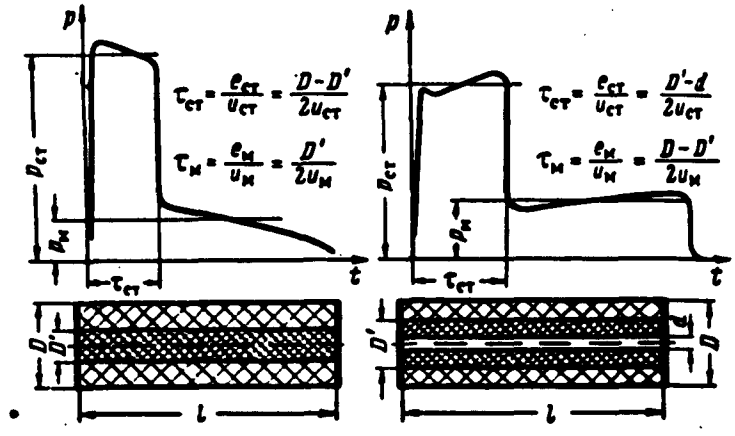

Fig. 5.40. Examples of charges which produce double thrust for medium periods of engine operation.

Given fixed charge geometry, the characteristics of engine operation can be changed only through the utilization of various propellant mixtures (for example, fast or slow burning powders, etc.) or by

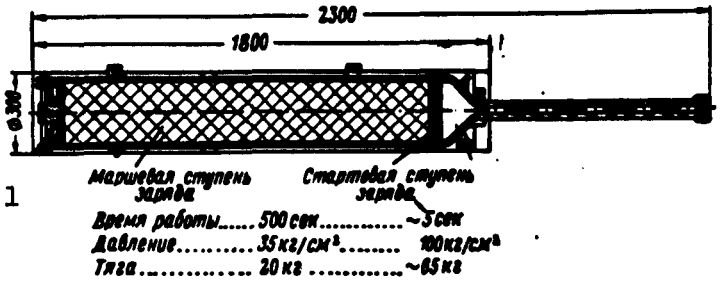

1

Fig. 5.41. Diagram of charge used in guided USA Naval Drone XKDT-1 "Til'-[sic]."

1) Cruising stage of charge		Starting stage of charge
Operating time	500 sec	~5 sec
Pressure	35 kg/cm^2	100 kg/cm^2
Thrust	20 kg	~65 kg

altering the operating pressure.

§6. THE PROBLEM OF INJECTING THE OPTIMUM VERSION OF A SINGLE-CHANNEL CYLINDRICAL GRAIN CHARGE INTO THE COMBUSTION CHAMBER

Almost all field-artillery missiles are being designed with a multigrain solid-propellant charge. This can be explained primarily by the fact that with an increase in the active flight phase (i.e., with an increase in the burning time of the charge) the firing accuracy of field rockets, as a rule, is reduced, so that for these missiles it is desirable to have a charge which exhibits a minimum of engine operating time. The increase in start overload in this case does not impose any particular restrictions on the magnitude of τ sec., since even the maximum realistically possible launch overloads, as a rule, do not produce any dangerous stresses in the elements of the missile structure.

In designing a multigrain charge, it is necessary first of all to select the number of grains with which the basic requirements of the tactical-technical requirements with respect to a rocket engine will be satisfied in the case of rather high ballistic and structural characteristics (density of charge, ω/q_p ratio, the length of the combus-

tion chamber, etc.). The problem here is to place a definite quantity of powder (ω, kg) - in the form of a charge - into the combustion chamber, and this quantity must guarantee the normal burning of the powder in the case of a maximum-density grain. The quantity ω kg is generally determined during the preliminary selection of structural and weight parameters for the missile. The dimension d_{vn} mm - the inside diameter of the combustion chamber - characterizes the volume (space) in which the charge can be held, and this can be found during the strength calculations for the chamber.

The problem of injecting into the combustion chamber the optimum version of a multigrain charge made of single-channel cylindrical grains can be solved in various ways - through simple empirical selection of various numbers of grains to the utilization of cumbersome analytical calculations. In first approximation, the solution of this problem, with a sufficient degree of accuracy (and at the same time, with comparative simplicity of calculation), can be obtained by employing the graphical-analytical method, and the procedure is desbribed below.

Let us have a charge consisting of n single-channel cylindrical grains whose butt-end surfaces are small in comparision with their side surfaces S_{bok} (for purposes of generality, we can, for example, assume that the butt-ends of the grains have been coated). For such a charge

$$S = S_{bok} = \pi (D+d) ln \qquad (5.36)$$

or taking into consideration

$$d = D - 4e,$$

where e is the combustion cupola,

$$S_{bok} = 2\pi (D-2e) ln. \qquad (5.36')$$

From this equation

$$D=2e+\frac{S_{бок}}{2\pi ln},$$

D, d, l are, respectively, the outside and inside diameters, and the length of the powder grain.

The obtained relationship establishes a link between the grain of a multigrain charge and some parameters (e, n) which determine the charge characteristics from the standpoint of the posed problem. However there is little practical use for this relationship, since it contains the quantity S_{bok} which, generally speaking, has not yet been determined and is in no manner associated with the parameters of either charge or engine. Let us express S_{bok} in terms of these parameters.

It is clear that

$$\omega=v_{заг}\gamma=\frac{\pi}{4}(D^2-d^2)l\eta\gamma,$$

where v_{zar} is the volume of the solid-propellant charge.

Separating the difference between the squared diameters into the cofactors and grouping the expression in the right-hand part of the equation in a certain manner, we will obtain

$$\omega=\pi(D+d)l\eta\frac{D-d}{4}\gamma=S_{бок}e\gamma,$$

whence

$$S_{бок}=\frac{\omega}{e\gamma}$$

and

$$D=2e+\frac{\omega}{2\pi l\eta\gamma}. \qquad (5.37)$$

Now it is possible to break down the over-all charge (ω,kg) into n grains having definite dimensions (D, d, l) so that the burning time corresponds to the required (e). However, we do not know whether such

a charge can be placed into the combustion chamber of the engine, and if it can be placed, we do not know whether the charge will burn stably there, i.e., the selection of a possible charge version is purely formal.

In a like manner, we will rearrange the equality

$$\omega = S_{бок} e \gamma$$

to the form

$$\omega = S_{бок} e \gamma \frac{F_{св}}{F_{св}} \frac{F_{вн}}{F_{вн}},$$

where $F_{vn} = (\pi d^2_{vn}/4)$ is the area of the lateral cross section of the combustion chamber; F_{sv} is the free cross section of the chamber when n grains of powder are placed into it.

We know that the parameter

$$\frac{S_{бок}}{F_{св}}$$

characterizes the stability of powder burning in the engine; we will denote this parameter by κ and rewrite the latter relationship, taking into consideration this denotation, and regrouping the remaining terms

$$\omega = \gamma e \varkappa \frac{F_{св}}{F_{вн}} F_{вн},$$

$$\frac{F_{св}}{F_{вн}} = \frac{F_{вн} - F_{торц}}{F_{вн}} = 1 - \frac{F_{торц}}{F_{вн}},$$

where F_{torts} is the area of the butt-end section of the charge.

We will assume that in first approximation the length of the combustion chamber is equal to the length of the grains contained within the chamber; then

$$1 - \frac{F_{торц}}{F_{вн}} = 1 - \frac{F_{торц} l}{F_{вн} l} = 1 - \frac{v_{пор}}{F_{вн} l} = 1 - \frac{\frac{\omega}{\gamma}}{F_{вн} l},$$

i.e.,

$$\omega = \gamma e x \left(1 - \frac{\omega}{\gamma F_{вн} l}\right) F_{вн},$$

whence the quantity ω will be determined in the following form:

$$\omega = \gamma F_{вн} \frac{exl}{ex + l}. \tag{5.38}$$

Substituting this ω into (5.37), we will obtain

$$D = 2e + \frac{F_{вн} \frac{ex}{ex + l}}{2ne} \frac{1}{n}. \tag{5.39'}$$

Let us introduce the dimensionless combinations

$$\left.\begin{aligned} \varepsilon &= \frac{ex}{l}, \\ \delta &= \frac{D}{d_{вн}}, \\ \xi &= \frac{e}{d_{вн}}. \end{aligned}\right\} \tag{5.40}$$

Dividing both parts of Eq. (5.39') by d_{vn}, we can easily obtain

$$\frac{D}{d_{вн}} = 2\frac{e}{d_{вн}} + \frac{1}{\delta} \frac{\frac{ex}{l}}{1 + \frac{ex}{l}\frac{e}{d_{вн}}} \frac{1}{n}, \tag{5.39"}$$

which in dimensionless terms is written as follows:

$$\delta = 2\xi + \frac{1}{\delta} \frac{\varepsilon}{1 + \varepsilon} \frac{1}{\xi} \frac{1}{n}. \tag{5.39}$$

Now the given weight of the powder ω, kg, can be divided into n such grains which are contained in the chamber of the engine being designed, and will burn there in a stable manner.

Naturally, the grain version which can be placed in the combustion chamber in dense packing will be the optimum version, i.e., the version for which d_{vn} will be the diameter of the described circumference. Graphically, this version is most simply defined as the point of intersection between the curve for Eq. (5.39) and the so-called curve

of dense-packing (Fig. 5.42). The dense-packing curve is constructed along the points of Table 5.3 which contains the dimensionless diameters of the various circumferences inserted around the given diameter d.

TABLE 5.3

Dimensionless diameters of inserted circumferences

n	δ	n	δ	n	δ	n	δ	n	δ	n	δ
1	1	7	0,333	13	0,230	19	0,200	25	0,175	31	0,160
2	0,5	8	0,294	14	0,220	20	0,196	26	0,168	32	0,156
3	0,464	9	0,269	15	0,220	21	0,189	27	0,165	33	0,156
4	0,414	10	0,256	16	0,213	22	0,184	28	0,165	34	0,150
5	0,370	11	0,247	17	0,206	23	0,176	29	0,160	35	0,150
6	0,333	12	0,244	18	0,200	24	0,172	30	0,160	36	0,150

The curve of Eq. (5.39) in coordinates δ, $1/n$ is a straight line which passes through point M $(0, 2\xi)$ at an angle φ to the axis of abscissas (Fig. 5.43) the tangent of which is

$$\tan\varphi = \frac{1}{8}\frac{\varepsilon}{1+\varepsilon}\frac{1}{\xi}.$$

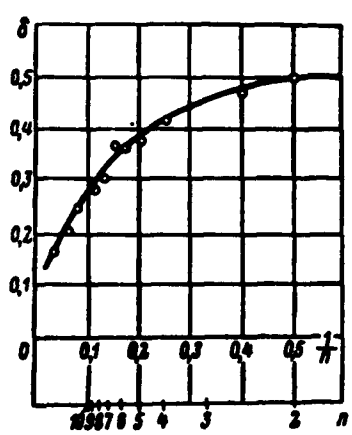

Fig. 5.42. Curve of dense packing for dimensionless grain diameters

This straight line may be directed with respect to the dense-packing curve in various ways. Here, if there is a single intersect point (Fig. 5.43) there is only one solution. However, if the curves intersect several times, there is a corresponding number of charge versions, each of which satisfies the optimum conditions. It is impossible to encounter a case in which the curves will not have any common points. In this case, if there are a pair of coordinates for which both curves come rather close, the solution is sought in the vicinity of this par-

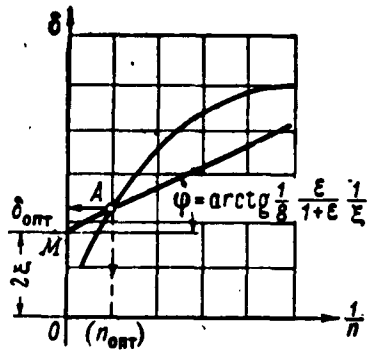

Fig. 5.43. For the selection of the optimum version of a multigrain charge made of single-channel cylindrical grains

ticular pair (Fig. 5.44) and a reverse calculation if performed, the initial parameters for charge and engine being refined here. If there is no such pair of coordinates, it becomes necessary to vary the initial quantities e, κ, l, etc., attaining the required change in the orientation of the line

$$\delta = 2\xi + \frac{1}{8}\frac{\varepsilon}{1+\varepsilon}\frac{1}{\xi}\frac{1}{n}.$$

In this case, the straight line can either be placed along the δ axis, so that

$$\delta = 2\xi_1 + \frac{1}{8}\frac{\varepsilon}{1+\varepsilon}\frac{1}{\xi_1}\frac{1}{n},$$

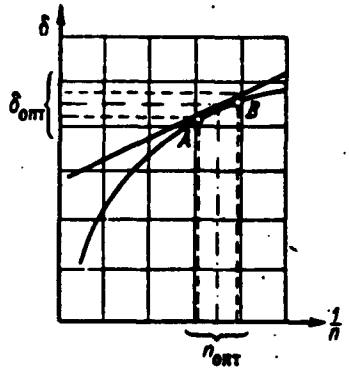

Fig. 5.44. Selection of optimum charge version in the absence of a point of intersection between the curves (the first case)

where $\xi_1 = e_1/d_{vn}$, and e_1 is the new magnitude of the combustion cupola, or the straight line can be turned about M (Fig. 5.45):

$$\delta = 2\xi + \left(\frac{1}{8}\frac{\varepsilon}{1+\varepsilon}\frac{1}{\xi_1}\right)\frac{1}{n}.$$

In both cases, the position of the straight line is sought so as to produce at least a single common, or, at least, sufficiently close point.

For an analysis of the methods used to achieve the practical change in the orientation of the straight line, let us examine the coefficients of Eq. (5.39):

$$1)\ 2\xi = \frac{2e}{d_{вн}}.$$

This coefficient can be increased (at d_{vn} = const) only by increasing the thickness of a grain cupola e. In this case, in order to maintain the given combustion time constant, it is necessary:

either to increase the pressure p_1 in the engine, in order to achieve the required degree of increase of powder-burning rate.

$$\frac{e}{u(p)} = \frac{e_1}{u(p_1)}, \tag{5.}$$

or to employ a different powder, exhibiting the required burning rate at the former pressure

$$\frac{e}{u(p)} = \frac{e_1}{u_1(p)}.$$

Thus the placement of the straight line along the δ axis is associated with the need to raise the operating pressure in the engine or to switch to a new, slower burning, propellant composition.

$$2)\ \left(\frac{1}{\delta}\frac{\varepsilon}{1+\varepsilon}\frac{1}{\xi}\right) = \frac{1}{\delta}\frac{\frac{\varkappa}{l}}{1+\frac{\varkappa}{l}\frac{e}{d_{vn}}}\frac{1}{}.$$

The magnitude of the coefficient is a function of e, κ, and l; since with a fixed ω, the values of e and l are mutually related, only two parameters can be arbitrarily changed; for example, κ and e. We can see from the formula that this coefficient increases with an increase in κ, in the limiting case tending to the magnitude determined by the following relationship:

$$\lim_{\varkappa\to\infty}\left(\frac{1}{\delta}\frac{\varepsilon}{1+\varepsilon}\frac{1}{\xi}\right) = \frac{1}{\delta}\frac{1}{\xi}\lim_{\varkappa\to\infty}\frac{\frac{\varkappa}{l}}{1+\frac{\varkappa}{l}} = \frac{1}{\delta}\frac{1}{\frac{e}{d_{vn}}}, \tag{5.41}$$

and increases with a drop in e_1, in which case

$$\lim_{\varepsilon\to 0}\left(\frac{1}{\delta}\frac{\varepsilon}{1+\varepsilon}\frac{1}{\xi}\right) = \frac{1}{\delta}\frac{\frac{\varkappa}{l}}{\frac{1}{d_{vn}}}\lim_{\varepsilon\to 0}\left(\frac{1}{1+\frac{\varkappa}{l}}\right) = \frac{1}{\delta}\frac{1}{\frac{e}{d_{vn}}}\varkappa. \tag{5.41'}$$

In actual practice, the coefficient is limited by even lower values, since in the case of κ being greater than some κ_{pr}, phenomena are observed in the engine which are characteristic of unstable powder-burning; because of the limits in the maximum burning rate for existing powder compositions, the quantity $\underline{e}$ cannot be lower than the following:

$$e_{min} = [u(p)]_{max}\tau.$$

With a drop in κ and an increase in $\underline{e}$, the coefficient tends to its minimum value, equal in both cases to zero:

$$\lim_{\varepsilon\to 0}\left(\frac{1}{\theta}\frac{\varepsilon}{1+\varepsilon}\frac{1}{\xi}\right)=\frac{1}{\theta}\frac{1}{\frac{e}{d_m}}\lim_{\varepsilon\to 0}\left(\frac{\frac{e\varkappa}{l}}{1+\frac{e\varkappa}{l}}\right)=0, \tag{5.42}$$

$$\lim_{e\to\infty}\left(\frac{1}{\theta}\frac{\varepsilon}{1+\varepsilon}\frac{1}{\xi}\right)=\frac{1}{\theta}\frac{\frac{\varkappa}{l}}{\frac{1}{d_m}}\lim_{e\to\infty}\left(\frac{1}{1+\frac{e\varkappa}{l}}\right)=0. \tag{5.42'}$$

Thus the turning of the straight line about point M (Fig. 5.45) can be achieved by a change in the parameter $\varkappa$ of the engine or by selecting a new calculation thickness for the cupola of the grain. In this case, an increase in κ and a decrease in $\underline{e}$ (the use of slow-burning powders and low operating pressures in the engine) will cause the straight line to turn in a counterclockwise direction.

Since $\underline{e}$ is included in both coefficients of the straight-line equation, if the straight line is placed along the δ axis, the straight line is additionally turned about M and with a single turn there is a slight shift of point M on the δ axis.

In conclusion, we would point out that the ordinates of the points of intersection, corresponding to Eq. (5.39), with the dense-packing curve, divide the plane into parts in which the curve either lies above the straight line or, conversely, the straight line lies above the curve. In the first region, for any number $\underline{n}$ grains corresponding

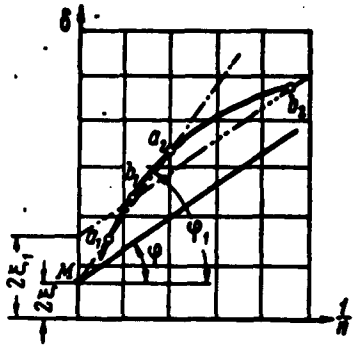

Fig. 5.45. Selection of optimum charge version in the absence of points of intersection between the curves (second case)

to the dimensionless diameter δ_{pl} can be packed densely into a diameter d_{vn}, and to place a charge ω, kg, into the combustion chamber, grains having a diameter $\delta<\delta_{pl}$ are required. Thus the charge can be placed in d_{vn}, but the packing will not be dense (Fig. 5.46). In areas where $\delta>\delta_{pl}$, the charge cannot be placed into the combustion chamber, since the grain diameter must be greater than the magnitude which corresponds to the maximum insertion of n circumferences in d_{vn}.

Let us assume that it has been possible to achieve an intersection of the curves which would determine the sought version of an optimum multigrain charge. Before finally deciding on this charge version, it is necessary, as a rule, to verify the κ for the grain channel of this charge, since a certain κ, average over the entire engine, has been introduced into the calculation. For this verification, we can use the following relationship:

$$\varkappa_{kan}=\frac{(S_{bok})_{kan}}{(F_{sv})_{kan}}=\frac{\pi dl}{\frac{\pi d^2}{4}}=\frac{4l}{d}, \qquad (5.43)$$

where $d = D - 4e$; κ_{kan} is the parameter of κ of the grain channel; $(S_{bok})_{kan}$ is the burning surface of the channel; $(F_{sv})_{kan}$ is the free cross section of the channel, in which case it is assumed

$$\varkappa_{nar}=(2\div3)\,\varkappa_{kan},$$

where κ_{nar} is the corresponding ratio of areas for the outer free cavity of the engine:

$$\varkappa_{зар} = \frac{(S_{сож})_{зар}}{(F_{св})_{зар}} = \frac{\pi D l n}{\frac{\pi d_{вн}^2}{4} - \frac{\pi}{4}(D^2 - d^2)n} = \frac{4Dln}{d_{вн}^2 - (D^2 - d^2)n}. \quad (5.44)$$

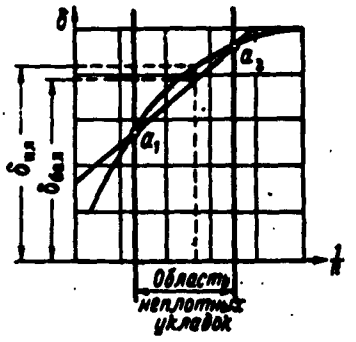

Fig. 5.46. Determination of range of values n and δ, corresponding to versions of nondense grain-packing into the combustion chamber. δ_{pl}) dimensionless diameter of grain providing for dense packing of charge in combustion chamber; δ_{bal}) dimensionless grain diameter providing form satisfaction of requirements with respect to parameters of interior ballistics; 1) region of nondense packing

§7. DESIGN OF IGNITION UNIT FOR BASIC PROPELLANT CHARGE

The basic charge of a rocket engine is ignited as a result of the combustion, in the combustion chamber, of an auxiliary charge consisting generally of black powder having definite grain dimensions. The black powders, in a special casing or cloth (calico) sack, are kept in the forward part of the combustion chamber, near the forward connection plate. For the transmission of the command pulse to igniter, the firing installations are equipped with special electrical fire control systems, a typical diagram of which is presented in Fig. 5.47. The electrical system closes on a contact device (pyrosparkplug) of the missile. The pyrosparkplug contains a special assembly referred to as the pyrocartridge which consists of a weighed portion of easily ignited powder mass into which a heating element has been inserted. (Fig. 5.48).

With the command "fire" a current appears in the circuit, and this current is transmitted through the combined contacts of the firing installation and missile to the pyrosparkplug. The heating element is actuated and the powder mass in the pyrocartridge burns up, producing a force from the flame which is transmitted to the igniter. As a result, the igniter receives the required command pulse. The products

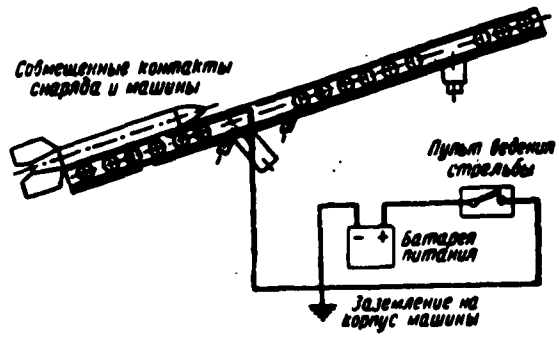

Fig. 5.47. Diagram of electrical system for firing of BM-13 weapon. 1) Combined contacts of missile and installation; 2) firing panels; 3) power supplies; 4) grounding of installation frame

of the combustion taking place in the igniter fill the combustion chamber, thus producing the initial increase in combustion-chamber pressure, and these products then stream out to the nozzle. The stream of products of combustion, flushing the powder grains of the basic charge, cause them to ignite.

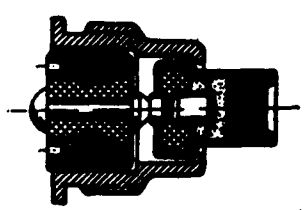

Fig. 5.48. Pyrocartridge (sparkplug) of M-13 rocket missile

The basic requirement imposed on an igniter is the necessity to provide for conditions within the combustion chamber, which will guarantee reliable ignition and entry into a regime of stable burning on the part of the basic charge of the engine, and primarily to increase the pressure in the combustion chamber to a point somewhat in excess of the pressure required for rated engine operation. Since the magnitude of the specific gas formation of the substance in the igniter is a physical constant, the pressure produced in the engine as the result of the burning up of the igniter can be entirely determined by the mass of consumed substance and the structural features of both charge and engine. In first approximation we

assume that the use of black powder as the igniter is necessary for reliable ignition of the basic charge, so that each liter of free combustion-chamber volume requires 1.5-2 g of the igniter, i.e.,

$$q_V = (1.5\text{-}2.0)v_{sv}\ g,$$

where q_V is the weighed portion of the ignition composition. In this case, the free volume can be

$$v_{св} \approx 1{,}15\left(\frac{\pi d_{вн}^2}{4} - n s_{торц}\right) l_ш$$

where 1.15 is employed to take into consideration the presence, in the engine, of the space behind the diaphragm as well as the free space at the forward connection plate; l_{sh} is the length of the grain charge; s_{torts} is the area of the butt-ends.

Thus to calculate the required weighed portion in the igniter, in first approximation, we can use the following formula:

$$q_в = (1{,}65 \div 2{,}2)\left(\frac{\pi d_{вн}^2}{4} - n s_{торц}\right) l_ш. \qquad (5.45)$$

Under actual conditions, the ignition process is a function not only of the magnitude of the initial free volume, but of the structural features of the charge and the engine. It is impossible to derive the theoretical formula for the determination of the required q_V, in terms of charge and parameters; therefore, the final weighed portion of igniter is selected on the basis of results obtained in experimental ignitions.

For the selection of the igniter for multigrain charges consisting of single-channel cylindrical grains, we can recommend the empirical relationship, obtained in the following form:

$$q_V = S_\Sigma[\text{dm}^2]\sigma_{kr}[\text{cm}^2]\ \text{g};$$

However, this formula makes no pretense at being universal, i.e., it does not cover all of the various engines employing multigrain charges.

FOOTNOTES

Manuscript Page No.	
201	Yu.Ya. Vayntraub Stekloplastiki i Vozmozhnost' ikh Primeneniya v Proizvodstve Vooruzheniya [Glass-filled Plastics and the Possibility of Their Utilization in the Production of Armaments] based on foreign materials], NTT [not identified in standard references], 1959
203	Yu.Ya. Vayntraub Stekloplastiki i Vozmozhnost' ikh Primeneniya y Proizvodstve Vooruzheniva
221	G.P. Sutton, Rocket Propulsion Elements 1957
240	J. Gates and S. Tinto, ASNE Reprint, N 59 T (March-April 1959)
250	EI VINITI AN SSSR, Seriya "Raketnaya Tekhnika" [not identified in standard references, Series "Rocket Engineering"] 1959, Vol. 6, No. RT 15
251	Journal of the Royal Aeronautical Society, 1959, 63, No. 580
256	R.N. Wimperss, Internal Ballistics of the Solid-Fuel Rockets, McGraw-Hill, New York 1950

Chapter 6

ELEMENTS OF THE EXTERIOR BALLISTICS OF AN UNGUIDED SOLID-PROPELLANT ROCKET MISSILE

§1. Flight Trajectory of Unguided Rocket Missile

Definitions. Coordinate Systems

Exterior ballistics study the laws governing the motion of missiles and rockets through the air as well as the methods of controlling these laws. The application of the fundamentals of exterior-ballistic theory to practice makes it possible to design a rocket missile which can satisfy the tactical-technical requirements in terms of firing range and accuracy.

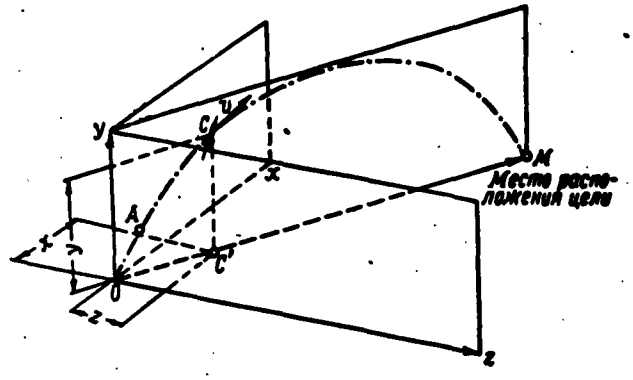

Fig. 6.1. Flight trajectory of unguided rocket in ground system of coordinates A) end of active phase; 1) position of target

In the general case, the flight trajectory of a rocket missile is a spatial curve having its origin at the point of missile launch. It is the practice to determine this curve in a so-called system of ground coordinates (Fig. 6.1).

The point that coincides with the point of rocket launch is generally taken as the origin of a ground system. The coordinate axes are positioned so that one of the axes, generally denoted Oy, is vertical. while the two remaining axes are arbitrarily oriented in the horizontal plane. If the target vector $\vec{OM}$ is drawn through the ground coordinate system, the plane defined by the Oy axis and the vector $\vec{OM}$ is referred to as the firing plane. The firing plane is a characteristic of the ground coordinate system.

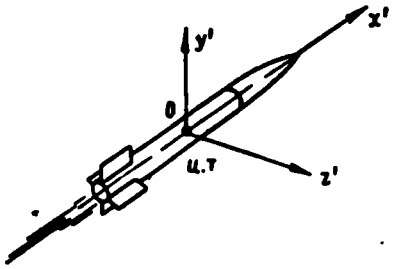

Fig. 6.2. Axes of a connected coordinate system

The flight trajectory of a rocket is completely determined if the mutual interrelationship of the ground coordinates $f(x, y, z) = 0$ is known; in this case, the nature of rocket motion along the trajectory will be a function of the law governing the time-variance of the rocket-position coordinates on the trajectory:

$$x=x(t),$$
$$y=y(t),$$
$$z=z(t).$$

The motion of a rocket along its trajectory represents only a transient phase of its total motion. The second part of this motion is the relative rotation of the rocket about a point of the rocket which lies on the trajectory line (the center of rocket gravity). This motion is generally referred to as relative and regarded as pertaining, in this case, to a flying rocket, with the introduction of an additional movable coordinate system associated with the shifting body. This is referred to as a connected coordinate system. The origin of the connected coordinate system coincides with the center of rocket gravity; the axes of the system are so chosen as to cause the Ox' axis

to coincide with the longitudinal axis of the rocket, and the Oy' axis is chosen so as to maintain the vertical position (in the absence of roll) of the coordinate plane x'Oy'. With this choice of axes for the connected coordinate system of a rocket situated, without roll, in the firing plane, the plane x'Oy' coincides with the firing plane. The axes of the connected coordinates are oriented with respect to the rocket, and this is presented in Fig. 6.2.

Through the introduction of the connected system of coordinates, the relative rotation of a rocket can be studied as a change in the relative position of the axes of both the ground and connected coordinate systems. In this case, the following coordinate angles are introduced: the angle of pitch θ, the angle of yaw ψ, and the angle of roll φ.

The pitch angle is the angle between the Ox' axis of the connected coordinate system and the plane xOz of the ground system. For the sake of clarity, the angle of pitch can be presented as the angle between the axis of the rocket and the horizontal plane. The angle of yaw is the angle between the axis of the rocket and the firing plane. This angle indicates the extent to which the rocket deviates from its position in the firing plane. And, finally, the angle of roll is the angle between the x'Oy' plane of the connected coordinate system and the firing plane. This angle characterizes the turning of the rocket about its longitudinal axis.

The angles θ, ψ, and φ are presented in Fig. 6.3. For simplicity, the diagrams show special cases which are best demonstrated graphically.

Thus to determine the position of a rocket in space at an arbitrary instant of time t, we must know the law governing the shift of the center of gravity for a rocket along the trajectory relative to

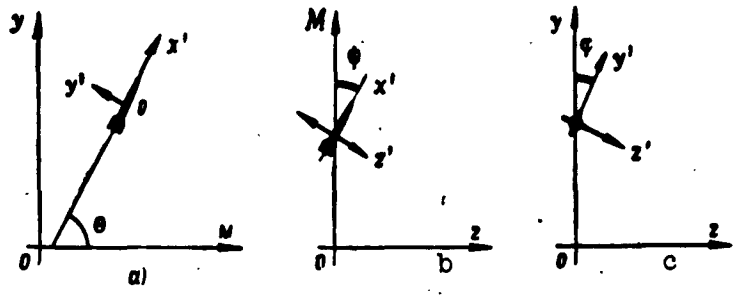

Fig. 6.3. Determination of angles of θ, ψ, and φ of the rocket. θ) angle of pitch for rocket situated in firing plane; ψ) angle of yaw for a rocket flying at an angle $\theta = 0$; φ) angle of roll for a rocket flying with $\theta = 0$, $\varphi = 0$

the ground system of coordinates:

$$\left.\begin{aligned} x &= x(t), \\ y &= y(t), \\ z &= z(t) \end{aligned}\right\} \qquad (6.1)$$

and the nature of the relative rotation of the rocket about the center of gravity, i.e., the position of the axes of the connected coordinate system relative to the coordinate planes of the ground system.

$$\left.\begin{aligned} \vartheta &= \vartheta(t), \\ \psi &= \psi(t), \\ \varphi &= \varphi(t). \end{aligned}\right\} \qquad (6.1')$$

Missile flight trajectories can, with a great degree of accuracy, be regarded as plane curves situated entirely in the firing plane, with the exception perhaps of individual phases in which the rocket shifts from its position in the firing plane as a result of external and internal disturbing forces. The trajectories of short-range rockets - field artillery rocket missiles - are particularly close to plane curves

If the flight trajectory is regarded as a plane curve, it is expedient to orient the ground coordinate system so that the xOy plane coincides with the firing plane. In this case, the trajectory can be examined in the xOy plane and the position of the rocket on the tra-

jectory can be determined by means of the following coordinates:

$$\left.\begin{aligned} x &= x(t), \\ y &= y(t), \\ \vartheta &= \vartheta(t), \\ \psi &= \psi(t), \\ \varphi &= \varphi(t). \end{aligned}\right\} \tag{6.2}$$

In addition to the ground and connected system of coordinates, we must use yet another coordinate system in the study of rocket motion; this new system takes into consideration the direction of the

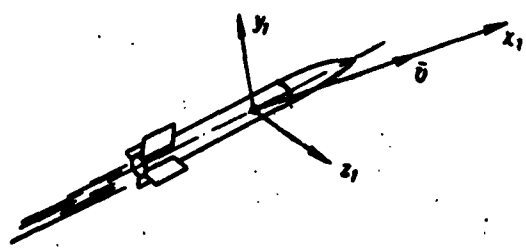

Fig. 6.4. The axes of a flow-system of coordinates

motion of the approaching stream of air with respect to the rocket. This coordinate system is referred to as a flow coordinate system. The axes of the flow coordinate system are selected so that the Ox_1 axis of the system coincides with the vector representing the absolute velocity of rocket motion (i.e., so that it coincides with the direction of the velocity of the approaching air stream and so that it is directed against this stream); the Oy_1 axis is selected so that in the case of $\psi = 0$ the x_1Oy_1 plane coincides with the firing plane; the third axis, the Oz_1 axis, is chosen to be perpendicular to the first two axes. The flow system of coordinates is examined in greater detail below. The axes of the flow system of coordinates are presented in Fig. 6.4.

Elements of the Trajectory in the Case of Unguided Flight

The basic external feature of a rocket flight trajectory is the presence on the trajectory of two successive phases - an active and a passive phase.

The active phase of the trajectory is the one over which the rocket flies with an operating engine. It is during this phase that the rocket is accelerated to the so-called velocity at the end of the active flight phase, and it is this velocity that is generally the maximum velocity for the entire trajectory.

In the passive phase of the trajectory (the free-flight phase) the engine is no longer in operation and the flight continues as a result of inertia due to the reserve of kinetic energy acquired by the rocket during the active phase of the flight. On the ascending branch of the passive trajectory phase the velocity of missile motion gradually diminishes to some minimum value which corresponds to the instant at which the missile attains the peak of the trajectory, and the velocity of missile motion then increases on the descending branch.

The firing of a solid-propellant rocket missile is generally carried out by means of a special launching installation that has a guide-rail device of a given design. The motion of the missile along the guide-rails, to the instant at which it leaves the rails, is sometimes isolated in an independent, so-called initial, trajectory phase. To attain the required flight range, the launching installation must be set up at a certain angle to the horizon. This angle is referred to as the firing angle.

A typical flight trajectory for an unguided rocket missile is presented (for the case of motion in the xOy plane which coincides with the firing plane) in Fig. 6.5. It should be borne in mind that if we refer to the $\vec{OM}$ vector as the target vector, drawn from the point

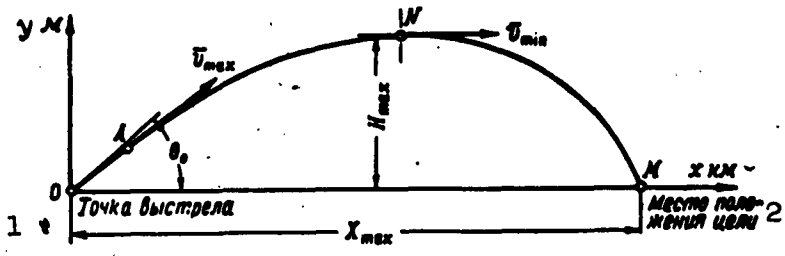

Fig. 6.5

Fig. 6.5. Diagram of flight trajectory for unguided rocket missile. OA) active phase of trajectory; AM) passive phase of trajectory; AN) ascending branch of passive phase; NM) descending branch of passive phase; X_{max}) maximum flight range; H_{max}) maximum height of trajectory; $\bar{v}_{max}$) missile velocity at end of active phase of trajectory; ζ_0) angle of firing installation (firing angle); $\bar{v}_{min}$) minimum rocket-missile velocities; 1) Firing point; 2) position of target.

of missile launch to the point which corresponds to the position of the target against which the firing is being carried out, then in the general case this vector might not coincide with the direction of the Ox axis (even in the case of a plane trajectory).

Fig. 6.6 shows how total missile velocity changes with its motion along the trajectory. The curve presents a qualitative illustration of the nature of velocity change.

The relative extent of the active trajectory phase, in comparison with the remaining portion of the trajectory, is not too great. For example, in the case of solid-propellant rockets having a range of several tens of kilometers, it may amount to several hundreds of meters, i.e., it has a relative extent of the order 10%. Therefore, in tentative ballistic calculations, the active phase of the trajectory need not be taken into consideration, and assuming that the missile requires its $\bar{v}_{max}$ virtually at the point of launching, we can examine a simplified trajectory diagram. (Fig. 6.7).

As an example of solid-propellant rocket missiles whose unguided flight trajectories can be schematically presented by the curves shown in Figs. 6.5 or 6.7, we can cite the well-known rockets of the USA Army: "Corporal" (exhibiting a range of 80 km); "Honest John" (exhibiting a range of the order of 35 km); "Lacrosse" (exhibiting a range of the order of 30 km); "Sergeant" (exhibiting a range of the order of 80 km), and many others.

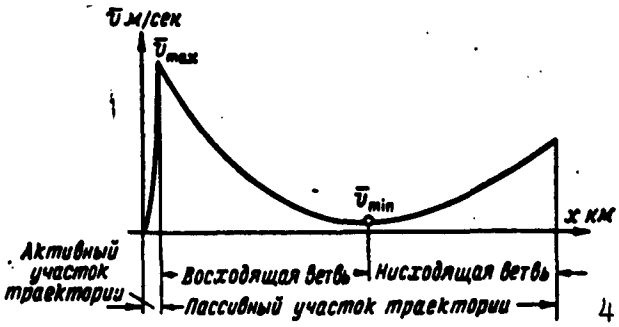

Fig. 6.6. Nature of change in velocity during motion of rocket along trajectory 1) active phase of trajectory; 2) ascending branch; 3) descending branch 4) passive phase of trajectory

Solid-propellant missiles can be made as guided rockets as well. As an example of such a rocket, we can cite the following missiles: "Falcon" (USA an "air-to-air" system); the "Sidewinder" (USA, an "air-to-air" system); the "Dart" (USA, antitank); the "Cobra" (Switzerland, antitank); the "Firestreak" (Great Britain, an "air-to-air" system); "SS-11" (France, antitank).

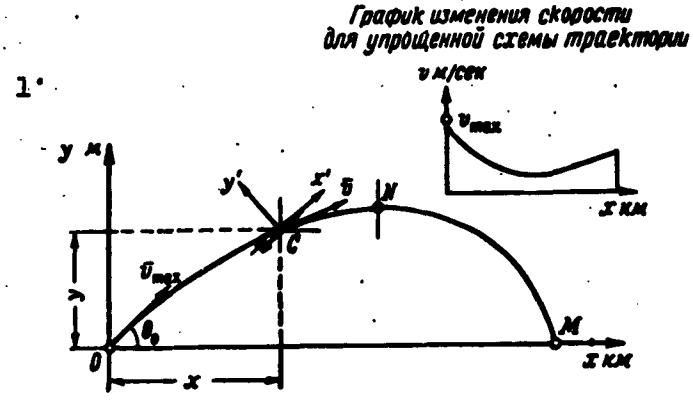

Fig. 6.7. Simplified diagram of a flight trajectory for unguided rocket missile 1) curve showing change in velocity for simplified trajectory diagram

The nature and form of the flight trajectories for these missiles are functions of many factors and primarily of the mutual position be-

tween the target and the launching site of the rocket at the instant of firing, as well as of the presence and nature of the defensive manuvers carried out by the target; in addition, they are functions of the tactical-technical data pertaining to the equipment and the entire guidance system or homing system employed by the missile, etc. The present work does not consider those problems associated with the theory of guided flight.*

§2. FORCES AND MOMENTS ACTING ON MISSILE DURING FLIGHT

Diagram of Forces and Moments

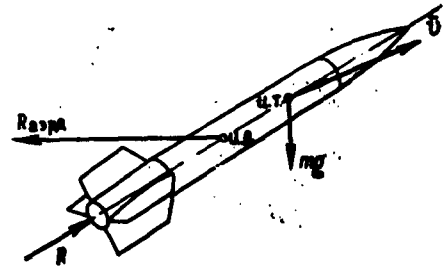

Fig. 6.8. Total diagram of forces acting on solid-propellant missile in flight

Any shift of a body in space is the result of the action of external forces and moments on that body.

Examining the flight of a rocket missile, we can see easily that the nature of rocket motion in space is determined by the action of three forces on that body: R_t is the force of rocket-engine thrust; R_{aerd} is the total force produced by the interaction of the rocket and the approaching air stream which decelerates the rocket motion and deflects the flight of the rocket from an ideal curve; mg is the mass gravitational force (weight of the rocket). A diagram of these forces can be seen in Fig. 6.8. In the case of a guided rocket, to the forces shown in Fig. 6.8, we must add the guidance forces applied to the control elements of rocket flight.

In the discussion of the problems relating to the interior ballistics of a solid-propellant rocket engine it was stated that the thrust of the engine is produced as a result of the action of the products of combustion of the solid-propellant working charge being discharged

through the nozzle of the engine. The direction of thrust coincides with the axis of the nozzle, i.e., with coaxial positioning of the engine in the missile, the direction of thrust coincides with the longitudinal axis of the missile. In calculating the thrust, we should employ Relationship (4.52) or the simplified Relationship (4.53).

The mass gravitational force (the weight of the rocket), as is generally the case, is the resultant of the gravitational forces acting on individual component parts of the solid-propellant missile. The point at which these forces are applied is referred to as the center of gravity. In terms of direction, the gravitational force coincides with the direction of the vertical at the corresponding point on the trajectory.

In the case of missile flight through the air, the approaching stream acts on the airframe of the rocket. The result of this action can be shown in the form of a rocket-surface distribution of excess normal pressure and the tangential forces, with the resultant of the

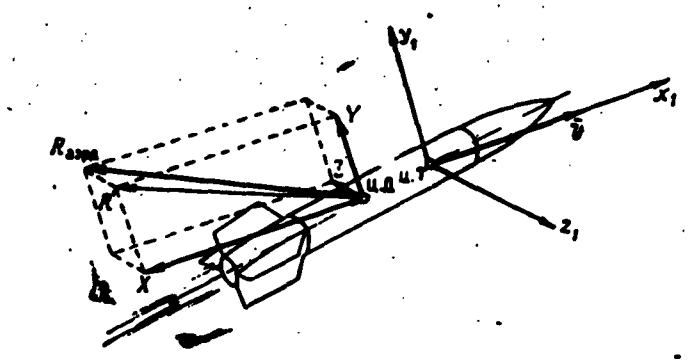

Fig. 6.9. Components of the resultant of aerodynamic force in the flow system of coordinates. X) force of frontal resistance (drag); Y) lift

total system referred to as the total aerodynamic resistance force. The point at which the total aerodynamic force is applied is referred to as the center of missile pressure. The position of the pressure

center is a function of the aerodynamic-force component distribution diagram. It is generally assumed that the center of pressure is situated on the rocket's axis at the point being calculated in each specific example. The vector of the total aerodynamic resistance force, in the general case, is arbitrarily oriented in space in a direction opposite to the direction of missile motion. This vector is conventionally associated with the flow system of coordinates and presented in the form of three components that are oriented along the axis of the system. The corresponding components are referred to as the force of resistance, lift, and lateral forces (Fig. 6.9).

Since it was assumed that in the tentative calculations the trajectory could be regarded as a plane curve, naturally the force Z can be neglected and the velocity vector $\vec{v}$ as coinciding with the firing plane. In this case, the true aerodynamic force $R_{aer.}$ is replaced by the force R' which is sufficiently close to it in magnitude, and it becomes therefore possible to simplify substantially the system of aerodynamic forces, reducing it to the resistance and lift forces lying above the plane that is coincident with the firing plane (Fig. 6.10). These components are generally examined in the investigation of aerodynamic forces acting on the rocket in flight.

We can see from Fig. 6.8 that there are two points of application of external forces on the rocket - the center of gravity and the center of pressure. It is convenient to refer the forces to some single point, such as, for example, the center of gravity at which the origins of both the flow and connected coordinate systems coincide.

For this purpose, two mutually balancing forces are applied at the reference point (in our case, the center of missile gravity); these two mutually balancing forces are coincident in terms of magnitude and line of action with the force being referred. The equili-

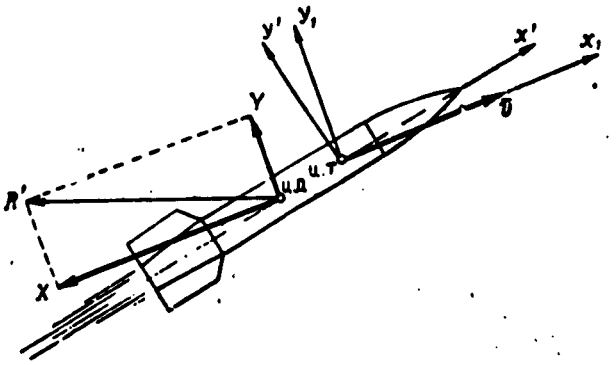

Fig. 6.10. Simplified diagram of components of total aerodynamic resistance force

brium of the body or the nature of its motion, given this application of forces, is not disturbed. Let us now examine all three forces, and we will see easily that they can be presented in the form of the sum of the force applied to the reference point and the moment of the couple of two forces about this point. The magnitude and direction of the force, upon its reference, are kept constant; the additional moment is determined by the magnitude of the force and the distance from the point of initial application of force to the reference point. Figure 6.11 is an example of the reference (reduction) of aerodynamic lift to the center of missile gravity for the particular case of the position of the vector of this force.

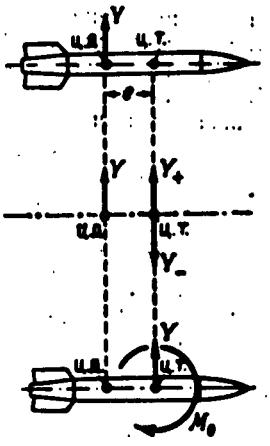

Fig. 6.11. Diagram referring force to center of missile gravity. Y_+ and Y_- are the conventional vectors referring Y to the center of missile gravity

Figure 6.12 shows the total calculation diagram of forces and moments referred to the center of missile gravity. This diagram of forces and moments for the simplified version of a plane trajectory, coincident with the firing plane, is presented in Fig. 6.13. A comparison of Figs. 6.12 and 6.13 shows that in the latter

case the lateral component of the aerodynamic force disappears, while all the remaining forces are referred to a single plane. With respect to the moments, the situation is the following; in the general case, even in a plane system of forces, it is expedient to examine all three moments M_θ, M_ψ, and M_φ, in which case the determining moment of finned missiles is M_θ, whereas M_ψ, and M_φ reflect only the possibility of the rocket executing oscillatory motions in the corresponding planes about the center of missile gravity, with limited possible angular displacements. In the case of turbojet missiles, rotating during flight, M_θ and M_φ are determining.

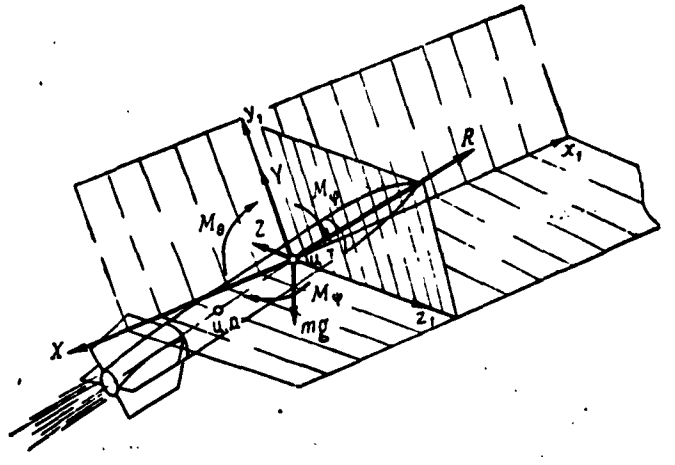

Fig. 6.12. Calculation diagram of forces and moments referred to the center of missile gravity

Since all three groups of forces acting on the rocket missile during flight were determined in various systems of coordinates, it is necessary to link these systems with one another. For the case of a plane trajectory, the indicated relationship is established if the coordinates of the centers of the movable systems (the connected and flow system) are assumed with respect to the ground coordinate system and the angles between positive directions of the coordinate axes.

The angle between the longitudinal axis of the rocket, coinci-

dent with the Ox' axis of the connected coordinate system and the Ox axis of the ground system is defined as the angle θ of rocket pitch.

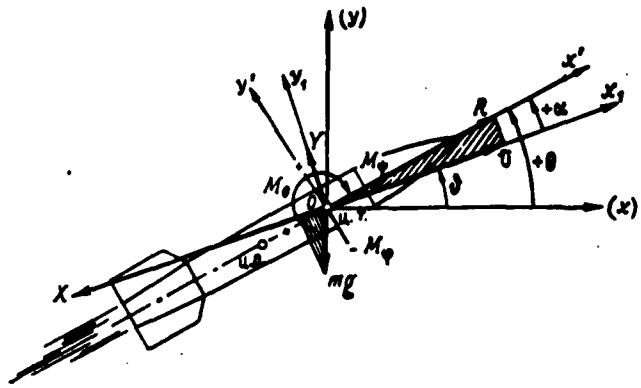

Fig. 6.13. Calculation diagram of referred forces and moments for the case of flight in the firing plane

In addition to this angle, we generally examine the angle between the Ox' and Ox_1 axes of the connected and flow coordinate systems, respectively. This angle is referred to as the angle of missile attack which is denoted by α.

The third angle - between the Ox_1 of the flow coordinate system and the Ox axis of the ground system - is determined in terms of the first two as follows: $\vartheta = \theta - \alpha$. The angle ϑ characterizes the direction of the tangent to the trajectory at the given point of flight, since the vector $\vec{v}$ of total velocity is always tangential to the trajectory:

$$\tan\vartheta = \frac{dy}{dx}\Big|_{x_k, y_k},$$

where x_k and y_k are instantaneous coordinates of the position of the center of gravity on the trajectory.

Now it is easy to separate those active forces from the entire system, which cause the rocket to move forward, as well as those forces which decelerate the motion of the rocket. For this it is enough to project all of the forces onto the Ox_1 axis which determines the direction of motion.

As a result of this projection it turns out that the only moving force is the projection of the thrust of the rocket engine.

$$F_{дв}=R_т \cos\alpha,$$

whereas frontal resistance X and the rocket-weight component represent forces offering resistance to this motion:

$$F_{сопр}=X+mg\sin(\vartheta-\alpha).$$

The second component of the force of gravity is offset by lift Y. For

i.e., when

$$F_{дв}>F_{сопр},$$

$$R_т>\frac{X+mg\sin(\vartheta-\alpha)}{\cos\alpha},$$

the resultant of these two forces

$$\Delta F_{дв}=F_{дв}-F_{сопр}$$

is directed so as to coincide with the motion of the rocket. Under the action of ΔF_{dv} the rocket accelerates, acquiring ever increasing velocity.

For the passive phase of the trajectory $R_t = 0$ is the resultant of the forces F_{dv} and F_{sopr} and is directed against the motion of the rocket thus causing the rocket to be decelerated.

Strictly speaking, the following equations

$$F_{дв}=R_т\cos\alpha \qquad F_{дв}=0,$$
$$F_{сопр}=X+mg\sin(\vartheta-\alpha)$$

are valid only for the ascending branch of the trajectory.

In motion over the descending branch of the trajectory, according to Fig. 6.14

$$F_{дв}=mg\sin(-\vartheta-\alpha),$$
$$F_{сопр}=X,$$

i.e., even in the absence of engine thrust there is a component directed to coincide with the direction of rocket motion. The pre-

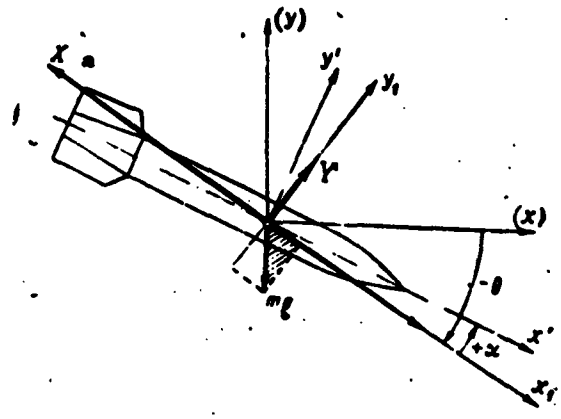

Fig. 6.14. Relationship of forces on the descending branch of the trajectory

sence of this force explains the nature of the change in missile velocity on the descending branch of the trajectory (Fig. 6.6).

As a result we find that the following basic forces and moments act on a rocket in flight: R_t, the thrust of the rocket engine; mg, the force of gravity, equal to the weight of the missile; X and Y, the components of the aerodynamic resistance; M_θ, the pitch moment; M_φ, the roll moment; M_ψ, the yaw moment, and for the passive phase of the trajectory $R_t = 0$.

Diagrams of the active forces on the ascending and descending branches of the trajectory are presented in Figs. 6.13 and 6.14. These diagrams can be used if it is assumed that the rocket moves along a trajectory lying in the firing plane.

The Force of Gravity. Calculation of Weight and Position of Center of Missile Gravity

In the case missile flight within the limits of the terrestrial gravitational field, among other forces, the force of terrestrial gravitation, referred to as the force of gravity, acts on the missile. The force of gravity P is proportional to the mass of the body. The

proportionality factor is referred to as the acceleration of the force of gravity:

$$P = mg$$

$g = 9.81$ m/sec^2 (at the surface of the earth)

The center of the gravitational forces acting on each individual part of this body is called the center of gravity for a solid (for example, a rocket missile).

The physical representation of the force of gravity is the weight of the body. Therefore, the point of application of the resultants of the system of vectors representing the weight of individual points in the system is another way of describing the center of gravity. Given this definition for the center of gravity, the action of the force of gravity on a system of material points or on a solid can be reduced to the total weight of the system of points or the given solid under consideration, said force applied at the center of gravity of this body.

As a result, in order to take into consideration the action of the force of gravity on a solid-propellant rocket missile moving in accordance with definite laws on its trajectory, it is necessary to find the weight of the missile and the point of application of this weight - the center of missile gravity.

The weight of a uniform solid is generally held to be proportional to the volume occupied by this body:

$$P = mg = \rho g V = \gamma V, \qquad (6.3)$$

where ρ is the density of the substance of the given body; γ is the specific weight of the body; V is the volume of the body.

On the whole, a missile cannot be regarded as a continuous uniform solid body; however, this assumption is completely valid for individual component parts of the missile. Consequently, in order to c-

calculate the weight of a missile, it is necessary to sum the weights of all component parts employed in the final assembly, in which case the weight of the individual component parts can be defined in terms of their volume and the specific weight of the material employed.

In the assembly of a solid-propellant reaction-thrust (rocket) missile we encounter component parts for which it is not difficult to calculate volume (for example, the cylindrical frame of the combustion chamber), in addition to component parts of complex configuration which introduce difficulties into the required calculations. In the latter case, it is accepted practice to separate a complex component part, through arbitrary sectioning, into a series of simpler shapes (cylinders, cones, etc.) and to calculate the volume of the component part as the total volume of its individual parts.

For example, given the problem of calculating the weight of the component parts shown in Fig. 6.15, it would seem at first glance that it is quite difficult to calculate the volume of such component parts; however, it is enough to divide the part arbitrarily into three sections I-I, II-II, and III-III, in order to separate the component part into five elements whose volumes can easily be calculated.

As a rule, complex component parts employed in the assembly of a solid-propellant rocket missile can be split into such elementary figures as a cylinder, a truncated cone, as well as certain combinations of these figures (Fig. 6.16), i.e., for the calculation of the volume of any component part, it is enough to know the following formula:

$$v_{цил}=\frac{\pi}{4}d^2l,$$

where d is the diameter of the cylinder base; l is the length of the cylinder generatrix,

$$v_{ус.кон}=\frac{\pi}{3}h(R^2+Rr+r^2),$$

where R and r are radii of the greater and smaller bases of the truncated cone; h is the height of the truncated cone.

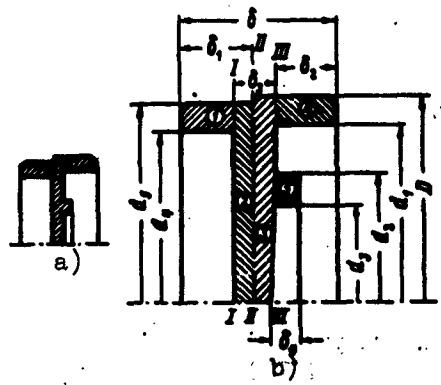

Fig. 6.15. For the calculation of the weight of the "connection plate" component part; a) sketch of component parts; b) calculation diagram I-I, II-II, and III-III) cross-sectional planes; D and d_1) diameters; δ_1) linear dimensions of the figure.

In fact, the volume of the connection plate (for generality, we will assume it to be some k-th component part of the assembly) is defined as the sum

$$V_k=\sum_{i=1}^{n} v_i, \qquad V_k=v_1+v_2+v_3+v_4+v_5 \tag{6.4}$$

(1, 2, 3, 4, 5 are the numbers of the elementary figures), where

$$v_1\approx\frac{\pi}{4}(d_5^2-d_4^2)(\delta-\delta_2-\delta_3);$$

$$v_2=\frac{\pi}{4}d_5^2(\delta_3-\delta+\delta_1+\delta_2);$$

$$v_3=\frac{\pi}{4}D^2(\delta-\delta_1-\delta_2);$$

$$v_1=\frac{\pi}{4}(D^2-d_1^2)\delta_1;$$

$$v_2=\frac{\pi}{4}(d_2^2-d_3^2)\delta_2;$$

$$V_k=\sum_{i=1}^{n} v_i.$$

The dimensions D, d_1, d_2, .., δ, δ_1, δ_2,... are shown in the drawing of the component part.

After the determination of the volume of k-th component part, the weight p_k of this component part is defined as

$$p_k=V_k\gamma, \tag{6.5}$$

$\gamma \approx 7.8$ g/cm^2 for steel component parts; $\gamma \approx 16$ g/cm^3 for the arming of the warhead (when armed with explosive material), as well as for individual elements of the solid-propellant charge for the engine.

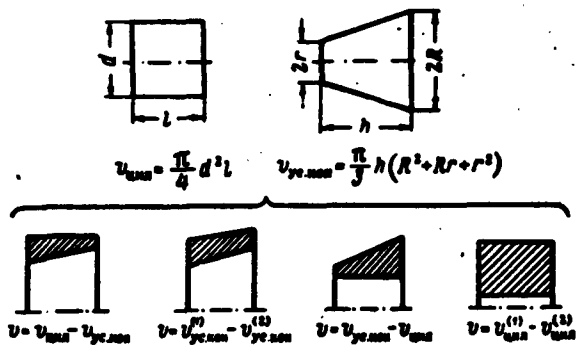

Fig. 6.16. Characterisitc elementary figures encountered in the calculation of the volume for various components.

Knowing the weight of the individual component parts, we can find the total weight of the missile by determining the sum

$$P_{ш}=\sum_{k=1}^{n} p_k, \tag{6.6}$$

where p_1 is the weight of the fuse; p_2 is the weight of the auxiliary detonator;

.....

.....

p_n is the weight of the hermetic-sealing end cap of the nozzle.

It has been demonstrated that it is important from the standpoint of exterior ballistics to know not only the magnitude of the active forces, but the point of their application as well. It is for this reason that the next problem is one which involves the determination of the coordinates of the center of missile gravity.

We will refer to the product of the mass and its distance from the plane as the static moment of the mass m concentrated at point A relative to some arbitrary plane N. With respect to the static moments of some material system of points the following theorem is valid: if the entire mass of the material system were concentrated at its center of gravity, the static moment of this mass with respect to some plane is equal to the sum of the static moments with respect to this same plane for the mass of all points in the system.

If we apply this theorem to the coordinate planes, we will obtain a system of equations which determine the coordinates of the system's center of gravity.

$$\left.\begin{aligned} m_{\text{с}} x_{\text{с.т}} &= \sum_{i=1}^{n} m_i x_i, \\ m_{\text{с}} y_{\text{с.т}} &= \sum_{i=1}^{n} m_i y_i, \\ m_{\text{с}} z_{\text{с.т}} &= \sum_{i=1}^{n} m_i z_i, \end{aligned}\right\} \tag{6.7}$$

whence

$$\left.\begin{aligned} x_{\text{с.т}} &= \frac{\sum_{i=1}^{n} m_i x_i}{m_{\text{с}}}, \\ y_{\text{с.т}} &= \frac{\sum_{i=1}^{n} m_i y_i}{m_{\text{с}}}, \end{aligned}\right\} \tag{6.8}$$

$$z_{ts.t} = \frac{\sum_{i=1}^{n} m_i z_i}{m_s}. \quad \Big| \qquad (6.8)$$

where $x_{ts.t}$, $y_{ts.t}$, and $z_{ts.t}$ are the coordinates of the system's center of gravity;

$$m_s = \sum_{i=1}^{n} m_i$$

is the total mass of all the points in the system; m_i, x_i, y_i, and z_i are, respectively, the mass and the coordinates of each material point in the system.

In calculating the coordinates of the center of gravity, it is useful to employ the following properties of the center of gravity:

1) if the system has a center of symmetry, the center of gravity coincides with the center of symmetry;

2) if the system has a plane of symmetry, the center of gravity lies in this plane;

3) for a system having an axis of symmetry, the center of gravity lies on this axis of symmetry

Since the longitudinal axis is, as a rule, the axis of symmetry for a solid-propellant rocket missile, the center of missile gravity must be sought on this axis. Having selected the coordinate system so that one of its axes coincides with the longitudinal axis of the missile, we will find that in order to find the center of missile gravity it is enough to determine only a single coordinate:

$$x_{ts.t} = \frac{\sum_{i=1}^{n} m_i x_i}{m_s}$$

or in terms of the weight of the component parts:

$$x_{ts.t} = \frac{\sum_{i=1}^{n} p_i x_i}{P_{ts}}, \qquad (6.9)$$

where p_i is the weight of the i-th component part; x_i is the coordinate of the center of gravity of the i-th component part;

$$P_{ra} = \sum_{i=1}^{n} p_i$$

is the weight of the missile.

We can see from the last formula that in order to determine the position of the center of missile gravity it is absolutely necessary to know not only the weight of the individual component parts but the positions of their centers of gravity.

The calculation of the center of missile gravity in terms of weight and the coordinates of the centers of gravity of individual component parts employed in the missile is possible on the basis of the so-called distribution properties of the centers of gravity.

This property indicates that if a system of material points having a total mass m_Σ is separated into parts having masses m', m",..., the center of gravity of the initial system remains the center of gravity of the total aggregate of m', m",..., in which case

$$m_\Sigma x_{\Sigma.T} = m' x'_{\Sigma.T} + m'' x''_{\Sigma.T} + \ldots$$

where $x'_{ts.t}$ and $x''_{ts.t}$ are the coordinates of the centers of gravity for the individual parts of the system.

Since the weight of an individual component part is generally calculated in terms of the weights of the elementary figures making up this component part, the coordinate of the center of gravity for the component part is calculated through the application of the theorem on the static moments, said theorem applied to the elementary figures (Fig. 6.17). In this case, the coordinate of the center of gra-ityyfor each elementary figure is calculated on the basis of a drawing of the component part, taking into consideration the fact that the position of the center of gravity for each individual element is

known (Fig. 6.18).

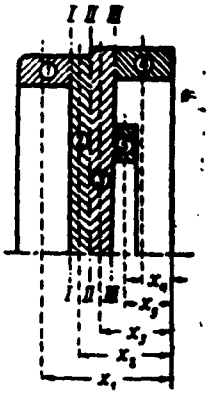

Fig. 6.17. Determination of position of center of gravity for a complex figure. 1-5) elements of figure; x_i) coordinate of the center of gravity of the i-th component of the figure.

Having determined the weight of the individual component parts and the positions of their centers of gravity for each individual unit in the assembly of a combat rocket, the position of the unit's center of gravity is calculated. However, if we know the coordinates of the centers of gravity for individual units in the assembly, it is not difficult to calculate the coordinate of the center of gravity for the entire missile.

The diagram for the calculation of the center of gravity for a solid-propellant rocket missile and its individual units (warhead) is presented in Fig. 6.19.

The final calculation formula for the determination of the coordinates of the center of missile gravity takes the following form:

$$x_{u.r}^{c.u} = \frac{P_{b.u} x_{u.r}^{b.u} + P_{p.u} x_{u.r}^{p.u}}{P_{c.u}},$$

in which case, for example, for the warhead

$$x_{u.r}^{b.u} = \frac{p_1 x_1 + p_2 x_2 + p_3 x_3 + p_4 x_4}{P_{b.u}},$$

where p_1 is the weight of the fuse; p_2 is the weight of the auxiliary detonator; p_3 is the weight of the warhead casing; p_4 is the weight of the explosive charge.

$$P_{b.u} = p_1 + p_2 + p_3 + p_4.$$

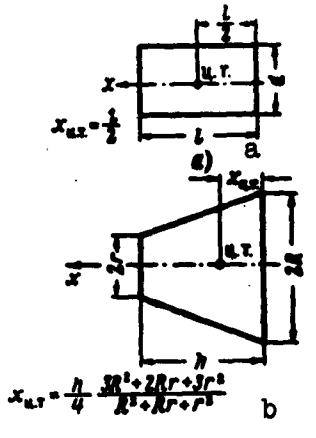

Fig. 6.18. Coordinates of centers of gravity for elementary figures a) cylinder b) truncated cone

We should turn our attention to the fact that when the theorem on the static moments is employed, we must have the coordinates of the centers of gravity

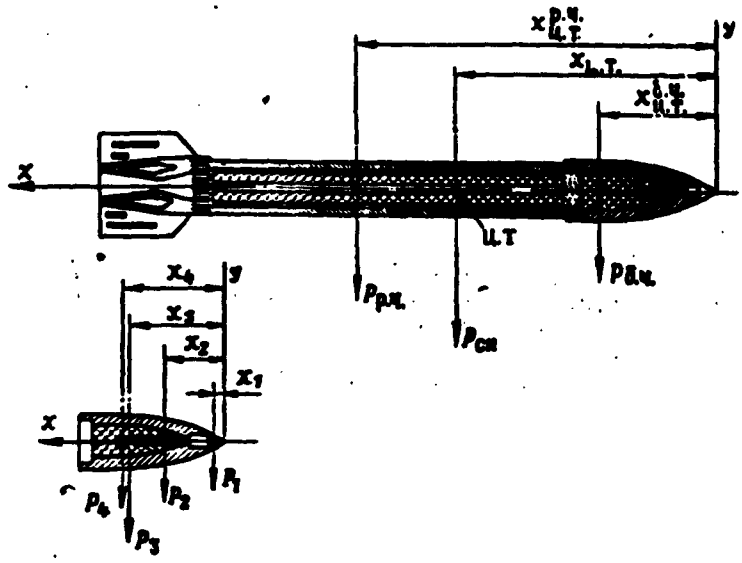

Fig. 6.19. Utililzation of theorem on statistical moments for the calculation of the position of the center of gravity for a solid-propellant rocket missile $P_{b.ch}$, $P_{r.ch}$) are the weights of the warhead and rocket parts of the missile; $x^{r.ch}_{ts.t}$, $x^{b.ch}_{ts.t}$) are the coordinates of the centers of gravity for the rocket and warhead parts of the missile

for the individual elements with respect to some common, although arbitrarily selected, coordinate origin. However, preliminary calculations yield the coordinate for the center of gravity for each individual element with respect to one of the characteristic points or boundaries of this element. Therefore, before employing the theorem, it is necessary to recalculate the coordinates of the individual elements in the given assembly to correspond with the drawing and the selected system of coordinates.

Aerodynamic Forces and Moments. Calculation of Aerodynamic Forces and Moments and the Determination of the Position of the Center of Pressure

Aerodynamic forces are produced as a result of the interaction between the missile and the approaching stream of air. This interaction can be reduced to the appearance at the surface of the missile of a continuously distributed normal pressure and tangential stresses (Fig. 6.20) and, in addition, to the development of a zone of reduced pressure (Fig. 6.21) in the region of the nozzle outlet (primarily when the missile engine is not in operation; in the case of an operating rocket engine, the stream of the products of combustion eliminates this zone of reduced pressure behind the nozzle outlet).

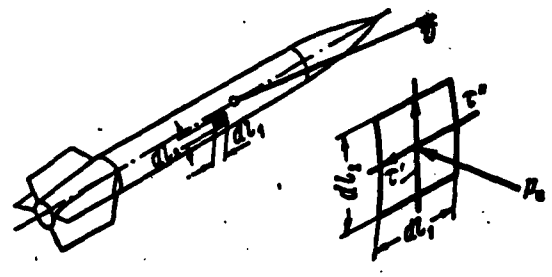

Fig. 6.20. Diagram of force components in interaction of missile with approaching stream, said forces acting on the elementary area of the surface. dl_1 and dl_2) dimensions of the elementary area; τ', τ'', and p_n) components of tangential and normal forces acting on area

The tangential stresses and the rarefaction which occurs at the rear produce forces which decelerate the motion of the rocket. These are, respectively, referred to as the force of frictional resistance and the force of tail drag. The resultant of the normal pressure distributed over the frame of the rocket is oriented with respect to the missile and the approaching stream rather

Fig. 6.21. Development of zone of reduced pressure behind nozzle outlet of rocket flying with inoperative engine

arbitrarily; however, having associated the resultant with the flow system of coordinates, it is possible to derive a component of resistance that is directed against the direction of motion velocity as well as a component that is normal to it. The first is referred to as the force of resistance (drag) due to normal pressure, and the second is referred to as lift.

Thus the total force produced by the aerodynamic interaction between the missile and the approaching stream of air can be presented in the form of two components; the force X of frontal resistance (drag) and lift Y. In this case, X appears as a result of friction, tail drag, and the components of normal pressure, directed along the Ox_1 axis of the flow coordinate system

$$X=X_f+X_a+X_p, \tag{6.10}$$

and the Y force appears as a result of the normal-pressure components directed along the Oy_1 axis of the flow system.

Strictly speaking, the notation

$$X=X_f+X_a+X_p.$$

is valid only when the effect of the forces of friction, tail drag, and pressure are independent, whereas in actual fact these components are interdependent.

However, since the hypothesis of the independence of the resistance-force components is quite convenient in engineering practice and since its utilization does not result in any substancial calculation errors, it is the accepted practice to use the above equation and to calculate the total aerodynamic force of resistance in terms of the individual components of this force.

The phenomenon of the flow of air past a body and the effect of the interaction of forces observed in this case, are extremely complex.

The nature of the above-mentioned interaction is determined by a great number of various factors which are difficult and sometimes even impossible to take into account. It is for this reason that the forces and moments acting on the missile in flight are determined most exactly by experimental procedures. The experiments are carried out in special installations - wind tunnels - where the missile, held fast by special means, is set into an air stream; the necessary measurements are carried out at this time, and when evaluated these measurements make it possible to calculate the components of the aerodynamic forces and moments.

It has been established that the basic parameters which determine the absolute magnitude of the aerodynamic forces are the following:

the velocity $\underline{v}$ of the approaching stream;

the density ρ of the gas in the approaching stream;

the geometrical dimensions of the body from which the characteristic dimension is generally taken, i.e., the area s_m of the midship cross section of the missile,

and therefore the relationship between the forces due to the above-enumerated parameters is presented in explicit form in the generally accepted standard form of notation for the aerodynamic forces, whereas the rest is included in the so-called coefficient of force. The standard form of the notation is the following:

$$\left.\begin{aligned} X &= C_x s_m \frac{\rho v^2}{2}, \\ Y &= C_y s_m \frac{\rho v^2}{2}. \end{aligned}\right\} \qquad (6.11)$$

in which case, since

$$X = X_f + X_a + X_p,$$

and

$$C_x = C_{xf} + C_{xd} + C_{xp}. \qquad (6.10')$$

Here C_x is the coefficient of frontal drag; C_y is the coefficient of lift; C_{xf}, C_{xd}, and C_{xp} are the coefficients of the components of total aerodynamic resistance.

The standard-form notation for aerodynamic forces is quite convenient. The fact that the relationship between the forces due to missile dimensions is accounted for by the factor s_m and is not contained in C_x (or C_y), makes it possible to model the phenomenon and to extend the results of the experiment to full-scale parts. For example, let a small-scale model of a missile be tested in a wind tunnel and let the force X_{mod} acting on the model during the wind-tunnel test be measured. In accordance with (6.11)

$$X_{мод} = C_{x\,мод} s_{м.мод} \frac{\rho v^2}{2},$$

where X_{mod} is the measured force; s_{mod} is the area of the midsection; ρ and $\underline{v}$ are the parameters of the flow; $C_{x\,mod}$ is the coefficient of model resistance, i.e., of the body of a certain configuration corresponding to the stream parameters ρ and $\underline{v}$. After the experiment it is easy to calculate

$$C_{x\,мод} = \frac{X_{мод}}{s_{м\,мод} \frac{\rho v^2}{2}}.$$

If we now turn to the full-scale object whose model was tested in the wind tunnel, and if we bear in mind the total geometric similarity between the model and nature (i.e., the full-scale object) it is natural to assume that for the same stream parameters - ρ and $\underline{v}$ - the force of aerodynamic resistance X_{nat} of the "natural" object will be

$$X_{нат} = C_{x\,мод} s_{м\,нат} \frac{\rho v^2}{2}$$

(since C_x is not a function of the dimensions of the body).

Thus by introducing the concept of the coefficient of aerodynamic force it becomes possible to simplify substantially the aerodynamic experiment, using data obtained in wind-tunnel tests of models for the determination of forces and moments acting on the "natural" missile under actual flight conditions.

The wind-tunnel testing of a missile is a complex experiment and is carried out only in the concluding stage of work on the missile. Tentative values for the aerodynamic forces and moments, calculated theoretically, are employed in the preliminary calculations (designs). The methods of approximate aerodynamic calculation, worked out to the present time, yield results that are in rather good agreement with the subsequent wind-tunnel tests, and the utilization of these calculations in the earlier stages of missile design is widespread practice.

Method of Calculating Aerodynamic Forces with the Utilization of a Simplified Model of the Flow of Air Past a Missile

The approximate methods of aerodynamic calculation are based on the conclusions reached in the so-called linearized theory of streamlining and the assumption as to the validity of the principle stating that the influences of the aerodynamic forces are independent for individual missile parts. With this assumption for a finned rocket missile, we will have

$$\left.\begin{aligned} X &= X_к + X_{оп} \\ Y &= Y_к + Y_{оп} \end{aligned}\right\} \qquad (6.12')$$

or in terms of the force coefficients:

$$\left.\begin{aligned} C_x &= C_{x\,к} + C_{x\,оп} \\ C_y &= C_{y\,к} + C_{y\,оп} \end{aligned}\right\} \qquad (6.12")$$

Below, the basic calculation relationships for the determination of the coefficients $C_{y\ к}$, $C_{y\ оп}$, $C_{x\ к}$, and $C_{x\ оп}$ for various flight conditions are presented without conclusion.

Calculation of the Lift Coefficient

Since the nature of streamlining and the mechanism responsible for the appearance of the components of the aerodynamic forces is a function of whether or not the flight velocity is subsonic (M < 1) or supersonic (M > 1), it becomes necessary to examine these two cases separately.

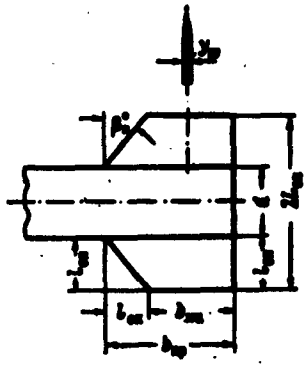

Fig. 6.22. Elements of fins for rocket missile. $2L_{op}$) total span of finning; $2l_{op}$) span of individual fin; β_p) sweepback angle of leading edge of stabilizer; β_z) sweepback angle of trailing edge of stabilizer (in Fig. 6.22, $\beta_z = 0$); y_t) profile thickness at section of middle chord of stabilizer; l_{sk}) sweepback of tail surfaces.

Subsonic flight velocities (M < 1)

Finning (empennage). The coefficient of lift for the finning of a missile is determined according to the following formula:

$$C_{y\,on} = \frac{1{,}84\pi\lambda_{on}\alpha}{2{,}4+\lambda_{on}}\frac{2s_{on}}{s_m}, \qquad (6.13')$$

λ_{op} is the elongation of the finning; α is the angle of attack; s_{op} is the area of the stabilizer fin; s_m is the area of the missile midsection.

Fig. 6.22 shows a diagram of the empennage (tail surfaces) of a rocket missile and its elements are denoted. In the denotation shown in the figure, the basic characteristics in the empennage are defined as follows:

elongation of tail surfaces

$$\lambda_{on} = \frac{2l_{on}^2}{2s_{on}}; \qquad (6.14)$$

area of stabilizer pairs

$$2s_{on} = 2b_{cp}l_{on} = (b_{kp}+b_{kn})l_{on},$$
$$b_{cp} = \frac{b_{kp}+b_{kn}}{2}; \qquad (6.15)$$

where b_{sr} is the middle chord of the stabilizer; b_{kr} is the root chord; b_{kts} is the tip chord;

the relative profile thickness of the empennage is

$$\Delta = \frac{2y_{\text{п}}}{b_{\text{ср}}}.$$

Strictly speaking, Formula (6.13') was derived for velocities at which the compressibility of the air can be neglected. However, this relationship can be extended to the entire range of near-sonic flight velocities with a sufficient degree of accuracy. With this, an additional term by means of which we take into consideration the effect of compressibility is introduced into the formula, which is then written in the following form:

$$C_{y\,\text{оп}} = \frac{1{,}84\pi\lambda_{\text{оп}}\alpha}{2{,}4+\lambda_{\text{оп}}} \frac{1}{\sqrt{1-M^2}} \frac{2s_{\text{оп}}}{s_{\text{н}}}. \qquad (6.13'')$$

The frame. For subsonic flight velocities

$$C_{y\,\text{к}} \approx \alpha, \qquad (6.16)$$

where α is the angle of attack for the missile in radians.

The total coefficient of missile lift. The total coefficient for a rocket missile with tail surfaces is defined as the sum

$$C_y = \frac{1{,}84\pi\lambda_{\text{оп}}\alpha}{2{,}4+\lambda_{\text{оп}}} \frac{1}{\sqrt{1-M^2}} \frac{2s_{\text{оп}}}{s_{\text{н}}} + \alpha$$

or

$$C_y = \left(1 + \frac{1{,}84\pi\lambda_{\text{оп}}}{2{,}4+\lambda_{\text{оп}}} \frac{1}{\sqrt{1-M^2}} \frac{2s_{\text{оп}}}{s_{\text{н}}}\right)\alpha. \qquad (6.17)$$

Supersonic flight velocities ($M > 1$)

Empennage (tail surfaces). To calculate the coefficient of lift for the empennage in the case of supersonic flight velocities, we use in first approximation the formula for lift in the case of a small-elongation wing that has a rectangular shape in the in-plan view:

$$C_{y\,\text{оп}} = \frac{4\alpha}{\sqrt{M^2-1}} \left(1 - \frac{1}{2\lambda_{\text{оп}}\sqrt{M^2-1}}\right) \frac{2s_{\text{оп}}}{s_{\text{н}}} \qquad (6.18')$$

for stabilizers with

$$\lambda_{\text{оп}} > \frac{1}{\sqrt{M^2-1}}$$

or we use the approximate relationship

$$C_{y\,\alpha} = 1{,}35\,\alpha\left(\lambda_{\alpha} + \frac{1}{\sqrt{M^2-1}}\right)\frac{2s_{\alpha}}{s_{м}} \qquad (6.18'')$$

for stabilizers with

$$\lambda_{\alpha} < \frac{1}{\sqrt{M^2-1}}.$$

The frame. The lift of a misille frame, at supersonic flight velocities, amounts to

$$C_{y\,к} \approx 2{,}4\alpha. \qquad (6.19)$$

The total coefficient of missile lift. The total coefficient of missile lift in the case of supersonic flight velocities will:

in the range of supersonic velocities to $M < 1 + \frac{1}{\lambda_{\alpha}^2}$

$$C_y = \left[1{,}35\left(\lambda_{\alpha} + \frac{1}{\sqrt{M^2-1}}\right)\frac{2s_{\alpha}}{s_{м}} + 2{,}4\right]\alpha \qquad (6.20')$$

and for velocities with $M > 1 + \frac{1}{\lambda_{\alpha}^2}$

$$C_y = \left[\frac{4}{\sqrt{M^2-1}}\left(1 - \frac{1}{2\lambda_{\alpha}\sqrt{M^2-1}}\right)\frac{2s_{\alpha}}{s_{м}} + 2{,}4\right]\alpha. \qquad (6.20'')$$

Calculation of Frontal-Resistance (Drag) Coefficient

Subsonic Flight Velocities

In calculating the coefficient of frontal resistance it is necessary to bear in mind that in accordance with (6.10') the total coefficient is presented in the form of a sum of the components, each of which is employed to take into consideration the effect on the total resistance of one of the factors responsible for this particular resistance. Generally speaking, (6.10') is satisfied exactly only in the case of $\alpha = 0$, thus for the $\alpha \neq 0$ the coefficient of resistance increases markedly as a result of the appearance of the so-called induced drag and because the increase in the component $C_{x\,p}$.

Let us examine the physical nature of this increase in drag during flight at some angle of attack. The primary feature of flight at

an angle of attack is the disturbance of the symmetry with which the approaching stream of air flows past the missile. As a result of this asymmetry in streamlining, downwash takes place from zones of elevated pressure to a zone of lower pressure. The losses produced by this downwash are taken into consideration by the induced drag (Fig. 6.23) The second component - ΔC_X - reflects the fact that during flight at an angle of attack the true midsection differs from the one according to which the calculation was carried out, so that the flow is decelerated over a greater area and as a result additional forces arise. The above-mentioned increase in the coefficient of drag is taken into consideration in the following form:

$$C_X = C_{X0} + C_{Xi} + \Delta C_X, \qquad (6.21)$$

where $C_{X0} = C_{Xf} + C_{X\,d} + C_{Xp}$ is the drag coefficient for $\alpha = 0$; C_{Xi} is the coefficient of induced drag; ΔC_X is the coefficient by means of which we take into consideration the additional resistance due to pressure as a result of the nonsymmetrical flow past the missile, for $\alpha = \emptyset$.

In the tentative calculation it turns out that it is enough to calculate the coefficient of frontal resistance without taking into consideration the effect of the angle of attack, i.e., the calculation can be done only on the basis of the elements C_{Xp}, C_{Xf}, and C_{Xd}.

The relationships for the calculation of individual components of the total coefficient of resistance for various flight conditions are presented below. As in the case in which the coefficient of lift was calculated, the validity of the principle of independent action is assumed for the aerodynamic forces on the airframe and tail surfaces of the missile.

The empennage. For the empennage it is natural to maintain that

$C_{X\,d} = 0$, so that

$$C_{X\,оп} = C_{Xp} + C_{Xf} + C_{Xl} + \Delta C_X. \qquad (6.21')$$

In practical calculations, the components of pressure and friction are combined for the empennage into the so-called profile resistance; in this case, Notation (6.21') is rearranged into the following form

$$C_{X\,оп} = C_{X\,пр} + C_{Xl} + \Delta C_X \qquad (6.21")$$

or for the negligibly small angles of attack

$$C_{X\,оп} \approx C_{X\,пр}.$$

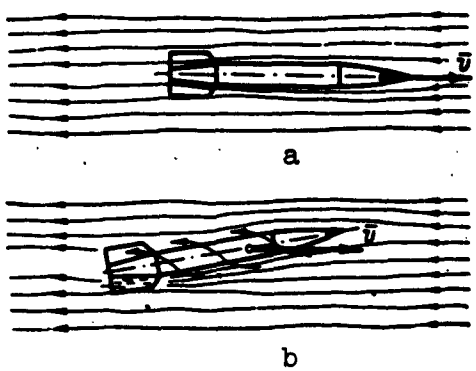

Fig. 6.23. Appearance of downwash in missile flight at some angle of attack. a) $\alpha = 0$; b) $\sigma \neq 0$.

if we take into consideration that $C_{X\,pr}$ represents the resistance of a single pair of stabilizers, and a rocket missile generally has two pairs, it is more convenient to write (6.21") in the following form:

$$C_{X\,оп} = 2C_{X\,пр} + C_{Xl} + \Delta C_X. \qquad (6.21")$$

and correspondingly for $\alpha \approx 0$

$$C_{X\,оп} \approx 2C_{X\,пр}$$

For the calculation of $C_{X\,pr[sic]}$ we can use the expression

$$C_{X\,пр} = \left(0{,}005 + \frac{0{,}031\Delta}{\sqrt{1-M^2}} + \frac{0{,}072\omega^2}{1-M^2}\right)\frac{2s_{оп}}{s_м}, \qquad (6.22)$$

where Δ is the relative thickness of the profile in the section of the middle chord; ω is the relative curvature of the profile (for rocket-missile stabilizers, generally $\omega = 0$).

The calculation of induced drag, if taken into consideration, is best carried out in terms of a calculation for the coefficient of empennage lift, using

$$C_{Xl} = \frac{C_{Y\,оп}^2}{\pi\lambda_{оп}}\frac{2s_{оп}}{s_м}. \qquad (6.23)$$

As a result, the coefficient of resistance for an empennage with zero curvature, in the case of subsonic velocities, is derived in the following form:

$$C_{X\,os}=\left(0{,}01+\frac{0{,}062\Delta}{\sqrt{1-M^2}}+\frac{C_{Y\,os}^2}{\pi\lambda_{os}}\right)\frac{2s_{os}}{s_m}. \tag{6.24}$$

Airframe. The concept of profile resistance is conveniently introduced for the calculation of C_{Xka} when

$$C_{X\,k}=C_{X\,pr}+C_{X\,a}+C_{X\,i}+\Delta C_X$$

or, neglecting the influence of the angle of attack,

$$C_{X\,k}=C_{X\,pr}+C_{X\,a}.$$

In the case of subsonic flight velocities, a substantial portion of the profile resistance is made up of frictional resistance; therefore, in rough calculations we can hold that

$$C_{X\,pr}\approx C_{X\,f}.$$

More exact results are obtained when the following calculation relationship is employed;

$$C_{X\,pr}=\frac{A_c C_{X\,f}}{\sqrt{1+0{,}2M^2}}, \tag{6.25}$$

where C_{Xf} is the coefficient of frictional resistance; A_s is the coefficient by means of which we take into consideration the influence on $C_{X\ pr}$ exerted by the component due to the distribution of pressure.

For the calculation of C_{Xf} we use

$$C_{X\,f}=0{,}0315\,\mathrm{Re}^{-0{,}166}\frac{s_{bok}}{s_m}, \tag{6.26}$$

where Re is the Reynolds number of the approaching stream; s_{bok} is the lateral surface of the missile airframe; s_m is the area of the midsection, and the correction factor A_s is determined on the basis of the following empirical formula

$$A_c=1{,}865-0{,}175\lambda_k\sqrt{1-M^2}+0{,}01\lambda_k^2(1-M^2), \tag{6.27}$$

where λ_k stands for the elongation of the rocket airframe:

$$\lambda_k = \frac{l_k}{d};$$

l_k is the length of the airframe; d is the caliber of the missile.

The airframe-resistance component, due to rarefaction, can be determined in accordance to the following formula:

$$C_{x\,k} = (0{,}05 + 0{,}25M^2)\frac{s_{dn}}{s_m}, \tag{6.28}$$

where s_{dn} is the area of rear outlet of the missile; s_m is the midsection area.

Thus, if we neglect the influence on resistance of the angle of attact, the total coefficient of aerodynamic resistance for the airframe of a rocket missile will be

$$C_{x\,k} = \frac{A_c C_{xf}}{\sqrt{1+0{,}2M^2}} + (0{,}05+0{,}25M^2)\frac{s_{dn}}{s_m}$$

or if we take into consideration (6.26)

$$C_{x\,k} = \frac{0{,}0315 A_c \mathrm{Re}^{-0{,}145}}{\sqrt{1+0{,}2M^2}}\frac{s_{bok}}{s_m} + (0{,}05+0{,}25M^2)\frac{s_{dn}}{s_m}. \tag{6.29}$$

The total coefficient of missile resistance (drag). Thus, at subsonic velocities.

$$C_x = \left(0{,}01 + \frac{0{,}062\Delta}{\sqrt{1-M^2}}\frac{C^2_{y\,op}}{\pi\lambda_{op}}\right)\frac{2s_{op}}{s_m} + \\ + \frac{0{,}0315 A_c \mathrm{Re}^{-0{,}145}}{\sqrt{1+0{,}2M^2}}\frac{s_{bok}}{s_m} + (0{,}05+0{,}25M^2)\frac{s_{dn}}{s_m} \tag{6.30}$$

or after substituting the value of $C_{y\,op}$

$$C_x = \left[0{,}01 + \frac{0{,}062\Delta}{\sqrt{1-M^2}} + \pi\lambda_{op}\left(\frac{1{,}84\alpha}{2{,}4+\lambda_{op}}\right)^2\right]\frac{2s_{op}}{s_m} + \\ + \frac{0{,}0315 A_c \mathrm{Re}^{-0{,}145}}{\sqrt{1+0{,}2M^2}}\frac{s_{bok}}{s_m} + (0{,}05+0{,}25M^2)\frac{s_{dn}}{s_m}. \tag{6.30"}$$

For the active phase of the flight, when $C_{x\,d} = 0$,

$$C_X^{выт} = \left[0{,}01 + \frac{0{,}062\Delta}{\sqrt{1-M^2}} + \pi\lambda_{оп}\left(\frac{1{,}84c}{2{,}4+\lambda_{оп}}\right)^2\right]\frac{2s_{оп}}{s_м} + \frac{0{,}0315\,A_c Re^{-0{,}146}}{\sqrt{1+0{,}2M^2}}\,\frac{s_{бок}}{s_м}.$$

The calculation data indicate that in the case of large missiles and rockets, approximately 95% of the total resistance can be attributed to the airframe.

The effect of the angle of attack on drag is a function of flight velocity and the magnitude of the angle. As an example we can cite the following data. For the M13 missile, during test launchings, with a flight velocity of ~275 m/sec (M = 0.8) the component due to the angle of attack did not exceed, in the over-all balance, a resistance of 8% at $\alpha = 0.1$ (~6°), and 27% at $\alpha = 0.2$ (~12°) and with a reduction in flight velocity the relative value of the component due to the angle of attack diminished.

Supersonic flight velocities.

In the case of a flight at supersonic velocities, the nature of resistance changes somewhat. While in the case of subsonic flight velocities the resistance occurs primarily as a result of the frictional forces, at velocities corresponding to M > 1 the basic role is played by resistance due to pressure distribution over the surface of the missile and in the stream about the missile. The very nature of this pressure distribution differs radically from the case of subsonic velocities; a system of so-called compression waves form about the missile; this system of compression waves involves shock waves of various intensities. The existence of shock waves in the stream is a characteristic feature of flight at velocities in excess of the speed of sound. This feature determines entirely the nature of the forces that are active at such flight velocities. The streamline pattern for the missile in the case of supersonic flow is presented in Fig. 6.24.

The coefficient of missile resistance in the case of supersonic

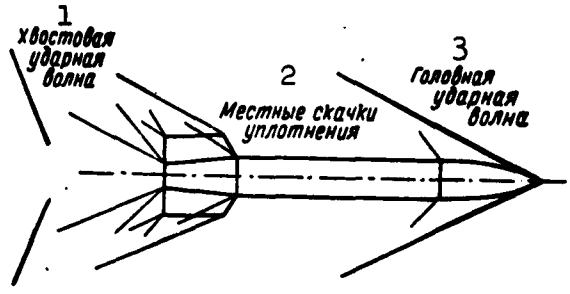

Fig. 6.24. System of compression waves formed during missile flight at supersonic velocity. 1) Tail shock wave; 2) local compression waves; 3) forward shock wave

flight velocities is presented in the form of the sum of the following components:

$$C_X = C_{X\,v} + C_{X\,a} + C_{Xf} + C_{Xl} + \Delta C_X = C_{X0} + C_{Xl} + \Delta C_X,$$

where $C_{X\,v}$ is the coefficient of resistance due to the forces of normal pressure, said coefficient in the case of supersonic velocities, referred to as the coefficient of wave resistance. The remaining denotations are the same as in (6.21).

The coefficient C_X of the missile for supersonic flight velocities is determined, as before, on the basis of missile elements.

Tail surface. The coefficient of wave resistance for the tail surfaces is calculated in accordance with the following formula:

$$C_{X\,a} = \frac{\frac{4}{b_{cp}}\int_0^{b_{cp}} (y')^2\,dx}{\sqrt{M^2-1}}\,\frac{2s_{cp}}{s_m}, \qquad (6.31)$$

where $y = y(x)$ is the equation for the contour of the tail-surface profile.

For a profile formed by parabolic arcs (Fig. 6.25),

$$\frac{1}{b_{cp}}\int_0^{b_{cp}} (y')^2\,dx = \frac{4}{3}\Delta^2,$$

where Δ is the relative thickness of the profile, so that for such a profile

$$C_{x_0} = \frac{\frac{16}{3}\Delta^2}{\sqrt{M^2-1}} \frac{2s_{ст}}{s_м},$$

i.e., the total wave resistance of the tail surfaces, taking into consideration that the missile has two pairs of stabilizers, will be

$$C_{x_0} = \frac{32\Delta^2}{3\sqrt{M^2-1}} \frac{2s_{ст}}{s_м}. \qquad (6.32)$$

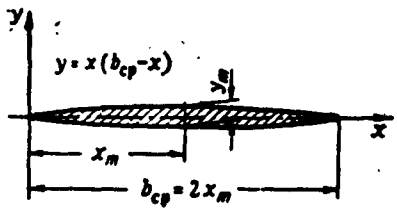

Fig. 6.25. Profile elements formed by parabolic arcs. x_m) Cross-sectional coordinates with maximum profile thickness (y_m)

The rear resistance for a symmetric profile is equal to zero, whereas in the case of stabilizers having a truncated rear edge, this resistance is negligibly small. In view of this, it is maintained that in the case of tail surfaces $C_{Xd} = 0$.

The quantity C_{Xf} for supersonic velocities is determined in accordance with following formula:

$$C_{xf} = 0{,}0315\,\mathrm{Re}^{-0{,}145} \frac{2s_{ст}}{s_м}, \qquad (6.33)$$

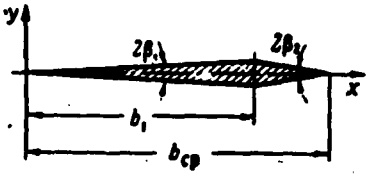

Fig. 6.26. Geometric elements of a rhomboid profile

where the Re number for the tail surfaces is as follows:

$$\mathrm{Re} = \frac{M a b_{ср}}{\nu} = \frac{v b_{ср}}{\nu},$$

where a is the speed of sound propagation in air ($a \approx 340$ m/sec); v is the flight velocity; ν is the coefficient of kinematic air viscosity, whose value for the conditions of flight close to the earth can be assumed to be $\nu = 1.45 \cdot 10^{-5}$ m^2/sec.

The components of the resistance which appear as a result of the angle of attack are most expediently evaluated in complex form. For this, we can employ the following formula:

$$\Delta C_x + C_{xi} = \frac{4c^2}{\sqrt{M^2-1}}\left(1-\frac{1}{2}\frac{1}{\lambda_{on}\sqrt{M^2-1}}\right)\frac{2s_{on}}{s_M}. \qquad (6.34)$$

In conclusion, the total resistance of the tail surfaces in the case of supersonic flight velocities amounts to

$$C_{x\,on} = \left[\frac{32\Delta^2}{3\sqrt{M^2-1}} + 4\cdot 0{,}0315\,\mathrm{Re}^{-0{,}145} + \right.$$
$$\left. + \frac{4c^2}{\sqrt{M^2-1}}\left(1-\frac{1}{2}\frac{1}{\lambda_{on}\sqrt{M^2-1}}\right)\right]\frac{2s_{on}}{s_M}. \qquad (6.35)$$

This formula was derived in the assumption that the cross-section of the stabilizer is a symmetric contour formed by parabolic arcs. In the general case, the formula is written as before, with the exception of the first term which must be determined in accordance with Formula (6.31).

In the practice of empennage design, in addition to the profile formed by parabolic arcs, widespread use is made of symmetric rhomboid profiles (Fig. 6.26). For such a profile

$$\frac{1}{b_{cp}}\int_0^{b_{cp}}(y')^2\,dx = \beta_1^2\frac{b_1}{b} + \beta_2^2\left(1-\frac{b_1}{b}\right)$$

or in the case of a symmetric rhomboid profile ($b_1 = (b/2)$, $\beta_1 = \beta_2$)

$$\frac{1}{b_{cp}}\int_0^{b_{cp}}(y')^2\,dx = \beta_1^2.$$

The airframe. In calculating the coefficient of airframe resistance, we generally take into consideration only the components of wave resistance, frictional resistance, and rear drag; the effect of the components due to the presence of an angle of attack (C_{Xi}, ΔC_X) on the magnitude of this coefficient can be neglected.

The component due to wave resistance can be estimated in accordance with the following formula:

$$C_{x\,0} = 0{,}415\bar{p}_0 - 0{,}667\left(0{,}327\bar{p}_0 + \frac{1{,}43}{M^2}\right)(1 - \nu_0), \quad (6.36)$$

(6.36)

where $\bar{p}_0$ is the so-called pressure coefficient on the cone at the tip of the missile (the conic angle is equal to the corresponding angle indicated on the drawing). The quantity $\bar{p}_0$ can be determined in accordance to the following empirical formula:

$$\bar{p}_0 = \left(0{,}083 + \frac{0{,}096}{M^2}\right)\left(\frac{\beta_0}{10}\right)^{1{,}65}; \quad (6.37)$$

β_0 is the cone angle at the tip of the missile;* ν_0 is the pressure-recovery factor; this factor is the ratio between the deceleration pressure of the stream after and prior to the pressure jump which appears in the case of a missile flying at supersonic velocities:

$$\nu_0 = \frac{p_0'}{p^*} = f(M\beta_0).$$

Detailed tables for $\nu_0 = f(M, \beta_0)$ can be found in the above-mentioned work by M.F. Krasnov.

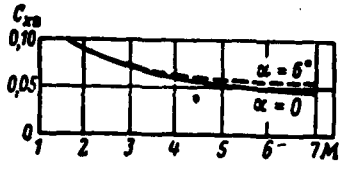

Fig. 6.27. Effect of angle of attack on magnitude of $C_{X\,v}$ of the missile airframe in the case of various M(ach) numbers

In approximate terms, the magnitude of $C_{X\,v}$ can be estimated in accordance with the following formula:

$$C_{x\,0} = \frac{2}{3}\frac{1}{\lambda_m^2}, \quad (6.38)$$

where $\lambda_m = (x_m/d_m)$ is the elongation of the missile; x_m is the coordinate of the section in which the missile diameter attains its maximum value of d_m.

Calculations show that with low flight velocities corresponding to M = 3-4, the changes in the magnitude of $C_{X\,v}$ as a result of the appearance of an angle of attack need not be taken into consideration. At greater velocities, the increment ΔC_X becomes substantial even in

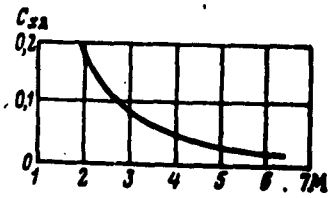

Fig. 6.28. Nature of change in coefficient $C_{X\,d}$ for the airframe of the missile with $s_{dn}/s_m = 1.0$ for various M(ach) numbers

the case of α and it must be taken into consideration (Fig. 6.27).

The coefficient of rear resistance is calculated in accordance with the following formulas:

$$C_{x\,a}=\frac{1,43}{M^2}-\frac{0,772}{M^3}(1-0,011M^2)^{2,5}\frac{s_{dn}}{s_m} \quad \text{for numbers } M<6 \qquad (6.39')$$

and

$$C_{x\,a}=\frac{1,43}{M^2}\frac{s_{dn}}{s_m} \quad \text{for numbers } M>8. \qquad (6.39'')$$

The nature of the change in $C_{X\,d}$ with respect to M(ach) numbers is shown in Fig. 6.28.

The coefficient $C_{X\,f}$ is defined as

$$C_{x\,f}=0,0315\,\mathrm{Re}^{-0,145}\frac{s_{bok}}{s_m}. \qquad (6.40)$$

In calculating C_{Xf} it should be borne in mind that the Re number is a function of the altitude of missile flight, since the density of the air and the speed of sound propagation in the air changes with altitude. Comparative values of the coefficient C_{Xf} for two various altitudes are shown in Fig. 6.29.

In conclusion, the total coefficient of frontal drag for the airframe is determined by the sum

$$C_{x\,a}=\frac{2}{3}\frac{1}{\lambda_m^2}+\left[\frac{1,43}{M^2}-\frac{0,772}{M^3}(1-0,011M^2)^{2,5}\right]\frac{s_{dn}}{s_m}+ \\ +0,0315\,\mathrm{Re}^{-0,145}\frac{s_{bok}}{s_m} \qquad (6.41')$$

for a flight at velocities corresponding to $M \leq 6$, or

$$C_{x\,a}=\frac{2}{3}\frac{1}{\lambda_m^2}+\frac{1,43}{M^2}\frac{s_{dn}}{s_m}+0,0315\mathrm{Re}^{-0,145}\frac{s_{bok}}{s_m} \qquad (6.41'')$$

for $M > 8$, where in the case of need for more exact calculations, the coefficient of wave resistance must be presented in the following form:

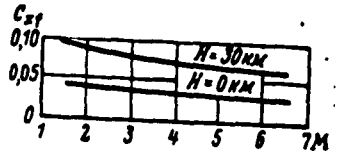

Fig. 6.29. C_{Xf} of the missile airframe as a function of altitude for varous M(ach) numbers

$$C_{x\,a}=0{,}415\bar{p}_0-0{,}667\left(0{,}327\bar{p}_0+\frac{1{,}43}{M^2}\right)(1-\nu_0)$$

instead of

$$C_{x\,a}=\frac{2}{3}\,\frac{1}{\lambda_m^2}.$$

The total coefficient of missile resistance. The coefficient of the frontal drag of a finned missile, in the case of supersonic velocities, is found as the sum of the resistance components due to the tail surfaces of the missile and the missile airframe.

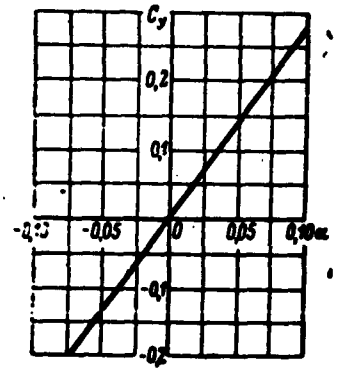

Fig. 6.30. Nature of function $C_Y = C_Y(\alpha)$ of solid-propellant rocket missile for small angles of attack

For a more extensive range of velocities, not exceeding M = 6, the calculation formula will be:

$$C_X=\frac{2}{3}\,\frac{1}{\lambda_m^2}+\left[\frac{1{,}43}{M^2}-\frac{0{,}772}{M^2}\left(1-0{,}011M^2\right)^{3{,}5}\right]\frac{s_{\text{ан}}}{s_M}+$$
$$+0{,}0315\,\mathrm{Re}^{-0{,}145}\,\frac{s_{\text{бок}}}{s_M}+\left[\frac{32\Delta^2}{3\sqrt{M^2-1}}+0{,}126\,\mathrm{Re}^{-0{,}145}+\right.$$
$$\left.+\frac{4a^2}{\sqrt{M^2-1}}\left(1-\frac{1}{2}\,\frac{1}{\lambda_{\text{оп}}\sqrt{M^2-1}}\right)\right]\frac{2s_{\text{оп}}}{s_M}. \qquad (6.42)$$

For the active flight phase, the calculation formula can be simplified somewhat:

$$C_X^{\text{акт}}=\frac{2}{3}\,\frac{1}{\lambda_m^2}+0{,}0315\,\mathrm{Re}^{-0{,}145}\,\frac{s_{\text{бок}}}{s_M}+$$
$$+\left[\frac{32\Delta^2}{3\sqrt{M^2-1}}+0{,}126\,\mathrm{Re}^{-0{,}145}+\right.$$
$$\left.+\frac{4a^2}{\sqrt{M^2-1}}\left(1-\frac{1}{2}\,\frac{1}{\lambda_{\text{оп}}\sqrt{M^2-1}}\right)\right]\frac{2s_{\text{оп}}}{s_M}$$

(for the case in which the missile has a tail surface whose section is formed (profiled) by parabolic arcs).

Thus Formulas (6.16) and (6.19) make it possible to calculate the coefficient of missile lift in the case of sub- and super-sonic velocities, and Formulas (6.30) and (6.42) make it possible to calculate

the coefficient of frontal drag. We can see from the sormulas that for a missile of some definite design, the coefficients are completely determined by the flight Mach number and the angle of missile attack.

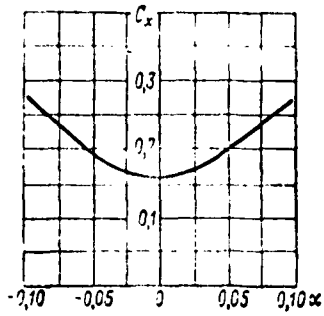

Fig. 6.31. Nature of change in $C_X = C_X(\alpha)$ of solid-propellant rocket missile for small angles of attack

Figs. 6.30 and 6.31 show tentative relationships $C_X = C_X(\alpha)$ and $C_Y = C_Y(\alpha)$, constructed for the case of M = const. A comparison of these curves leads one easily to the conclusion that given small angles of attack (below 3-5°) $C_X > C_Y$, where for α close to zero $C_Y \to 0$, whereas as C_X even with a zero angle of attack has a certain definite value. Since the possible angles of attack as a rule, are limited, we frequently examine only the coefficient C_X of the missile. The nature of the change in this missile with respect to the Mach numbers and the angles α is an important characteristic of the missile being designed. The tentative form of the family of corresponding curves is presented in Fig. 6.32.

For exterior-ballistic calculations it is important to know not only the magnitude of the active aerodynamic forces, but the position

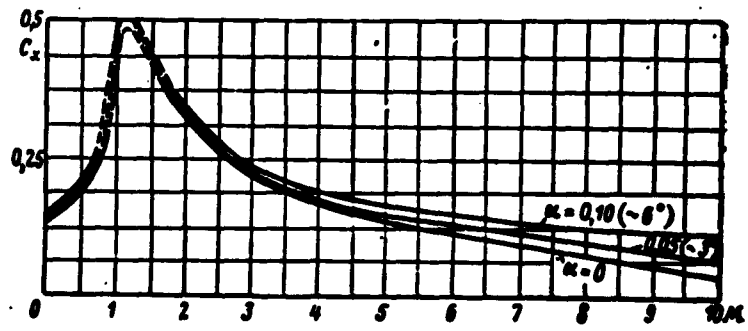

Fig. 6.32. Summary curves $C_X = C_X(M)$ of the finned solid-propellant rocket missile for various angles of attack α (for the case of flight during the passive phase)

of the point of application of the resultant of these forces, called the center of missile pressure, since as will be shown below, the mutual position of the center of pressure and the center of missile gravity determines the degree of missile stability on its trajectory. It is general practice to regard the center of pressure as being situtated on the axis of the missile at a distance of $x_{ts.d}$ from its nose, and it is for this reason that the calculation of the center-of-pressure coordinates can be reduced to the determination of the coordinate $x_{es.d}$.

In aerodynamics, we generally use the dimensionless coordinate

$$\frac{x_{s.s}}{x_k},$$

where x_k is the total length of the body being considered.

This coordinate is referred to as the coefficient of the center of missile pressure and is denoted as follows:

$$C_{s.s}=\frac{x_{s.s}}{x_k}. \tag{6.43}$$

It can be demonstrated that at supersonic velocities for a solid of revolution, consisting of an ogive curve and a cylindrical part, (for the airframe of the missile),

$$C_{s.s.x}=\frac{0{,}733+0{,}667\alpha\lambda_m\left(\bar{x}_k^2-1\right)}{x_k\left[1{,}57+1{,}334\alpha\lambda_m\left(\bar{x}_k-1\right)\right]}, \tag{6.44}$$

where α is the angle of attack; $\lambda_m = (x_m/d)$ is the elongation of the forward part of the missile; $\lambda_k = (x_k/d)$ is the elongation of the entire airframe; $\bar{x}_k = (x_k/x_m)$ is the dimensionless airframe length (λ_k/λ_m).

The basic denotations adopted in (6.44) are illustrated in Fig. 6.33.

In practical calculations we can assume that for airframes of rockets having an elongation of the order 7–10, the coefficient of the

center of pressure is equal to 0.5.

Since in the transition from subsonic flight velocities to supersonic flight velocities the rocket stability margin diminishes somewhat, $C_{ts.d}$ for $M < 1$, need not be calculated, since the rocket that is stable at supersonic velocities will obviously be stable at subsonic velocities.

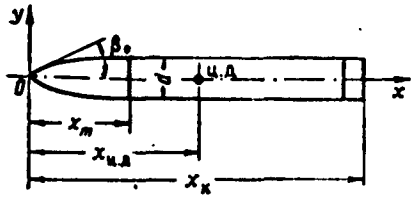

Fig. 6.33. Geometric elements of airframe of rocket missile. $\lambda_m = (x_m/d)$ is the elongation of the forward part of missile; $\lambda_k = x_k/d$ is missile airframe elongation; $\bar{x}_k = \lambda_k/\lambda_m$ is the dimensionless missile length

With respect to the tail surfaces of the missile, it is assumed that the center of tail-pressure lies in the middle of the central fin chord (Fig. 6.34). This makes it possible, given a certain missile assembly and tail-surface geometry (Fig. 6.35), to calculate the coordinate of the center of tail-pressure $x_{ts.d.o}$ and to find $C_{ts.d.o}$:

$$x_{ц.д.о} = x_к + m - b_{ср},$$

$$C_{ц.д.о} = \frac{x_к + m - b_{ср}}{x_к} = 1 - \frac{b_{ср} - m}{x_к}.$$

For the calculation of the center of pressure coordinates for the entire missile, we employ the theorem on the static moments for a system of parallel forces applied at the center of airframe and tail-surface pressure. The component Y_k and Y_{op} for the forces of missile lift are conveniently employed as such a system. Employing the theorem on static moments and assuming that for small angles of attack ($\alpha \sim 0.05$), the vectors of the forces Y_k and Y_{op} are perpendicular to the axis of the missile, we will obtain (Fig. 6.36).

$$C_{y\,к} x_{ц.д.к} + C_{y\,оп} x_{ц.д.о} = C_y x_{ц.д.}$$

where C_y is the force of missile lift, equal to the sum of the airframe and tail-surface components; $x_{ts.d.k}$ and $x_{ts.d.o}$ are, respectively, the coordinates of the center of pressure for the airframe and

the tail surfaces of the missile; $x_{ts.d}$ is the coordinate of the center of missile pressure.

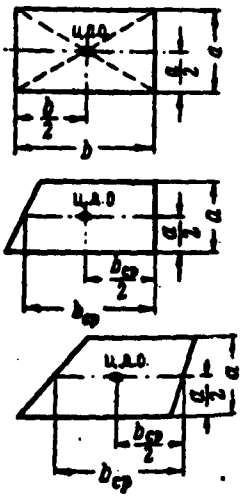

Fig. 6.34. Position of center of pressure (ts.d.o. - center of tail-surface pressure) for certain types of stabilizers

From this equation

$$x_{n.s}=\frac{C_{y\,k}x_{n.s.k}+C_{y\,os}x_{n.s.o}}{C_y}, \qquad (6.45)$$

i.e., the coefficient of the center of missile pressure will be

$$C_{n.s}=\frac{x_{n.s}}{x_k}=\frac{\frac{x_{n.s.k}}{x_k}C_{y\,k}+\frac{x_{n.s.o}}{x_k}C_{y\,os}}{C_y}. \qquad (6.46)$$

In addition to the above-discussed method of an approximate calculation of the aerodynamic forces acting on a finned rocket missile in flight, we sometimes employ the relationships that come into play in rocket engineering from the theory of conventional artillery. These relationships make it possible, as a rule, to evaluate more rapidly, although with a lower degree of accuracy, the parameters of the stress-bearing interaction of the missile with the approaching air stream and may be useful for preliminary calculations.

Fig. 6.35. Calculation diagram of missile for determination of center of tail-surface pressure in system of coordinates connected to missile

<u>Method of estimating the aerodynamic forces in terms of the coefficient of missile shape</u>

It is easy to derive the formula for the calculation of the force of frontal missile resistance (drag) in terms of the shape coefficient from the standard form of denotation for the aerodynamic force:

$$X=C_X S_m \frac{\rho v^2}{2}.$$

In this denotation, the term v^2 characterizes the relationship be-

tween aerodynamic forces and the flight velocity, assuming this relationship to be squared. This quadratic function is valid only for a certain definite range of velocities. In the more general form, for any flight velocities, instead of v^2, it is expedient to introduce simply some velocity function F(v). This function is referred to as the resistance (drag) function. The factor ρ is employed to take into consideration the effect on the magnitude of the aerodynamic forces exerted by the density of the approaching air stream. Since the density of the air is a function of the altitude of the given air layer above sealevel, the factor ρ may, in the general case, be replaced by some missile flight-altitude function H(y). Finally, C_X and s_m reflect the relationship between aerodynamic forces and the shape and dimensions of the body. In artillery, this relationship is generally taken into account by the ballistic missile coefficient C_0. Thus the denotation

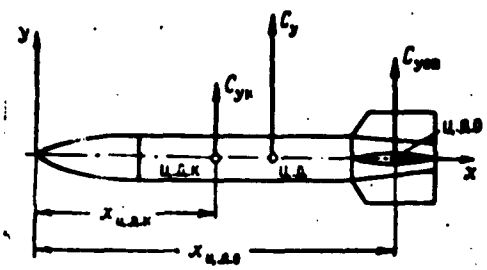

Fig. 6.36. Calculation diagram of missile for application of theorem on static moments on determination of position of missile center of pressure

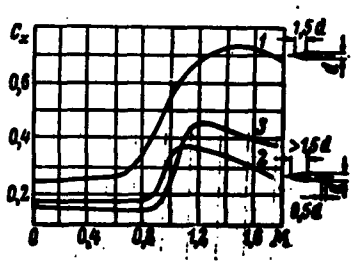

Fig. 6.37. Laws governing resistance of standard missiles 1) The Siachchi [sic] law; 2) The law of the year "1930"; 3) The law of the year "1943."

$$X = C_X s_m \frac{\rho v^2}{2}$$

is modified to the following equivalent form

$$X = C_0 H(y) F(v), \qquad (6.47)$$

where C_0 is the ballistic missile coefficient; A(y) is the altitude function; F(v) is the resistance function.

The ballistic missile coefficient is associated with the basis design parameters of the missile by the following relationship:

$$C_0 = \frac{id^2 \cdot 1000}{q}, \tag{6.48}$$

where i is the coefficient of missile shape; d is the calibre of the missile, in inches; q is the weight of the missile, in kg.

Let us introduce the ratio q/d^3, generally referred to as the lateral load on the missile, and denoted by

$$C_q = \frac{q}{d^3}.$$

if we take into consideration C_q, (6.48) will be

$$C_0 = \frac{1000i}{C_q d}. \tag{6.48'}$$

The quantity C_q amounts to, for example, $C_q = 15$ kg/dm^3 for the finned rocket missiles of the USSR M-8 system, and for the USSR M-13 system, $C_q = 19$ kg/dm^3.

The established practice of preliminary ballistics calculations reduces the calculation of the coefficient C_0 to a comparison of this coefficient with the ballistic missile coefficient adopted as the standard, so that

$$C_0 = iC_{0\,et}. \tag{6.49}$$

where $C_{0\,et}$ is the ballistic coefficient of a standard missile; i is the shape factor of the given missile.

The quantity $C_{0\,et}$ for various velocities is determined experimentally. Frequently, the curve first derived by Siachchi [sic] is chosen as the standard curve $C_{0\,et}$ (M). However, generally speaking, other curves taken for missiles of definite configurations can be selected as the standard. In addition to the Siachchi [sic] curve, the curves which are conventionally referred to as the curves of the "1930 law" and the "1943 law" (Fig. 6.37) have also found widespread application.

Experience in the design of rocket missiles shows that for the preliminary calculations of the coefficient of shape for finned missiles employed in the field artillery can be assumed to be equal to $i_s = 0.8$ is accordance with the Siachchi resistance law; it can be assumed to be equal to $i_{30} = 1.35$ in accordance with the "1930 law"; and in accordance with the "1943 law," it can be assumed to be equal to $i_{43} = 1.45$, so that the ballistic coefficient of the missile can be estimated as follows:

$$\left.\begin{aligned} C_0 &= 0{,}8\,(C_{0\,ст})_{\text{Сиаччи}},\\ C_0 &= 1{,}35\,(C_{0\,ст})_{1930\ г.},\\ C_0 &= 1{,}45\,(C_{0\,ст})_{1943\ г.} \end{aligned}\right\} \qquad (6.49')$$

where the value of C_0 of the standard missiles is taken from the corresponding curves, and in first approximation the curves shown in Fig. 6.37 can be employed.

If we compare the curve $C_0(M)$ of a true finned rocket missile against the standard curves (Fig. 6.38), it is easy to show that

$$\frac{C_0}{C_{0\,ст}} = f(M),$$

i.e., the shape factor, strictly speaking, cannot be assumed to be constant for the various flight velocities. For example, for a missile whose resistance-function curve is shown in Fig. 6.38, the magnitude of the ratio changes as shown in Fig. 6.39. We can see from this figure that while with respect to the "1930 resistance function" we can examine some average value of the coefficient of $\underline{i}$ in terms of flight Mach numbers, such averaging in the case of the Siachchi [sic] law (function) such an averaging may possibly produce serious calculation errors. Therefore, in the case of refined calculations as a

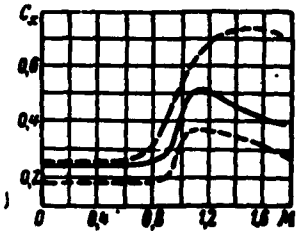

Fig. 6.38. Comparison of law governing resistance of a finned solid-propellant rocket missile with standard curves

rule, the relationship between the shape factor of the missile and velocity is taken into consideration.

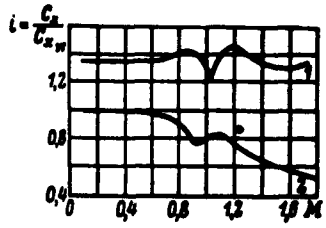

Fig. 6.39. Shape factor i of finned rocket missile as function of the flight Mach number 1) the "1930 law"; 2) the Siachchi [sic] law.

The relationship i = f(M) can be taken into consideration with an adequate degree of accuracy if the values of the shape factor presented in Table 6.1 are employed in the calculations.

Thus a calculation of the force of frontal missile drag in the second case can be reduced to a determination of the shape factor of this missile with respect to one of the standard resistance functions. However, if we know the shape factor i, it is easy to find the required calculation magnitudes, using the above-presented relationship. It is clear that this method is applicable only for an evaluation of the active forces in the case of rough preliminary calculations.

TABLE 6.1.
Recommended Calculation Values of Shape Factor for Finned Rocket Missile for Various Laws of Resistance

M	1 Коэффициент формы		
	2 к закону Сиаччи	3 к закону 1930 г.	4 к закону 1943 г.
0,1	0,980	1,350	1,000
0,5	0,975	1,350	1,000
1,0	0,805	1,230	1,355
1,5	0,595	1,325	1,205
5 Среднее значение коэффициента формы в рассматриваемом диапазоне скоростей			
0,1—1,5	0,772	1,337	1,430

1) Shape factor; 2) for the Siachchi [sic] law; 3) for the 1930 law; 4) for the 1943 law; 5) mean value of the shape factor in the velocity range being examined.

Calculation of Aerodynamic Moments Acting on Missile in Flight

It has been shown that in referring the aerodynamic forces to the

center of gravity, there appear moments whose magnitude is determined by the magnitudes of the aerodynamic forces X and Y and the distance between the center of gravity and the center of missile pressure. Denoting this distance by

$$e=x_{ц.д}-x_{ц.т},$$

we will obtain (Fig. 6.40)

$$M=Ye\cos\alpha+Xe\sin\alpha. \tag{6.50}$$

The standard form of writing out the aerodynamic moment M is given by the following expression:

$$M=C_M s_м x_к \frac{\rho v^2}{2}, \tag{6.51}$$

where C_M is the moment coefficient; s_m is the area of the rocket's midsection; x_k is the characteristic linear dimension of the rocket which is generally assumed to be the length of the missile airframe.

Taking into consideration (6.51) and the standard form of denoting aerodynamic forces, we will derive Eq.(6.50) in the following form:

$$C_M s_м x_к \frac{\rho v^2}{2}=C_y s_м \frac{\rho v^2}{2} e\cos\alpha+C_x s_м \frac{\rho v^2}{2} e\sin\alpha,$$

whence for the moment coefficient C_M we obtain the following relationship

$$C_M=\frac{e}{x_к}(C_y\cos\alpha+C_x\sin\alpha) \tag{6.52}$$

or for the case of small angles of attack, when we can assume $\cos\alpha\approx 1.0$, $\sin\alpha\approx a$.

$$C_M=\frac{e}{x_к}(C_y+aC_x). \tag{6.52"}$$

It is evident that given a zero angle of attack, the aerodynamic moment will vanish.

The components of the total aerodynamic moment with respect to the Ox', Oy', and Od' axes of the connected coordinate system are re-

ferred to, respectively, as the moments of roll M_φ, yaw M_ψ, and pitch M_θ. These are generally expressed in terms of the corresponding coefficients, in standard form:

$$\left.\begin{aligned} M_\theta &= C_{M\theta} S_M x_k \frac{\rho v^2}{2}, \\ M_\psi &= C_{M\psi} S_M x_k \frac{\rho v^2}{2}, \\ M_\varphi &= C_{M\varphi} S_M x_k \frac{\rho v^2}{2}, \end{aligned}\right\} \qquad (6.51')$$

where $C_{M\theta}$, $C_{M\psi}$, and $C_{M\varphi}$ are standard coefficients.

A shift of the missile in space as a result of the action of moments M_θ, M_ψ, and M_φ hinders the forces of viscous friction and those

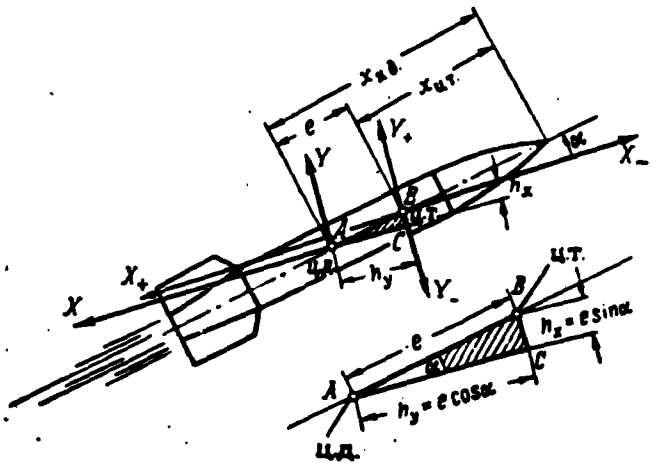

Fig. 6.40. Calculation of aerodynamic moment in terms of the forces which produce the appearance of this moment. $h_y = e \cos \alpha$) arm of lift force with respect to center of missile gravity $h_x = e \sin \alpha$) arm of force of frontal resistance with respect to center of missile gravity

forces which appear as a result of certain secondary phenomena which can be observed in the case of the missile turning about the center of gravity. This counteraction is generally taken into consideration through the introduction of the concept of the damping moment by which we mean the moment which is proportional to the total counteraction of

the medium. Each of the moments M_θ, M_ψ, and M_φ is assigned a damping moment of the same designation:

M'_θ is the damping moment of pitch;

M'_ψ is the damping moment of yaw;

M'_φ is the damping moment of roll.

To distinguish them from the damping moment, the moments M_θ, M_φ, and M_ψ are sometimes referred to as the stabilizing moments.

Thus there is always some effective moment ΔM_{ef}, acting on the missile, said moment determined by the following equation

$$\Delta M_{эф} = M_{ст} - M_{демпф},$$

where M_{st} is the stabilizing moment; M_{dempf} is the damping moment.

The calculation of the coefficients $C_{M\theta}$, $C_{M\psi}$, $C_{M\varphi}$ and $C'_{M\theta}$, $C'_{M\psi}$, and $C'_{M\varphi}$ is the comparitively complex. In first approximation, the damping moments need not be taken into consideration, and $C_{M\theta}$, $C_{M\varphi}$, and $C_{M\psi}$, can be taken into consideration in terms of C_Y, C_X and the geometric characteristics of the missile.*

§3. GENERAL SYSTEM OF EQUATIONS OF MISSILE MOTION IN AIR IN A SPATIAL SYSTEM OF COORDINATES

In the general case, in accordance with the basic principles of mechanics, the complex motion of a missile with respect to a ground system of coordinates can be presented as the sum of the forward (translational) and relative motions. In this case, the forward (translational) motion will be the translation of the center of missile gravity, the nature of which is determined by the well-known relationships for translational motion:

$$\left.\begin{aligned} m\ddot{x} &= \sum_{i=1}^{n} (F_i)_x, \\ m\ddot{y} &= \sum_{i=1}^{n} (F_i)_y, \\ m\ddot{z} &= \sum_{i=1}^{n} (F_i)_z. \end{aligned}\right\} \qquad (6.53')$$

The rotation of the missile about the center of gravity, in accordance with the following equations, is referred to as relative motion:

$$\left.\begin{aligned} J_e\ddot{\theta} &= \sum_{j=1}^{n_2} M_{\theta j}, \\ J_e\ddot{\psi} &= \sum_{j=1}^{n_2} M_{\psi j}, \\ J_p\ddot{\varphi} &= \sum_{j=1}^{n_2} M_{\varphi j}. \end{aligned}\right\} \qquad (6.53'')$$

In the systems of equations (6.53') and (6.53") the following denotations have been adopted: $\underline{m}$ is the mass of the rocket missile, at some arbitrary instant of time; $\ddot{x}$, $\ddot{y}$, and $\ddot{z}$ are the second derivatives with respect to time of the coordinates of the center of missile gravity in a ground coordinate system (the components of acceleration along the axes of the ground system of coordinates); $(F_i)_x$, $(F_i)_y$ and $(F_i)_z$ are projections of the i-th components from the system of forces acting on the missile during flight onto the Ox, Oy, and Oz axes; m_1 is the number of forces acting on the missile; J_e is the moment of missile inertia with respect to one of the lateral axes of the connected system of coordinates (Oy' or Oz'), referred to as the equatorial moment of inertia; J_p is the moment of missile inertia with respect to the Ox' axis of the connected coordinate system, referred to in the established terminology as the polar moment of inertia; $\ddot{\vartheta}$, $\ddot{\psi}$, and $\ddot{\varphi}$ are the second derivatives with respect to time of the angular coordinates of the two moving coordinate systems with respect to the ground coordinate system (the components of conditional acceleration with respect to the corresponding axes); $M_{\theta j}$, $M_{\varphi j}$, and $M_{\psi j}$ are the magnitudes of the j-th moment with respect to the corresponding angles from the

total system of moments acting on the missile; n_2 is the number of moments acting on the missile in flight.

Bearing in mind what was said earlier about the system of forces and moments acting on an unguided rocket missile in flight, we will obtain a general system of differential equations of missile motion having the following form:

$$\left.\begin{aligned} m\ddot{x} &= R_x - X_x - Y_x - Z_x, \\ m\ddot{y} &= R_y - mg + Y_y - X_y - Z_y, \\ m\ddot{z} &= R_z - X_z - Y_z - Z_z, \end{aligned}\right\} \qquad (6.54)$$

$$\left.\begin{aligned} J_\vartheta\ddot{\vartheta} &= M_\vartheta - M'_\vartheta, \\ J_\psi\ddot{\psi} &= M_\psi - M'_\psi, \\ J_\varphi\ddot{\varphi} &= M_\varphi - M'_\varphi, \end{aligned}\right\}$$

where R_x, R_y, and R_z are the components of the force of thrust from a rocket engine, along the axes of a ground system of coordinates; mg is the force of gravity (the weight of the missile); if we assume the earth is flat, this force is projected only on Oy'; X_x, Y_y, and X_z are the components of the force of frontal resistance along the coordinate axes; Y_x, Y_y, and Y_z are the corresponding components of lift; Z_x, Z_y, and Z_z are components of lateral force; M_ϑ, M_ψ, and M_φ are the stabilizing aerodynamic moments with respect to the coordinate angles of pitch, yaw, and roll; M'_ϑ, M'_ψ, and M'_φ are the corresponding damping moments.

Generally speaking, the Coriolis force which takes into consideration the rotation of the earth about its own axis should be added to the above-enumerated forces. However, for solid-propellant rocket missiles having a flight range of 50 to 80 km, the Coriolis effect need not be taken into consideration and the system of forces can be considered in the form in which it is presented in Eqs. (6.54).

System (6.54) is somewhat too complex in order to solve it in its general form. In fact, the mass m of the missile changes with respect

to time, at least during the active phase of the flight, i.e., m = = m(t).

The thrust R of a solid-propellant rocket engine also changes with respect to time because, first of all, it can be programmed in some way, and, secondly, because it changes with flight altitude as a result of the drop in the pressure of the surrounding medium. Thus, in the general case

$$R=R(t_{пр}, y),$$

where t_{pr} is the instantaneous instant of time of programmed flight.

Finally, the aerodynamic forces and moments also change with respect to time, and these are functions of altitude and flight velocity:

$$X=X(y, x, \dot{y}, z, t),$$
$$\ldots\ldots\ldots\ldots$$
$$M_\vartheta=M_\vartheta(y, x, \dot{y}, z, t).$$
$$\ldots\ldots\ldots\ldots$$

Taking these remarks with respect to the active forces into consideration, we can write the system of equations (6.54) in expanded form:

$$m(t)\ddot{x}=R_x(t_{пр}, y)-X_x(y, \dot{x}, \dot{y}, \dot{z}, t)-Y_x(y, \dot{x}, \dot{y}, \dot{z}, t)-$$
$$-Z_x(y, \dot{x}, \dot{y}, \dot{z}, t),$$
$$m(t)\ddot{y}=R_y(t_{пр}, y)-mg(y, t)-X_y(y, \dot{x}, \dot{y}, \dot{z}, t)+$$
$$+Y_y(y, \dot{x}, \dot{y}, \dot{z}, t)-Z_y(y, \dot{x}, \dot{y}, \dot{z}, t),$$
$$m(t)\ddot{z}=R_z(t_{пр}, y)-X_z(y, \dot{x}, \dot{y}, \dot{z}, t)-$$
$$-Y_z(y, \dot{x}, \dot{y}, \dot{z}, t)-Z_z(y, \dot{x}, \dot{y}, \dot{z}, t),$$
$$J_z(t)\ddot{\vartheta}=M_\vartheta(y, \dot{x}, \dot{y}, \dot{z}, t)-M'_\vartheta(y, \dot{x}, \dot{y}, \dot{z}, t),$$
$$J_\psi(t)\ddot{\psi}=M_\psi(y, \dot{x}, \dot{y}, \dot{z}, t)-M'_\psi(y, \dot{x}, \dot{y}, \dot{z}, t),$$
$$J_\varphi(t)\ddot{\varphi}=M_\varphi(y, \dot{x}, \dot{y}, \dot{z}, t)-M'_\varphi(y, \dot{x}, \dot{y}, \dot{z}, t).$$

This system consists of six conventional linear differential equations with variable coefficients, a portion of which (for example, the aerodynamic forces) cannot even be presented in analytical form, as formulas which relate the variables $\dot{y}$, $\dot{x}$, $\dot{y}$, ...t.

The cited general system of equations for missile motion is generally simplified for practical application. In this case, the most substantial simplifications are associated with the property of missile stability on the trajectory.

§4. THE CONCEPT OF MISSILE STABILITY ON THE TRAJECTORY

The motion of a missile on its trajectory is regarded as stable if in the case of chance deflection of the missile from the trajectory there arise forces and moments which act to return the missile to its initial trajectory.

In the design of a missile, special measures are taken to provide for missile stability in flight. The flight of a missile on its trajectory can stabilized through the use of tail surfaces (empennage) or rotation (or the combined effect of tail surfaces and rotation). Empennage stabilization is attained as a result of the fact that additional aerodynamic forces act on the tail surfaces, and these forces can return the missile to its initial trajectory in the case of missile deflection. Stabilization by means of rotation is based on the so-called property of gyroscopic stability that is inherent in bodies of certain shape (including the shape of a missile) rotating at a great angle of velocity about its longitudinal axis.

Without dwelling in too great detail at the moment on the problem the stabilization of solid-propellant missiles, we will say only that it would be impossible to fire at some target if chance disturbances (wind gusts, local drops in air density, etc.) could move the missile from its trajectory and cause the missile to continue in its deflected course from the initial flight heading, i.e., if the missile were unstable on its trajectory (Fig. 6.41).

For a stabilized missile trajectory, the latter is an almost

The cited general system of equations for missile motion is generally simplified for practical application. In this case, the most substantial simplifications are associated with the property of missile stability on the trajectory.

§4. THE CONCEPT OF MISSILE STABILITY ON THE TRAJECTORY

The motion of a missile on its trajectory is regarded as stable if in the case of chance deflection of the missile from the trajectory there arise forces and moments which act to return the missile to its initial trajectory.

In the design of a missile, special measures are taken to provide for missile stability in flight. The flight of a missile on its trajectory can stabilized through the use of tail surfaces (empennage) or rotation (or the combined effect of tail surfaces and rotation). Empennage stabilization is attained as a result of the fact that additional aerodynamic forces act on the tail surfaces, and these forces can return the missile to its initial trajectory in the case of missile deflection. Stabilization by means of rotation is based on the so-called property of gyroscopic stability that is inherent in bodies of certain shape (including the shape of a missile) rotating at a great angle of velocity about its longitudinal axis.

Without dwelling in too great detail at the moment on the problem the stabilization of solid-propellant missiles, we will say only that it would be impossible to fire at some target if chance disturbances (wind gusts, local drops in air density, etc.) could move the missile from its trajectory and cause the missile to continue in its deflected course from the initial flight heading, i.e., if the missile were unstable on its trajectory (Fig. 6.41).

For a stabilized missile trajectory, the latter is an almost

ideally flat curve situated in the firing plane. Consequently, if for purposes of studying the motion of such a missile the plane xOy of the ground system of coordinates were made to coincide with the firing plane, the lateral coordinate of the position of the center of missile gravity would be constant and equal to zero, i.e., the third equation in System (6.54) could be eliminated.

Moreover, the property of missile flight stability assumes that the oscillatory motion of a missile about the center of gravity is limited and is damped after the disturbance has been removed. This allows us in certain cases to neglect the equations of rotational motion in System (6.54). As a result, for known stable flight System (6.54) is substantially simplified.

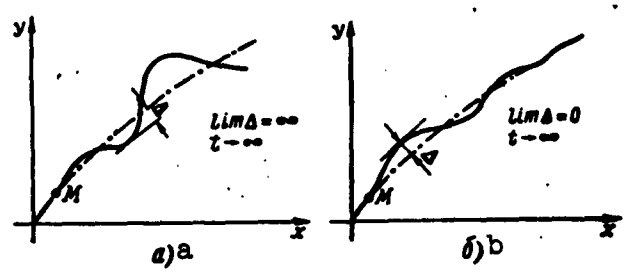

Fig. 6.41. Unstable and stable missile motion on the trajectory a) Unstable motion; b) stable motion; M) the point on the trajectory at which a certain disturbance is applied on the missile by external forces

§5. SYSTEM OF EQUATIONS FOR MISSILE MOTION STABILIZED BOTH ALONG THE TRAJECTORY AND IN THE FIRING PLANE

Having taken into consideratinn the above with respect to the features encountered in the stabilized flight of missiles, we obtain the system of equations of missile motion in the firing plane in the following form

$$\left.\begin{aligned} m\ddot{x} &= R_x - X_x - Y_x - Z_x, \\ m\ddot{y} &= R_y - mg - X_y + Y_y - Z_y \end{aligned}\right\} \qquad (6.55')$$

for missiles stabilized with tail surfaces, or

$$\left.\begin{aligned} m\ddot{x} &= R_x - X_x - Y_x - Z_x, \\ m\ddot{y} &= R_y - mg - X_y + Y_y - Z_y, \\ J_z\ddot{\varphi} &= M_z - M_z' \end{aligned}\right\} \qquad (6.55'')$$

for turbojet missiles, stabilized by rotation.

In the preliminary calculations, the forces Y and Z and Eqs. (6.55') and (6.55") may be assumed to be equal to zero, so that

$$Y_{x(y)}=0,\ Z_{x(y)}=0,$$

and the system will be

$$\left.\begin{aligned} m\ddot{x}&=R_x-X_x,\\ m\ddot{y}&=R_y-mg-X_y,\\ (J_p\ddot{\varphi}&=M_\varphi-M'_\varphi). \end{aligned}\right\} \tag{6.55}$$

System (6.55) can be presented in another somewhat more convenient form, by examining the translational motion of the center of missile gravity in a system whose axes coincide at each and every instant of time with the direction of the normal and the tangent to the trajectory (a special case of the connected system of coordinates) rather than in a ground system of coordinates.

The equations of translational motion in projections onto the normal and the tangent take the following form:

$$\left.\begin{aligned} m\dot{v}&=R-mg\sin\theta-X,\\ mv\dot{\theta}&=Y-mg\cos\theta. \end{aligned}\right\} \tag{6.56'}$$

The total system of equations for this case, assuming flight stability, will be:

$$\left.\begin{aligned} m\dot{v}&=R-mg\sin\theta-X,\\ mv\dot{\theta}&=Y-mg\cos\theta,\\ (J_p\ddot{\varphi}&=M_\varphi-M'_\varphi). \end{aligned}\right\} \tag{6.56}$$

The systems of equations (6.55) and (6.56) have been simplified only in a formal fashion in comparison with a general system of equation of missile motion (6.54); the number of equations has been reduced and the components of the forces Y and Z have been dropped from the equations of translational motion. For all intents and purposes, however, these systems are as complex to solve as is System (6.54).

§6. SIMPLIFIED SYSTEM OF EQUATIONS FOR THE MOTION OF THE CENTER OF MISSILE GRAVITY IN AIRLESS SPACE

Let us imagine a missile in the form a material point having a mass m and let us examine the motion of this point in airless space.

Since the missile is being regarded as a point, there is no sense in considering the rotational motion of the missile, i.e., the system of equations describing the motion of such a missile is reduced to two equations of translational motion (for the case of stabilized flight in the firing plane).

In view of the fact that the missile motion is assumed to be taking place in airless space, the aerodynamic forces of missile interaction with the surrounding medium are naturally assumed to be equal to zero, so that the corresponding equations are simplified to the following form:

$$\begin{aligned} m\ddot{x} &= R_x, \\ m\ddot{y} &= R_y - mg. \end{aligned}$$

The force of thrust R (R_x, R_y) acts on the missile only during the active phase of the flight. The magnitude of the active phase, in comparison with the entire trajectory, is relatively small, and in approximate terms it may be held that the missile acquires a certain velocity virtually at the launch site as a result of the action of engine thrust.

Taking these comments and assumptions into consideration, we can present the motion of a missile along its trajectory in the form of the following system of equations:

$$\left.\begin{aligned} m\ddot{x} &= 0, \\ m\ddot{y} &= -mg \end{aligned}\right\} \qquad (6.57)$$

with the initial condition that $v = v_a$ (the velocity at the end of the active phase of the trajectory, calculated in accordance with the K.E.

Tsiolkovskiy formula) at t = 0.

System (6.57) is referred to as a simplified system of equations for the motion of the center of missile gravity in airless space. This system can be integrated in quadratures.

§7. CALCULATION OF MISSILE TRAJECTORY ELEMENTS

In calculating the trajectory of a missile, we are primarily interested in missile flight range (for a certain initial flight velocity) or we want to know the required initial velocity in order to enable the missile to attain a certain given flight range. Of secondary importance, as a rule, are questions relating to the laws governing missile motion along a trajectory, i.e., relating to the time sequence in which the missile will pass individual points on the trajectory, and how missile flight velocity will change in this case, etc.

In first approximation, the answer to all these questions can be attained by integrating System (6.57). Since in the derivation of this system we employed such gross assumptions as to neglect the forces of aerodynamic interaction between the missile and the approaching airstream and the elimination of the active phase from our consideration, etc., the corresponding calculation results will be somewhat limited in nature.

Estimate of limit trajectory elements by integrating the simplified system of equations

Let us examine System (6.57):

$$m\ddot{x}=0,$$
$$m\ddot{y}=-mg.$$

Since the missile mass m in the equation of this system is constant and not equal to zero, it is possible to present this system in the following form:

$$\ddot{x}=0,$$
$$\ddot{y}=-g.$$

The integration of the last equations can be reduced to the following.

The equation

$$\ddot{x}=\frac{dx^2}{dt^2}=\frac{d}{dt}\left(\frac{dx}{dt}\right)=\frac{d}{dt}(\dot{x})=0$$

indicates that

$$\dot{x}=\text{const}=C_1.$$

Equation

$$\ddot{y}=\frac{d^2y}{dt^2}=\frac{d}{dt}(\dot{y})=-g$$

after separation of the variables leads to the equation

$$d(\dot{y})=-g\,dt,$$

which, after integration

$$\int d(\dot{y})=\int -g\,dt$$

yields

$$\dot{y}=-gt+C_2.$$

The integration constants C_1 and C_2 are determined from the initial conditions:

at $t = 0$, $v = v_a$ (the velocity at the end of the active phase), i.e., at $t = 0$

$$\dot{x}=v_x=v_{ax}=v_a\cos\theta_0,$$
$$\dot{y}=v_y=v_{ay}=v_a\sin\theta_0.$$

Thus, we will obtain

$$\left.\begin{aligned}\ddot{x}&=0\\ \ddot{y}&=-g\end{aligned}\right\}\quad\left.\begin{aligned}\dot{x}&=C_1=v_a\cos\theta,\\ \dot{y}&=-gt+C_2=-gt+v_a\sin\theta.\end{aligned}\right.$$

Repeated integration yields:

$$\dot{x}=\frac{dx}{dt}=C_1,$$

whence after the separation of the variables and integrating

$$x=C_1t+C_3$$

and correspondingly

$$\dot{y} = \frac{dy}{dt} = -gt + C_3,$$
$$y = -\frac{gt^2}{2} + C_3 t + C_4.$$

Bearing in mind that the coordinate origin coincides with the point of missile launch, we define the integration constants C_3 and C_4, as being equal to zero. In conclusion, we will obtain

$$\left.\begin{aligned} \ddot{x} &= 0 \\ \ddot{y} &= -g \end{aligned}\right\} \quad \left.\begin{aligned} \dot{x} &= v_0 \cos\theta_0 \\ \dot{y} &= v_0 \sin\theta_0 - gt \end{aligned}\right\} \quad \left.\begin{aligned} x &= v_0 t \cos\theta_0 \\ y &= v_0 t \sin\theta_0 - \frac{gt^2}{2}, \end{aligned}\right\} \tag{6.58}$$

where the equalities

$$\left.\begin{aligned} \ddot{x} &= 0, \\ \ddot{y} &= -g \end{aligned}\right\} \tag{6.58'}$$

show how the acceleration components of missile motion change with time; the equations

$$\left.\begin{aligned} \dot{x} &= v_0 \cos\theta_0, \\ \dot{y} &= v_0 \sin\theta_0 - gt \end{aligned}\right\} \tag{6.58"}$$

show how the velocity components of missile motion change; and finally, the equations

$$\left.\begin{aligned} x &= v_0 t \cos\theta_0 \\ y &= v_0 t \sin\theta_0 - \frac{gt^2}{2} \end{aligned}\right\} \tag{6.58'''}$$

show how the coordinates of missile position on the trajectory change in time with respect to altitude and range.

The last relationships make it possible to estimate the maximum flight range of the missile. The formula for maximum range is most simply derived by employing the following conditions: at $x = X_{max}$, $y = 0$. From the following equation

$$y = v_0 t \sin\theta_0 - \frac{gt^2}{2} = 0$$

we will find that $y = 0$ is valid in the following case:

$$t_1 = 0,$$
$$t_2 = \frac{2v_a \sin\theta_0}{g}.$$

The case $t_1 = 0$ corresponds to the position of the missile at the point of missile launch and, consequently, the value of time t_2 corresponds to the position of the missile at point M on the trajectory (Fig. 6.42). Consequently,

$$X_{max} = x(t_2) = v_a \frac{2v_a \sin\theta_0}{g} \cos\theta_0 = \frac{v_a^2}{g} \sin 2\theta_0. \tag{6.59}$$

We see that $X_{max} = f(v_a, \theta_0)$, i.e., given the same velocity at the end of the active flight phase, the maximum range will be a function of the initial θ_0. In this case, the greatest value of X_{max} will correspond to the following case:

$$\sin 2\theta_0 = 1,$$
$$\theta_0 = \frac{1}{2} \arcsin 1 = 45°.$$

and amounts to

$$(X_{max})_{max} = \frac{v_a^2}{g}. \tag{6.60}$$

Solving Formula (6.59) for v_a, we find that in order to achieve a range of X_{max} the missile must attain a velocity no less than

$$v_{a\,min} = \sqrt{\frac{g X_{max}}{\sin 2\theta_0}}, \tag{6.61}$$

if the initial launch angle (the setting angle of the weapon launch installation) amounts to θ_0 degrees to the horizon.

We will now determine the maximum altitude H_{max} of missile ascent along the trajectory. This quantity can be determined, for example, from the maximum of the function $y = f(x)$. In our case, $y = f(x)$ is presented in the form of two equations:

$$y = \varphi_1(t),$$
$$x = \varphi_2(t),$$

and it is therefore necessary at the beginning to eliminate the para-

meter t and express y directly in terms of x. The appropriate transformations will result in a relationship of the following form:

$$y = -\frac{g}{2v_0^2\cos^2\theta_0}x^2 + \frac{\sin\theta_0}{\cos\theta_0}x. \tag{6.62}$$

Equation (6.62) is the equation of the missile's flight trajectory. If we examine the nature of the curve corresponding to this equation, we can demonstrate that the curve is a parabola shifted with respect to the coordinate origin and we can show that this curve has an axis of symmetry that is parallel to the Oy axis (Fig. 6.43).

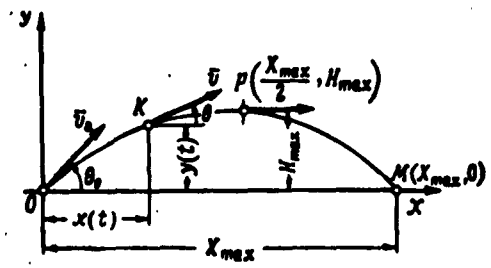

Fig. 6.42. Trajectory diagram for calculation of maximum missile flight range in airless space

The maximum of Function (6.62) has the following form:

$$\frac{dy}{dx} = 0,$$

$$\frac{dy}{dx} = -\frac{g}{2v_0^2\cos^2\theta_0}2x + \frac{\sin\theta_0}{\cos\theta_0} = 0,$$

whence the value of x at which y attains its maximum value of H_{max} is determined in the following form:

$$x_{H\,max} = \frac{v_0^2\sin\theta_0\cos\theta_0}{g} = \frac{v_0^2}{2g}\sin 2\theta = \frac{X_{max}}{2}, \tag{6.63}$$

and the value of H_{max} itself will be

$$H_{max} = y(x_{H\,max}) = -\frac{g}{2v_0^2\cos^2\theta_0}\frac{v_0^4\sin^2\theta_0\cos^2\theta_0}{g^2} + \frac{\sin\theta_0}{\cos\theta_0}\frac{v_0^2\sin\theta_0\cos\theta_0}{g}$$

or after reducing and canceling

$$H_{max} = \frac{v_0^2}{2g}\sin^2\theta_0. \tag{6.64}$$

It is clear that the greatest value of H_{max} will be found in the case of $\sin\theta_0 = 1$, i.e., for $\theta_0 = 90^\circ$ (vertical ascent)

$$(H_{max})_{max} = \frac{v_0^2}{2g}. \tag{6.65}$$

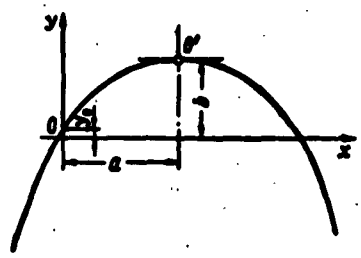

Fig. 6.43. Parabola of missile trajectory in airless space. y_0) altitude coordinate of point of missile launch; 0') trajectory peak

We can see from (6.65) that the minimum velocity required to attain an altitude of H_{max} in vertical flight will be

$$v_{0\,min} = \sqrt{2gH_{max}}. \qquad (6.66)$$

Relationship (6.58") makes it possible to estimate the time in which the rocket missile will attain a certain altitude y* or will reach a distance x* from the launch site. These time, respectively, will be:

$$\left.\begin{aligned} t_{x^*} &= \frac{x^*}{v_0 \cos\theta_0}, \\ t_{y^*} &= \frac{v_0}{g}\sin\theta_0 \pm \sqrt{\frac{v_0^2}{g^2}\sin^2\theta_0 - \frac{2y^*}{g}}. \end{aligned}\right\} \qquad (6.67)$$

By the way, the total flight time for the missile can be determined from Eq. (6.67) in the following form

or

$$\left.\begin{aligned} t_{max} &= \frac{X_{max}}{v_0 \cos\theta_0} \text{ (from condition } x^* = X_{max}) \\ t_{max} &= \frac{2v_0 \sin\theta_0}{g} \text{ (from condition } y^* = 0). \end{aligned}\right\} \qquad (6.68)$$

It is easy to see that both of these relationships are equivalent.

The cited calculation relationships yield results that are substantially different from those observed in practice. This is not surprising, since in the derivation of these relationships excessively gross assumptions were employed, and the most important of these being the failure to take into consideration the aerodynamic forces. This method is employed only for tentative calculations in the preliminary design of a rocket missile.

Substantially more exact results are obtained if Systems (6.55) or (6.56) are integrated in the place of the simplfied system; however,

it is impossible to carry out the calculation in the general form and it becomes necessary to resort to approximate numerical integration methods. The integration results are obtained not in the form of formulas but in the form of tables in which the basic elements of the trajectory are determined for various values of flight time. The method of the numerical integration of the equations of motion for a solid-propellant rocket missile is presented below.

Calculation of Trajectory Elements by the Method of the Numerical Integration of the Equations of Missile Motion in the Firing Plane

It basically makes no difference which systems of equations — (6.55) or (6.56) — is used to calculate the trajectory elements by the method of numerical integration. However, it is held that System (6.56) is, nevertheless, more convenient, and it is this system, written in the following form, that is most frequently used:

$$\left.\begin{aligned} m(t)\frac{dv}{dt} &= R(t) - m(t)g\sin\theta(t) - X(t), \\ m(t)v(t)\frac{d\theta}{dt} &= -m(t)g\cos\theta(t), \\ \frac{dy}{dt} &= v_y = v(t)\sin\theta(t), \\ \frac{dx}{dt} &= v_x = v(t)\cos\theta(t), \end{aligned}\right| \qquad (6.69)$$

where the last two equations are clear from the definition of the concept of flight velocity.

From (6.69) we obtain the following system of calculation equations:

$$\left.\begin{aligned} \Delta v &= \left(\frac{R_t}{m_t} - g\sin\theta_t - \frac{X_t}{m_t}\right)\Delta t, \\ v_{t+\Delta t} &= v_t + \Delta v, \\ \Delta\theta &= -\frac{g\cos\theta_t}{v_t}\Delta t, \\ \theta_{t+\Delta t} &= \theta_t + \Delta\theta, \\ \Delta y &= (v_t\sin\theta_t)\Delta t, \\ y_{t+\Delta t} &= y_t + \Delta y, \\ \Delta x &= (v_t\cos\theta_t)\Delta t, \\ x_{t+\Delta t} &= x_t + \Delta x. \end{aligned}\right| \qquad (6.70)$$

To solve this system, the initial parameters of motion must be given: v_0 is the initial velocity of missile motion, equal to zero or the velocity v_{skh} which the missile attains as it leaves the guide rails of the launch installation as a function of the selection of the coordinate origin; θ_0 is the initial angle of trajectory rise, equal to the setting angle of the launch installation; x_0 and y_0 are the coordinates of the point selected as the coordinate origin (the beginning or the end of the weapon launch installation). We can maintain, with sufficient accuracy, that

$$x_0=0,\ y_0=0.$$

Moreover, the missile characteristics $X = X(M)$ and the rocket-engine characteristics $R = R(t)$ and $m = m(t)$ must be given. The calculation sequence can, in this case, be presented in the following form:

1. Let us assume the integration interval Δt, i.e., the time interval in which the values of the trajectory elements will be derived by calculation. In selecting Δt it is necessary to bear in mind that with an increase in Δt the accuracy of the calculation diminishes, and if somewhat too low values of Δt are selected the calculations become extremely cumbersome. Generally, for the active phase of the trajectory Δt is assumed to be equal to

$$\Delta t = 0.001 - 0.01 \text{ sec.},$$

and for the passive phase of the trajectory

$$\Delta t = 0.1 - 1.0 \text{ sec.}$$

2. For sake of simplicity, let $x_0 = y_0 = 0$ and $v_0 = v_{skh}$; the initial setting angle is θ_0. Further, let the engine be operating at a constant thrust $R = \text{const}$, so that the mass of the missile changes in accordance with the following function:

$$m(t)=m_0-m_{sek}t,$$

where m_0 is the initial mass of the missile; m_{sek} is the per-second

propellant flow rate, and the force of resistance is given in the form of some flight velocity function X = X(M) such as, for example, in the form of a graph or a table.

Given these initial conditions and missile and engine characteristics, after Δt the missile will have the following velocity:

$$v_1 = v_0 + \Delta v = v_{cx} + \Delta v_1,$$

in which case

$$\Delta v_1 = \left(\frac{R}{m_0} - g \sin \theta_0 - \frac{X(M_0)}{m_0}\right) \Delta t,$$

where

$$M_0 = \frac{v_{cx}}{a_0};$$

a_0 is the speed of sound corresponding to a flight altitude of y_0.

The angle θ after Δt changes by

$$\Delta \theta_1 = -\frac{g \cos \theta}{v_{cx}} \Delta t$$

and amounts to

$$\theta_1 = \theta_0 + \Delta \theta_1.$$

The missile will be at a point having the following coordinates

$$x_1 = x_0 + \Delta x_1 = \Delta x_1,$$
$$y_1 = y_0 + \Delta y_1 = \Delta y_1,$$

where

$$\Delta x_1 = (v_{cx} \cos \theta_0) \Delta t,$$
$$\Delta y_1 = (v_{cx} \sin \theta_0) \Delta t.$$

3. In the subsequent time interval, the missile velocity will increase to

$$v_2 = v_1 + \Delta v_2,$$

where

$$\Delta v_2 = \left(\frac{R}{m_0 - m_{cx} \Delta t} - g \sin \theta_1 - \frac{X(M_1)}{m_0 - m_{cx} \Delta t}\right) \Delta t;$$
$$M_1 = \frac{v_1}{a_1};$$

a_1 is the speed of sound corresponding to a flight altitude of y_1.

The angle θ of the trajectory will change by

$$\Delta\theta_2 = -\frac{g\cos\theta_1}{v_1}\Delta t$$

and will amount to

$$\theta_2 = \theta_1 + \Delta\theta_2.$$

The missile will shift to the point having the following coordinates:

$$x_2 = x_1 + \Delta x_2,$$
$$y_2 = y_1 + \Delta y_2,$$

where

$$\Delta x_2 = (v_1 \cos\theta_1)\,\Delta t;$$
$$\Delta y_2 = (v_1 \sin\theta_2)\,\Delta t.$$

4. As a result, we will obtain a series of successive points 1, 2, 3... in space with known parameters of missile motion at each point (Fig. 6.44), determined in their totality by the trajectory of the missile flight.

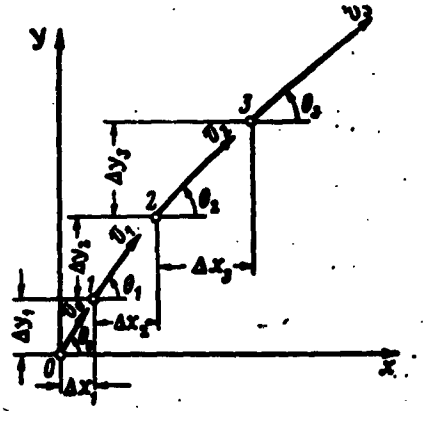

Fig. 6.44. Calculation of trajectory by means of numerical integration of equations of missile motion

During the calculation process, there will be an instant in which the engine ceases to function. The corresponding point A determines the end of the active flight phase and establishes the missile parameters for the end of the active phase.

It is interesting to point out that if prior to point A the nature of the trajectory was a strong function of the parameters and features of the missile engine, beyond this point - throughout the entire passive phase of the trajectory - the nature of motion is determined only by the parameters of missile motion at A and the ballistic coefficient of the missile. This makes it possible to calculate in ad-

vance the trajectory elements for various values of v_a, θ_a, and C_0, reducing the calculation result into a ballistic table, as is the widespread practice in design procedures.

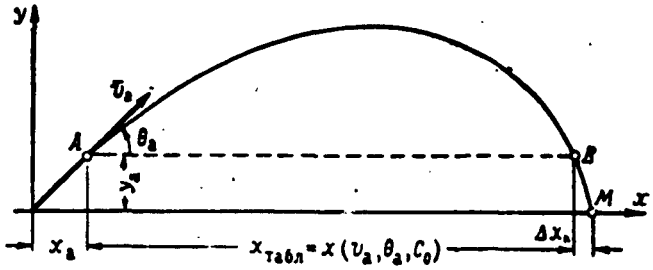

Fig. 6.45. Calculation diagram for trajectory to determine trajectory elements through utilization of ballistic tables. $x_a y_a$) coordinates of the end of the active trajectory phase; v_a) velocity at the end of the active trajectory phase; θ_a) the angle of inclination of the tangent to the trajectory at the end of the active phase.

It should be stipulated that the tables should be employed for the calculation not of the entire passive phase of the trajectory but only of arc AB of this segment (Fig. 6.45), otherwise it being impossible to generalize the calculation results for missiles having various active phases.

The segment BM should be calculated separately for each individual case. However, as a rule, this is not done and in first approximation the following assumptions are made

$$\Delta x_в = \frac{2}{3} x_a,$$

$$v_M \approx v_B,$$

where v_B is the velocity at point B; v_M is the velocity at point M.

In conclusion, the total missile flight range is defined as the sum

$$X_{max} = x_a + x_{табл} + \Delta x_в,$$

while taking into consideration

$$\Delta x_a = \frac{2}{3} x_a$$

$$X_{max} \approx x_{табл} + 1{,}667\, x_a. \qquad (6.71)$$

where x_a is obtained as a result of the numerical integration of the active trajectory phase; x_{tabl} is taken from tables.

The maximum trajectory height is defined as

$$H_{max} = y_{табл} + y_a. \qquad (6.72)$$

The results of the trajectory calculation by the method of numerical integration differ subtantially from the case in which the simplified system of equations of motion was employed, where the effect of aerodynamic forces was neglected. For example, the flight range may amount to only 0.5 - 0.6, the trajectory altitude may amount to only 0.7 - 0.8, the distance to the peak of the trajectory may amount to only 0.7 - 0.8, and the velocity at the target may amount to only 0.3 – 0.4 of the values for the corresponding quantities (X_{max}, H_{max}, $X_{max}/2$,...) calculated according to the formulas for flight in airless space.

For contemporary rocket artillery , requiring increased firing accuracy, it is necessary to make extensive use of the method of numerical integration of the equations of motion which make it possible to carry out calculations with high accuracy. In this case, the difficulty in carrying out these calculations can be substantially reduced through the use of computer equipment.

§8. STABILIZATION OF MISSILE ON TRAJECTORY

As has already been indicated, in order to provide for firing accuracy against the target the missile must be stabilized along its trajectory. This means that measures must be implemented in order to restrict the possible deviations of the missile axis from the direc-

tion of the tangent to the trajectory.

It has been established that a missile can be stabilized on its trajectory either by the introduction of special stabilization elements into the design of the missile - tail surfaces (stabilizers) - or by using the effect of gyroscopic stability (stabilization through rotation). Both stabilization methods are used successfully in the practical design of various types of rocket missiles

Selection of Tail Surfaces which will provide for Stabilization with the Given Stability Margin

The idea of stabilizing rockets by means of tail surfaces is based on the following property of bodies moving in a resisting medium; it turns out that such a body moves stably, i.e., its seeks to preserve its initial orientation during its motion only in the case in which the center of the body's gravity is situated in front of the center of pressure. And conversely, if the center of gravity is situated behind the center of pressure, the position of the body on the trajectory becomes unstable and upon the interference of random disturbances, and this interference can result in a change in position. Let the center of gravity of a missile flying along a certain trajectory be situated in front of the center of pressure (Fig. 6.46), and let the axis of the missile be deflected through an angle α ($\pm\ \alpha$) from the direction of the tangent to the trajectory at some instant of time under the action of a random disturbance. We can see from Fig. 6.46 that in this case there will appear a moment of aerodynamic forces directed against the direction of the increasing angle α, i.e., seeking to return the missile to its initial position. The initial position of the missile is stable on the trajectory.

Let us now examine the motion of a missile whose center of pressure is situated in front of the center of gravity (Fig. 6.47). From

the diagrams presented in this figure we can see that in this case, given the random appearance of a positive or negative angle of attack, there will appear a moment which seeks to increase the angle α, i.e., to deflect the missile even further from its initial position. In this case, the missile is unstable on its trajectory.

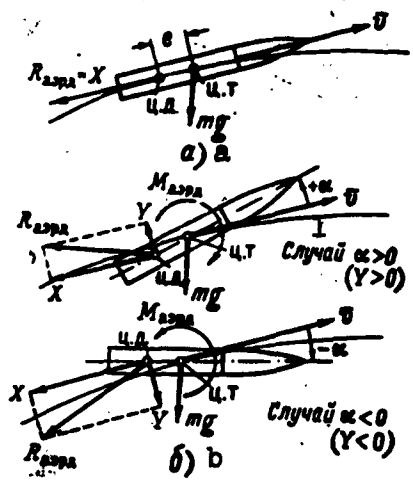

Fig. 6.46. Diagram of mutual position of center of gravity and center of pressure which provide for missile stability (the forward position of the center of gravity with respect to the center of pressure). a) initial position of missile on trajectory; b) disturbed position of missile on trajectory M_{aerd}) aerodynamic moment; 1) case $\alpha > 0$.

Thus a nonrotating missile is stable on its trajectory only in the case in which the center of missile gravity lies in front of the center of pressure. The degree of stability is a function of the distance e between the above-mentioned two points. The quantitative measure of stability is generally evaluated in terms of the stability margin by which we mean the ratio

$$\xi_{уст} = \frac{e}{x_к} 100\ \%, \qquad (6.73)$$

where $e = x_{ts.d} - x_{ts.t}$ is the eccentricity of the missile; x_k is the length is the length of the missile airframe.

The center of gravity for a solid-propellant rocket missile without tail surfaces and consisting of a warhead and a rocket part will be situated at a point shifted somewhat forward of the geometric center of the missile. However, the center of missile pressure lies somewhere in the vicinity of missile-warhead gravity. Thus the mutual positions of the center of gravity and the center of pressure coincide exactly with the case in which there are no stability properties on the

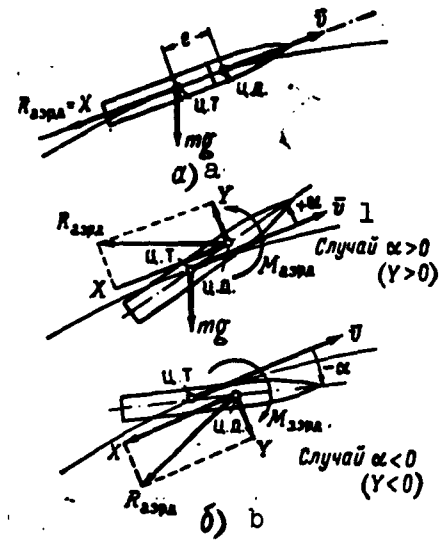

Fig. 6.47. Diagram of mutual position of center of gravity and center of pressure resulting in missile instability (rear position of center of gravity with respect to center of pressure a) initial positon of missile on trajectory; b) disturbed position of missile on trajectory; 1) case $\alpha > 0$.

trajectory, so that a rocket missile without tail surfaces, as a rule, is unstable in flight.

For the stabilization of such a missile, it is necessary markedly to shift the center of pressure to the rear, behind the center of gravity. In this case, if the missile has to have a stability margin of $\xi\%$, the center of pressure must be shifted to a point having the following coordinate:

$$x_{ц.д} = x_{ц.т} + \frac{\xi_{уст}}{100} x_{ц}. \qquad (6.74)$$

We know from mechanics that if there is a system of parallel forces referred to some resultant force, then with the addition of an additional force to the system, the point of application of this new resultant shifts toward the point of application of this force by a certain definite magnitude proportional to the value of the newly applied force. In accordance with this, to shift the center of missile pressure backward behind the center of gravity it is necessary for additional aerodynamic forces to appear in the tail portion of the missile.

It is well known that in terms of their physical nature the aerodynamic forces represent the result of the interaction between the approaching stream and those surfaces or bodies situated in this stream. Therefore, to shift the center of missile pressure backward

to the tail portion, stabilizers are employed here as sources for this additional force.

Stabilizers are made, as a rule, in the form of thin plates and installed parallel to the axes of the missile in order to reduce the drag component to its absolute minimum in the interaction of the stabilizers with the stream, i.e., so that the introduction of the stabilizers into the design of the missile shifts the center of missile pressure in the required direction by the necessary magnitude, and if possible without increasing the total resistance of the missile.

In accordance with (6.45)

$$x_{a.a} = \frac{C_{Y\,a} x_{a.a.a} + C_{Y\,op} x_{a.a.o}}{C_{Y\,a} + C_{Y\,op}}.$$

On the other hand, in order to provide for missile stabilization with a stability margin of ξ_{ust}%, it is necessary for the center of pressure to be situated at a point having the following coordinate:

$$x_{a.a} = x_{a.t} + \frac{\xi_{yct}}{100} x_a.$$

Hence, for the stabilization of the given solid-propellant missile ($x_{ts.t}$, x_k, $x_{ts.d.k}$, $C_{Y\,k}$,...) it is necessary to select such tail surfaces for the missile as to yield

$$x_{a.t} + \frac{\xi_{yct}}{100} x_a = \frac{C_{Y\,a} x_{a.a.a} + C_{Y\,op} x_{a.a.o}}{C_{Y\,a} + C_{Y\,op}}. \qquad (6.75)$$

The derived equation contains, generally speaking, two unknowns – $C_{Y\,op}$ and $x_{ts.d.o}$; however, bearing in mind that the tail surfaces are situated in the rear part of the missile and the position of the center of pressure for the basic types of stabilizers is approximately known (see Fig. 6.34), the magnitude of $x_{ts.d.o}$ can be assumed quite accurately, so that (6.75) will, in its capacity as an unknown, contain only the parameter $C_{Y\,op}$.

Taking the above into consideration, we will have

$$C_{y\,on}=C_{y\,k}\frac{x_{u.t}-x_{u.d.k}+\frac{\xi_{yct}}{100}x_k}{x_{u.d.o}-x_{u.t}-\frac{\xi_{yct}}{100}x_k}.$$

In first approximation, it is expedient to assume $x_{ts.d.o} = x_k$ and the above-mentioned relationship lends itself to solution and the quantity $C_{Y\ op}$ is easily determined:

$$C_{y\,on}=C_{y\,k}\frac{x_{u.t}-x_{u.d.k}+\frac{\xi_{yct}}{100}x_k}{x_k-x_{u.t}-\frac{\xi_{yct}}{100}x_k}, \tag{6.76}$$

where $C_{Y\ k}$ is calculated in accordance with (6.16) or (6.19) as a function of missile flight velocity; $x_{ts.t}$ is the coordinate of the center of missile gravity, determined in the weight calculation; x_k is the length of the missile airframe; $x_{ts.d.k}$ is the coordinate of the center of pressure for the airframe of the missile, assumed to be equal to 0.5 x_k for M < 1 and calculated with (6.44), if the missile exhibits supersonic velocity; ξ_{ust}% is the given stability margin.

Thus in order to stabilize the missile with a stability margin of ξ_{ust}%, it is necessary to select tail surfaces for which the coefficient of lift would coincide with (6.76). The geometric dimensions of such tail surfaces can be determined for various flight velocities through the utilization of (6.13'), (6.18'), and (6.18"). In first approximation calculations we can assume an elongation λ_{op} = 2.0 and for sake of simplicity we can examine stabilizers that are rectangular in shape in the in-plan view. After a rough estimate of the required tail-surface dimensions, the initial parameters are corrected and the final calculations are carried out with selection of the optimum shape for the stabilizer fin under the given conditions.

If the calculation shows that the required tail surfaces are somewhat too large with respect to dimensions and therefore unaccept-

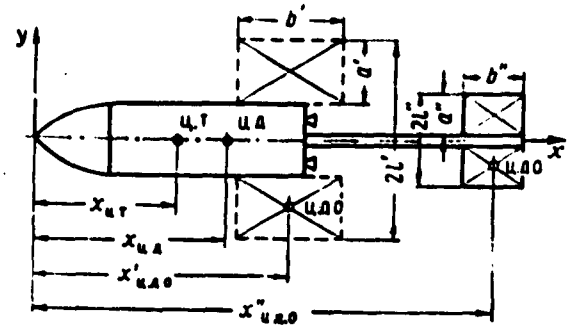

Fig. 6.48. Comparative dimensions of tail surfaces required for the stabilization of a missile for cases of various position distances from coordinate origin.

able, it becomes necessary either to move the tail surfaces further back along the tail (or even behind the tail, as is shown in Fig. 6.48), or to increase the number of stabilizer fins, or to undertake even more radical means, including the entire redesigning of the missile.

On the other hand, cases are possible in which the designed tail surfaces for the version in which the stabilizers are positioned at the rear have intolerably small dimensions. In these cases, the tail surfaces must be moved forward (Fig. 6.49). The final solution to the problem of selecting the shape, dimensions, and position of the tail surfaces depends on the results obtained in wind-tunnel tests of a missile with theoretically calculated tail surfaces. In recent times, wind-tunnel experimentation has given way, in a number of countries, to free-flight tests or tests on rocket sleds.

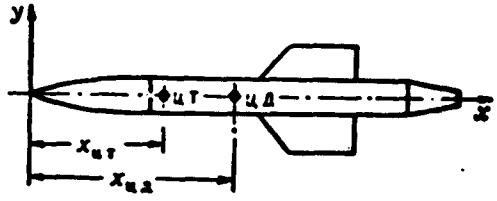

Fig. 6.49. Missile with tail surfaces shifted forward

Calculation of an angle for nozzle outlet to provide for stability in the case of turbojet missile

A missile with a rear center of gravity can be stabilized on its tra-

jectory not only by means of tail surfaces, thus shifting the center of pressure behind the center of gravity but also by causing the missile to rotate about its longitudinal axis with a certain definite angular velocity.

Stabilization by means of rotation is based on the application of the so-called gyroscopic effect. Let us examine this effect on the well-known example of its appearance in the case of a spinning top. We know that for bodies having a small-support-base area, the position of vertical equilibrium is unstable. Such a body need be deflected only through an angle α at which the resultant of the gravity forces no longer intersects the support-base area, when a toppling moment arises, thus forcing the body out of its equilibrium position; the body will fall as a result.

The vertical position of the top, in the general case, is also unstable. However, if the top is forced to spin at a great angular velocity about its longitudinal axes, forces will appear to prevent the top from falling as it moves from its position of vertical equilibrium. The vertical position of a spinning top thus seems to become stable. The random disturbances which deflect the axis of the top from the vertical only produce the additional motion of the top's axis about the initial direction (Fig. 6.50). In gyroscope theory, this motion is referred to as the precession of the gyroscope axis. The conic angle α of the precession and the angular velocity ω_{pr} of the precession are determined by the magnitude of the active disturbance (P or M_{vneshn}), the angular velocity ω_0 of rotation, and the geometric characteristics of the spinning body. All other conditions being equal, the greater ω_0, the smaller the angle α, i.e., the more stable the vertical position of the top.

Let us now compare a top with a missile moving along its trajec-

tory and rotating at a velocity ω_0 about its longitudinal axis. If the center of pressure is in a forward position, a missile of this type is much like the top, fixed to its trajectory at point 0 which coincides with the center of missile gravity (Fig. 6.51). In analogy with the example of the top, in the case of random deflections of the missile axis from its original zero position, the missile seeks not to move further away from its initial position, but rather it seeks to keep that position constant. In this case, missile axis precession appears, and the angular amplitude is given by the magnitude of ω_0, the geometric characteristics of the missile, and the magnitude of the external disturbing moment.

The property of gyroscopic stability appears only in the case of sufficiently great angular velocity of rotation. In first approximation it may be maintained that stability will be guaranteed if

$$n > \frac{2\sqrt{RJ_e e}}{J_p}, \tag{6.77}$$

where n is the number of revolutions of the rotating body; R is the active disturbing force; e is the eccentricity of the missile; J_p and J_e are, respectively, the polar and equatorial moments of inertia.

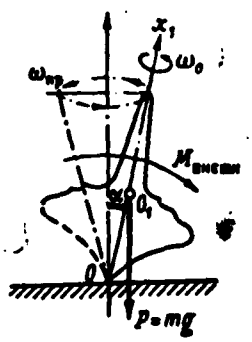

Fig. 6.50. Diagram of gyroscopic stability of top. x_1) longitudinal axis of top; 0) support point; 0_1) point of application of disturbing external force.

Taking (6.77) into consideration we find that the problem of missile flight stabilization by means of rotation consists in providing for the rotation of the missile over the entire trajectory, and an angular velocity not lower than the corresponding number of revolutions:

$$n_{min} = \frac{2\sqrt{RJ_e e}}{J_p}.$$

The rotation of the missile about its longitudinal axis is described by the following equation:

$$J_p\ddot{\varphi}=\sum M_\varphi.$$

where the active stabilizing moment and the damping moment of resistance enter into ΣM_φ.

If the missile is caused to rotate by means of nozzle-turbines, the stabilizing moment acts on the missile only during the active phase of the trajectory, for which

$$J_p\ddot{\varphi}_{\dot{\varphi}\to\omega_{max}}=M_{cr}-M'_\varphi\approx M_{cr}. \tag{6.78}$$

since the moment of resistance is generally small in comparison with M_{st}. During the passive phase, $M_{st} = 0$ and the equation of rotational motion for the missile is written in the following form:

$$J_p\ddot{\varphi}_{\omega_{max}\to\omega_k}=-M'_\varphi. \tag{6.79}$$

We can see that during the passive phase of the trajectory the angular velocity of rotation gradually dimenishes to some ω_k which corresponds to the following number of revolutions

$$n_k=\frac{30\omega_k}{\pi}.$$

Hence, to provide for stability over the entire flight trajectory it is necessary to turn the missile so during the active phase that it exhibits the following to the end of the flight:

$$n_k>\frac{2\sqrt{RJ_{\varphi e}}}{J_p}. \tag{6.80}$$

The ω_{max} required for this at the end of the active phase is easily found from (6.79):

$$J_p\ddot{\varphi}=-M'_\varphi,$$

$$\ddot{\varphi}=\frac{d\omega}{dt},$$

$$J_p\frac{d\omega}{dt}=-M'_\varphi.$$

whence, separating the variables, we will obtain

$$\int_{\omega_{max}}^{\omega_k} d\omega = -\frac{1}{J_p}\int_{t_a}^{t_k} M'_\varphi\, dt,$$

which yields

$$\omega_k = \omega_{max} - \frac{1}{J_p}\int_{t_a}^{t_k} M'_\varphi\, dt. \qquad (6.81')$$

The relationship between M'_φ and time, not expressed explicitly, makes it necessary to calculate the second integral numerically:

$$\omega_k = \omega_{max} - \frac{1}{J_p}\sum_n (M'_\varphi)_i \Delta t, \qquad (6.81'')$$

where the summing is carried out over the entire Δt into which the time interval $t_a - t_k$ has been divided. If we take (6.80) into consideration, the required ω_{max} at the end of the active phase is determined in the following form:

$$\omega_{max} > \frac{\pi}{30}\frac{2\sqrt{RJ_{\varphi e}}}{J_p} + \frac{1}{J_p}\sum_n (M'_\varphi)_i \Delta t. \qquad (6.82)$$

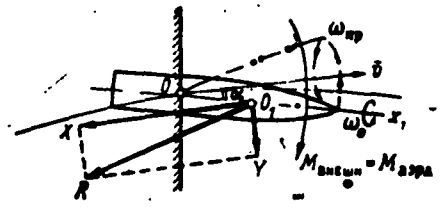

Fig. 6.51. Diagram of gyroscopic missile stability

Assuming that we can employ the following approximate equation for the active phase of the flight:

$$J_p\ddot{\varphi} = M_{ст},$$

we will find the required moment M_{st}:

$$J_p\frac{d\omega}{dt} = M_{ст},$$

$$d\omega = \frac{M_{ст}}{J_p}dt,$$

$$\int_0^{\omega_{max}} d\omega = \int_0^{t_p}\frac{M_{ст}}{J_p}dt.$$

The quantity M_{st} may be regarded as constant for the entire active phase of the trajectory. However, the value of J_p changes as a result of the consumption of propellant. Taking this into considera-

tion,

$$\omega_{max} = M_{cr} \int_0^{t_p} \frac{1}{J_p} dt \qquad (6.83')$$

or in a form convenient for numerical calculation,

$$\omega_{max} = M_{cr} \sum_m \frac{1}{(J_p)_t} \Delta t, \qquad (6.83")$$

where $\sum_m \frac{1}{(J_p)_t} \Delta t$ is computed over all $\underline{m}$ intervals of Δt into which the flight time for the active trajectory phase has been divided.

From (6.83") the required stabilizing moment is determined in the following form:

$$M_{cr} = \frac{\omega_{max}}{\sum_m \frac{1}{(J_p)_t} \Delta t},$$

which with consideration of (6.82) yields

$$M_{cr} = \frac{\frac{\pi}{30} \frac{2\sqrt{RJ_p\varepsilon}}{J_p} + \frac{1}{J_p} \sum_n (M'_\varphi)_t \Delta t}{\sum_m \frac{1}{(J_p)_t} \Delta t}. \qquad (6.84)$$

Here J_p and J_e characterize the properties of the missile during the passive phase of the trajectory, and M'_φ is regarded as a given aerodynamic characteristic of the missile, so that the values of $(M'_\varphi)_t$ for any instant of time can be found from a graph or table; $(J_p)_t$ is calculated for various points of the active phase of the flight, taking into consideration the gradual burning up of the propellant.

The stabilizing moment is developed as a result of the engine-thrust component which is directed perpendicular to the axis of the missile and which appears when the nozzle outlet is slanted at an angle ψ to the axis of the missile (Fig. 6.52). The magnitude of this moment

$$M_{cr} = R_{r1} \sin\psi \frac{d'}{2} x_c = -R_r \sin\psi \frac{d'}{2}, \qquad (6.85)$$

where R_{t1} is the magnitude of thrust referred to a single nozzle; n_s is the number of nozzles; d'/2 is the arm of nozzle position with respect to the longitudinal axis of the missile; R_t is the total thrust developed by the engine.

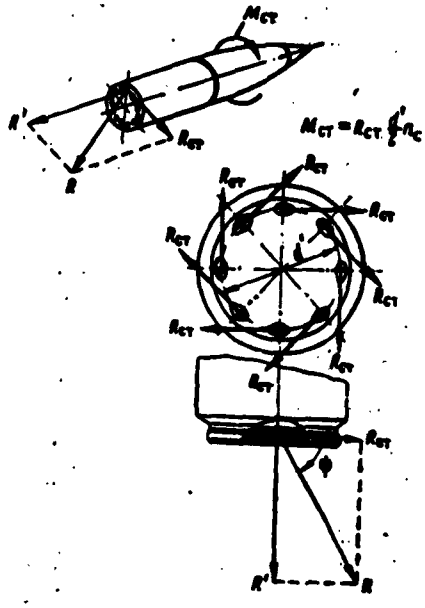

Fig. 6.52. Diagram of the appearance of the stability moment in the case of a turbojet missile

From (6.85) the required angle of nozzle outlet is defined as

$$\psi = \arcsin\left(\frac{M_{ст}}{R_t \frac{d'}{2}}\right), \qquad (6.86)$$

where M_{st} is calculated in accordance with (6.84); d' is the diameter of the circle around which the nozzle turbines have been positioned.

With this nozzle outlet angle, the turbine develops a moment M_{st} adequate to maintain the missile stable over the entire flight trajectory.

The proposed method of calculating the required nozzle outlet angle in the case of turboject missiles is extremely tentative, since the reduction of missile motion to the elementary diagram of a top is a rather gross approximation.

§ 9. SCATTERING OF UNGUIDED MISSILES OVER TARGET AREA. CONCEPT OF FIRING ACCURACY

The flight trajectory of an actual missile is always somewhat different from a theoretical trajectory.

A missile is made industrially with definite dimensional and weight allowances; in conclusion, the ballistic coefficients of individual missiles

$$C_i = \frac{1000 i d^2}{q}$$

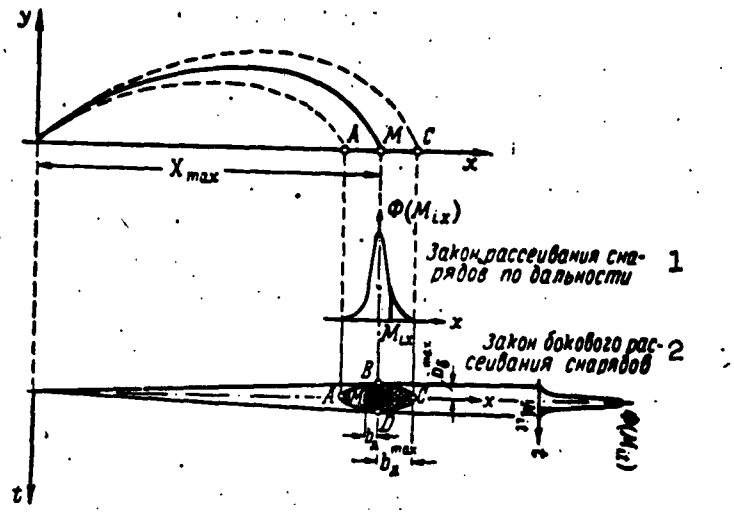

Fig. 6.53. Regional elements of target area over which unguided rocket missiles are scattered. M_{ix}) Probability of missile striking i-th point along x axis of scattering region; $\Phi(M_{ix})$) function of probability distribution of missile striking i-th point along x axis of scattering region; M_{it}) probability of missile striking i-th point along t axis of scattering region; $\Phi(M_{it})$) function of probability distribution of missiles striking i-th point along t axis of scattering region; 1) missile scattering function with respect to range; 2) lateral missile scattering function

differ somewhat from one another and amount to

$$C_i = C_{теор} + \Delta C_i,$$

where C_i is the true ballistic coefficient of the missile; C_{teor} is the theoretical value of the ballistic coefficient; ΔC_i is the difference in magnitude between the ballistic coefficient and its theoretical value.

The scattering of the interior ballistic parameters for each individual engine and the difference in weight between various missiles leads to a situation in which the missile velocity at the end of the

active phase of the flight is not identical for the various missiles:

$$(\Delta v_{max})_i = (\Delta v_{max})_{теор} + \Delta(\Delta v_{max})_i,$$

where $(\Delta v_{max})_{teor}$ is calculated in accordance with the K.E. Tsiolkovskiy formula.

Finally, the possible eccentricity or distortion of the reaction-force vector with respect to the longitudinal axis of the nozzle and the defects in the mounting of the stabilizers on the missile may serve as sources resulting in the additional deflection of a true missile from its theoretical curve.

An important consequence of the deflection of missile flight trajectories from the theoretical trajectories is the fact that the points of missile incidence do not coincide with one another and the calculated point M. The distribution of the points M_1 over the target area about point M is generally referred to as the scattering of missiles. It has been established that the scattering of unguided missiles is subject to a number of quantitative relationships: all of the points are located within the limits of the so-called scattering ellipse (Fig. 6.53), and in this case it becomes possible to construct a curve which characterizes, for example, the distribution of the number of points of incidence along the given direction of the scattering ellipse. This curve coincides with the classical curve from the theory of probability, said curve describing the normal probability-distribution function for the occurence of some random event (for example, the missiles striking the given point within the given area). The points A, B, C, and D which coincide with the ends of the semiaxes of the scattering ellipse characterize the magnitude of the maximum probable deviation of the points of missile incidence from the point M with respect to range and lateral direction. It is the general practice to denote the corresponding distances as follows:

$AM = B_A^{max}$; $BM = B_B^{max}$

and to employ the range and lateral direction points of missile incidence as the maximum deflection.

We can discern a ractangular region within the scattering ellipse within which limits ~ 50% of all strikes are distributed. In evaluating the effectiveness of the firing, generally not the entire scattering ellipse is taken into consideration, but precisely this region, the coordinates of whose boundaries are, respectively, referred to as the probable deviation of the missile from the target in terms of range B_d and in terms of lateral direction B_b.

The probable deflection is an inadequate characteristic of scattering. A more general evaluation of scattering is offered by the dimensionless parameter

$$\frac{B_d B_b}{X_{max}},$$

referred to as the combat or firing accuracy of missiles with respect to range (or with respect to side direction).

To calculate the firing accuracy, it is necessary to determine the probable deflection with respect to range and lateral direction for a missile of any given design and known firing conditions.

In first approximation, for this purpose we can use the simplified calculation of relationships in which it is assumed that the individual factors responsible for deflecting a missile from the target are indepent in their effect on said deflection of the missile.

Since the deviation from the calculated values of the ballistic coefficient, the velocity at the end of the active phase, the angle of pitch ϑ at the end of the active phase, the eccentricity of the distortion of the reaction-force vector, and the defects in the mounting of stabilizers on the missile can be regarded as the primary factors

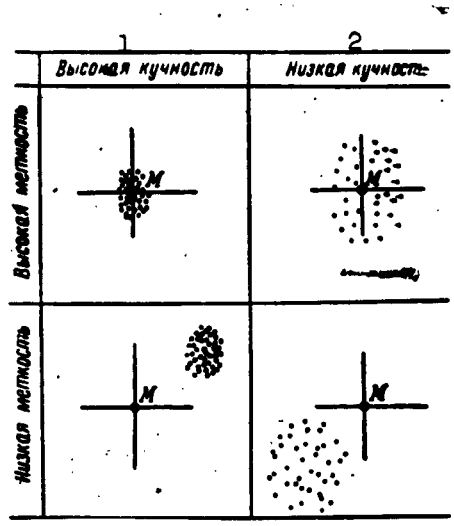

Fig. 6.54. Illustration of concept of firing accuracy and grouping 1) Close grouping; 2) scattered grouping

responsible for the scattering of range in the case of rocket missiles with tail surfaces, the formula for the evaluation of B_d of a missile with tail surfaces can be presented in the following form:

$$B_d=\sqrt{(\Delta x_c)^2+(\Delta x_v)^2+(\Delta x_\vartheta)^2+(\Delta x_R)^2+(\Delta x_{on})^2}, \quad (6.87$$

where B_d is the probable deviation of the missile from the calculated point of impact, with respect to range; Δx_s is the deviation with respect to range resulting from the fact that the ballistic coefficient for the missile does not coincide with the calculated coefficient:

$$C_i=C_{reop}+\Delta C_i.$$

The quantity Δx_s is generally calculated in the following manner

$$\Delta x_c=\frac{\partial x}{\partial C}\Delta C_i,$$

where $\partial x/\partial C$ characterizes the degree to which the magnitude of the ballistic coefficient exerts influence on the flight range; Δx_v is the deviation, with respect to range, resulting from the inconstancy of velocity at the end of the active phase:

$$\Delta x_v=\frac{\partial x}{\partial v}\Delta v_{max\,i};$$

Δx_ϑ, Δx_R, Δx_{op} are, respectively, the deviations with respect to range resulting from the remaining factors which affect range.

To calculate the individual components of Δx_k for various cases, we can employ a number of various relationships. These relationships, as a rule, are derived through the generalization of data from a great number of monitoring missile launchings and these relationships are comparatively simple calculation formulas that have been completed by

means of experimental graphs and tables.

An estimate of the mean-probable deviation of a missile with tail surfaces in the lateral direction (along the OZ axis) can be carried out in accordance with the following formula:

$$B_6 = \sqrt{(\Delta z_\psi)^2 + (\Delta z_{\bar{R}})^2 + (\Delta z_{st})^2}, \qquad (6.88)$$

since the lateral deviation occurs primarily because of the deviation of the missile in the firing plane from the direction of $\Delta\psi$ and the errors that are associated with the direction of the reaction-force vector, as well as with the fact that the stabilizers have not been mounted in an ideal fashion on the missile.

For the specific calculation of Δz_ψ, $\Delta z_{\bar{R}}$, and Δz_{st}, we employ the empirical calculation relationships and the statistical data from experimental launching.

Turbojet missiles do not have any tail surfaces and are characterized by the fact that because of the great number of nozzles the total eccentricity of the nozzle assembly, and consequently, the eccentricity of the thrust vector $\vec{R}_t$, are virtually equal to zero.

In this connection, for such missiles

$$B_z = \sqrt{(\Delta x'_c)^2 + (\Delta x'_v)^2 + (\Delta x'_v)^2}, \qquad (6.89)$$

where $\Delta x'_s$, $\Delta x'_v$, and $\Delta x'_v$, despite the similar notation, are calculated in accordance with formulas that are different from the formulas for the case of missiles with tail surfaces, although even these may be identical in form.

The cited relationships make it possible, in first approximation, to estimate the probable deflections and firing accuracy (grouping) of the reaction-thrust missiles stabilized by means of tail surfaces or rotation for the given firing conditions. Finally, the scattering and firing-accuracy (grouping) parameters are verified through firing-range tests of experimental missile models.

In conclusion, we should turn our attention to the difference between the concept of firing accuracy (grouping) and accuracy (precision). The difference between these concepts is clearly shown in the diagrams presented in Fig. 6.54.

[Footnotes]

Manuscript Page No.

228 A detailed discussion of these can be found, for example, in the following books: A. Lokk, Upravleniye smaryadami. IL [Control of Missiles. Foreign Literature Press], 1958. V.I. Feodos'yev and G.B. Sinyarev. Vvedeniye v raketnuyu tekhniku, Oborongiz [Introduction into Rocket Engineering, State Defense Industry Press], 1956 etc.

321 Detailed tables for $\overline{p}_0 = \overline{p}_0\ (M/\beta_0)$ are presented, for example, in the book by N.F. Krasnov "Aerodinamika" [Aerodynamics," Part 2. Certain Problems in Applied Aerodynamics. MVTU Press of the Moscow Bauman Higher Technical School], 1954.

334 The problems dealing with the calculation of instantaneous missile characteristics are discussed in greater detail, for example, in the book by N.F. Krasnov entitled "Aerodinamika" [Part 2. Certain Problems in Applied Aerodynamics. MVTU Press], 1954.

[Transliterated Symbols]

288 ц.д = ts.d = tsentr davleniya = center of pressure

288 ц.д = ts.d = tsentr tyazhesti = center of gravity

293 tg = tan

294 $F_{дв} = F_{dv} = F_{dvizheniye} = F_{motion}$

294 $F_{сопр} = F_{sopr} = F_{soprotivleniye} = F_{resistance}$

297 $v_{цил} = v_{tsil} = v_{tsilindr} = v_{cylinder}$

Manuscript Page No.

[List of Transliterated Symbols (Continued)]

297 $v_{ус.кон} = v_{us.kon} = v_{usechennyy\ konus} = v_{truncated\ cone}$

299 $P_{сн} = P_{sn} = P_{snaryad} = P_{missile}$

303 $x_{б.ч} = x_{b.ch} = x_{boyeveya\ chast'} = x_{warhead}$

303 $x_{р.ч} = x_{r.ch} = x_{raketnya\ chast'} = x_{rocket\ part}$

310 $\lambda_{оп} = \lambda_{op} = \lambda_{opereniye} = \lambda_{tail\ surfaces}$

310 $b_{ср} = b_{sr} = b_{srednyaya\ khordda} = b_{middle\ chord}$

310 $\beta_{п} = \beta_{p} = \beta_{perednaya\ (kromka)} = \beta_{leading\ (edge)}$

310 $\beta_{з} = \beta_{z} = \beta_{zadnaya\ (kromka)} = \beta_{trailing\ (edge)}$

310 $y_{т} = y_{t} = y_{tolshchina} = y_{thickness}$

310 $l_{ск} = l_{sk} = l_{skos} = l_{sweepback\ angle}$

310 $b_{кр} = b_{kr} = b_{kornevaya\ (khorda)} = b_{root\ (chord)}$

310 $b_{кц} = b_{kts} = b_{kontsevaya\ (khorda)} = b_{tip\ (chord)}$

315 $s_{бок} = s_{bok} = s_{bokovaya\ (poverkhnost')} = s_{side\ (surface)}$

315 $s_{м} = s_{m} = s_{midel'} = s_{midsection}$

316 $l_{к} = l_{k} = l_{korpus} = l_{airframe}$

334 $M_{эф} = M_{ef} = M_{effektivnyy} = M_{effective}$

334 $M_{ст} = M_{st} = M_{stabiliziruyusachiy} = M_{stabilizing}$

334 $M_{дэмпф} = M_{dempf} = M_{dempriruyushchiy} = M_{damping}$

337 $t_{пр} = t_{pr} = t_{programmiruyemyy\ (polet)} = t_{programmed\ (flight)}$

Chapter 7

TESTS OF EXPERIMENTAL MODELS OF ROCKET MISSILES

The testing of experimental models of rocket missiles is carried out by each planning organization in accordance with its own program; it is therefore impossible to speak of a uniform method for the carrying out of such tests; moreover, the range of problems associated with the testing of rocket missiles is so extensive that a separate book would be required for their elucidation. The present chapter gives only some general considerations involved in the testing of rocket missiles.

The approximate nature of the theoretical calculations into which it becomes necessary to introduce various simplifications as well as to employ the experimental data taken from similar classes of missiles and the present inability to use theoretical calculations and the fact that the required data can be obtained only experimentally makes it necessary for the missile to be tested and checked through test-stand firings and firing-range launchings.

§1. STATIC TESTS OF A ROCKET ENGINE

The design of a missile and its engine are adjusted during the static tests in accordance with the requirements imposed by the tactical-technical designation of the missile, and during these tests the igniter and powder grains are selected and checked.

The successful solution of these problems depends primarily on the coincidence of the interior-ballistic characteristics of an actual engine and those of the engine being designed. Therefore, the following

missile characteristics are taken during the static tests:

1) the pressure curve;

2) the reaction-force curve;

3) the total reaction-force impulse.

Before the hot-firing tests are carried out, any engine (we have reference here to the shell) must of necessity be checked for strength and hermetic sealing, and this is, as a rule, carried out in a specially equipped shop of the production plant. The engine is set into a device, the outlet orifice is closed, all of the other openings are sealed, and then water under pressure greater than the maximum theoretical pressure produced by the combustion gases from the chamber is fed through the engine. The engine is kept under this pressure for a certain period of time in order to enable all of the destructive processes which may possibly be attributed to the effect of pressure to make themselves felt.

After the pressure is reduced, the engine is carefully checked and if no failures of the structure are observed, the hermetic sealing of the engine is checked, and this is generally carried out by employing the same device as was used for strength tests. The method used to test hermetic sealing were somewhat different. It is not water that is fed into the chamber, but air or kerosene. It is impossible to test an engine for strength with air, since in the case of engine failure the effect would be similar to that of an explosion, whereas a liquid can burst only a portion of a weak structure, or penetrate a weak spot, which of course is very much safer.

With the use of air (in the case of small volumes) hermetic sealing is checked by immersing the engine in water or covering its outer surface with a soapy solution. In either case, the air bubbles which form indicate the degree of the hermetic sealing of the structure.

Hermetic-sealing tests are generally carried out under a pressure equal to the maximum magnitude of the theoretical pressure to be produced in the combustion chamber.

An engine having passed the above-described production tests can be used for the subsequent static operations.

The pressure curve is generally taken by means of sensing elements and oscillographs of various designs. The records can be obtained, for example, by means of an aneroid sensing element and a tensometric oscillograph (Fig. 7.1). An installation assembled in this manner functions as follows. The pressure of the exhaust gases is transmitted to the sensing element 3 through the tubing 2. Here a change in pressure is recorded by the sensing element 4 - an aneroid chamber - (Fig. 7.2), which is connected to the potentiometer 5 which changes the resistance of the electric circuit. This change in resistance produces a pulse that is transmitted to the oscillograph where the change in pressure with time is recorded on a special paper tape. The tape with its recording is processed in a photography dark room and the pressure curve is obtained (Fig. 7.3), and the beginning of engine operation (the point at which the curve rises above the zero level) and the end of engine operation are noted on this curve.

On the basis of these extreme points and the calibrated graph it is possible to carry out an analysis of engine operation. For example, the time of engine operation is calculated from the line of time marking 1. In proceeding from point A on the pressure curve of interest to us to the origin we count 20 peaks, and we know (from the oscillograph scale) that each peak is equal to 1/20 sec; consequently, the time is $1/20 \times 20 = 1$ sec.

The magnitude of pressure at, for example, this same point A is determined as simply. For this, the distance from the zero level to

point A on the pressure curve is measured on the oscillogram and the magnitude of the pressure at point A is determined by carrying out measurements further along the calibrated graph.

The calibrated graph is constructed in the following manner. In the installation employed for the measuring of pressure, instead of the engine, a press is connected to the sensing element. Then the sensing element is subjected to step-wise pressure increases such as 10, 20 and 30 atm, etc., and each pressure increase is recorded by the oscillograph on paper. Subsequently a graph is constructed with the distance between the zero line and the pressure line plotted along one axis and the magnitude of pressure plotted along the other axis. The pressure curve can, of course, be obtained in such other ways as, for example, by means of a loop oscillograph and the sensing unit of a deformation measuring device.

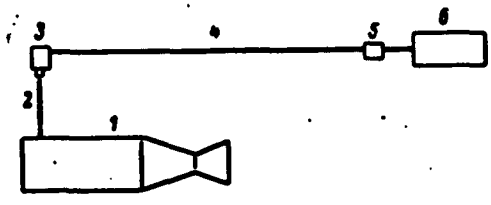

Fig. 7.1. Diagram of installation for determination of pressure curve. 1) Engine being tested; 2) tubing through which gas is fed from engine to sensing element; 3) aneroid sensing elements; 4) cable; 5) attachment; 6) oscillograph.

The thrust characteristics of the engine are obtained on specially equipped test stands. Here the engine is fastened onto a moving cradle (Fig. 7.4) from which the force developed by the engine is transmitted to a receiving device. A dynamometer (Fig. 7. can serve as such a receiving device.

The operating principle of such a unit is quite simple. The force from the engine is transmitted from the cradle of the test-stand installation through the coupling rod to the dynamometer where it is transformed into pressure whose magnitude is indicated by the manometer that is connected to the dynamometer. The dynamometer is calibrated prior to the test, i.e., regularly increasing loads are applied

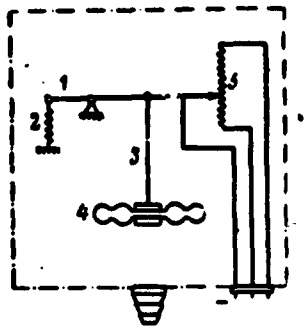

Fig. 7.2. Basic circuit of sensing element. 1) Wiper rod; 2) return spring; 3) transmission-instrument multiplier; 4) sensing mechanism; 5) potentiometer.

to the coupling rod: 500, 1000 kg, etc., and the corresponding manometer readings are marked. In accordance with the derived data it becomes possible to construct a calibrated graph - the loads on the coupling rod, in kilograms, are plotted along one axis, and the manometer readings, in atmospheres, are plotted along the other axis.

In addition to test-stand installations equipped with dynamometers, engine thrust is also measured on test-stand installations equipped with round scales to which the thrust developed by the engine is transmitted from the cradle by means of a special lever system.

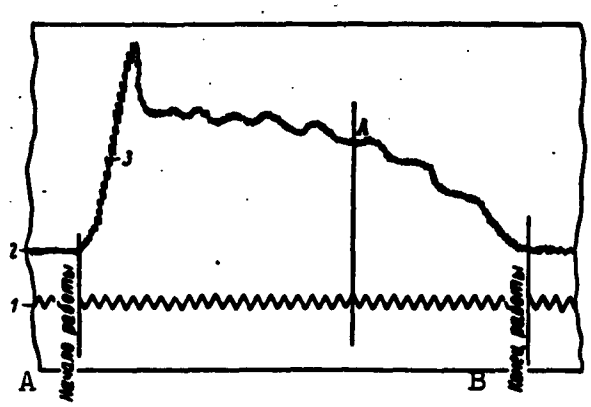

Fig. 7.3. Pressure curve recorded on paper tape by means of oscillograph. 1) Time mark; 2) zero level; 3) pressure curve; A) beginning of operation B) end of operation

To derive the magnitude of the total reaction-force impulse, we frequently employ the graph for the change in thrust developed by the engine with respect to time.

In the case of engines that are in operation for long periods of time, this graph can be constructed on the basis of the points measured

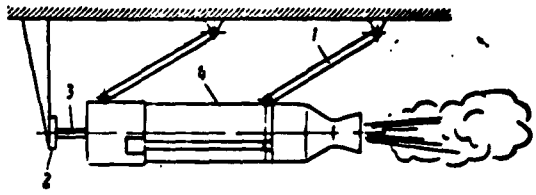

Fig. 7.4. Simplified diagram of testing installation. 1) Rocking cradle 2) dynamometer; 3) dynamometer coupling rod; 4) engine being tested.

at definite intervals of engine-operating time, and the construction of this graph can be carried out in accordance with one of the methods described above. However, this method for obtaining the reaction-force curve yields extremely approximate results. It is preferable to write this curve automatically. For this purpose we can use a test-stand installation equipped with a dynamometer.

Instead of manometers, the sensing element employed to detect the pressure is connected to the dynamometer and the operation is then carried out in the same manner as the derivation of the pressure curve. The only difference here is in the calibration of the sensing element. In this case, the calibration is carried out by applying step-wise loads such as, for example, 500, 1000 kg, etc., to the dynamometer, and each increase is marked by means of an oscillograph. Thus the calibrated graph is constructed in the following coordinates: the distance of the reaction-force curve from zero level, i.e., force in kg.

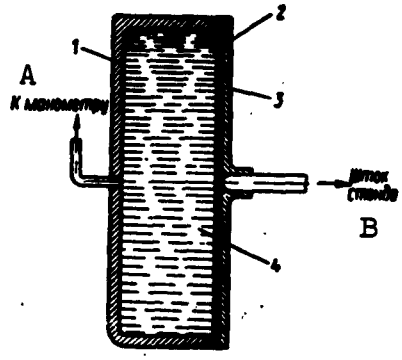

Fig. 7.5. Diagram of dynamometer: 1) Frame of dynamometer; 2) flexible padding; 3) frame lid; 4) oil; A) to manometer; B) coupling rod to stand

The total impulse can be obtained by integrating the reaction-force curves that have been derived by means of the oscillograph, with this curve scaled down to millimeter graph paper; then the area beneath this curve is calculated either by means a planimeter or by means of counting the boxes on this millimeter graph paper contained within the reaction-force curve.

To obtain the magnitude of impulse directly, it is necessary to multiply the computed area by a scale. For example, the area calculated according to boxes is equal to 2000 mm^2, and we know that 1 mm along the axis of ordinates corresponds to 5 kg of thrust, and 1 mm along the axis of abcissas relates to 2 seconds of engine operation. Then the magnitude of the impulse will be equal to

$$J = 2000\ (1/5 \cdot 2) = 200\ kg \cdot sec.$$

In certain cases, if necessary, additional tests of the missile's combustion chamber are carried out, and the following determinations, for example, are made:

1) the powder burning rate in various sections of the chamber;

2) the heat losses in the combustion chamber;

3) the eccentricity of the reaction force, etc.

We will dwell in some detail on the most interesting tests - the determination of the powder burning rate. For this purpose a combustion chamber made of special transparent material is fabricated, and this chamber has an inside profile that is identical to the combustion chamber being designed. Powder grains selected for the engine being designed are burned in this chamber. The process of burning the grains is recorded on film by means of a motion-picture camera. Since the filming rate is known, the film can be used to determine the burning rate for the powder.

In the case of an engine in operation for long periods of time, the powder burning rate can be determined in a simpler manner, i.e., by burning the powder and interrupting the burning. Of course, here as well as in the previous case, it is necessary to have a special chamber. However, this chamber differs from a conventional chamber only in that a device to eject the charge from combustion chamber is installed in the engines used for the measurement of the burning rate.

The rate is measured directly in the following manner. A second-timer is connected and synchronized with the engine start. Upon completion of an earlier set time, this device is actuated and the powder charge is ejected from the combustion chamber into some space (a barrel, a tank, etc.) filled with water. The extinguished powder grains are measured.

This operation is repeated several times, increasing the time intervals for the burning each time, and each time the extinguished grain is measured. The obtained results are evaluated and the powder-burning rate is thus determined.

Thorough experimental investigations of the operation of a solid-propellant engine make it possible to coordinate the theory of solid-propellant rocket missiles with experiment and to refine the basic parameters required for the remaining calculations.

It should be pointed out that combustion chambers from regular rocket missiles can sometimes be employed as the experimental chambers in static tests, and holes can be drilled and connection pipes welded to the walls of such chambers. But as a rule, special thick-walled chambers are used for these tasks, since such chambers make it possible to undertake repeated starts. Such chambers are equipped with diaphragms of various designs, as well as with an assembly of nozzles having various throat diameters and various outlet shapes; here, if only the pressure in the chamber is being investigated (rather than the reaction force), it is possible to use a nozzle without a diverging outlet section - the so-called eyelet nozzle.

The combustion chamber is prepared for the test in the following manner. A nozzle with a definite d_{kr} corresponding to the given charging conditions and the anticipated calculated pressure is selected. Then, a weighed specimen of an igniter is selected and charged into

the combustion chamber; all of the instruments are mounted and the final completed assembly is installed on the test stand. After a check of the readiness of the system, the engine is started on the stand and the appropriate readings for the subsequent evaluation are taken.

Up to this point we have described static tests for elements of interior ballistics, but the test-stand conditions can also be employed to carry out tests for elements of the exterior ballistics.

The most common method of deriving the aerodynamic characteristics is the testing of missile models or actual missiles in wind tunnels. In essence, this is a structure that consists of a tube through which a blower accelerates air. The object being tested (or a model of this object) - depending on the dimensions of the tube - is mounted in the tube in such a fashion as to become immobile, and thus the wind tunnel reflects a situation that is opposite to that actually encountered in the flight of a missile through the air, but which, of course, produces no change whatsoever in the aerodynamic characteristics.

At the same time, the fact that the object being tested is immobile is convenient from the standpoint of employing measuring devices whose measurement accuracy is substantially higher than it would be in the case of instruments used with a body moving with respect to a fixed medium (for example, air).

Moreover, the possibility of creating an artificial stream of air makes it possible to select the conditions for the experiment so as to more closely approximate the actual conditions of missile flight. Since missile flight under actual conditions takes place in a fixed undisturbed medium such as air, it is necessary to create similar conditions in the wind tunnel. If the missile is simply mounted on a support that is not fixed in place, and with a blower to di-

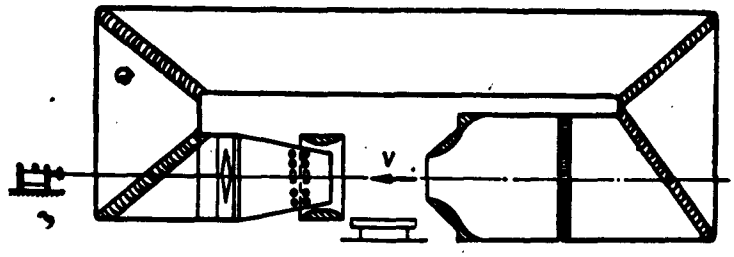

Fig. 7.6. Diagram of wind tunnel

rect a stream of air against the missile, the stream in this case would develop considerable turbulence beyond the blower and exhibit a variable velocity both in terms of magnitude as well as in terms of direction. In addition, the stream would also be subject to strong pulsations. All of these shortcomings have gradually been eliminated in the design of wind tunnels and at the present time a wind tunnel is a complex and highly refined mechanism which can reproduce extremely accurately the disposition and magnitude of aerodynamic forces on a body flying through the air.

Figure 7.6 shows the diagram of a wind tunnel. Structurally, this wind tunnel is a closed circuit with an open working section. The air passes from the working section - the narrowest portion of the tunnel - to an expanding receiver attachment. Beyond the receiver fitting (diffuser), there is a cylindrical liner which contains the blower. Beyond the blower, the stream of air changes its direction of motion through an angle of 90° and flows through the so-called first bend in the tube. Subsequently, the air passes through the second and third bends of the tube, each of which involves a 90° turn, and the air then enters into the forward chamber - the widest portion of the tube (tunnel). Here we have a rectification grid and a fitting which compress the stream and accelerate it. In order to reduce losses, special shaped blades have been installed in each of the turns.

By testing a missile in a wind tunnel it is possible to determine the coefficient C_x of frontal resistance, the position of the center of pressure, the coefficient C_y of lift, etc.

§2. FIRING-RANGE TESTS OF ROCKET MISSILES

After completion of the static tests of the missile, firing-range tests are carried out. Here, as a rule, the flight of a missile over the initial section of the trajectory is first checked, i.e., the correctness of the manner in which the missile is made to leave its launching installation and its entry into the given trajectory, as well as the correspondence between the magnitudes of calculated and actual initial velocity of missile motion over the trajectory. Then the over-all flight range of the missile is checked, and finally, the effectiveness of the missile is investigated in the following manner.

Firing-Accuracy Tests of Rocket Missiles

Firing-accuracy (grouping) tests are carried out with individual shots into the target area or according to a screen, over the entire effective range of the launching installation, both in the vertical and horizontal planes.

The coordinates of the points of incidence (explosion) of the missile at the target area can be determined in two ways:

directly, by measuring with a measuring tape and by marking the direction; the accuracy of the measurement must not be lower than 1 mm;

by a triangulation method involving the use of optical instruments.

In fire against a shell-hole screen, the shell-hole coordinates (1, 2, 3, etc.) are taken from a coordinate grid plotted onto the screen before the firing (Fig. 7.7).

The results obtained in the firing are evaluated in accordance with following formulas:

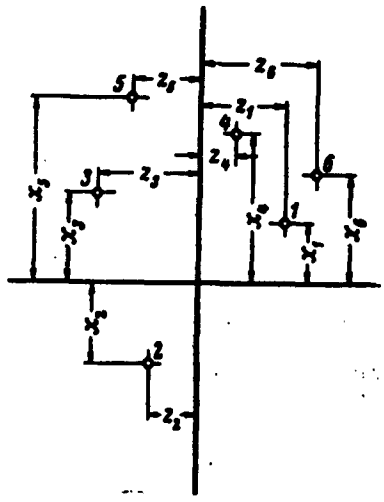

Fig. 7.7. Appearance of shell-hole screen after evaluation

$$x_0=\frac{\sum_{i=1}^{n} x_i}{n},\quad z_0=\frac{\sum_{i=1}^{n} z_i}{n},$$

where x_0 and z_0 are the coordinates of the central point of incidence; x_i and z_i are coordinates of the points of incidence for individual missiles; n is the number of shots counted.

The coordinates of the points of missile explosions obtained in the control group of shots makes it possible to evaluate the probable deviation of the missile in terms of lateral direction and range, and these are calculated as follows:

$$b_b=0{,}6745\frac{\sqrt{\sum_{i=1}^{n}(x_i-x_0)^2}}{n-1},$$

$$b_d=0{,}6745\frac{\sqrt{\sum_{i=1}^{n}(z_i-z_0)^2}}{n-1},$$

where b_b is the probable lateral deviation; b_d is the probable deviation with respect to range.

With known firing range x, missile firing accuracy in terms of lateral direction and range will, respectively, be equal to (b_b/x) and (b_d/x).

The obtained firing accuracy must correspond to that set in the tactical-technical requirements.

With great divergence of a missile from the group with respect to range and lateral direction, if it is established that the factor responsible for this divergence is unsatisfactory quality of stabilizer fabrication or nonnormal engine operation, the shot is not counted.

The scattering magnitude should be determined only from results of valid measurements, and here only a single shot may be classified as valid. An invalid measurement is generally one which deviates from the arithematic mean by more than four mean-probable deviations calculated from the given group of measurements.

The above-cited sequence of calculating firing accuracy is useful for firing both at a target area as well as firing against a screen, but in the latter case the calculation is simplified somewhat because here the coordinates x_0 and z_0 are the coordinates of the sighting points indicated in the center of the screen.

The shell-hole coordinates are measured from the sighting point after each shot by means of a unique surveying rod or by means of an optical viewing device.

Determination of Demolition Effect of Rocket Missiles by Means of Underground Explosions and Firing at Target Area

The demolition effect of a missile is tested on a firing range, as a rule, in two stages. The first stage involves the static explosion of the weapon beneath the soil at various depths; the second stage involves the actual firing of the missile against obstacles in the target area.

In accordance with their tactical-technical designation, demolition missiles are generally intended for action against structures and enemy fortifications; however, it has been demonstrated in practice that the effectiveness of their force can be evaluated on the basis of the dimensions of the craters produced by a demolition missile in the soil, regardless of the nature and strength of the target.

Therefore, the demolition effect is estimated on the basis of the missile's action in the ground, thus substantially simplifying the analysis of the demolition effect, the systematization of the ex-

perimental material, and the methods employed for the verification tests.

Test involving the underground explosions can be reduced to the following : a vertically positioned missile is exploded beneath the groun at various depths and the crater formed in this case is measured. As a result of soil nonuniformites and the asymmetries of the missile and the explosive charge, the craters as a rule exhibit rather irregular shapes..

In firing-range practice a crater is generally assumed to have the shape of a simple truncated cone whose larger base is flush with the surface of the ground.

The demolition effect of missiles is measured by the absolute volume of the crater or by the volume of the explosive charge, referred to its weight; in this case, it is clear that the volume and shape of the crater produced in the explosion are single-valued functions of the weight and quality of the explosive charge on the one hand, and unique functions of missile geometry, depth of explosion, and soil properties on the other hand. One of the goals in these static explosions of weapo is the determination of the optimum depth of warhead explosion. During static tests, the weapons are exploded by means of a special electric detonating machine housed in a reinforced bunker situated in a safety area. The crater produced by the explosion is measured by means of special surveying and marker rods.

In the second stage of the firing-range test of the combat effecti ness of a demolition missile, the effect of the missile against the ground and structures is tested; in this case, one of the most importan tasks in these firings is the verification of the agreement between th fuse time lag for the optimum depth of missile explosion determined during the static tests.

The shortcomings in missile designs, engine operation, etc., brought out during the firing-range tests, are eliminated during the subsequent adjustment of the weapon.

Determination of Fragmentation Effect of Rocket Missiles

The combat effectiveness of a fragmentation missile is determined by two parameters: the number and weight characteristics of the fragments and the range over which the effectiveness of these fragments is preserved.

The number of fragments formed in the explosion of a weapon, and the distribution of these fragments in terms of weight, can be determined by the method of static explosions in a protected pit which is a structure made of reinforced-concrete walls filled with sand. There is a well in the central part of this pit into which the specimen to be exploded is inserted. The entire structure is covered with a massive covering plate. This protected pit is situated in a special ditch or in an underground labyrinth.

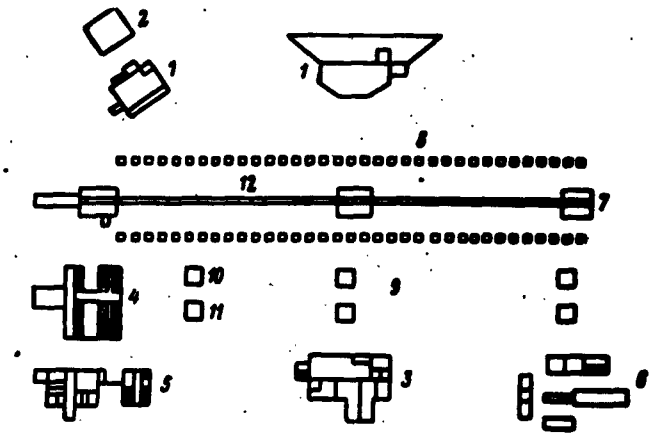

Fig. 7.8. Complex of industrial (technical) structures at Holloman. 1) Shelter; 2) housing for adjustment and preparation of rocket engines; 3) information-gathering point; 4) assembly shop; 5) repair shop; 6) test stand; 7) launching pad; 8) 35 distributor panels; 9) 70 supports for mounting of equipment; 10) photography intallation; 11) photomonitoring installation; 12) track.

The model of the weapon to be tested is lowered into the well of the test pit and exploded. The fragments that are formed as a result of the explosion scatter into the surrounding sand, and here the strength of the pit walls is such as to prevent even a single fragment from flying out beyond the pit. After the explosion, the walls of the pit are dismantled, and the sand is sifted. The collected fragments are weighed and sorted in weight groups. The data of the explosion are recorded.

The second stage of the static firing-range test of fragmentation missiles involves the explosion of the weapon in a circle of divided screens. These divided screens are positioned in a circle, each screen a definite distance from the other, so that the entire scattering range is covered. The missile is exploded in the very center. The fragments formed in the explosion scatter in various directions, striking the screens and marking these with holes. After the explosion, the screens are examined and the number of holes in each screen are counted. The data from these tests make it possible to evaluate the nature of fragment scattering after the explosion as well as to find the radius of continuous damage, i.e., the radius of the zone in which the density of the flying fragments is adequate in order to have at least two fragments strike the target.

After the static explosion tests, the fragmentation missiles are checked through control firings. Here firing is conducted in single shots or in salvos along specially prepared corridors, against tow targets, etc.

The basic purpose of firing rocket missiles to determine the fragmentation is to verify the radius of continuous damage for a missile carrying a given fuse and the agreement of the parameters for this fuse with the design of the weapon.

In recent times, in order to derive the aerodynamic characteristics, it has become the practice to employ closed tracks and rocket sleds. As a rule, models are employed for the track tests. The basic advantages of the use of tracks are the following:

the possibility of obtaining identical meteorological conditions for each shot (an aeroballistic track), since over a closed track the model is not subject to the effects of rain, snow, wind, etc.;

the possibility of obtaining various densities, temperatures, as well as the possibility of modeling missile flight at various altitudes (hermetically sealed barometric and thermobaric tracks).

In comparison with wind tunnels, tracks exhibit the advantage that there are, in this case, no errors attributable to the effect of holders and walls in the testing of models, as is the case with wind tunnels

With tracks it is comparatively simple to note changes in M(ach) and Re(ynolds) numbers over wide ranges.

With respect to track shortcomings, we can cite the fact that models can be used only once, and we can also mention the fact that it is impossible to obtain the aerodynamic characteristics by direct measurements. In processing the experimental results, calculations must be employed.

Abroad, aeroballistic tracks are structuraly made in the form of closed stuctures some 150 - 200 m long. The models are fired from a weapon having a caliber of up to 300 mm. The flight velocity of the model is determined by means of an obturator and a chronograph. During the flight, the model is photographed continuously. The coefficients of longitudinal and lateral stability are frequently calculated by means of cardboard screens set up along the track.

The thermobaric and barometric tracks are made almost identically from a structural standpoint, and as a rule they are made in the form of

a metallic tube having a diameter of 1000 m and a length of 100 – 150 m These tubes are also fitted out with a special photography installation and such other measuring equipment as may be necessary.

Tests with rocket sleds have recently become a more common practice, since they have proved to be the most promising. In this case, particularly in the case of tests conducted on actual objects, the test conditions more closely approximate the actual conditions to be encountered.

For example, in the USA rocket sleds are employed to test fuses, to determine the effectiveness of warheads, and a variety of ballistic problems are solved with these devices; in addition, many of the other experiments associated with rocket and aviation engineering are carried out in this manner.

As an example, below we present the description of a rocket-sled track employed at the Holloman Missile Developement Center (USA).

The track (Fig. 7.8) is a set of rails installed on a reinforced concrete base that is 2.9 m wide, 1.5 m in height, and sloped at a ratio of 1:1000.

The entire track is 10,670 m long, and the gauge of the track is 2.13 m. The sleds are capable of developing velocities of 900 m/sec, and they are capable of developing up to 100 g during acceleration and 150 g during deceleration.

In order to decelerate the sled, a water channel 0.355 m deep and 1.525 m wide has been constructed into the base of the track. A wedge-like blade is mounted on the sled, and this blade is employed to decelerate the sled. The various sled designs make possible the installation of from 1 to 18 engines, the largest of which is capable of developing a thrust of 27 tons.

The information-gathering center receives data from two telemetry

systems: a frequency-modulation system and a pulse-code modulation system. The incoming data are processed through computers.

The firing range has been fitted out with a variety of equipment, including an optical system of obturation photography.

The velocity of the rocket sleds on this track is calculated as follows.

First the maximum possible velocity of the sled is determined:

$$v_т = \sqrt{\frac{2R_т}{C_x \rho s_м}},$$

where R_t is the thrust developed by the power plant; C_x is the coefficient of the frontal resistence of the sled, with the influence of the surface having been taken into consideration; ρ is the air density; s_m is the area of the sled midsection.

But since the actual velocity of the sled, after consumption of the propellant, is a function of the mass ratio

$$\mu = \frac{m_0}{m_к}$$

and the specific impulse J_{ud},

$$v = v_т \frac{\mu^k - 1}{\mu^k + 1},$$

where M_0 is the mass of the sled prior to launch; m_k is the mass of the sled after the consumption of the propellant;

$$k = \frac{2g \cdot J_{уд}}{v_т}.$$

Other Tests of Rocket Missiles

In addition to the described group of basic firing-range tests, both fragmentation and demolition missiles are subject to a number of additional tests, including the following:

1) control tests for normal functioning within the given temperature intervals;

2) control tests for transportability and conservation of all combat properties during transportation, etc.

REFERENCES

1. Abramovich G.N. Prikladnaya gazovaya dinamika, GITTL, [Applied Gasdynamics], 1953.
2. Vaintraub Yu.Ya., Stekloplastiki i vozmozhnost' ikh primeneniya v proizvodstve vooruzheniya(po zarubezhnym materialam), NTI, [Glass-Filled Plastics and the Possibility of their Application in the Production of Armaments (from foreign data)], 1959.
3. Voprosy raketnoy tekhniki, [Problems of Rocket Engineering] 1959 No. 4 (46), 1957, No. 4 (40), 1951, No. 4; 1954, No. 2 (20); 1955, No. 1 (25); 1956, No. 4.
4. Yefimov M.G., Kurs artilleriyskikh snaryadov, Oborongiz [Course in Artillery Missiles, State Defense Industry Press], 1939.
5. ZhETF, [Journal of Experimental and Theoritical Physics], 1942, Vol. 12, No. 11-12.
6. Izvestiya AN SSSR, Otd. tekhn. nauk, [Bulletin of the Academy of Sciences USSR, Department of Technical Sciences], 1958, No. 9.
7. Krasnov N.F., Aerodinamika, Part 2, Nekotoryye voprosy prikladnoy aerodinamiki. Izd. MVTU, [Aerodynamics, Part 2, Certain Problems of Applied Aerodynamics. Publishing House of the Moscow Higher Technical School], 1954.
8. Krasnov N.F. Aerodinamika tel vrashcheniya, [Aerodynamics of Solids of Revolution], Oborongiz, 1958.
9. Lokk A., Osnovy proyektirovaniya upravlyayemykh snaryadov, Upravleniye reaktivnymi snaryadami. IL, [Fundamentals of Designing Guided Missiles, Control of Reaction-Thrust Missiles. Foreign Literature Press], 1959.
10. Merill G., Gol'dberg G., Gel'mgol'ts R., Osnovy proyektirovaniya upravlyayemykh snaryadov. Issledovaniye operatsiy. Boyevyye chasti. Pusk snaryadov. [Fundamentals of Designing Guided Missiles.

Investigation of Operations. Warheads. Missile Launchings], IL, 1959.

11. Prikladnaya matematika i mekhanika, [Applied Mathematics and Mechanics], 1952, Vol. XVI, No. 4; 1958, Vol. XXII No. 3.
12. Sinyarev G.B. and Dobrovol'skiy, M.V. Zhidkostnyye raketnyye dvigateli, [Liquid Rocket Engines], Oborongiz, 1957.
13. Sonkin M., Russkaya raketnaya artilleriya (istoricheskiye ocherki), Voyenizdat, [Russian Rocket Artillery (historical notes), Military Press], 1952.
14. Tret'yakov G.M. Boyepripasy artillerii, [Artillery Weapons], Voyenizdat, 1940.
15. Feodos'yev V.I. and Sinyarev G.B. Vvedeniye v raketnuyu tekhniku, [Intruduction to Rocket Engineering], Oborongiz, 1956.
16. Satton D., Raketnyye dvigateli, [Rocket Engines] IL., 1952.
17. EI VINITI AN SSSR, seriya "Raketnaya tekhinka", [Rocket Engineering], Issue 29, No. RT-87; 1959, Issue 41, No. RT-123; 1959, Issue 25, No. RT-73; 1959, Issue 5, No. RT-13; 1959, Issue 2 No. RT-4; 1959, Issue 6, No. RT-15.
18. Aeronautical Engineering Review, 1958, Vol. 16, No. 8; 1957, 16, No. 10; 1957, 16, No. 11.
19. American Aviation, 1955. Vol. 18, No. 3.
20. ARJ Journal, 1959. Vol. 29, No. 7; 1959, Vol. 29, No. 4.
21. Astronautics, 1958, Vol. 3, No. 3; 1958. 3, No. 4.
22. Astronautica Acta, 1959, Vol. 5, No. 1.
23. Aviation Week, 1957, Vol. 67, No. 17; 1958, Vol. 68, No. 25; 1958, Vol. 68, No. 8.
24. Aviation Age, 1958, Vol. 28, No. 8; 1958, Vol. 28, No. 7.
25. Jet Propulsion, 1958, Vol. 28, No. 7; 1954, Vol. 24, No. 1; 1958, Vol. 28, No. 3; 1956, Vol. 26, No. 8; 1958, Vol. 28, No. 6;

1958, Vol. 28, No. 7; 1958, Vol. 28, No. 12; 1956, Vol. 26, No. 4; 1958, Vol. 28, No. 9; 1958, Vol. 28, No. 3; 1955, Vol. 25, No. 10; 1958, Vol. 28, No. 4; 1958, Vol. 28, No. 11; 1956, Vol. 26, No. 2; 1955, Vol. 25, No. 1; 1956, Vol. 26, No. 7; 1956, Vol. 26, No. 9; 1956, Vol. 26, No. 2.

26. Journal of the Royal Aeronautical Society, 1959, 63, No. 580.
27. Journal of the Aeronautical Sciences, 1956, II Vol. 23, No. 2.
28. Journal of the American Chemical Society, 1955, 77.
29. Journal of the Aero/Space Sciences, 1958, VIII, Vol. 25, No. 8.
30. Journal of the British Interplanetary Society, 1957, Oct. - Dec.
31. Engineering, 1958, No. 4793, 185.
32. Flight, 1958, Vol. 73, No. 2576.
33. Combustion Colloquium Cambrige University, England, Butterworths Scientific Publications, 1954.
34. Missiles and Rockets, 1958, 3, No. 1; 1957, 2, No. 8.
35. Wimpress R.N., Internal. Ballistics of the Solid-Fuel Rockets, McGraw-Hill, New York, 1950.
36. Bonni E.A. Zakrou M. Dzh., Besserer K.U., Aerodinamika. Reaktivnyy dvigateli. Praktika konstruirovaniya i rascheta, Fiamatgiz, [Aerodynamics. Jet Engines. Design Practice and Calculation, Publishing House for Literature in Physics and Mathematics], 1960.

DISTRIBUTION LIST

DEPARTMENT OF DEFENSE	Nr. Copies
HEADQUARTERS USAF	
AFCIN-3D2	1
ARL (ARB)	1
OTHER AGENCIES	
CIA	1
NSA	6
ATD	2
OTS	2
AEC	2
PWS	1
NASA	1
RAND	1
SPECTRUM	1

MAJOR AIR COMMANDS	Nr. Copies
AFSC	
SCFTR	1
ASTIA	25
TD-B1a	5
TD-B1b	3
TD-E3d (Merkle)	1
TD-E3b (Shafer)	4
AEDC (AEY) (Thru B2b)	2
SSD (SSF)	2
BSD (BSF)	1
AFFTC (FTY)	1
APGC (PGF)	1
AFSWC (SWF)	1